R&D 7342-PH-03
N68171-94-M-5711.

PREFACE

It is both a privilege and a pleasure to contribute a short Preface to this Volume. The Proceedings of the 18th International Workshop on Condensed Matter Theories held in Valencia, Spain in June 1994 are recorded in the present book.

These Workshops have a tradition of bringing together many–body theorists with a wide variety of interests. Evidently condensed matter is always the central focal point, but techniques from other areas having potential for solid and liquid state theories have frequently been discussed in this Series of Workshops. In this respect, the 1994 Workshop was no exception. Techniques useful in a variety of nuclear many–body problems were well represented, as were interconnections between various theoretical techniques, ranging through the coupled cluster method, variational Jastrow–like approaches, parquet theory etc. Particular emphasis was placed in the present Workshop on the technique of density functional theory (plus a little on density matrices), a wide range of applications including atomic cluster theory, inhomogeneous liquids and especially ^{4}He, simple metals and metal surfaces. In this context, there was a Special Session, with two papers related to the density–functional technique; one by S. Stringari on time–dependent theory and the other by E. Krotscheck on the many–body construction of density functionals with illustrative applications. Other especially notable contributions applied information theory in ingenious ways to quantal many–body systems.

Turning from (mainly) techniques to physical areas in condensed matter, there was considerable emphasis on the quantal liquid ^{4}He, with discussion not only of bulk properties but of wetting, surface tension and ^{3}He–^{4}He mixtures. Contact with new neutron scattering experiments was highlighted in connection with bulk ^{4}He. Some papers on high T_c materials, plus a discussion of recent progress, both experiment and theory, on electron solids, reflected important growth areas in condensed matter. In the latter area, the equilibrium between Laughlin electron liquid and electron solid was considered, the electron liquid being treated in a number of papers, including a study by quantal hypernetted chain methods.

Finally, the organizers are to be congratulated on the fine, stimulating Workshops they created, and on the efficiency with which they have brought these Proceedings to fruition. As a participant in this Workshop, in the lovely setting of the City of Valencia, the author can only now look ahead with eager anticipation to the 19th Workshop in the Series, to be held in Caracas, Venezuela.

N.H. March
July, 1st. 1994

FOREWORD

The 18th International Workshop on Condensed Matter Theories was held in Valencia (Spain) from 6 to 10 June 1994 and attended by about 70 scientists from all over the world.

In planning for an interdisciplinary workshop focussing on new developments in many-body theories, the Program Committee selected some forty talks collected herewith. We thank the members of this Committee for their help in the program. We also thank the International Advisory Committee members, and specially professor R. Guardiola, for their valuable suggestions and comments.

The Workshop has been made possible with the financial support of several institutions. The Universidad Internacional Menéndez y Pelayo hosted the Workshop at *Palau de Pineda*, its beautiful branch site in Valencia, and assisted the local organizers in numerous administrative tasks. We acknowledge its staff, and specially its director in Valencia, Professor J. Azagra, for his interest and generous support to the Workshop. The Workshop also benefited from the financial support of Dirección General de Investigación Científica y Tecnológica (Ministerio de Educación y Ciencia), Institut de Física i Matemàtiques (Institució Valenciana d'Estudis i Investigació), Consejo Superior de Investigaciones Científicas, Instituto de Física Corpuscular and Universitat de Valencia. Finally, the US Army Research Office helped some participants with travel expenses.

We are also grateful to all participants for their presentations and careful preparation of manuscripts which sustain the scientific quality of this workshop and guarantee its future. Numerous enthusiastic and useful discussions during walks through the historic quarter of Valencia, where the *Palau de Pineda* is located, created a friendly and productive atmosphere throughout the Workshop.

Finally we express our gratitude to Professor N.H. March for kindly accepting to write the Preface to this volume, and to Professor M. de Llano for his invaluable help in the edition of the series *Condensed Matter Theories.*

The Local Organizing Committee:

M. Casas, J. Navarro and A. Polls

Text of an Invited Talk given at the
18th International Workshop on Condensed Matter Theories, held at
Valencia, Spain; 6-10 June 1994

TWO-BODY CORRELATIONS IN QUANTUM MANY-BODY SYSTEMS: A CONFRONTATION BETWEEN DIFFERENT TECHNIQUES

R.F. Bishop

Department of Mathematics, UMIST
(University of Manchester Institute of Science and Technology)
P.O. Box 88, Manchester M60 1QD, UK

Abstract. The important effects of two-body correlations between interacting particles in a quantum many-body system are included in very different ways, depending both on the technique used to study the system and the level of approximation made in its implementation. Our aim here is to study in depth the relationships between various important fundamental techniques by applying them at this level to a specific model, namely the so-called Lieb model of an infinite one-dimensional system of bosons interacting via a pairwise repulsive delta-function potential. We focus particularly on microscopic *ab initio* methods, including the coupled cluster method, variational techniques based on Jastrow-correlated wave functions, planar (or parquet) theory, and a nonlinear integro-differential equation approach due to Lieb.

1. INTRODUCTION

The best of the currently available microscopic techniques in *ab initio* quantum many-body theory have been widely applied to many different physical systems, where they have often been found to be capable of high precision in relatively low orders of implementation. Most practitioners nowadays believe that the state of the art in quantum many-body theory is such that it is less important to develop fundamentally new techniques, for which there seems to be no real need, than to explore the relationships between existing methods which are capable of systematic improvement via well-defined hierarchical approximation schemes. Although different such schemes in principle agree when carried out to the highest (usually infinite) order necessary for

a complete description of the system under study, they will naturally differ in practice when truncated. In particular, the incorporation of the important, and usually dominant, two-body correlation effects depends critically on the formalism adopted.

The aim of the present paper is to examine in depth the relationships between different methods of building two-body correlations into the many-body wave function in various theoretical frameworks. We are particularly interested in studying fully microscopic approaches, as opposed to the more phenomenological techniques that are not intended or designed for systematic improvement. We therefore focus on the following approaches: (i) the coupled cluster method [1-7]; (ii) variational techniques based on Jastrow-correlated wave functions [8-16]; (iii) planar (or parquet) theory [13,17-22]; and (iv) a nonlinear integro-differential equation approach due to Lieb [23-25].

The comparison is made by applying each technique to a particular model problem for which exact results are known. This is chosen to be the so-called Lieb model [26-30] of an infinite system of bosons constrained to move on the one-dimensional line, at a fixed density, and interacting via a pairwise repulsive delta-function potential. The strong-coupling limit thus corresponds to the case of one-dimensional hard-core bosons. The model is known to be exactly integrable *for all values of the coupling constant* by the Bethe-ansatz technique [30-32]. Like most exactly soluble models, the Lieb model provides an especially stringent test for the universal techniques of quantum many-body theory considered here.

One of our main aims in this work has been to show that by bringing the various theoretical methodologies into confrontation by applying each of them to a specific model, we can gain valuable insight both into the methods themselves and, perhaps even more importantly, into the various interconnections between them. We shall also show how, by bringing into conjunction the best elements of the existing methods described, we might produce powerful new calculational schemes.

The remainder of the paper is organized as follows. The Lieb model and its exact solution are first described in Sec. 2. In Secs. 3-5 we then describe in turn the elements of the coupled cluster method (CCM), the local parquet approximation (LPA), and the nonlinear integro-differential equation approach (NIEA) of Lieb. The CCM is also applied in Sec. 3 to the Lieb model at the so-called SUB2 level of approximation, and corresponding results are given in Secs. 4 and 5 for the LPA and NIEA methods. In the light of the latter results we return in Sec. 6 to consider improved truncation schemes within the CCM framework. We conclude in Sec. 7 with a critical discussion of the results obtained.

2. THE LIEB MODEL OF INTERACTING BOSONS

The so-called Lieb model [26-30] considered here consists of a homogeneous system of N bosons constrained to lie on a line of length L interacting via a repulsive pairwise delta-function potential, $v(x) = 2c\delta(x)$, where $c > 0$ and x is the interparticle spacing. The Hamiltonian for the system, in units in which $\hbar = 2m = 1$, is given by,

$$H = -\sum_{i=1}^{N} \partial^2/\partial x_i^2 + 2c \sum_{1 \le i < j \le N} \delta(x_i - x_j) \quad . \tag{2.1}$$

We are particularly interested here in the ground-state Schrödinger equation,

$$H\Psi = E\Psi \quad , \tag{2.2}$$

in the thermodynamic limit where $N \to \infty$, $L \to \infty$, such that $\rho \equiv N/L$ remains finite; and with a bosonic solution $\Psi = \Psi(x_1, \cdots, x_n)$ which is symmetric under the interchange of any two coordinates, and which obeys periodic boundary conditions in each coordinate separately.

Lieb and Liniger [26] first showed that Eqs. (2.1) and (2.2) could be solved exactly by a Bethe ansatz [32] form for the wave function. This general technique has now become of great importance as a method of solution for a number of exactly integrable quantum field theory and statistical mechanical models in two space-time dimensions. All such models solvable by means of the Bethe ansatz share the following feature, namely that they can be reduced to two-body dynamics, in complete analogy with the reduction of free models to one-body dynamics. More precisely, the many-particle scattering matrix simply becomes a product of two-particle scattering matrices, with the latter obeying a particular self-consistency relation. This relation is just the corresponding Yang-Baxter equation (and see Ref. [33]) for the model. The latter equation is nowadays regarded as perhaps the fundamental concept for exactly soluble models. Indeed, the role of the Yang-Baxter equation extends beyond the theory of dynamical systems into both knot theory and the theory of quantum groups. Furthermore, from a modern viewpoint, the coordinate-space Bethe ansatz generalizes into an algebraic counterpart and thence into the quantum inverse scattering method which lies at the heart of present treatments of exactly integrable two-dimensional models in quantum field theory and quantum statistical mechanics. The interested reader is referred to Ref. [31] for a modern treatment of the subject, which actually begins with a detailed discussion of the Lieb model, brief details of the solution to which are given below.

Due to the symmetry of Ψ it is sufficient to consider the solution in the domain R where $0 \leq x_1 < x_2 < \cdots < x_N \leq L$. The wave function in R is simply an eigenfunction of the *free* Hamiltonian,

$$-\sum_{i=1}^{N} \partial^2\Psi/\partial x_i^2 = E\Psi; \quad \text{in } R \quad , \tag{2.3}$$

together with the boundary conditions,

$$(\partial/\partial x_{j+1} - \partial/\partial x_j - c)\Psi = 0; \quad x_{j+1} = x_j + 0 \quad . \tag{2.4}$$

Equations (2.3) and (2.4) are fully equivalent to Eqs. (2.1) and (2.2). Now, it is readily verified that the (unnormalized) function Ψ specified in R as

$$\Psi = \prod_{1 \leq i < j \leq N} (\partial/\partial x_j - \partial/\partial x_i + c) \det[\exp(ik_m x_n)] \quad , \tag{2.5}$$

satisfies Eqs. (2.3) and (2.4) with

$$E = \sum_{i=1}^{N} k_i^2 \quad , \tag{2.6}$$

and where the parameters $\{k_i; i = 1, \cdots, N\}$ are any set of distinct numbers. One also observes that Ψ given by Eq. (2.5) is an antisymmetric function of the parameters $\{k_i\}$. Hence $\Psi = 0$ if $k_i = k_j, i \neq j$, and this forms the basis of the set $\{k_i\}$ forming *a filled Fermi (or Dirac) sea*, which appears strange at first sight for a bosonic problem.

Finally, the set $\{k_i\}$ is determined by requiring that $\Psi(x_1, \cdots, x_i, \cdots, x_N) = \Psi(x_1, \cdots, x_i + L, \cdots, x_N)\ \forall i$, or equivalently that $\Psi(0, x_2, \cdots, x_N) = \Psi(x_2, \cdots, x_N, L)$ for Ψ defined in the domain R. These requirements result in the following Bethe equations for the permitted values of $\{k_j\}$,

$$\exp(ik_j L) = -\prod_{l=1}^{N} \frac{k_j - k_l + ic}{k_j - k_l - ic}\ ; \quad j = 1, \cdots, N\ , \tag{2.7}$$

or equivalently,

$$(-1)^{N-1} \exp(-ik_j L) = \exp\left[i \sum_{l=1}^{N} \theta(k_l - k_j)\right]\ ; \quad j = 1, \cdots, N\ , \tag{2.8a}$$

$$\theta(k) \equiv -2\tan^{-1}(k/c)\ ; \quad -\pi < \theta < \pi, \quad k \in \mathbf{R}\ . \tag{2.8b}$$

Although Eqs. (2.7) or (2.8) comprise N equations in N unknowns they have many sets of solutions (corresponding to the different eigenfunctions of the Hamiltonian). Equation (2.8a) may be rewritten as

$$\delta_j \equiv (k_{j+1} - k_j)L = \sum_{i=1}^{N} [\theta(k_i - k_j) - \theta(k_i - k_{j+1})] + 2\pi n_j\ ; \quad j = 1, \cdots, N-1\ , \tag{2.9}$$

where n_j is an integer. Equation (2.9) comprises $(N-1)$ simultaneous equations for the set $\{\delta_j\}$, from the solution to which the set $\{k_j\}$ may be found once k_1 is fixed from Eq. (2.8a). One can show that with all $n_j \geq 1$ there is a solution to Eq. (2.8) with real $\delta_j > 0$.

If we pass now to the bulk thermodynamic limit the ground state will be obtained with all $n_j = 1$, since this clearly minimizes E from Eq. (2.6). In this limit, furthermore, the set $\{k_j\}$ becomes dense over the "Dirac sea" $-K \leq k \leq K$ with a (non-uniform) distribution $f(k)$ such that $Lf(k)dk$ is the number of k parameters in the range $k \to k + dk$. One can then easily show that Eq. (2.9) reduces to the integral equation,

$$1 = -2c \int_{-K}^{K} dk' \frac{f(k')}{c^2 + (k - k')^2} + 2\pi f(k)\ , \tag{2.10a}$$

with the condition that the number of particles is N given by,

$$\int_{-K}^{K} dk\ f(k) = \rho\ , \tag{2.10b}$$

and the ground-state energy given from Eq. (2.6) by,

$$E = L \int_{-K}^{K} dk\ k^2 f(k)\ . \tag{2.10c}$$

It is now convenient to introduce the dimensionless coupling constant,

$$\gamma \equiv c/\rho \quad , \tag{2.11}$$

in terms of which the ground-state energy E may be written as,

$$E \equiv N\rho^2 e(\gamma) \quad . \tag{2.12}$$

By writing $c \equiv K\lambda, k \equiv Kx, f(Kx) \equiv g(x)$, Eqs. (2.10a-c) become,

$$1 + 2\lambda \int_{-1}^{1} dx' \frac{g(x')}{\lambda^2 + (x - x')^2} = 2\pi g(x) \quad , \tag{2.13a}$$

$$\gamma \int_{-1}^{1} dx \; g(x) = \lambda \quad , \tag{2.13b}$$

$$e(\gamma) = \left(\frac{\gamma}{\lambda}\right)^3 \int_{-1}^{1} dx \; x^2 g(x) \quad . \tag{2.13c}$$

We have solved Eqs. (2.13a-c) numerically. The values are tabulated in Tables 1 and 2 given in later Sections. The method of solution is first to solve Eq. (2.13a) for $g(x)$ for a given value of λ. Equation (2.13b) then determines $\gamma = \gamma(\lambda)$. This process is repeated until the solution for a required value of γ is obtained.

The above exact solutions lead to the following analytic results for e in the small- and large-γ limits,

$$e(\gamma) \underset{\gamma \to 0}{\longrightarrow} \gamma - \frac{4}{3\pi}\gamma^{\frac{3}{2}} \quad , \tag{2.14}$$

$$e(\gamma) \underset{\gamma \to \infty}{\longrightarrow} \frac{\pi^2}{3} \quad . \tag{2.15}$$

We also note an interesting feature of the Lieb model, namely that the integral equation (2.13a) is easy to solve for large c (or γ), but as $c \to 0$ (or $\gamma \to 0$) the solution becomes increasingly singular. This feature seems to be true of all the exactly soluble models, and is the opposite of what one finds from their approximate treatments by the general many-body formalisms discussed below, where the weak-coupling limit is the simplest regime to obtain correctly but the strong-coupling limit is difficult. Finally, we note that, although we do not discuss them further here, the elementary excitations of the Lieb model for all $c > 0$ look like the spectrum of ideal fermions (rather than bosons), for reasons to which we have already alluded.

3. COUPLED CLUSTER METHOD: SUBn APPROXIMATION

The basic coupled cluster method (CCM) approach is by now well known, and we refer the reader to the literature [5-7] for the details of the underlying philosophy and its most general features. Instead, we concentrate here on its specific application to the bosonic systems of interest. We consider a zero-temperature system comprising N bosons in a d-dimensional volume Ω, and we shall mostly be concerned with the thermodynamic limit where $N \to \infty$, $\Omega \to \infty$, such that $\rho \equiv N/\Omega$ remains finite.

The basic boson destruction and creation operators are $b(\mathbf{q})$ and $b^\dagger(\mathbf{q})$ respectively in the momentum-space representation, with the usual canonical commutation relations,

$$[b(\mathbf{q}), b(\mathbf{q}')] = 0 \; ; \quad [b(\mathbf{q}), b^\dagger(\mathbf{q}')] = (2\pi)^d \Omega^{-1} \delta(\mathbf{q} - \mathbf{q}') \quad , \tag{3.1}$$

where $\delta(\mathbf{q})$ is the d-dimensional Dirac delta function. The zero-momentum term is conveniently separated explicitly as,

$$b(\mathbf{q}) = \bar{b}(\mathbf{q}) + \Omega^{-1}(2\pi)^d \delta(\mathbf{q}) b_0 \; ; \quad \bar{b}(q = 0) = 0 \quad . \tag{3.2}$$

Introducing the definition of the Fourier transform of the destruction operator $b(\mathbf{q})$ as,

$$b(\mathbf{x}) = \Omega \int \frac{d\mathbf{q}}{(2\pi)^d} \mathrm{e}^{-i\mathbf{q}\cdot\mathbf{x}} b(\mathbf{q}) \Longleftrightarrow b(\mathbf{q}) = \frac{1}{\Omega} \int d\mathbf{x} \; \mathrm{e}^{i\mathbf{q}\cdot\mathbf{x}} b(\mathbf{x}) \quad , \tag{3.3}$$

the coordinate-space analogue of the boson destruction operator is,

$$b(\mathbf{x}) = \bar{b}(\mathbf{x}) + b_0 \quad . \tag{3.4}$$

The two-body potential term in the many-body Hamiltonian of Eq. (2.1) may be written quite generally in second-quantized form as,

$$\begin{aligned} \hat{V} &= \frac{1}{2} \frac{1}{\Omega^2} \int d\mathbf{x}_3 \int d\mathbf{x}_4 v(\mathbf{x}_3, \mathbf{x}_4) b^\dagger(\mathbf{x}_3) b^\dagger(\mathbf{x}_4) b(\mathbf{x}_4) b(\mathbf{x}_3) \\ &\equiv \frac{1}{2} \int \int_{34} v(34) b^\dagger(3) b^\dagger(4) b(4) b(3) \quad , \end{aligned} \tag{3.5}$$

where $v(34) \equiv v(\mathbf{x}_3, \mathbf{x}_4) = v(\mathbf{x}_3 - \mathbf{x}_4)$ and $b(i) \equiv b(\mathbf{x}_i)$, and in a notation where,

$$\int \cdots \int_{1 \cdots n} f(1 \cdots n) \equiv \frac{1}{\Omega^n} \int d\mathbf{x}_1 \cdots \int d\mathbf{x}_n \; f(\mathbf{x}_1, \cdots, \mathbf{x}_n) \quad . \tag{3.6}$$

The exact ground-state wave function $|\Psi\rangle$ of the many-body Hamiltonian H is now written in the general CCM form,

$$|\Psi\rangle = \mathrm{e}^S |\Phi\rangle \quad , \tag{3.7}$$

in terms of an exponentiated correlation operator S and some suitable model state $|\Phi\rangle$. For bosons we choose $|\Phi\rangle$ to be the normalized zero-momentum condensate,

$$|\Phi\rangle = (N!)^{-\frac{1}{2}} (b_0^\dagger)^N |0\rangle \; ; \quad \langle\Phi|\Phi\rangle = 1 \quad , \tag{3.8}$$

in terms of the bosonic vacuum state $|0\rangle$,

$$b_0|0\rangle = 0 = \bar{b}(\mathbf{q})|0\rangle \quad . \tag{3.9}$$

The correlation operator S may be decomposed into its n-body partitions,

$$S = \sum_{n=2}^{N} S_n \quad , \tag{3.10}$$

where S_n may be expressed in the coordinate-space representation as,

$$S_n = \frac{1}{n!} \int \cdots \int_{12\cdots n} S_n(12\cdots n)\bar{b}^\dagger(1)\bar{b}^\dagger(2)\cdots\bar{b}^\dagger(n)b_0^n \quad , \tag{3.11}$$

where $S_n(12\cdots n)$ is a completely symmetric function of its n position coordinates. We note that Eqs. (3.7) and (3.8) imply the intermediate normalization condition for $|\Psi\rangle$,

$$\langle\Phi|\Psi\rangle = \langle\Phi|\Phi\rangle = 1 \quad . \tag{3.12}$$

It is also convenient to define the momentum-space matrix elements of the operator S_n as follows,

$$S_n(\mathbf{q}_1,\cdots,\mathbf{q}_n) \equiv \frac{1}{\Omega}\int d\mathbf{x}_1\cdots\int d\mathbf{x}_n\ \mathrm{e}^{i\mathbf{q}_1\cdot\mathbf{x}_1}\cdots\mathrm{e}^{i\mathbf{q}_n\cdot\mathbf{x}_n}S_n(\mathbf{x}_1,\cdots,\mathbf{x}_n) \quad . \tag{3.13}$$

We note that translational invariance implies that for an arbitrary translational vector $\mathbf{a}$,

$$S_n(\mathbf{x}_1+\mathbf{a},\cdots,\mathbf{x}_n+\mathbf{a}) = S_n(\mathbf{x}_1,\cdots,\mathbf{x}_n) \quad , \tag{3.14a}$$

or, equivalently, in momentum-space representation,

$$S_n(\mathbf{q}_1,\cdots,\mathbf{q}_n) = S_n(\mathbf{q}_1,\cdots,\mathbf{q}_n)(2\pi)^d\Omega^{-1}\delta(\mathbf{q}_1+\cdots+\mathbf{q}_n) \quad . \tag{3.14b}$$

For example, in the case $n=2$ we have $S_2(\mathbf{x}_1,\mathbf{x}_2) = S_2(\mathbf{x}_1-\mathbf{x}_2)$; and we also write $S_2(\mathbf{q},-\mathbf{q}) \equiv S_2(q)$. Finally, we note that translational invariance implies that the one-body partition $S_1 \equiv 0$, as assumed in Eq. (3.10).

By projecting the ground-state Schrödinger equation,

$$H|\Psi\rangle = E|\Psi\rangle \quad , \tag{3.15}$$

with the non-interacting bra state $\langle\Phi|$, and with $|\Psi\rangle$ given by the CCM parametrization of Eq. (3.7), we readily find that the ground-state energy E is given by,

$$E = \tfrac{1}{2}N(N-1)\int\int_{34} v(34)[1+S_2(34)] \quad . \tag{3.16}$$

We may similarly derive an equation for $S_2(12)$ by projecting Eq. (3.15) onto the bra state $\langle\Phi|b_0^{\dagger 2}\bar{b}(2)\bar{b}(1)$. After some algebra we find,

$$\begin{aligned}
&[t(1)+t(2)]S_2(12) + v(12) + (N-2)\int_3 [v(13)S_2(32)+v(23)S_2(31)] \\
&+(N-2)(N-3)\int\int_{34} S_2(13)v(34)S_2(42) + v(12)S_2(12) \\
&+(N-2)S_2(12)\int_3 [v(13)+v(23)] - (2N-3)S_2(12)\int\int_{34} v(34) \\
&-(2N-3)S_2(12)\int\int_{34} v(34)S_2(34) \\
&+(N-2)\int_4 [v(14)+v(24)]S_3(124) + \tfrac{1}{2}(N-2)(N-3)\int\int_{34} v(34)S_4(1234) = 0 \quad ,
\end{aligned} \tag{3.17}$$

where $t(i) \equiv -\nabla_i^2$, and where we continue to use units where $\hbar = 2m = 1$.

In the thermodynamic limit the two terms in the third line of Eq. (3.17) cancel, and we may use the translational invariance to write Eq. (3.17) for $S_2(x) \equiv S_2(\mathbf{x}_1, \mathbf{x}_2)$ with $\mathbf{x} \equiv \mathbf{x}_1 - \mathbf{x}_2$,

$$-2\nabla^2 S_2(x) + v(x) + 2\rho \int d\mathbf{x}' v(\mathbf{x} - \mathbf{x}') S_2(x')$$

$$+\rho^2 \int d\mathbf{x}' \int d\mathbf{x}'' S_2(\mathbf{x} - \mathbf{x}') v(\mathbf{x}' - \mathbf{x}'') S_2(x'') + v(x) S_2(x)$$

$$-2\rho S_2(x) \int d\mathbf{x}' v(x') S_2(x') + 2\rho \int d\mathbf{x}' v(\mathbf{x} - \mathbf{x}') S_3(0, \mathbf{x}, \mathbf{x}')$$

$$+\tfrac{1}{2}\rho^2 \int d\mathbf{x}' \int d\mathbf{x}'' v(\mathbf{x}' - \mathbf{x}'') S_4(0, \mathbf{x}, \mathbf{x}', \mathbf{x}'') = 0 \quad . \tag{3.18}$$

The ground-state energy is given in the same thermodynamic limit as,

$$\frac{E}{N} = \tfrac{1}{2}\rho \int d\mathbf{x} v(x)[1 + S_2(x)] \quad . \tag{3.19}$$

Equations (3.18) and (3.19) may equivalently be written in the momentum-space representation for $S_2(q) \equiv S_2(\mathbf{q}, -\mathbf{q})$ as,

$$2q^2 S_2(q) + v(q)[1 + \rho S_2(q)]^2 + \int \frac{d\mathbf{q}'}{(2\pi)^d} v(\mathbf{q} - \mathbf{q}') S_2(q')$$

$$-2\rho S_2(q) \int \frac{d\mathbf{q}'}{(2\pi)^d} v(q') S_2(q') + 2\rho \int \frac{d\mathbf{q}'}{(2\pi)^d} v(q') S_3(\mathbf{q}, \mathbf{q}', -\mathbf{q} - \mathbf{q}')$$

$$+\tfrac{1}{2}\rho^2 \int \frac{d\mathbf{q}'}{(2\pi)^d} v(q') S_4(\mathbf{q}, -\mathbf{q}, \mathbf{q}', -\mathbf{q}') = 0 \quad , \tag{3.20}$$

and

$$\frac{E}{N} = \tfrac{1}{2}\rho \left[v(q = 0) + \int \frac{d\mathbf{q}'}{(2\pi)^d} v(q') S_2(q') \right] \quad . \tag{3.21}$$

In Eqs. (3.20) and (3.21) the Fourier transforms $v(q)$ and $S_2(q)$ are defined as,

$$v(q) \equiv \int d\mathbf{x}\ \mathrm{e}^{i\mathbf{q}\cdot\mathbf{x}} v(x) \ ; \quad S_2(q) \equiv \int d\mathbf{x}\ \mathrm{e}^{i\mathbf{q}\cdot\mathbf{x}} S_2(x) \quad , \tag{3.22}$$

where the latter is consistent with Eqs. (3.13) and (3.14b).

We note that Eqs. (3.18)–(3.21) are exact in the thermodynamic limit, but that they involve coupling of the two-body correlation coefficients to their three- and four-body counterparts. Comparable equations can be derived for the latter, which will also involve couplings to higher-order clusters. In order to use the resulting coupled set of equations in practice, the hierarchy must be broken by a suitable approximation scheme. The most common such scheme is the so-called SUBn scheme in which all correlation operators S_m with $m > n$ are set to zero. It is this scheme upon which we focus in the remainder of this Section, and we return in Sec. 6 to discuss alternatives. Since we are primarily interested in pair correlations we focus attention on the SUB2

Table 1. Ground-state energy per particle, $E/N = \rho^2 e(\gamma)$, for the one-dimensional Lieb model as a function of the dimensionless coupling constant $\gamma = c/\rho$, with $\rho = N/L$. We show the exact results and the results from the RPA, LAD+SE, and the full CCM SUB2 and SUB3 approximations.

γ	$e_{\rm exact}$	$e_{\rm RPA}$	$e_{\rm LAD+SE}$	$e_{\rm SUB2}$	$e_{\rm SUB3}$
0.1	0.0872	0.0866	–	0.0895	–
0.3	0.236	0.230	–	0.251	–
1.0	0.639	0.576	0.632	0.750	0.718
2.0	1.050	0.800	1.136	1.374	–
3.0	1.352	0.795	1.586	1.940	1.80
4.0	1.584	0.605	2.000	2.466	–
5.0	1.769	0.255	2.388	2.963	–
10.0	2.311	-3.421	4.077	5.155	4.50
20.0	2.724	-17.961	–	8.743	–
30.0	2.893	-39.738	–	11.764	9.42
$\rightarrow \infty$	$\frac{\pi^2}{3} \approx 3.290$	$-\frac{4}{3\pi}\gamma^{\frac{3}{2}}$	$2(2\gamma)^{\frac{1}{2}}$	$4\gamma^{\frac{1}{2}}$	–

scheme, in which we set $S_3 = 0 = S_4$ in Eqs. (3.18) and (3.20). The remaining four terms in Eq. (3.20) now represent respectively: (i) the kinetic energy (KE) contribution; (ii) the term that together with the KE term generates precisely the ring or bubble diagrams summed in the random phase approximation (RPA); (iii) the term that generates the two-boson ladder (LAD) diagrams for the repeated scattering of a pair from out of the condensate; and (iv) the term that generates the self-consistent self-energy insertions on the zero-momentum hole lines, namely the condensate potential (CP) term.

If we now specialize to the one-dimensional Lieb model introduced in Sec. 2, for which $v(q) = 2c$, the SUB2 approximation can be written from Eqs. (3.20) and (3.21) as,

$$[\rho S_2(z)]^2 + \left(z^2 + 4 - 2\frac{e}{\gamma}\right)\rho S_2(z) + \frac{e}{\gamma} = 0 \quad , \tag{3.23}$$

$$e = \gamma + \gamma^{\frac{3}{2}} \int_{-\infty}^{\infty} \frac{dz}{2\pi} \rho S_2(z) \quad , \tag{3.24}$$

in terms of the dimensionless variables e and γ defined in Eqs. (2.11) and (2.12), and a dimensionless momentum variable z defined as $q \equiv \gamma^{\frac{1}{2}}\rho z$. The self-consistent solution for the ground-state energy $e = e(\gamma)$ in this CCM SUB2 approximation is easy to obtain numerically, and results are shown in Table 1. Both the weak- and strong-coupling limits of Eqs. (3.23) and (3.24) can also be found analytically. We readily derive,

$$e_{\rm SUB2} \underset{\gamma \to 0}{\longrightarrow} \gamma - \frac{4}{3\pi}\gamma^{\frac{3}{2}} \quad , \tag{3.25a}$$

$$e_{\rm SUB2} \underset{\gamma\to\infty}{\longrightarrow} \frac{4\gamma}{\gamma^{\frac{1}{2}}+4} \quad . \tag{3.25b}$$

Whereas Eq. (3.25a) agrees with the exact weak-coupling limit of Eq. (2.14), Eq. (3.25b) is not only in strong disagreement with the constant strong-coupling limit of $\frac{\pi^2}{3}$ for the exact result given by Eq. (2.15), but it is clearly unbounded for large γ. Thus, the CCM SUB2 approximation gives a very poor result in the strong-coupling limit. We shall examine the reasons for this in greater depth below. For the moment we simply remind the reader that in the limit $\gamma \rightarrow \infty$, the Lieb potential becomes a hard-core interaction in the sense that the wave function must vanish when two particles overlap. Indeed, in this one-dimensional case the particles cannot pass through or around each other as $c \rightarrow \infty$, so that they behave in this limit like non-interacting fermions. It is precisely because of this (albeit one-dimensional) hard-core property that the Lieb model is of special interest in the present work, since it is well known that the SUBn truncation scheme cannot satisfactorily handle such hard-core systems [4]. The deficiencies of the SUBn schemes in general, and the SUB2 scheme in particular, can thus be well illustrated by the Lieb model, as can the various ways for compensating for them that we discuss below.

Before leaving the SUB2 scheme, however, it is instructive to consider various sub-approximations contained within it. The first of these is the random phase approximation (RPA), which is contained within the CCM SUB2 scheme by ignoring all but the first two terms in Eq. (3.20). In terms of the dimensionless variables introduced previously, the RPA equation is,

$$[\rho S_2(z)]^2 + (z^2+2)\rho S_2(z) + 1 = 0 \quad , \tag{3.26}$$

with physical solution,

$$\begin{aligned} \rho S_2(z) &= -\tfrac{1}{2}[z^2+2-(z^4+4z^2)^{\frac{1}{2}}] \\ &= -\frac{(z^4+4z^2)^{\frac{1}{2}}-z^2}{(z^4+4z^2)^{\frac{1}{2}}+z^2} \quad . \end{aligned} \tag{3.27a}$$

Insertion of the RPA expression of Eq. (3.27a) into Eq. (3.24) yields the result,

$$e_{\rm RPA} = \gamma - \frac{4}{3\pi}\gamma^{\frac{3}{2}} \quad , \tag{3.27b}$$

which holds for *all* γ. We note that the RPA expression becomes exact in the $\gamma \rightarrow 0$ limit. This is scarcely surprising since this is just the uniform limit in which the ring diagrams generated by the RPA dominate the ground-state energy.

The next SUB2 sub-approximation that we shall consider is the bare ladder sum (LAD), in which we retain in Eq. (3.17) only the first, second and fifth terms. Equivalently, in Eq. (3.20) we retain only the first and third terms together with the bare potential term $v(q)$ from the second term. However, it is trivial to show that the solution to Eq. (3.20) is now $\rho S_2(z) = -e/\gamma z^2$, which leads to a divergent expression for the energy. This problem is overcome by the inclusion also of the fourth (self-energy or SE) term in Eq. (3.20), in order to renormalize the bare kinetic energy denominators appearing in the ladder approximation. The resulting (LAD+SE)

SUB2 sub-approximation is readily expressed in terms of our dimensionless variables as,

$$(z^2 - 2e + 2\gamma)\rho S_2(z) + e = 0 \quad , \tag{3.28a}$$

with a corresponding ground-state energy from Eq. (3.24) given by the cubic equation,

$$8(e-\gamma)^3 + e^2\gamma^2 = 0 \; ; \quad e = e_{\mathrm{LAD+SE}} \quad . \tag{3.28b}$$

In the interesting weak- and strong-coupling limits we obtain,

$$e_{\mathrm{LAD+SE}} \underset{\gamma\to 0}{\longrightarrow} \gamma \quad , \tag{3.29a}$$

$$e_{\mathrm{LAD+SE}} \underset{\gamma\to\infty}{\longrightarrow} 2(2\gamma)^{\frac{1}{2}} \quad . \tag{3.29b}$$

From our discussion to date it is clear that the complete neglect in the SUB2 approximation of the coupling terms to three- and four-body clusters in Eqs. (3.18) or (3.20) for the S_2 amplitude is a very poor approximation for the Lieb model at intermediate and large values of γ. One might imagine naively that a possible solution is to proceed to higher SUBn approximations with $n > 2$. For example, in the SUB3 scheme we first derive an equivalent equation to Eq. (3.17) for the S_3 amplitude. This equation contains coupling terms to the S_2, S_4 and S_5 amplitudes. In the SUB3 approximation one now solves simultaneously for S_2 and S_3 by setting S_4 and S_5 to zero. We have also solved the full SUB3 equations (which we do not present here) for the Lieb model, and numerical results are also shown in Table 1. The weak-coupling limit of Eq. (3.25a) is again reproduced in SUB3 approximation. Although we were unable to obtain an analytic form for the energy in the $\gamma \to \infty$ limit, the numerical evidence strongly suggests that the energy again diverges, although perhaps not quite as rapidly as in the SUB2 case. Although the SUB3 results are marginally better than the SUB2 results, both approximations are extremely poor. We return in Sec. 6 to a more detailed discussion of the reasons why, where we also consider new approximations to improve the CCM performance. Before doing so, however, we discuss two alternative many-body formalisms as an aid to our later discussion.

4. PARQUET THEORY

We now turn our attention to an alternative method of quantum many-body theory, namely the so-called planar or parquet theory [13,17-22]. Since it will be particularly useful for later purposes to draw analogies between the CCM and parquet theory, we derive the basic ingredients of parquet theory below in a way which emphasises their similarities. We stress from the outset, however, that rather than deriving the (two-body) parquet equations in their most general form, we shall make certain simplifying assumptions concerning the locality properties of the fundamental two-body amplitudes that underpin the method. In this way we consider only the so-called local parquet approximation (LPA). Our reasons for making the simplification are threefold. Firstly, the derivation of the full parquet equations is sufficiently complicated that it has often obscured the underlying simplicity of the method. Secondly, the complexity of the full equations usually necessitates further approximations in practice.

Finally, although our resulting LPA equations are known [19] from making a suitable localizing approximation to the full parquet equations, our greatly simplified direct derivation of the LPA appears not to have appeared previously in the literature.

The LPA is conceptually extremely simple since it contains only two principal ingredients, namely generalized versions of the two-body ladder diagrams familiar from Brueckner-Bethe-Goldstone theory, and generalized versions of the ring diagrams familiar from RPA. As is well known, the ladder diagrams are necessary for a proper description of short-range correlations, at least for potentials with strongly repulsive cores, whereas the ring diagrams are necessary for describing the long-range behaviour. A correct description of the important intermediate-range effects clearly requires some degree of mixing of these two elements. The great strength of parquet theory, even in its present LPA form, is the very high degree to which this is achieved.

From our discussion in Sec. 3 it should be clear to the reader that the CCM also includes at the SUB2 level of approximation all of the bare ring and bare ladder diagrams, as well as many additional diagrams which include a fusion of both elements (e.g., ladders in which the rungs are composed of chains of rings; and rings connected by ladders of two-body interactions). As we shall see later, however, although a large degree of self-consistency is built into the set of rings and ladders iterated together in the CCM SUB2 approximation, nevertheless some important terms of this sort are still missing, which are present in the LPA.

Thus, the basic motivation of the LPA is to include the *full* self-consistent union of ring and ladder diagrams. To this end we introduce two new *local* two-body operators, written in the momentum-space representation as $W(q)$ and $G(q)$. They are extensions of the bare two-body potential $v(q)$, associated with the momentum transfer $\mathbf{q}$, which is henceforth represented diagramatically by a dashed line. The new ingredients $W(q)$ and $G(q)$, denoted by wavy and sawtooth lines respectively, are defined to be *local approximations* to the sum of particle-particle (s-channel) irreducible diagrams and the sum of particle-hole (t-channel) irreducible diagrams, respectively. We use here the standard terminology that a particle or a hole (denoted by a solid line with an arrow pointing upwards or downwards, respectively) are defined with respect to the non-interacting zero-momentum condensate state of Eq. (3.8). Furthermore, a diagram is said to be particle-particle (or particle-hole) irreducible if it cannot be made disconnected simply by cutting two internal particle lines (or one internal particle and one internal hole line).

In terms of Goldstone diagrams, the self-consistent definitions of $W(q)$ and $G(q)$ are given in Fig. 1, from which we clearly see that both operators are really nonlocal. We also introduce two related functions $\tilde{G}(q)$ and $\tilde{W}(q)$ which are defined exactly as in Fig. 1 except that the bare potential (driving) term $v(q)$ is replaced respectively by $W(q)$ in the corresponding equation for $\tilde{G}(q)$ and by $G(q)$ in the corresponding equation for $\tilde{W}(q)$. Thus,

$$\tilde{G}(q) = G(q) - v(q) + W(q) \quad , \tag{4.1a}$$

$$\tilde{W}(q) = W(q) - v(q) + G(q) \quad , \tag{4.1b}$$

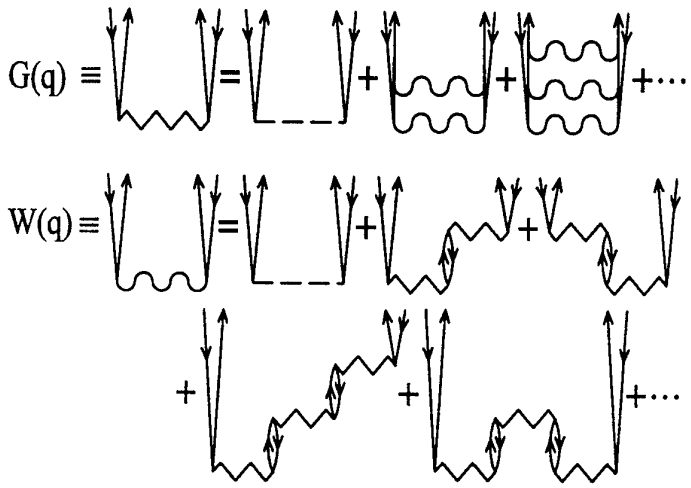

Fig. 1. The self-consistent diagrammatic definitions of the LPA amplitudes $G(q)$ and $W(q)$.

from which we have trivially the manifest self-consistency relation,

$$\tilde{G}(q) = \tilde{W}(q) \quad , \tag{4.2}$$

which demonstrates the completely symmetric fashion in which the particle-particle and particle-hole channels are treated in the LPA treatment.

Before proceeding we note that the LPA makes no provision for any self-energy insertions which dress the bare propagators, although these can be included in full parquet theory. Furthermore, the above analysis can also be extended to higher orders by replacing the bare potential term $v(q)$ in the two equations represented diagramatically in Fig. 1 by a larger class of fully irreducible diagrams. For present purposes, however, we consider neither of the above extensions.

We now introduce our final LPA amplitude $S(q)$, which is defined as,

$$S(q) \equiv -\frac{1}{2q^2}\tilde{G}(q) = -\frac{1}{2q^2}\tilde{W}(q) \quad . \tag{4.3}$$

By recalling that we are using units in which $\hbar^2/2m = 1$, we see that the term $(-2q^2)^{-1}$ in Eq. (4.3) is simply the bare two-particle/two-hole energy denominator. Equation (4.3) has the trivial Fourier transform,

$$\tilde{G}(r) = \tilde{W}(r) = 2\nabla^2 S(r) \quad . \tag{4.4}$$

From Fig. 1 and from Eqs. (4.1)-(4.3), we may express the equation determining $S(q)$ in either of the two forms represented in Fig. 2, where the solid horizontal line now represents the energy denominator explicit in Eq. (4.3). They are easily seen to have

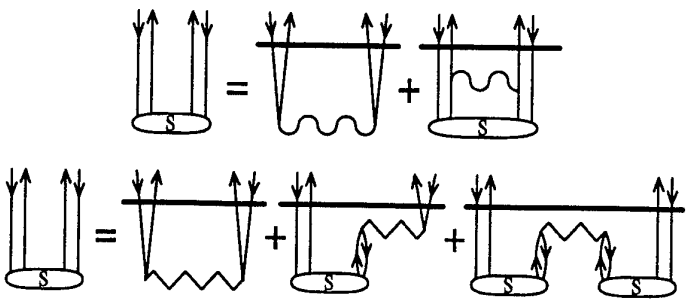

Fig. 2. The equations for the basic LPA amplitude $S(q)$.

the algebraic forms,

$$-2q^2S(q) = W(q) + \int \frac{d\mathbf{q}'}{(2\pi)^d} W(\mathbf{q}-\mathbf{q}')S(q') \quad , \tag{4.5}$$

$$-2q^2S(q) = G(q)[1+\rho S(q)]^2 \quad . \tag{4.6}$$

We note the strong similarity between Eq. (4.6) and the equation obtained by retaining only the first two terms in Eq. (3.20), where this latter approximation exactly generates the RPA, as described in Sec. 3. Equations (4.1a), (4.3) and (4.6) readily yield the relation,

$$W(q) = v(q) + 2C(q) \quad , \tag{4.7}$$

$$C(q) \equiv -q^2\rho S^2(q)\frac{[2+\rho S(q)]}{[1+\rho S(q)]^2} \quad . \tag{4.8}$$

Finally, the insertion of Eq. (4.7) into Eq. (4.5) gives the final equation to determine the basic LPA amplitude $S(q)$,

$$2q^2S(q) + v(q) + \int \frac{d\mathbf{q}'}{(2\pi)^d} v(\mathbf{q}-\mathbf{q}')S(q') + 2C(q)$$

$$+2\int \frac{d\mathbf{q}'}{(2\pi)^d} C(\mathbf{q}-\mathbf{q}')S(q') = 0 \quad . \tag{4.9}$$

Once $S(q)$ is determined from Eqs. (4.8) and (4.9), the ground-state energy is finally computed from the analogues of Eqs. (3.16) and (3.21),

$$\frac{E}{N} = \tfrac{1}{2}\rho\int d\mathbf{x}v(x)[1+S(x)] = \tfrac{1}{2}\rho\left[v(q=0) + \int \frac{d\mathbf{q}}{(2\pi)^d} v(q)S(q)\right] \quad . \tag{4.10}$$

We note that the final LPA equations encapsulated in Eqs. (4.8)-(4.10) are identical to those derived from the full parquet theory [19] by making the localizing approximation made here. Before applying the LPA to the Lieb model, we make one further point of considerable importance for later discussion, namely that the LPA presented here is extremely closely related to the optimized Jastrow hypernetted chain (JHNC)

approach. Indeed, the diagrammatic content of the two approaches is identical, although the weighting factors of some mixed diagrams do differ [19]. Both methods sum all pure ring and pure ladder diagrams (i.e., those formed with links and rungs respectively equal to the bare two-body potential) with the correct weighting however. Further important work in this area [20] has shown that the optimized JHNC approach is actually *identical* to a similar (but different) local form of exact parquet theory to that considered here.

We now apply the LPA to the Lieb model of Sec. 2. In terms of the previously introduced dimensionless coupling constant γ and energy e, and a dimensionless momentum variable z with $q \equiv \gamma^{\frac{1}{2}} \rho z$, it is not difficult to show that the LPA equations (4.8)–(4.10) can be written in the form,

$$\gamma z^2 \rho S(z) + e + \rho^{-1} C(z) + \gamma^{\frac{1}{2}} \int_{-\infty}^{\infty} \frac{dz'}{2\pi} C(z - z') S(z') = 0 \quad , \tag{4.11a}$$

$$C(z) = -\gamma z^2 \rho^3 S^2(z) \frac{[2 + \rho S(z)]}{[1 + \rho S(z)]^2} \quad , \tag{4.11b}$$

$$e = \gamma + \gamma^{\frac{3}{2}} \int_{-\infty}^{\infty} \frac{dz}{2\pi} \rho S(z) \quad , \tag{4.11c}$$

which may be compared with the corresponding CCM SUB2 equations (3.23) and (3.24). We have solved Eqs. (4.11a-c) numerically and the results are tabulated in Table 2. We observe the excellent agreement with the exact results over the whole range of coupling constants.

In the weak-coupling limit it is not difficult to show that,

$$e_{\rm LPA} \underset{\gamma \to 0}{\longrightarrow} \gamma - \frac{4}{3\pi} \gamma^{\frac{3}{2}} \quad , \tag{4.12}$$

in agreement with the exact result of Eq. (2.14). Furthermore, to this accuracy, one may shown that the last term in Eq. (4.11a) does not contribute. If we denote the sub-approximation to the LPA where the last term in Eq. (4.9) or (4.11a) is omitted as LPAa, the resulting set of equations (4.11a-c) can be solved exactly. We find,

$$e_{\rm LPAa} = \gamma \left(1 - \frac{4}{3\pi} e_{\rm LPAa}^{\frac{1}{2}} \right) \Longleftrightarrow e_{\rm LPAa} = \gamma + \frac{8\gamma^2}{9\pi^2} - \frac{4\gamma^{\frac{3}{2}}}{3\pi} \left(1 + \frac{4\gamma}{9\pi^2} \right)^{\frac{1}{2}} \quad . \tag{4.13}$$

This LPAa sub-approximation is itself interesting since it turns out to be identical to a sub-approximation to the NIEA of Lieb discussed in Sec. 5 As here, the motivation behind the Lieb sub-approximation [23,25] was to keep just those terms needed to obtain the correct second term in the small-γ expansion for the energy. As was pointed out by Lieb [25], Eq. (4.13) actually gives a quite good approximation to e for *all* values of γ. In particular, unlike the CCM SUB2 approximation, it approaches a constant value for large γ,

$$e_{\rm LPAa} \underset{\gamma \to \infty}{\longrightarrow} \frac{9\pi^2}{16} \quad , \tag{4.14}$$

which may be compared with the exact value from Eq. (2.15). Finally, before turning to Lieb's NIEA method, we remark that the full LPA result for the energy also approaches a constant value as $\gamma \to \infty$. Although we have been unable to calculate this limit analytically, the numerical solution shows that

Table 2. Ground-state energy per particle, $E/N = \rho^2 e(\gamma)$, for the one-dimensional Lieb model as a function of the dimensionless coupling constant $\gamma = c/\rho$, with $\rho = N/L$. We show the exact results and the results from the local parquet approximation (LPA) and its sub-approximation (LPAa), Lieb's nonlinear integro-differential equation approach (NIEA), and the CCM approximations JSUB2 and HC-JSUB2.

γ	$e_{\rm exact}$	$e_{\rm LPA}$	$e_{\rm LPAa}$	$e_{\rm NIEA}$	$e_{\rm JSUB2}$	$e_{\rm HC-JSUB2}$
0.1	0.08723	0.08725	0.08745	0.08731	–	0.08765
0.3	0.2361	0.2363	0.2379	0.2364	0.2453	0.2387
1.0	0.6392	0.6417	0.6562	0.6382	0.7042	0.6571
3.0	1.352	1.374	1.461	1.329	1.692	1.439
10.0	2.311	2.433	2.843	2.145	3.886	2.649
30.0	2.893	3.150	4.129	2.493	7.289	3.535
100.0	3.162	3.498	5.009	2.593	12.88	4.013
300.0	3.246	3.606	5.355	2.615	20.11	4.173
1000.0	3.277	3.645	5.491	2.622	31.33	4.232
$\rightarrow \infty$	$\frac{\pi^2}{3} \approx 3.290$	3.66	$\frac{9\pi^2}{16} \approx 5.552$	2.63	$\approx 3.2\gamma^{\frac{1}{3}}$	4.26

$$e_{\rm LPA} \underset{\gamma\to\infty}{\longrightarrow} 3.66 \ , \tag{4.15}$$

which is only 11% higher than the exact value of $\frac{\pi^2}{3}$.

5. LIEB'S NONLINEAR INTEGRO-DIFFERENTIAL EQUATION APPROACH

Lieb's analysis of the imperfect Bose gas [26,27] begins by defining the exact n-body ground-state subsystem amplitudes characteristic of the configuration-interaction method (CIM). In the same notation as that adopted in Sec. 3, these are defined in terms of the ground-state N-body wave function, $\Psi = \Psi(\mathbf{x}_1, \cdots, \mathbf{x}_N)$, as,

$$\psi_n(1\cdots n) = \psi_n(\mathbf{x}_1, \cdots, \mathbf{x}_n)$$

$$\equiv \int \cdots \int_{(n+1)\cdots N} \Psi(\mathbf{x}_1, \cdots, \mathbf{x}_N) \Big/ \int \cdots \int_{1\cdots N} \Psi(\mathbf{x}_1, \cdots, \mathbf{x}_N) \ . \tag{5.1}$$

Integration of both sides of the N-body Schrödinger equation (2.2), with a Hamiltonian comprising a sum of one-body kinetic energies and a potential energy term given by Eq. (3.5), yields the exact relation,

$$E = \tfrac{1}{2} N(N-1) \int \int_{12} v(12)\psi_2(12) \ . \tag{5.2}$$

To find an equation for $\psi_2(12)$, the Schrödinger equation is integrated over all variables except 1 and 2. This yields,

$$[t(1)+t(2)+v(12)]\psi_2(12) = E\psi_2(12) - 2(N-2)\int_3 \psi_3(123)v(23)$$

$$-\tfrac{1}{2}(N-2)(N-3)\int\int_{34} \psi_4(1234)v(34) \equiv M(12) \ , \tag{5.3}$$

which is formally equivalent to the CCM Eq. (3.17).

Following Lieb, we now make a careful analysis of the quantity $M(12)$, realizing that although this quantity is expected to be of order unity, its first term in Eq. (5.3) scales like the particle number N. We must therefore be very careful in taking the thermodynamic limit. (Indeed, one of the great attractions of the CCM parametrization of Eq. (3.7) is that this cancellation of $O(N)$ terms is automatically done properly.) By using the cluster property that $\psi_3(123)$ must factorize when particle 1 is far removed from particles 2 and 3, $\psi_3(123) \to P(1)Q(23)$, and the first of the two relations,

$$\int_1 \psi_3(123) = \psi_2(23) \ ; \quad \int\int_{12} \psi_4(1234) = \psi_2(34) \ , \tag{5.4}$$

which follow immediately from the definition of Eq. (5.1), it follows that to leading order in the volume Ω or particle number N, $P = 1$ and $Q = \psi_2$. Similarly, as particles 1 and 2 become far removed from particles 3 and 4, we find $\psi_4(1234) \to \psi_2(12)\psi_2(34)$. By inserting these leading asymptotic forms into Eq. (5.3), and by making use of Eq. (5.2), we verify that $M(12) \to 0$ as the separation of the two particles tends to infinity.

In order to proceed we now need to obtain the leading corrections to the above asymptotic forms for ψ_3 and ψ_4. Lieb was guided in his further analysis by his unproven assumption that, at least at low enough densities, the functions ψ_3 and ψ_4 would have a superposition form akin to a Jastrow-type product,

$$\psi_3(123) = s[1+w(12)][1+w(13)][1+w(23)] \ , \tag{5.5}$$

$$\psi_4(1234) = t\prod_{i<j=1}^{4}[1+z(ij)] \ . \tag{5.6}$$

The constants s and t and the functions w and z may now be determined from the relations (5.4). By writing ψ_2 as,

$$\psi_2(12) \equiv [1+\Sigma(12)]/(1+\delta) \ ; \quad \delta \equiv \int\int_{12} \Sigma(12) \ , \tag{5.7}$$

we see that $\Sigma(\mathbf{x}_1, \mathbf{x}_2) \equiv \Sigma(\mathbf{x}_1 - \mathbf{x}_2) \to 0$ as $|\mathbf{x}_1 - \mathbf{x}_2| \to \infty$. Also, $\delta \to 0$ in the bulk limit, $\Omega \to \infty$. We readily find,

$$s = 1 - 3\delta + o(\Omega^{-1}) \ ,$$

$$t = 1 - 6\delta + o(\Omega^{-1}) \ ,$$

$$w(12) = \Sigma(12) - \psi_2(12)\int_3 \Sigma(13)\Sigma(23) + o(\Omega^{-1}) \ ,$$

$$z(12) = \Sigma(12) - 2\psi_2(12)\int_3 \Sigma(13)\Sigma(23) + o(\Omega^{-1}) \quad , \tag{5.8}$$

where the second term in each case is $O(\Omega^{-1})$, and the standard notation $o(x)$ means that the quantity x is of order *lower* than x. The reason for retaining the terms of order Ω^{-1} in Eq. (5.8) is, as explained above, that the first and third terms in $M(12)$ of Eq. (5.3) are both of order N. They cancel to this order, leaving a residue of order unity. The sources of this residue are threefold in the last term of $M(12)$, namely: (i) that $\psi_4(1234)$ goes asymptotically to $\psi(12)\psi(34) + O(\Omega^{-1})$ for particles 3 and 4 far removed from particles 1 and 2; (ii) the contribution to the integral when particle 3 and/or 4 is close to particle 1 and/or 2; and (iii) the presence of the factor $(N-2)(N-3)$ rather than the corresponding $N(N-1)$ in the expression (5.2) for E. By inserting Eqs. (5.5)-(5.7) into Eq. (5.3), and passing to the bulk thermodynamic limit, we obtain the final form of the Lieb NIEA approximation,

$$[t(1)+t(2)]\Sigma(12) + v(12)[1+\Sigma(12)] + 2N[1+\Sigma(12)]\int_3 \Sigma(13)[1+\Sigma(23)]v(23)$$

$$+N^2[1+\Sigma(12)]\int\int_{34}\Sigma(13)\Sigma(24)\{1+\Sigma(14)+\Sigma(23)+\tfrac{1}{2}\Sigma(14)\Sigma(23)\}$$

$$\times[1+\Sigma(34)]v(34) = 0 \quad . \tag{5.9}$$

By applying Eq. (5.9) to the Lieb model of Sec. 2 we readily find,

$$-\frac{d^2\Sigma(x)}{dx^2} + \rho e\delta(x) + 2\rho^2 e[1+\Sigma(x)]\Sigma(x) + \rho^3 e[1+\Sigma(x)]$$

$$\times\left\{\int_{-\infty}^{\infty} dy\Sigma(x-y)\Sigma(y) + 2\int_{-\infty}^{\infty} dy\Sigma(x-y)\Sigma^2(y) + \tfrac{1}{2}\int_{-\infty}^{\infty} dy\Sigma^2(x-y)\Sigma^2(y)\right\}$$

$$= 0 \quad , \tag{5.10a}$$

$$e = \gamma[1+\Sigma(x=0)] \quad . \tag{5.10b}$$

We have solved Eq. (5.10) numerically after Fourier transformation into the momentum representation. The results are shown in Table 2. For small values of γ (and hence e) we expect $\Sigma(x)$ to be small, and it is thus convenient to define new variables $x \equiv e^{-\frac{1}{2}}s/\rho$ and $\Sigma(e^{-\frac{1}{2}}s/\rho) \equiv e^{\frac{1}{2}}\phi(s)$. We readily find,

$$-\frac{d^2\phi}{ds^2} + \delta(s) + [1+e^{\frac{1}{2}}\phi(s)]\left\{2\phi(s) + \int_{-\infty}^{\infty} dt\phi(s-t)\phi(t)\right.$$

$$\left.+2e^{\frac{1}{2}}\int_{-\infty}^{\infty} dt\phi(s-t)\phi^2(t) + \tfrac{1}{2}e\int_{-\infty}^{\infty} dt\phi^2(s-t)\phi^2(t)\right\} = 0 \quad , \tag{5.11a}$$

$$e = \gamma[1+e^{\frac{1}{2}}\phi(s=0)] \quad . \tag{5.11b}$$

Thus, we see that to obtain $\phi(s=0)$ to leading order, we may safely neglect the last two terms inside the brace in Eq. (5.11a). In this way we arrive at the equation,

$$-\frac{d^2\phi}{ds^2} + \delta(s) + 2\phi(s) + \int_{-\infty}^{\infty} dt\phi(s-t)\phi(t) = 0 \quad , \tag{5.12}$$

which is readily seen (upon Fourier transformation) to be precisely the same sub-approximation to the NIEA as the sub-approximation LPAa to the LPA discussed in Sec. 4. Thus, the NIEA gives the correct weak-coupling expansion of Eq. (2.14). Further, just like the above (LPAa) sub-approximation to it, the full NIEA also gives a constant value for e as $\gamma \to \infty$. This limiting value is determined numerically to be approximately 2.63, or about 20% lower than the exact value of $\frac{\pi^2}{3}$.

6. COUPLED CLUSTER METHOD: ALTERNATIVE APPROXIMATIONS

It is now of considerable interest to revisit the CCM, and particularly its SUBn approximation scheme, in the light of the LPA and NIEA techniques already discussed. We first recall the exact Eq. (3.17) for the CCM correlation function S_2, where, in the bulk thermodynamic limit, the two terms on the third line cancel each other, and the remaining terms may be represented diagrammatically as in Fig. 3. It is clear by iteration that, as we have already noted, the SUB2 approximation (in which S_3 and S_4 are set to zero) generates all of the pure ring and pure ladder diagrams, as well as many mixed diagrams composed of both ring and ladder elements, such as that illustrated in Fig. 4(a). Nevertheless, there are still many such mixed diagrams which are not present at the SUB2 level of the CCM. Examples are those in Figs. 4(b) and 4(c), which are only contained in the CCM by the inclusion of S_3 (and hence which would only appear in SUBn approximations with $n \geq 3$). By contrast, Figs. 1 and 2 clearly show that all three diagrams in Fig. 4 are generated in the LPA. There are many other such diagrams present in the LPA but absent in CCM SUB2 approximation. Conversely, by neglecting only the self-energy insertions (which merely renormalize the bare propagators), *all* diagrams occurring in SUB2 approximation also occur in the LPA.

The differences between the LPA and CCM SUB2 approximations can also be discussed more formally, by examination of the structure that each method assumes for the ground-state wave function. In the SUB2 approximation we have

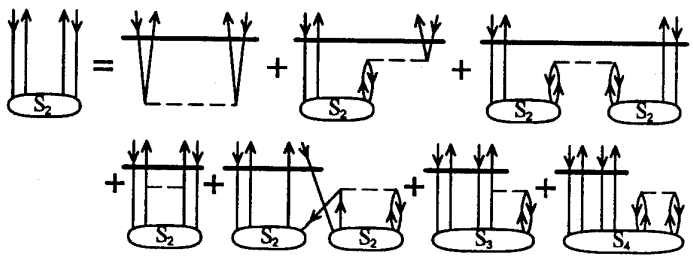

Fig. 3. Diagrammatic representation of the exact equation (3.17) for the CCM amplitude S_2 in the bulk thermodynamic limit.

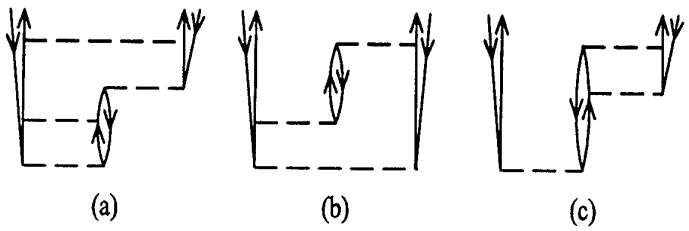

Fig. 4. Three Goldstone diagrams which are generated in the LPA scheme. Note that only diagram (a) appears in the CCM SUB2 expansion.

$$|\Psi\rangle_{\rm SUB2} = \exp(S_2)|\Phi\rangle \quad , \tag{6.1}$$

where S_2 is a two-body operator with the definite structure that it contains only creation operators with respect to the model state $|\Phi\rangle$. Thus, any two S_2 operators commute. Conversely, in a Jastrow-type approach, such as the LPA, the ansatz for the wave function has the form,

$$|\Psi\rangle_{\rm Jastrow} = \exp(U_2)|\Phi\rangle \quad , \tag{6.2}$$

where U_2 is now a *general* two-body operator, which may have both creation and destruction pieces with respect to $|\Phi\rangle$. Hence, two U_2 operators do not, in general, commute. A consequence is that the Jastrow wave function of Eq. (6.2) is a much more complex object than its CCM SUB2 counterpart of Eq. (6.1).

Expressed in terms of the Goldstone diagram formalism used here, in which time is taken to run in the upwards direction, S_2 is thus a "bottom amplitude" in the sense that the four legs of this four-point function always emerge from the top of its corresponding diagram. This is simply a reflection of the fact that S_2 can only create particles and holes from the vacuum state $|\Phi\rangle$ implicit in the diagrams. By contrast, U_2 can be both a "middle amplitude" and "top amplitude" as well as a "bottom amplitude," as is evident from the representations of the elements W, G and S in Figs. 1 and 2. Thus, the four legs of the U_2 amplitude may emerge from either the top or the bottom of its diagrammatic equivalent. It is clear that the fact that S_2 is purely a bottom amplitude implies a considerable restriction on the class of diagrams obtained by iteration of its defining equation, by contrast with the Jastrow-type methods. For example, in the LPA scheme, we see that we can build onto every part of the parquet diagrams, and not just the bottom as in the CCM SUB2 scheme.

For all of these reasons it seems likely that the SUBn approximation scheme may, for many purposes, be too drastic. Thus, recalling that Eq. (3.17) (and see Fig. 3) is *exact*, we turn our attention to alternative truncation schemes in which the higher S_n amplitudes are not neglected entirely, but are instead represented in some self-consistent fashion in terms of the lower amplitudes retained. One obvious way of doing this is via the so-called super-SUBn approximation discussed by Robinson [34]. For example, at the super-SUB2 level, we approximate for S_3 and S_4 in the two-body

equation (3.17) by reference to the corresponding CCM equations which determine S_3 and S_4. In the three-body equation we retain only those terms which include either S_2 or S_3 alone, or which are simple factorizable products of S_2 and S_3. We thus derive an approximation for S_3 in terms of S_2. A similar treatment of the four-body CCM equation gives S_4 in terms of S_2.

Although we expect that the super-SUBn scheme is likely to be one of the most accurate available, we do not discuss it further here. Instead, for present purposes we choose to develop an alternative, namely the so-called Jastrow SUB2 or JSUB2 scheme, which is motivated by the previous discussion of the LPA and NIEA approaches, and in which we employ a Jastrow-like decomposition of the amplitudes S_3 and S_4.

We thus attempt to equate the CCM and Jastrow forms of the wave function parametrization,

$$\Psi(1\cdots N) \equiv \langle 1\cdots N| \exp\left(\sum_{n=2}^{N} S_n\right)|\Phi\rangle = \prod_{i<j=1}^{N} [1+\sigma(ij)] \quad . \tag{6.3}$$

In fact, we only need to assume the product form for the specific cases $N = 3$ and 4. By choosing $N = 2, 3, 4$ respectively in Eq. (6.3) we find the JSUB2 approximations,

$$\Psi_2(ij) = 1 + S_2(ij) = 1 + \sigma(ij) \quad , \tag{6.4a}$$

$$\begin{aligned}\Psi_3(ijk) &= 1+S_2(ij)+S_2(ik)+S_2(jk)+S_3(ijk) \\ &= 1 + \sigma(ij) + \sigma(ik) + \sigma(jk) + \sigma(ij)\sigma(ik) + \sigma(ij)\sigma(jk) \\ &\qquad +\sigma(ik)\sigma(jk) + \sigma(ij)\sigma(ik)\sigma(jk) \quad ,\end{aligned} \tag{6.4b}$$

$$\begin{aligned}\Psi_4(ijkl) &= 1 + S_2(ij) + S_2(ik) + S_2(il) + S_2(jk) + S_2(jl) + S_2(kl) \\ &\qquad +S_2(ij)S_2(kl) + S_2(ik)S_2(jl) + S_2(il)S_2(jk) \\ &\qquad +S_3(ijk) + S_3(ijl) + S_3(ikl) + S_3(jkl) + S_4(ijkl) \\ &= [1+\sigma(ij)][1+\sigma(ik)]\cdots[1+\sigma(kl)] \quad .\end{aligned} \tag{6.4c}$$

Equations (6.4a,b) clearly yield the JSUB2 approximation for S_3,

$$S_3(ijk) = \sigma(ij)\sigma(ik) + \sigma(ij)\sigma(jk) + \sigma(ik)\sigma(jk) + \sigma(ij)\sigma(ik)\sigma(jk) \quad . \tag{6.5}$$

Similarly, Eq. (6.4c) yields the JSUB2 approximation for S_4 in terms of S_2, which we do not write down here due to its length. It includes 16 terms involving products of 3 S_2 functions, 15 involving products of 4 S_2 functions, 6 involving products of 5 S_2 functions, and one term containing a product of all 6 S_2 functions.

By inserting Eq. (6.5) and its counterpart for S_4 into Eq. (3.17) we arrive at the JSUB2 approximation. After a considerable amount of algebra, it may be written in the form,

$$[t(1)+t(2)]\sigma(12) + v(12)[1+\sigma(12)] + 2N[1+\sigma(12)]\int_3 \sigma(13)[1+\sigma(23)]v(23)$$

$$+N^2[1+\sigma(12)]\int\int_{34} \sigma(13)\sigma(24)\{1+\sigma(14)+\sigma(23)+\tfrac{1}{2}\sigma(14)\sigma(23)\}[1+\sigma(34)]v(34)$$

$$+N^2\sigma(12)\int\int_{34}\sigma(13)\sigma(14)[1+\sigma(34)]v(34)$$

$$+2N^2\sigma(12)\int\int_{34}\sigma(13)\sigma(34)v(34)$$

$$+N^2[1+\sigma(12)]\int\int_{34}\sigma(13)\sigma(23)\sigma(34)v(34)=0 \quad . \tag{6.6}$$

It is interesting to compare Eq. (6.6) with its NIEA counterpart of Eq. (5.9). We see that every term in the NIEA method is also contained in the CCM JSUB2 approach, and the latter also contains some additional terms.

By applying Eq. (6.6) to the Lieb model of Sec. 2 we find,

$$-\frac{d^2\sigma(x)}{dx^2}+\rho e\delta(x)+2\rho^2 e[1+\sigma(x)]\sigma(x)+\rho^3 e[1+\sigma(x)]$$

$$\times\left\{\int_{-\infty}^{\infty}dy\sigma(x-y)\sigma(y)+2\int_{-\infty}^{\infty}dy\sigma(x-y)\sigma^2(y)+\tfrac{1}{2}\int_{-\infty}^{\infty}dy\sigma^2(x-y)\sigma^2(y)\right\}$$

$$+\rho^3 e\sigma(x)\int_{-\infty}^{\infty}dy\sigma^2(y)$$

$$+\rho^3(e-\gamma)\left\{2\sigma(x)\int_{-\infty}^{\infty}dy\sigma(y)+[1+\sigma(x)]\int_{-\infty}^{\infty}dy\sigma(x-y)\sigma(y)\right\}=0 \quad , \tag{6.7a}$$

$$e=\gamma[1+\sigma(x=0)] \quad . \tag{6.7b}$$

We have solved Eq. (6.7a) numerically after Fourier transformation into the momentum representation and the ground-state energy results are shown in Table 2. For small values of γ, the analysis of Eq. (6.7) proceeds exactly as for the NIEA, and we find that the JSUB2 approach gives the correct weak-coupling expansion of Eq. (2.14).

Conversely, in the large-γ limit, the JSUB2 approximation, unlike its NIEA subapproximation, does not converge to a constant value for e, like the exact result of Eq. (2.15). Instead, from the numerical results, it appears to diverge as $\gamma^{\frac{1}{3}}$. The reason for this difference between the NIEA and JSUB2 results can clearly only lie in the terms in the last three lines of Eq. (6.6) or, equivalently, the last two lines of Eq. (6.7a). Each of these terms emanates from the Jastrow decomposition of the four-body cluster term S_4 in the exact CCM two-body equation (3.17), and we might wonder why there is such a large difference between the two sets of results. The reason is simple. It stems from the hard-core nature of the Lieb model at strong coupling. For hard-core systems it is well known that for a perturbative or diagrammatic treatment to give meaningful results, the whole treatment must be formulated in terms of complete G-matrices. Equivalently, no bare interaction term v must appear in the formulation except in conjunction with an infinite sum of particle-particle ladders.

It is clear from its construction that the LPA possesses the G-matrix property, which partly explains why the method is so successful in treating the Lieb model, especially at large γ. Conversely the CCM SUB2 approximation does not possess this property. This is easily seen from Fig. 4. Thus, whereas diagrams like that in Fig. 4(a) do appear in SUB2 approximation, those like Fig. 4(c) do not. This drawback of

the SUB2 scheme, and indeed the whole SUBn hierarchy is well known [2,4]. Indeed, an alternative truncation scheme, the so-called hard-core restricted SUBn (or HC-SUBn), has been used in the nuclear physics context to circumvent this problem. In this scheme only those terms in the SUBn equations are retained which when iterated together lead only to diagrams which are still contained in the original SUBn class when each bare interaction v is replaced by a ladder-summed G-matrix, and when the relative time-orderings of the remaining interactions are kept fixed. Clearly, the HC-SUB2 is just the LAD approximation discussed in Sec. 3, which does not converge for the Lieb model. Furthermore, even higher order HC-SUBn schemes will not take proper account of the ring diagrams.

Let us turn finally to a diagrammatic interpretation of the JSUB2 scheme. The most important thing to note now is that although S_2 as it appears in ordinary SUBn calculations is purely a bottom amplitude, this is not true any longer for its JSUB2 counterpart σ. This is a direct consequence of the Jastrow-like superposition ansatz for S_3 and S_4. For example, the terms $\int_3 \sigma(13)\sigma(23)v(23)$ and $\sigma(12)\int_3 \sigma(13)v(23)$ which appear in the second term in Eq. (6.6) may now be represented diagrammatically as in diagrams (a) and (b) respectively of Fig. 5. Upon iteration, these terms clearly generate, for example, the diagrams (c) and (a) respectively of Fig. 4. By similarly iterating together other terms of the JSUB2 equation, we generate many more diagrams which are absent from the SUB2 scheme. However, the complete JSUB2 scheme does not possess the G-matrix property, since for it to do so each bare interaction $v(ij)$ would need to occur in conjunction with the product $v(ij)\sigma(ij)$ and vice versa, i.e., every term involving $v(ij)$ in the defining equation should contain a factor $[1+\sigma(ij)]$. However, it is clear that the terms in the last two lines of Eq. (6.6) do not possess this property. Dropping these terms thereby results in the so-called HC-JSUB2 approximation, to which the NIEA is still a sub-approximation. The HC-JSUB2 results for the Lieb model are also shown in Table 2. They correspond to solving Eq. (6.7a) with the last line omitted. We observe that, as expected, the energy e now approaches a constant value in the $\gamma \to \infty$ limit. This value is about 30% higher than the exact value.

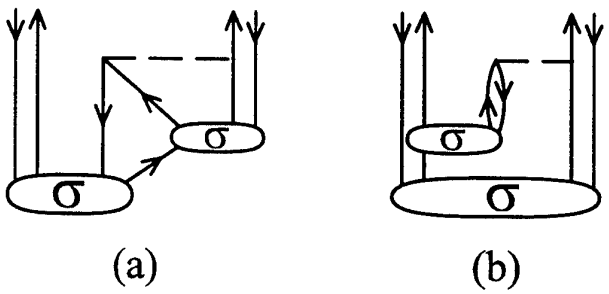

Fig. 5. Diagrammatic representation of two terms from the JSUB2 equation (6.6).

7. DISCUSSION AND CONCLUSIONS

The incorporation of two-body correlations into the treatment of many-body systems has been attempted many times in the past within different contexts and as part of different more general microscopic theories. Most modern treatments have realized that the dual incorporation of ring and ladder terms is vital for an accurate treatment, but as we have seen their self-consistent union is an extremely subtle matter. Different treatments and different formalisms achieve this union to quite different degrees. In many respects the maximal union has been achieved through parquet theory. This is hardly surprising, since it is the primary motivation for (two-body) parquet theory. Essentially the same degree of mixing is also achieved in the Jastrow variational framework, at least via a localized version of optimal hypernetted chain theory.

Later formal developments of parquet theory have included a possible extension to fermionic systems [35,36]; the inclusion of three-body terms [37]; and parquet perturbation theory for bosons [21] as an expansion in the difference between the exact and approximate propagators, in order to improve systematically upon the local parquet equations. However, despite what is now a rather large corpus of formal developments, the parquet method has not yet been widely applied and tested. This is undoubtedly partly due to the rather complicated derivation and nature of the full parquet equations, before any localizing approximations are made. In this respect we hope that our own rather simple and direct derivation of the LPA will prove useful. In particular, it would be extremely useful to repeat the derivation given here for fermions, and we hope to report on this extension elsewhere.

By contrast to parquet theory, the CCM has been very widely applied in physics and chemistry (and see Ref. [6] for a recent review). We have seen how some of the deficiencies of the standard SUBn truncation of the CCM equations, that we have explored in detail here, can be remedied by attempting to mimic within the CCM some of the successes of the LPA and variational treatments employing Jastrow trial wave functions. In particular, we have shown how in the JSUB2 scheme, instead of setting the matrix elements of the higher-order partitions S_3 and S_4 of the correlation operator to zero, as in the standard SUB2 scheme, they have been themselves represented as functions of the S_2 matrix elements. The JSUB2 scheme essentially allocates them the values they would have if the exact wave function were precisely of Jastrow type. We also note that such an approach can be systematically improved upon by enlarging the Jastrow trial wave functions to the more general Jastrow-Feenberg type. In this way one could derive a general JSUBn scheme, in principle. The success of the JSUB2 scheme also encourages us to explore further the more natural super-SUBn extension of the SUBn scheme which we have already mentioned. In this scheme one does not need to make appeals to other approaches for guidance on how to approximate the higher-order partitions S_m with $m > n$, which are otherwise set to zero in a standard SUBn scheme.

Finally, we note that the comparison made between the methods discussed here has focused on the Lieb model interaction. One reason has been that due to its short-range nature it is a particularly sensitive probe in the strong-coupling limit of methods which do not possess the G-matrix property. Nevertheless, a similar comparison using other potentials would also be useful. An obvious example would be the Coulomb potential, and we shall report comparable results using this potential

elsewhere.

ACKNOWLEDGEMENT

Much of the work reported here has been done in collaboration with my students S.R. Hughes and R.G. McGarry, and I thank them both for their assistance. The support of a research grant from the Science and Engineering Research Council (SERC) of Great Britain is gratefully acknowledged. I also thank the European Research Office of the United States Army for partial travel support.

REFERENCES

1. F. Coester, Nucl. Phys. **7**, 421 (1958); F. Coester and H. Kümmel, *ibid.* **17**, 477 (1960).
2. H. Kümmel, K.H. Lührmann, and J.G. Zabolitzky, Phys. Rep. **36C**, 1 (1978).
3. R.F. Bishop and K.H. Lührmann, Phys. Rev. B **17**, 3757 (1978).
4. H.G. Kümmel, in *Nucleon-Nucleon Interaction and Nuclear Many-Body Problems* (eds. S.S. Wu and T.T.S. Kuo), World Scientific, Singapore, 1984, p. 46.
5. R.F. Bishop and H.G. Kümmel, Phys. Today **40(3)** 52 (1987).
6. R.F. Bishop, Theor. Chim. Acta **80**, 95 (1991).
7. R.F. Bishop, in *Dirkfest '92 – A Symposium in Honor of J. Dirk Walecka's Sixtieth Birthday* (eds. W.W. Buck, K.M. Maung, and B.D. Serot), World Scientific, Singapore, 1992, p. 21.
8. R. Jastrow, Phys. Rev. **98**, 1479 (1955).
9. E. Feenberg, *Theory of Quantum Fluids*, Academic Press, New York, 1969.
10. M. Gaudin, J. Gillespie, and G. Ripka, Nucl. Phys. **A176**, 237 (1971).
11. S. Fantoni and S. Rosati, Nuovo Cim. **20A**, 179 (1974).
12. E. Krotscheck and M.L. Ristig, Phys. Lett. **48A**, 17 (1974); *idem.*, Nucl. Phys. **A242**, 389 (1975).
13. G. Ripka, Phys. Rep. **56**, 1 (1979).
14. J.W. Clark, in *Progress in Particle and Nuclear Physics*, Vol. **2** (ed. D.H. Wilkinson), Pergamon, Oxford, 1979, p. 89.
15. S. Rosati and S. Fantoni, in *The Many-Body Problem: Jastrow Correlations Versus Brueckner Theory* (eds. R. Guardiola and J. Ros), (Lect. Notes in Phys., Vol. **138**), Springer, Berlin, 1981, p. 1.

16. S. Rosati and M. Viviani, in *First International Course on Condensed Matter* (eds. D. Prosperi, S. Rosati, and G. Violini), (ACIF Series, Vol. 8), World Scientific, Singapore, 1988, p. 231.

17. I.T. Diatlov, V.V. Sudakhov, and K.A. Ter-Matirosian, Sov. Phys. – JETP **5**, 631 (1957).

18. R. Roulet, J. Gavoret, and P. Nozières, Phys. Rev. **178**, 1072 (1969).

19. A.D. Jackson, A. Lande, and R.A. Smith, Phys. Rep. **86**, 55 (1982).

20. A.D. Jackson, A. Lande, and R.A. Smith, Phys. Rev. Lett. **54**, 1469 (1985); E. Krotscheck, R.A. Smith, and A.D. Jackson, Phys. Rev. A **33**, 3535 (1986).

21. A.D. Jackson, A. Lande, R.W. Guitink, and R.A. Smith, Phys. Rev. B **31**, 403 (1985).

22. R.A. Smith, in *Condensed Matter Theories*, Vol. **4** (ed. J. Keller), Plenum, New York, 1989, p. 129.

23. E.H. Lieb, Phys. Rev. **130**, 2518 (1963).

24. E.H. Lieb and A.Y. Sakakura, Phys. Rev. **133**, A899 (1964).

25. E.H. Lieb and W. Liniger, Phys. Rev. **134**, A312 (1964).

26. E.H. Lieb and W. Liniger, Phys. Rev. **130**, 1605 (1963).

27. E.H. Lieb, Phys. Rev. **130**, 1616 (1963).

28. J.B. McGuire, J. Math. Phys. **5**, 622 (1964).

29. C.N. Yang, Phys. Rev. Lett. **19**, 1312 (1967).

30. M. Gaudin, *La Fonction d'Onde de Bethe*, Masson, Paris, 1983.

31. V.E. Korepin, N.M. Bogoliubov, and A.G. Izergin, *Quantum Inverse Scattering Method and Correlation Functions*, Cambridge Univ. Press, 1993, p. 3.

32. H. Bethe, Z. Phys. **71**, 205 (1931).

33. M. Jimbo, *Yang-Baxter Equation in Integrable Systems*, Advanced Series in Mathematical Physics **10**, World Scientific, Singapore, 1990.

34. N.I. Robinson, PhD Thesis, Manchester University, 1987.

35. A. Lande and R.A. Smith, Phys. Lett. **131B**, 253 (1983).

36. R.A. Smith and A.D. Jackson, in *Recent Progress in Many-Body Theories*, Vol. **1** (eds. A.J. Kallio, E. Pajanne, and R.F. Bishop), Plenum, New York, 1988, p. 327; A. Lande and R.A. Smith, in *ibid.*, p. 335.

37. R.A. Smith and A. Lande, in *Condensed Matter Theories*, Vol. **3** (eds. J.S. Arponen, R.F. Bishop, and M. Manninen), Plenum, New York, 1988, p. 1.

THERMODYNAMICS OF A SUPERFLUID BOSE GLASS

Eugene P. Bashkin

Fachbereich Physik, Philipps–Universität Marburg
35032 Marburg (Lahn), Germany
and
P. L. Kapitza Institute for Physical Problems
117334 Moscow, Russia

Macroscopic properties of a many–body system in a random external potential are actively studied both in theory and experiment throughout the world. Under certain conditions such systems can exhibit an universal behavior independent on the particular structure of the random potential at microscopic distances. For example, all glasses show the linear temperature dependence of the specific heat due to the constancy of the density of states of the two–level excitations [1]. The Bose–Einstein condensation in a random potential may also possess quite unusual features [2,3]. For that reason superfluidity in these systems can manifest itself in a very unusual way. In this paper we will consider the thermodynamic properties of a many–particle Bose fluid with a finite condensate fraction in a random potential. If the number density of potential wells is not too high one can expect that the main contribution to the thermodynamic features is provided by shallow energy levels. This enables one to define specific elementary excitations in the system and calculate all macroscopic characteristics in terms of the corresponding density of states. Under these conditions a quantum Bose fluid can simultaneously exhibit the features pertaining to glassy materials. Liquid helium isotopes in a porous medium can provide a direct experimental realization of the system in question. Instead of formulating the "general principles" of the approach we will begin with some experimental data on quantum ^{3}He–^{4}He solutions, which will help us understand the most significant statements of the theory.

A ^{3}He–^{4}He superfluid mixture in a porous medium can exhibit unique macroscopic properties which are quite different from the behavior in bulk. Recent measurements of Kim, Ma, and Chan on the ^{3}He–^{4}He mixture in aerogel [4] revealed an unusual phase diagram that possesses a large number of very exciting features. In contrast to the phase diagram of the solution in bulk [5]–[6] the coexistence curve of the mixture in aerogel *does not have* a tricritical point and demonstrates *a finite*

strands.

In the very dilute limit, $N_4 \to 0$, the number of ^{4}He particles (per unit volume) off the condensate is given by the obvious equation:

$$\mathcal{N}_4^{(0)} = \frac{(MT)^{3/2}}{2^{1/2}\pi^2\hbar^3}\int_0^\infty \frac{z^{1/2}dz}{\exp(\alpha+z)-1}\ ,\ \alpha = \frac{|\Delta|+E_4^{(0)}}{T}\ , \tag{2}$$

which has the following asymptotic solution at high temperatures, $\alpha << 1$:

$$\mathcal{N}_4^{(0)} = \Big(\frac{MT}{2\pi\hbar^2}\Big)^{3/2}\Big[\zeta(3/2) - 2\pi^{1/2}\Big(\frac{|\Delta|+E_4^{(0)}}{T}\Big)^{1/2}\Big]\ . \tag{3}$$

Here $\zeta(n)$ is the Riemann function. The λ-line on the phase diagram is then described simply by putting $\mathcal{N}_4^{(0)} = N_4$ and $T = T_C$ (where T_C is the Bose–Einstein phase transition temperature) in Eqs.(2)–(3). With the same accuracy Eq.(3) can be rewritten to explicitly calculate the critical temperature:

$$T_C = T_C^{(0)}\Big[1 + \frac{4\pi^{1/2}}{3\zeta(3/2)}\Big(\frac{|\Delta|+E_4^{(0)}}{T_C^{(0)}}\Big)^{1/2}\Big]\ , \tag{4}$$

where $T_C^{(0)}$ is the critical temperature of the Bose–Einstein condensation in a perfect (non–interacting) gas. Notice that the transition temperature in the case in question is higher than $T_C^{(0)}$. In the opposite limiting case, $\alpha >> 1$, the number of the off–condensate particles and the equation of the λ–curve take the form:

$$\mathcal{N}_4^{(0)} = \Big(\frac{MT}{2\pi\hbar^2}\Big)^{3/2}\exp\Big(-\frac{|\Delta|+E_4^{(0)}}{T}\Big)\ . \tag{5}$$

The total energy, $\mathcal{E}_4^{(0)}$, of the ^{4}He specie is given by the following expression:

$$\mathcal{E}_4^{(0)} = -|\Delta|(N_4 - \mathcal{N}_4^{(0)}) + \frac{(MT)^{3/2}}{2^{1/2}\pi^2\hbar^3}\int_0^\infty \frac{z^{3/2}dz}{\exp(\alpha+z)-1}\ ,\ \alpha = \frac{|\Delta|+E_4^{(0)}}{T}\ , \tag{5}$$

which reduces to the power–law dependence at high temperatures, $\alpha << 1$:

$$\mathcal{E}_4^{(0)} = -|\Delta|(N_4 - \mathcal{N}_4^{(0)}) + \frac{3}{2}T\Big(\frac{MT}{2\pi\hbar^2}\Big)^{3/2}\Big[\zeta(5/2) + \frac{4\pi^{1/2}}{3}\Big(\frac{|\Delta|+E_4^{(0)}}{T}\Big)^{3/2}\Big]\ . \tag{6}$$

At low temperatures, $\alpha >> 1$, the thermal corrections in the total energy are, of course, exponentially small, $\mathcal{E}_4^{(0)} = -|\Delta|(N_4 - \mathcal{N}_4^{(0)}) + (3/2)\mathcal{N}_4^{(0)}T$, where the number of thermally activated particles, $\mathcal{N}_4^{(0)}$, is determined by Eq.(5).

Indeed, the ^{4}He states in continuum are not stable. Strictly speaking, it means that the ^{4}He component is not in equilibrium and at finite temperatures after a long enough period of time the ^{4}He particles will "evaporate" from their localized states (exactly like the atmosphere around the Earth). Nevertheless, this does not prevent

us from considering the local equilibrium and taking into account the continuum states when calculating the thermodynamic properties.

Such a simple "one level theory" certainly does not work either at higher densities of ^{4}He or in the presence of more than one localized states. It should be emphasized that the Bose–Einstein condensation of the ^{4}He impurities into the quantum–mechanical state with the lowest energy is accompanied by a real "condensation" and spatial localization of the ^{4}He quasiparticles within the potential well. As long as the number of captured ^{4}He quasiparticles is not too large, so that the mean free path, $d \sim (N_4 r_0^2)^{-1}$, calculated for the ^{4}He–^{4}He collisions is larger than the characteristic localization length, $L \sim \hbar/(M|\Delta|)^{1/2}$, the problem under consideration reduces in fact to the question of how a one particle moves in a given potential box. However, when the concentration of ^{4}He accumulated in the potential box becomes higher, the situation drastically changes. If the lowest energy level Δ is deep enough, the localization length, *i.e.* the "effective size" of the box, is very small. For that reason, if the second particle were placed at the same level Δ, a strong repulsion–core interaction between the particles would come into effect and result in a big increase in the total energy. This effect makes the second particle occupy a higher level or a level with the same energy but located in another potential well if available. A shallower energy state possesses a larger localization length and can adopt a bigger number of ^{4}He impurities. When adding ^{4}He atoms one by one and thus increasing the concentration, the repulsive interparticle interaction at short distances will cause the particles to fill upper levels. Inasmuch as the typical geometric scale of the randomly distributed strand network in aerogel is of the macroscopic order of magnitude (a large open volume fraction of about 98% [4]) one can expect the total number of potential wells to be much less than N_4 at all reasonable macroscopic concentrations. Thus we end up with the picture that as a result of the Bose–Einstein condensation at $T = 0$ all deep–lying states are filled with just a few particles each. Since the number of such states is not large, their contribution to the thermodynamics is negligibly small. On the contrary, the shallow levels may be populated with a macroscopic number of ^{4}He particles, and, consequently, they provide the main contribution to the thermodynamic properties. In the real space a shallow level occupied with a big number of particles, corresponds to a macroscopically large patch with a high enough ^{4}He concentration.

The shallow states can be classified in terms of the *only one* quantum number, namely: the energy of the level ϵ [10]. (In the case of a deep level the quantum–mechanical state is described by the entire set of parameters pertaining to the given potential well.) Thus the localization length and, consequently, the occupation number, n, of each shallow state depend on and are determined by ϵ only no matter what a "profile" of the potential well is and where this potential well is located. The thermodynamic functions of such a system can be expressed in terms of the occupation numbers, $n(\epsilon)$, for each energy level ϵ, and by means of the corresponding density of the low–lying states, $\nu(\epsilon)$. The latter is the most important feature of the theory. It is determined by the specifics of the random potential provided by the aerogel strands. We will begin with the description of the excited states which are responsible for all temperature–dependent terms in the thermodynamic functions.

At finite temperatures, $T > 0$, an essential contribution from the excited states (above the ground state) comes along. Inasmuch as the entropy of the ^{4}He particles

distributed over the shallow states can be defined in a purely combinatoric way [11]:

$$S = -\int_{-\infty}^{0} [(1+n)\log(1+n) - n\log n]\nu(\epsilon)d\epsilon\,, \tag{7}$$

maximizing S at constant energy E and number of particles N_4 leads to the equilibrium distribution function of a traditional form:

$$n(\epsilon) = \left[\exp\left(\frac{\epsilon-\mu_4}{T}\right) - 1\right]^{-1}. \tag{8}$$

Let us recall that due to the interaction between ^{4}He atoms ϵ itself is a functional of n, so that expression (8) is, in fact, a complicated integral equation. The critical temperature of the superfluid transition as well as the number density of the "off-condensate" ^{4}He particles can be calculated by means of the common equation:

$$\mathcal{N}_4 = \int_{-|\mu_{40}|}^{0} \frac{\nu(\epsilon)d\epsilon}{\exp\left(\frac{\epsilon+|\mu_{40}|}{T}\right) - 1} + \mathcal{N}_4^{cont}\,, \tag{9}$$

where term $\mathcal{N}_4^{cont}$ is related to the contribution of the ^{4}He impurity states in continuum and in the low density limit is given by Eq.(2). Here μ_{40} is the chemical potential of ^{4}He in the ground state (in the low-density limit $\mu_{40} = -|\Delta|$). To assure the convergence of the integral in Eq.(9) the density of states $\nu(\epsilon)$ should vanish fast enough when $\epsilon \to \mu_{40}$. The thermal properties of the ^{4}He component can be found using the total energy in the form:

$$\mathcal{E}_4 = \mathcal{E}_{40} + \int_{-|\mu_{40}|}^{0} \frac{(\epsilon+|\mu_{40}|)\nu(\epsilon)d\epsilon}{\exp\left(\frac{\epsilon+|\mu_{40}|}{T}\right) - 1} + \mathcal{E}_4^{cont}\,. \tag{10}$$

Here $\mathcal{E}_{40}$ is the ground state energy at $T = 0$, and $\mathcal{E}_4^{cont}$ describes the continuum contribution similar to Eq.(6) in the case of a rarefied ^{4}He component.

If the ^{4}He concentration is not too high, and the ^{4}He quasiparticles fill basically only the deepest of the shallow levels (let the coresponding binding energy be defined again as $-|\Delta|$), one can easily convince onself that in the high-temperature limit, $T >> |\Delta|$, Eqs.(9–10) take the form:

$$\mathcal{N}_4 = \mathcal{N}_4^{(0)} + T\nu(0)\,,\ \mathcal{E}_4 = \mathcal{E}_4^{(0)} + T|\Delta|\nu(0)\,. \tag{11}$$

Here quantities $\mathcal{N}_4^{(0)}$ and $\mathcal{E}_4^{(0)}$ are the same as in Eqs.(3,7). One can see that at high temperatures the localized states provide only a relatively small correction to the contribution of a perfect gas. The magnitude of this correction is determined by the density of the localized states when $\epsilon \to 0$.

The situation is quite different at low enough temperatures, $T << |\Delta|$. In this case the contibutions of the continuum states, $\mathcal{E}_4^{cont}$ and $\mathcal{N}_4^{cont}$, are exponentially small, and the temperature dependence of $\mathcal{N}_4$ and $\mathcal{E}_4$ is given by the power-law

terms due to the localized states. As was mentioned above, $\nu(-|\Delta|) = 0$. Let us then assume that the density of states can be presented in the form:

$$\nu(-|\Delta| + \epsilon)\Big|_{\epsilon \to 0} \approx a\epsilon^{\gamma} \ , \ \gamma > 0 \ . \tag{12}$$

In the most natural case where $\nu(\epsilon)$ is a normal analytic function, one would simply have $\gamma = 1$, and $a = \partial\nu/\partial(-|\Delta|)$. Keeping in mind definition (21) after some algebra one obtains:

$$\begin{aligned} \mathcal{N}_4 &= a\Gamma(1+\gamma)\zeta(1+\gamma)T^{1+\gamma} \\ \mathcal{E}_4 &= -|\Delta|(N_4 - \mathcal{N}_4) + a\Gamma(2+\gamma)\zeta(2+\gamma)T^{2+\gamma} \ . \end{aligned} \tag{13}$$

Here $\Gamma(n)$ is the common gamma function. Putting $\mathcal{N}_4 = N_4$ and $T = T_C$ in the first of Eqs.(13) one immediately obtains the ^{4}He concentration dependence of the superfluid transition temperature (the λ-curve). Differentiating the second one provides the specific heat:

$$C_V = a(1+\gamma)\Gamma(1+\gamma)\zeta(1+\gamma)|\Delta|T^{\gamma} \ . \tag{14}$$

(In Eq.(14) we keep only the biggest term.) Term (14) can easily be detected in experiment when lowering the temperature as the contribution of superfluid ^{3}He falls off exponentially. Using the thermodynamic identities:

$$\frac{\partial\mu_4}{\partial T} = -\frac{\partial S}{\partial N_4} \ , \ T\frac{\partial S}{\partial T} = C_V \ , \tag{15}$$

where S is the entropy, one can easily calculate the coexistence curve (the solubility of ^{4}He in ^{3}He as a function of temperature):

$$N_4^C(T) - N_4^C(0) = \frac{\partial N_4}{\partial \mu_{40}} \cdot \frac{\partial}{\partial N_4} \int_0^T S dT \ . \tag{16}$$

Substituting Eqs.(13–16) into Eq.(25) yields:

$$N_4^C(T) = N_4^C(0) + \frac{1}{\gamma}\Gamma(1+\gamma)\zeta(1+\gamma)\frac{\partial N_4}{\partial \mu_{40}} \cdot \frac{\partial}{\partial N_4}(a|\Delta|) \cdot T^{1+\gamma} \ . \tag{17}$$

To calculate $N_4^C(0)$ one has to consider the ground state properties.

In principle the ground state energy E_{40} of the ^{4}He component at $T = 0$ can be expressed in terms of the occupation numbers, $n_0(\epsilon)$, in a common way as a sum over all energy states:

$$\acute{E}_{40} = \sum_n \epsilon_n n(\epsilon_n) = \int_{-\infty}^{0} \epsilon n_0(\epsilon)\nu_0(\epsilon) d\epsilon \ . \tag{18}$$

Here index "0" refers to the ground state. At $T = 0$ the distribution function, $n_0(\epsilon)$, is, indeed, normalized to the total particle density, N_4:

$$\int_{-\infty}^{0} n(\epsilon)\nu(\epsilon) d\epsilon = N_4 \ . \tag{19}$$

As mentioned above, the interaction between particles and, hence, the level populations may strongly affect the energetics of the states themselves. In other words it means that the energy of the level is a functional of the occupation number, $\epsilon = \epsilon[n]$, and a quantitative measure of this "effective interaction" can be represented in the form:

$$\frac{\delta\epsilon}{\delta n_0(\epsilon')} = f(\epsilon, \epsilon') \; . \tag{20}$$

Function $f(\epsilon, \epsilon')$ (similar to the interaction function in the fermi–liquid theory) is in turn a functional of $n_0(\epsilon)$ and describes the interaction between the levels. In contrast to the thermally excited states where the population is always small at low enough temperatures, the ground state calculations are much more complicated due to the high population density and interaction between levels. Here we will restrict ourselves to considering the low–density limit where only one lowest level is populated at $T = 0$, and the population density is not too high. In this case one can use sort of a virial expansion:

$$\epsilon = \epsilon_0 + \int_{-\infty}^{0} f(\epsilon_0, \epsilon') n_0(\epsilon') \nu_0(\epsilon') d\epsilon' \; , \tag{21}$$

where ϵ_0 is the energy of the level in the absence of ^{4}He. After simple manipulations one can easily obtain:

$$E_{40} = \bar{\epsilon} N_4 + \frac{1}{2} \bar{f} N_4^2 \; , \tag{22}$$

where quantities $\bar{\epsilon}$ and $\bar{f}$ are defined as follows:

$$\begin{aligned} \bar{\epsilon} N_4 &= \int_{-\infty}^{0} \epsilon_0 n_0(\epsilon_0) \nu_0(\epsilon_0) d\epsilon_0 \; , \\ \bar{f} N_4^2 &= \int_{-\infty}^{0} \int_{-\infty}^{0} f(\epsilon_0, \epsilon_0') n_0(\epsilon_0) n_0(\epsilon_0') \nu_0(\epsilon_0) \nu_0(\epsilon_0') d\epsilon_0 d\epsilon_0' \; . \end{aligned} \tag{23}$$

Simply differentiating yields the chemical potential of the ^{4}He component: $\mu_{40} = \bar{\epsilon} + \bar{f} N_4$. From the condition of constancy of the chemical potential, $\mu_{40} = const$, one immediately finds the equilibrium concentration of ^{4}He in the phase rich with ^{3}He at $T = 0$:

$$N_4^C(0) = \frac{\mu_4^{(6.4)} - \bar{\epsilon}}{\bar{f}} \; , \tag{24}$$

where $\mu_4^{(6.4)}$ is the chemical potential of ^{4}He in a 6.4% mixture of ^{3}He in ^{4}He, which ranges from –7K at saturated vapour pressure to –1K at $P = 25 atm$ [12]. According to the experimental data [4] the critical concentration, N_4^C, is about 19%. One can make a very crude estimate of the average binding energy, $\bar{\epsilon}$, when using the theory of a weakly–interacting Bose gas in the s–wave scattering approximation [13]. Within this approach the magnitude of $\bar{f}$ can be calculated as:

$$\bar{f} = \frac{4\pi\hbar^2 a N_4}{M} \; , \tag{25}$$

where $a = 2.2\mathring{A}$ [13] is the s-wave scattering length. A simple calculation shows that the magnitude of $\bar{\epsilon}$ is just slightly less than the ^{4}He chemical potential in bulk: $(|\bar{\epsilon}| - |\mu_4^{(6.4)}|/|\mu_4^{(6.4)}| \sim 0.1$. This, actually, demonstrates that the virial expansion holds very badly in the case in question. The accuracy of the estimate obtained is very poor, and improved ground state computations are certainly needed.

Let us point out that no information about the continuum states of ^{4}He is required when considering the low–temperature part of the phase diagram and other thermodynamic properties. All the characterisics are expressed in terms of the energy spectrum and density of levels for the shallow localazed states only. It means that the physical foundation of the theory is based on the bosonic macroscopic condensation of ^{4}He atoms onto the shallow bound states in a random potential no matter what the state of a ^{4}He impurity in the bulk ^{3}He background is. That is why the low–temperature calculations should be valid at the temperatures higher than the superfluid transition temperature of ^{3}He as well. There is no need to have the ^{3}He background superfluid in order to cause the macroscopic accumulation of ^{4}He atoms in the ground state. The theory, indeed, cannot be applied to ^{3}He atoms as the Fermi–Dirac statistics prohibits to get more than two particles at the same level. In case of the ^{3}He component the continuum states in bulk are stable and provide the main contribution to the thermodynamics. At high temperatures the critical fluctuations come into effect and strongly affect the thermodynamics. Nevertheless, naively extrapolating the developed theory to that temperature range would result in the absence of the tricritical point. A more elaborated theory should, however, take into account various surface effects (like the existence of a solid inert layer of ^{4}He *etc*) as the surface–to–volume ratio in aerogel be rather high.

This research was supported in part by the Deutsche Forschungsgemeinschaft under Grant No. BA 1229/4-1, the U.S. National Science Foundation under Grant No. DMR–9022681, Petroleum Researh Fund of ACS, and the European Research Office of the U.S. Army. The author greatly appreciates the warm hospitality extended to him at the Pennsylvania State University where a part of this work was done. The work has benefited from stimulating discussions with J. Banavar, M. Chan, and M. Cole.

REFERENCES

[1] P. W. Anderson, B. I. Halperin, and C. M. Varma, Phil. Mag. **25**, 1 (1972).
[2] M. P. A. Fisher, P. B. Weichman, *et al.* Phys. Rev. **B40**, 546 (1989).
[3] D. K. K. Lee and J. M. F. Gunn, J. Low Temp. Phys. **89**, 101 (1992).
[4] S. B. Kim, J. Ma, and M. H. W. Chan, Phys. Rev. Lett. **71**, 2268 (1993).
[5] E. H. Graf, D. M. Lee, and J. D. Reppy, Phys. Rev. Lett. **19**, 417 (1967).
[6] E. M. Ifft, D. O. Edwards, *et al.* Phys. Rev. Lett. **19**, 831 (1967).
[7] A. Maritan, M. Cieplak, M. Swift, *et al.* Phys. Rev. Lett. **69**, 221 (1992).
[8] D. D. Osheroff, W. J. Gully, *et al.* Phys. Rev. Lett. **29**, 920 (1972).
[9] L. D. Landau and I. Pomeranchuck, Dokl. Akad. Nauk SSSR **59**, 669 (1948).
[10] L. D. Landau and E. M. Lifshitz, Quantum Mechanics (Pergamon, NY, 1977).
[11] L. D. Landau and E. M. Lifshitz, Statistical Physics (Pergamon, NY, 1977).
[12] C. Ebner and D. O. Edwards, Phys. Reports **2C**, 77 (1970).
[13] R. K. Pathria, Statistical Mechanics (Pergamon, NY, 1980).

BOSE QUANTUM FILMS AT FINITE TEMPERATURE

B. E. Clements[1], E. Krotscheck[2], M. Saarela[3] and C. E. Campbell[4]

[1]Institute Laue-Langevin, 38042 Grenoble Cedex, France

[2]Department of Physics, Texas A&M University, College Station, Texas 77843

[3]Department of Theoretical Physics, University of Oulu, SF-90570 Oulu, Finland

[4]School of Physics and Astronomy, University of Minnesota, Minnesota 55455

1. INTRODUCTION

In this work we focus on the low temperature properties of ^{4}He films adsorbed to weakly attractive substrates. To date, the most sophisticated and accurate microscopic approach for studying the structural properties of helium films is variational Euler-Lagrange (EL) theory. At the present level of implementation, *i.e.* including optimized triplet correlations, the theory reproduces the zero temperature Green's function Monte Carlo (GFMC) and experimental equations of state in the two- and three-dimensional limits, respectively. Since the theory is analytic and microscopic, it is not hampered by finite size effects and statistical uncertainties, as in Monte Carlo simulations, nor does it require additional input regarding the bulk helium system, which is a limitation of approximate applications of density functional theory. The finite temperature generalization of the EL theory, has been applied extensively to bulk ^{4}He as well as to the infinite half space ($d \times d \times t; -\infty \leq d \leq \infty, -\infty \leq t \leq 0$). Although the finite-temperature theory is at a much cruder level of implementation compared to the ground-state theory, it does reproduce the bulk ^{4}He liquid-gas phase diagram with quite good accuracy. For example, the liquid-gas critical temperature and density determined by the theory is $T = 4.3K$ and $\rho = 0.009\text{Å}^{-3}$ whereas the experimental values are $T \approx 5.2K$ and $\rho \approx 0.009\text{Å}^{-3}$. Since a goal of the theory is to describe the thermodynamic phase diagram for the film, similar success is expected.

Although the physics that governs the growth of helium films depends on the particular choice of substrate (in some cases dramatically), we will concentrate on a graphite substrate, leaving substrate dependent effects to latter studies. Graphite substrates are rather unique for several reasons:

(a) The interaction between the graphite and the ^{4}He is sufficiently strong to cause

the first two layers of adsorbed helium to freeze. The outermost frozen layer provides a very flat substrate upon which further *liquid* ^{4}He can be adsorbed. In this work the substrate is the combined graphite *plus* the two frozen layers of helium.

(b) Because of the substrate strength, the liquid ^{4}He wets the substrate. The finite-temperature behavior of a nonwetting substrate provides an additional complication that should be considered only when the simpler wetting case is fully understood.

(c) The liquid film is truly layered in the sense that the density profile $\rho_1(\mathbf{r})$ shows substantial oscillations as one moves away from the substrate. The distance between oscillations is approximately a broadened atomic layer. The layering is experimentally observed for as many as 9 layers away from the substrate [1].

(d) The film grows by adsorbing more and more ^{4}He atoms to the existing film. The simplest growth scenario imaginable would be for the film's thickness to increase continuously as the number of atoms increases. There is strong evidence that this is not the case for liquid helium on the graphite/solid ^{4}He substrate, at least for the first few liquid layers. Variational EL theory asserts that the film passes through a series of first-order phase transitions as the film grows [2]. Near the completion of a given layer it eventually becomes energetically unfavorable to compress it further. After the film broadens slightly, the uniform-covering phase gives way to a clustering phase where two-dimensional ^{4}He clusters coexist with the surrounding vacuum. Upon adding a sufficient amount of ^{4}He, the clusters connect whereby a low density covering phase is again reached. This process repeats for the growth of at least three layers.

In the next section we will briefly describe the ground-state theory. Following that discussion, the growth scenario outlined in (d) will be expanded upon [3]. We argue that evidence for the proposed scenario has been provided by torsional oscillator experiments and recent path integral Monte Carlo (PIMC) simulations. In Sec. 3, a brief description of finite-temperature variation theory is outlined. A low-temperature expansion provides useful insight into the behavior of the full set of finite-temperature equations. Of special interest to us here is the role of the excitations in determining the thermodynamic behavior of the films. In our numerical work, we will limit ourselves to the case of a monolayer. Already at this level much interesting physics takes place. In Sec. 4 we close with some speculative remarks about the thermodynamic phase diagram for a thin film.

2. GROUND-STATE THEORY

Ground-state variational theory has been reviewed in considerable detail elsewhere [4, 5]. Our intent here is only to summarize the relevant ground-state formulation so that we can appropriately discuss the issues important to this work, such as the film's stability and the low-lying excitations. This summary will culminate with a discussion on the predicted growth scenario. For details concerning the treatment of triplet correlations we refer the reader to Ref. [5] .

The starting point of the theory is the many-body wave function:

$$\Psi_0(\mathbf{r}_1,\ldots,\mathbf{r}_N) = \exp\frac{1}{2}\left[\sum_i u_1(\mathbf{r}_i) + \sum_{i<j} u_2(\mathbf{r}_i,\mathbf{r}_j) + \sum_{i<j<k} u_3(\mathbf{r}_i,\mathbf{r}_j,\mathbf{r}_k)\right]. \quad (2.1)$$

The pseudo-potential $u_1(\mathbf{r}_i)$ is required because of the broken symmetry caused by the substrate, $u_2(\mathbf{r}_i,\mathbf{r}_j)$ is the Jastrow pseudo-potential, and the triplet correlation pseudo-potential $u_3(\mathbf{r}_i,\mathbf{r}_j,\mathbf{r}_k)$ is needed to make the theory quantitatively precise. The Hamiltonian has contributions coming from kinetic energy, and the ^{4}He-^{4}He interaction, and the substrate-^{4}He potential.

$$H = \sum_i \left[-\frac{\hbar^2}{2m}\nabla_i^2 + U_{sub}(\mathbf{r}_i)\right] + \sum_{i<j} V(|\mathbf{r}_i - \mathbf{r}_j|). \quad (2.2)$$

In our numerical work we used the *old* Aziz potential [6] for the ^{4}He-^{4}He potential. The explicit form for the substrate potential can be found in Ref. [5]. The pseudo-potentials are determined by invoking the optimization condition:

$$\frac{\delta E}{\delta u_n(\mathbf{r}_1,\ldots,\mathbf{r}_n)} = 0 \quad (2.3)$$

where

$$E \equiv \frac{\langle\Psi_0|H|\Psi_0\rangle}{\langle\Psi_0|\Psi_0\rangle}. \quad (2.4)$$

In practice, it is significantly more convenient to use the BBGKY and hypernetted-chain equations to eliminate the $u_1(\mathbf{r}_i)$ and $u_2(\mathbf{r}_i,\mathbf{r}_j)$ in favor of the (physically observable) single-particle density and the pair distribution function,

$$\rho_1(\mathbf{r}_1) = N\frac{\int d\mathbf{r}_2\cdots d\mathbf{r}_N\,|\Psi_0|^2}{\int d\mathbf{r}_1\cdots d\mathbf{r}_N\,|\Psi_0|^2}, \quad (2.5)$$

$$g(\mathbf{r}_1,\mathbf{r}_2) = \frac{N(N-1)}{\rho_1(\mathbf{r}_1)\rho_1(\mathbf{r}_2)}\frac{\int d\mathbf{r}_3\cdots d\mathbf{r}_N\,|\Psi_0|^2}{\int d\mathbf{r}_1\cdots d\mathbf{r}_N\,|\Psi_0|^2}. \quad (2.6)$$

The Euler equation for $\rho_1(\mathbf{r})$ has the form of a Hartree equation:

$$\frac{\delta}{\delta\sqrt{\rho_1(\mathbf{r})}}[E - \mu N] = 0 \quad (2.7)$$

that is,

$$\left[-\frac{\hbar^2}{2m}\nabla^2 + U_{sub}(\mathbf{r}) + V_H(\mathbf{r})\right]\sqrt{\rho_1(\mathbf{r})} = \mu\sqrt{\rho_1(\mathbf{r})} \quad (2.8)$$

with a Hartree potential

$$V_H(\mathbf{r}) \equiv \frac{\delta}{\delta\rho(\mathbf{r})}E_c. \quad (2.9)$$

Here E_c is the correlation energy; the explicit form for it, V_H, and V_{p-h} (discussed below) are not important for this paper and may be found in Refs. [4] and [5].

As a result of solving the Hartree equation, one obtains the chemical potential μ, and $\rho_1(\mathbf{r})$, for a given surface coverage n

$$n = \int dz \rho_1(\mathbf{r}). \tag{2.10}$$

Next we consider the two body-equation which may be cast into the form of an eigenvalue equation that is written in terms of a particle-hole interaction. Formally $V_{p-h}(\mathbf{r}, \mathbf{r}')$ may be defined from the second variation in density of the correlation energy.

$$\hat{V}_{p-h}(\mathbf{r}, \mathbf{r}') = \sqrt{\rho_1(\mathbf{r})} \frac{\delta^2 E_c}{\delta\rho_1(\mathbf{r})\delta\rho_1(\mathbf{r}')} \sqrt{\rho_1(\mathbf{r}')} \tag{2.11}$$

Introducing a generalized kinetic energy operator

$$H_1(\mathbf{r}) \equiv -\frac{\hbar^2}{2m} \frac{1}{\sqrt{\rho_1(\mathbf{r})}} \nabla\rho_1(\mathbf{r})\nabla \frac{1}{\sqrt{\rho_1(\mathbf{r})}} \tag{2.12}$$

the eigenvalue equation may be expressed as:

$$\int d^3r' \left[H_1(\mathbf{r})\delta(\mathbf{r} - \mathbf{r}') + 2\hat{V}_{p-h}(\mathbf{r}, \mathbf{r}') \right] H_1(\mathbf{r}')\psi_m(\mathbf{r}') = \hbar^2\omega_m^2\psi_m(\mathbf{r}). \tag{2.13}$$

For an homogeneous system this equation reduces to the Bogoljubov expression for the excitation energy with the important exception that V_{p-h} replaces the bare interaction found in the usual weakly-interacting case,

$$\hbar\omega_k = \sqrt{\frac{\hbar^2k^2}{2m}\left(\frac{\hbar^2k^2}{2m} + 2V_{p-h}(k)\right)}. \tag{2.14}$$

Indeed linear response theory [7] has been used to show that the poles of the density-density response function are completely equivalent to the eigenvalues of Eq. (2.13).

$$\chi(\mathbf{r}, \mathbf{r}'; \omega) = 2\sum_m \delta\rho_1(\mathbf{r}, \omega_m) \frac{1}{(\hbar\omega)^2 - (\hbar\omega_m)^2 + i\eta} \delta\rho_1(\mathbf{r}', \omega_m). \tag{2.15}$$

Here $\delta\rho_1(\mathbf{r}, \omega)$ is the transition density and is related to the eigenstates $\psi_m(\mathbf{r})$ by:

$$\delta\rho_1(\mathbf{r}, \omega_m) = \sqrt{\rho_1(\mathbf{r})} \frac{1}{\hbar\omega_m} H_1\psi_m(\mathbf{r}) \equiv \sqrt{\rho_1(\mathbf{r})}\phi_m(\mathbf{r}). \tag{2.16}$$

Using the fluctuation-dissipation theorem, we obtain from Eqs. (2.15) and (2.16) the spectral representation of the static structure function $S(\mathbf{r}, \mathbf{r}')$:

$$S(\mathbf{r}, \mathbf{r}') = -\frac{1}{\pi} \int d\hbar\omega \chi(\mathbf{r}, \mathbf{r}'; \omega) = \sum_m \phi_m(\mathbf{r})\phi_m(\mathbf{r}'). \tag{2.17}$$

For our model of the substrate the symmetry in the plane parallel to the substrate is not broken and consequently the eigenstates may be factored into z (perpendicular distance from the substrate) and parallel position vector $\mathbf{r}_{||}$ parts:

$$\psi_m(\mathbf{r}) \equiv \psi_n(q_{||}, z)e^{i\mathbf{q}_{||}\cdot\mathbf{r}_{||}}. \tag{2.18}$$

When it is clear to do so, we will use m to refer collectively to the discrete quantum number n and the parallel momentum $\mathbf{q}_{||}$. The eigenstates are normalized by the condition

$$\langle\psi_n(\mathbf{r})|H_1|\psi_m(\mathbf{r})\rangle = \hbar\omega_m\delta_{n,m}. \tag{2.19}$$

Finally, from the spectral representation (2.17) of $S(\mathbf{r},\mathbf{r}')$ and the normalization (2.19), an equivalent definition of the excitation functions is through the eigenvalue problem

$$H_1\psi_m(\mathbf{r}) = \hbar\omega_m \int d^3r' S(\mathbf{r},\mathbf{r}')\psi_m(\mathbf{r}') \tag{2.20}$$

which becomes, in the homogeneous limit,

$$\hbar\omega_k = \frac{\hbar^2k^2}{2mS(k)}. \tag{2.21}$$

In Eq. (2.21) $S(k)$ is the momentum space structure function in the homogeneous system. It is now clear that the eigenvalues of the two-body equation (2.13) are Feynman excitation energies generalized to the inhomogeneous system.

The self-consistent solutions to these equations enable us to study the ground-state structure and energetics of the film. This has been done in considerable detail in Ref. [5]. Here, we focus on the zero-temperature phase diagram and for this purpose it is most relevant to consider the sound velocity as a function of the coverage. By sound we specifically refer to the long-wavelength, lowest energy mode (*i.e.*, $n = 1, q_{||} \to 0$). Generically, the sound velocity in a liquid film will be driven in large part by the substrate as in third sound or, for thick films, by the surface tension. In the initial case the dispersion is linear in $q_{||}$ and in the latter case the excitations have a $q_{||}^{3/2}$ dispersion and are referred to as ripplons. In this work, we will restrict ourselves to thin films, i.e., the third-sound c_3 limit. Two points of substantial importance need to be stated [8, 9]:

(a) The lowest energy, long wavelength mode does not always propagate at the surface of the film: For a low density monolayer, sound is a longitudinal phonon propagating down the length of the monolayer. Above a cross-over coverage, as discussed below, the nature of the excitation changes — it now has a component of it's motion that is out of the plane of the layer and has substantial strength at the surface.

(b) When the film is in the clustering phase it will not support sound until the clusters percolate.

It is the latter point that implies that a map of the coverage dependence of the third sound provides a convenient representation of the phase diagram.

The sound velocity can be theoretically determined several ways. The first is to calculate the chemical potential determined from the Hartree equation, and then differentiate it with respect to the coverage:

$$mc_3^2 = n\frac{d\mu}{dn} = \frac{1}{n\kappa_T}, \tag{2.22}$$

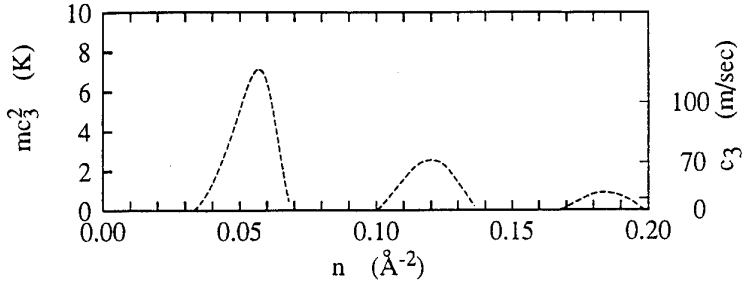

Figure 1. The surface coverage dependence for the sound velocity. The regions of no sound propagation correspond to the outer most layer being in a coexistence phase.

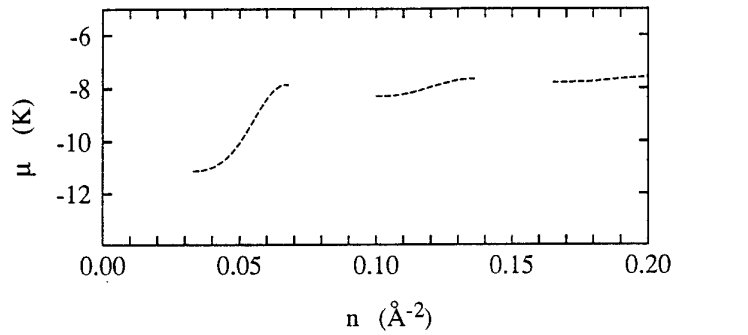

Figure 2. The surface coverage dependence of the chemical potential. The solutionless coverages correspond to the first-order phase transitions.

where κ_T is the isothermal compressibility. Alternatively, a more microscopic approach is to calculate c_3 from the long wavelength limit of the excitation energies, *i. e.* from the eigenvalues of Eq. (2.13) in the limit $q_{||} \to \infty$.

$$mc_3^2 = \frac{\hbar^2}{2m} \frac{n}{\left(\sqrt{\rho}\left|\left[H_1(0) + 2\hat{V}_{p-h}(0)\right]^{-1}\right|\sqrt{\rho}\right)}. \tag{2.23}$$

These two approaches lead to the same answer only in an exact theory, otherwise they provide a convenient consistency check for the theory. Finally, in the next section it will be useful to discuss the local compressibility $\kappa(z)$ defined as:

$$\frac{1}{mc^2} = n \int dz \kappa(z). \tag{2.24}$$

This quantity tells us about the z dependence of the stability of the film.

In Figs. 1 and 2 the sound velocity and chemical potential is plotted as a function of the coverage. Three regions of cluster/vacuum coexistence are shown in these figures corresponding to coverages (i) $n \leq 0.033\text{Å}^{-2}$ (ii) $0.068\text{Å}^{-2} \leq n \leq 0.100\text{Å}^{-2}$ and (iii) $0.138\text{Å}^{-2} \leq n \leq 0.170\text{Å}^{-2}$.

A pictorial representation of the growth scenario, as determined by the EL theory is displayed in Fig. 3. The coverages can be grouped as follows.

(a) For $n \leq 0.033\text{Å}^{-2}$, the film consists of 2-d clusters existing on top of the substrate (graphite plus two frozen helium layers).

(b) For $0.033\text{Å}^{-2} \leq n \leq 0.045\text{Å}^{-2}$ the layer uniformly covers the substrate and is described well as a low density 2-d liquid layer.

(c) For $0.045\text{Å}^{-2} \leq n \leq 0.055\text{Å}^{-2}$ the film is increasingly compressed, its stability is rapidly increasing as is indicated by the increasing sound velocity.

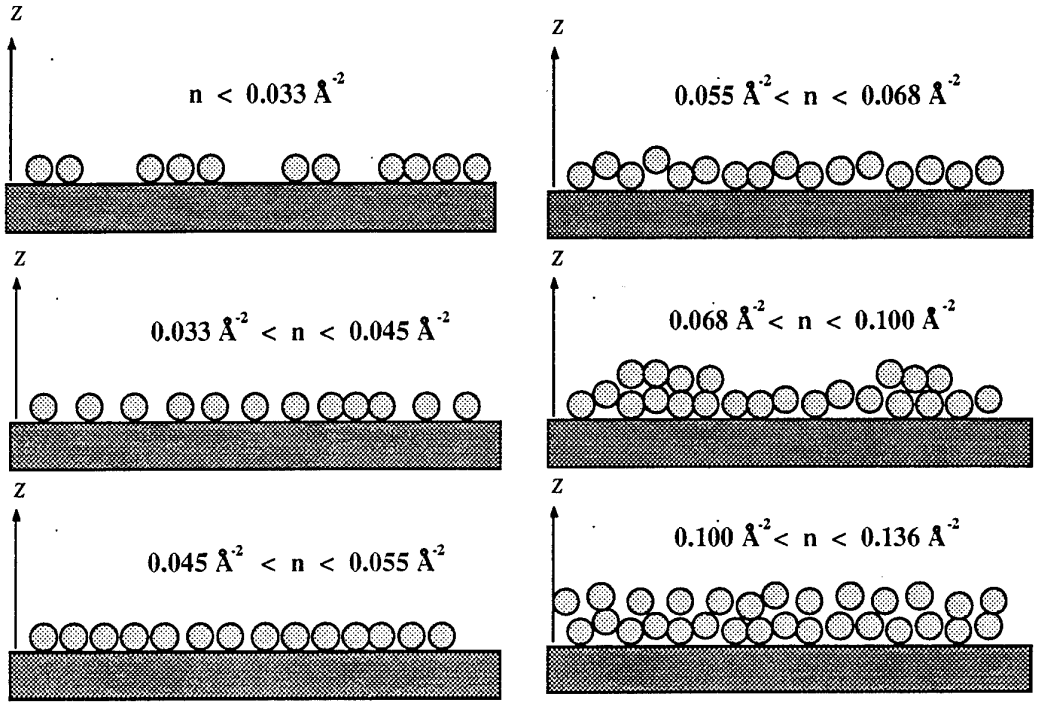

Figure 3. Growth of the liquid film for the first two liquid layers.

(d) For $0.055\text{Å}^{-2} \leq n \leq 0.068\text{Å}^{-2}$ a dramatic change in physics takes place. At $n = 0.055\text{Å}^{-2}$ there is a dimensional cross-over where the film now starts to occupy the third dimension. A shoulder forms in the profile and this largely determines the stability of the film. As n approaches 0.068Å^{-2} the shoulder becomes progressively softer.

(e) For $0.068\text{Å}^{-2} \leq n \leq 0.100\text{Å}^{-2}$ the second layer begins to grow, but its growth is by the formation and growth of clusters, on top of the previously formed first layer. Above 0.100Å^{-2} the helium once again uniformly covers the surface. Meanwhile the local density of the first layer continues to increase. This process is repeated for still another layer.

There is new, further evidence for the proposed growth scenario. First, since the superfluidity in the system will be appreciably altered by the layering transitions, we have proposed [10] that layering transitions provide a natural explanation to the staircase behavior observed in the superfluidity measured in recent torsional oscillator experiments of liquid ^{4}He adsorbed to a graphite substrate [11]. Second, PIMC studies done at 0.5 K and on a corrugated solid hydrogen substrate, find at least two layering transitions [12].

3. FINITE-TEMPERATURE THEORY

Our goal in this section is to present an overview of the finite-temperature variational theory. The fundamental theory is equivalent to the one first used by Gernoth

and coworkers [13] and reviewed in his contribution to this workshop. The theory is a straight-forward extension of the bulk finite-temperature theory first developed by Campbell *et al* [14]. Consequently, we take the liberty of only summarize the main points of the theory.

The starting point for the theory is the minimum principle for the free energy

$$F \leq F_t = tr(\hat{H}\hat{\Re}_t) + \frac{1}{\beta} tr(\hat{\Re}_t \ln \hat{\Re}_t), \tag{3.1}$$

where the first and second terms are the internal energy and the entropy, respectively. Here, $\hat{\Re}_t$ is the trial statistical operator. As in the ground-state calculation, we work in the real space representation for which

$$\langle \mathbf{r}_1^\alpha, \cdots, \mathbf{r}_N^\alpha | \hat{\Re} | \mathbf{r}_1^\beta, \cdots, \mathbf{r}_N^\beta \rangle = \Re(\mathbf{r}_1^\alpha, \cdots, \mathbf{r}_N^\alpha, \mathbf{r}_1^\beta, \cdots, \mathbf{r}_N^\beta), \tag{3.2}$$

where the density matrix is given by

$$\Re_t = \frac{1}{Z_t} \Psi(\mathbf{r}_1^\alpha, \cdots, \mathbf{r}_N^\alpha) Q(\mathbf{r}_1^\alpha, \cdots, \mathbf{r}_N^\alpha; \mathbf{r}_1^\beta, \cdots, \mathbf{r}_N^\beta) \Psi(\mathbf{r}_1^\beta, \cdots, \mathbf{r}_N^\beta), \tag{3.3}$$

Z_t is the normalization integral,

$$\Psi = \exp \frac{1}{2} \left[\sum_i u_1(\mathbf{r}_i) + \sum_{i<j} u_2(\mathbf{r}_i, \mathbf{r}_j) + \sum_{i<j<k} u_3(\mathbf{r}_i, \mathbf{r}_j, \mathbf{r}_k) \right], \tag{3.4}$$

and the incoherence function, which is also of the Jastrow form, is given by

$$Q = \exp \frac{1}{2} \left[\sum_{i,j} \{ \omega_2(\mathbf{r}_i^\alpha, \mathbf{r}_j^\beta) - \frac{1}{2}\omega_2(\mathbf{r}_i^\alpha, \mathbf{r}_j^\alpha) - \frac{1}{2}\omega_2(\mathbf{r}_i^\beta, \mathbf{r}_j^\beta) \} \right]. \tag{3.5}$$

The pseudopotentials, u_1, u_2, u_3, and ω_2, are implicitly temperature dependent, and are determined by solving the self-consistent set of Euler equations for the F_t

$$\begin{aligned} \frac{\delta F_t}{\delta u_n} &= 0 \\ \frac{\delta F_t}{\delta \omega_2} &= 0. \end{aligned} \tag{3.6}$$

At this point two paths may be taken; we may return to Eq. (3.1) and Eq. (3.3) and use the replica and the Jackson-Feenberg identities [14] to calculate the the entropy and the internal energy, respectively. Alternatively, we may start immediately with the free energy of the bulk system and take the inhomogeneous limit. The second approach, which is possible only because we know, *a priori*, the results of the inhomogeneous zero-temperature theory, assumes that the approximations used in the bulk finite-temperature theory are adequate for the inhomogeneous theory. The first

path is the one taken by Gernoth *et al* in this Proceedings, we choose the later. The free energy is

$$\begin{aligned} F_t = & \int d^3r \left[\frac{\hbar^2}{2m} \left| \nabla \sqrt{\rho_1(\mathbf{r})} \right|^2 + \rho_1(\mathbf{r}) U_{sub}(\mathbf{r}) \right] \\ & + E_c \left[g(\mathbf{r}, \mathbf{r}'), \rho_1(\mathbf{r}) \right] + \frac{1}{N} \sum_{\mathbf{q}_\parallel, m} \hbar \omega_m^*(\mathbf{q}_\parallel) n_m(\mathbf{q}_\parallel) \left[n_m(\mathbf{q}_\parallel) + 1 \right] \cdot \\ & - T\mathcal{S}_t - \mu N \end{aligned} \tag{3.7}$$

The additional contribution to the internal energy (the fourth term in Eq. (3.7)) is Eq. (5.1) in the bulk studies of Ref. [15]. The trial entropy $\mathcal{S}_t$ is given the form:

$$\mathcal{S}_t = k_B \sum_{\mathbf{q}_\parallel, m} \left[(n_m(\mathbf{q}_\parallel) + 1) \ln(n_m(\mathbf{q}_\parallel) + 1) - n_m(\mathbf{q}_\parallel) \ln \ n_m(\mathbf{q}_\parallel) \right], \tag{3.8}$$

where $n_m(\mathbf{q}_\parallel)$ are the usual bose (quasiparticle) occupation numbers for the state $(m, q_\parallel)$, and serve as a means of introducing a temperature dependent excitation spectrum

$$n_m(\mathbf{q}_\parallel) = \frac{1}{e^{\beta \omega_m(\mathbf{q}_\parallel)} - 1}. \tag{3.9}$$

The pair distribution function is defined in terms of the density matrix as:

$$g(\mathbf{r}_1, \mathbf{r}_2) = \frac{N(N-1)}{\rho_1(\mathbf{r}_1)\rho_1(\mathbf{r}_2)} \int d(\mathbf{r}_3, \cdots, \mathbf{r}_N) \hat{\Re}_t(\mathbf{r}_1, \cdots, \mathbf{r}_N; \mathbf{r}_1, \cdots, \mathbf{r}_N). \tag{3.10}$$

In Eq. (3.7) the ω^* are the eigenvalues of an auxiliary equation:

$$H_1 \psi_m^*(\mathbf{r}) = \hbar \omega_m^* \int d^3r' S(\mathbf{r}, \mathbf{r}') \psi_m^*(\mathbf{r}'), \tag{3.11}$$

which is recognized as being a T-dependent generalization of Eq. (2.20). Choosing $n_m(\mathbf{q}_\parallel)$ to be one of the independent Euler functions one immediately sees that

$$\omega_n^*(\mathbf{q}_\parallel) = \omega_n(\mathbf{q}_\parallel) \tanh(\beta \omega_n(\mathbf{q}_\parallel)/2), \tag{3.12}$$

which has an equivalent expression in the bulk calculation.

While the ground-state theory is at a much higher level of accuracy than the finite-temperature theory, the latter can be improved by including multiphonon effects. In the present formulation this means including higher-order correlations in the incoherence function. For example, by including $\omega_3(\mathbf{r}_i^\alpha, \mathbf{r}_j^\beta, \mathbf{r}_k^\nu)$, one finds in the *bulk system* that a series of correction terms to the Feynman energy are generated.

$$\begin{aligned} \omega^* = & \frac{\epsilon_o(k)}{S(k)} \\ & + \frac{1}{Z_t^2 N} \sum_{\mathbf{q}} \frac{|\langle \Psi | \rho_{\mathbf{q}} \rho_{\mathbf{k}-\mathbf{q}} \delta H \rho_{-\mathbf{k}} | \Psi \rangle|^2}{S(k) S(\mathbf{k}-\mathbf{q}) S(q) [\omega^*(k) - \omega_{BF}(q) - \omega_{BF}(\mathbf{k}-\mathbf{q})]} + \cdots \end{aligned} \tag{3.13}$$

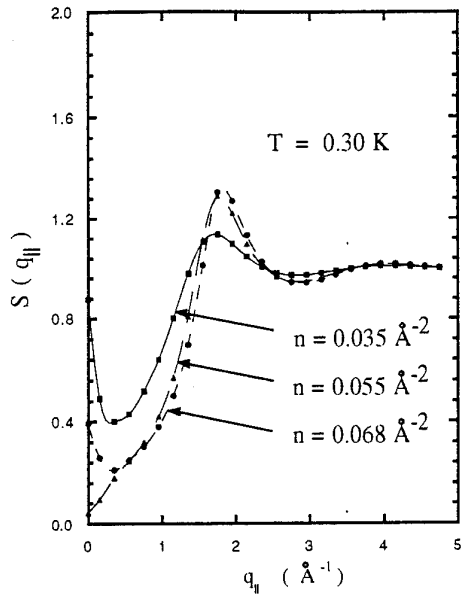

Figure 4. The z-integrated static structure function. In the long-wavelength limit $S(q_{\|})$ approaches $k_B T/mc_3^2$

Here, $\delta H \equiv H - E_o - \omega_{BF}(k)$ and $\omega_{BF}(k) \equiv \epsilon_o(k)/S(k)$. The higher order terms have a kernel which is a Bethe-Salpeter-like equation. In principle one can use the inhomogeneous generalization of this equation to improve the the accuracy of the theory (this has already been done for zero-temperature films [16]). At low temperatures these corrections are small since only those states with small k will be populated, but for small k the Feynman approximation is quite sufficient.

Working directly on Eq. (3.7) it is possible to construct the finite-temperature Euler equations for the film. We summarize the main results:

(a) The distribution functions $\rho_1(\mathbf{r})$ and $g(\mathbf{r}_1, \mathbf{r}_2)$ have implicit temperature dependence.

(b) $V_{PH}(\mathbf{r}_1, \mathbf{r}_2)$ and $V_H(z)$ that have terms with explicit T-dependence. So for example, the zero temperature Hartree equation is replaced by:

$$\left[-\frac{\hbar^2}{2m}\nabla_z^2 + U_{sub}(z) + V_H(z) + V_H^T(z)\right]\sqrt{\rho_1(z)} = \mu\sqrt{\rho_1(z)}. \tag{3.14}$$

(c) The stability of the film is strongly influenced by finite-temperature effects. The well known bulk system result that $\lim_{k\to 0} S(k) = 1/\beta mc_3^2$ is replaced by a similar expression for the z-integrated static structure function

$$\lim_{\mathbf{q}_{\|}\to 0}\int dz dz' S(z, z', \mathbf{q}_{\|}) = \frac{1}{\beta mc_3^2}. \tag{3.15}$$

In Fig. 4, the monolayer $S(\mathbf{q}_{\|})$ is shown for typical coverages.

(d) As the temperature approaches 1 K, a non-superfluid gas should be present and this has been neglected in our calculation. The gas may have non-negligible consequences — it is know experimentally that by 1 K there is a measurable gas pressure and this pressure will undoubtedly influence the film.

(e) The eigenvalue equation (Eq. (2.13)) remains unchanged in form but a more appropriate normalization condition for the states is

$$\langle\psi_n^*(\mathbf{r})|H_1|\psi_m^*(\mathbf{r})\rangle = \hbar\omega_m^*\delta_{n,m}. \tag{3.16}$$

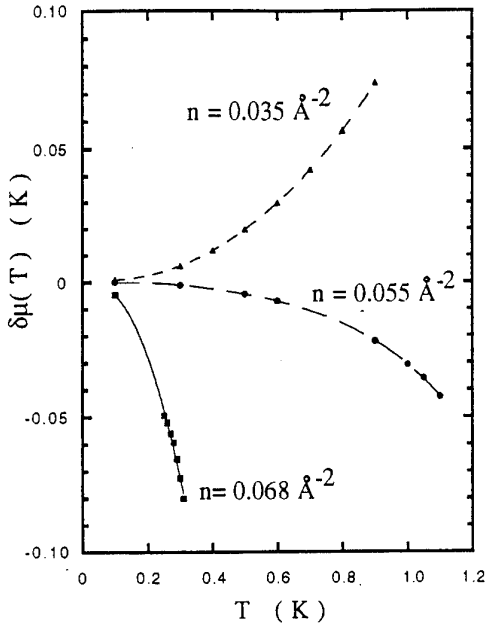

Figure 5. The shift in the chemical potential for the monolayer. Depending on the surface contribution $\delta\mu(T)$ can be either positive or negative. A positive $\delta\mu(T)$ indicates the film's rigidity is increasing as the temperature increases while the negative $\delta\mu(T)$ indicates the surface term contributes.

The full finite-temperature expressions do not lend themselves to elucidating the underlying physics (nor are they very numerically tractable) and for that purpose it useful to use some trustworthy approximation scheme to simplify them. First, since we are always in the low temperature regime, only the $n = 1$ state is important for the thermodynamics of the film. The relevant quantity is the $n = 1$, long-wavelength, transition density. Up to a z-independent normalization factor, we will refer to this as the the ripplon wavefunction, $\psi_R(z)$. More explicitly, the eigenvalue equation (Eq. (2.13)), along with the known long-wavelength properties of the eigenstates [17], allows us to write

$$\frac{n}{2mc^2}\psi_R(z) = \left[H_1(0) + 2\hat{V}(0)\right]^{-1}\sqrt{\rho_1(z)},$$

where the zeros imply $q_{\|} \to 0$. Inspection of Eqs. (2.23) and (2.24) immediately allow one to deduce that $\psi_R(z)$ can be interpreted as being the local compressibility of the film (again, up to z-independent factors). Consequently a physically appealing picture emerges which links the surface excitations, the films stability and the thermodynamics. The link is apparent in the next discussion.

Expanding the finite-temperature theory in the low-temperature limit, it can be shown that the leading order correction $\delta\mu(T) = \mu(T) - \mu(0)$, to the chemical potential is

$$\delta\mu(T) = \frac{1}{2}\int \frac{d^2q}{(2\pi)^2 n} n(q)\hbar\omega(q)\left[1 - \frac{t_q}{\hbar^2\omega^2(q)}E_\perp\right], \tag{3.17}$$

where $E_\perp$ is roughly the energy that can be associated with motion out of the symmetry plane:

$$E_\perp = \frac{3\hbar^2 n^2}{2m}\int dz\sqrt{\rho_1(z)}\psi_R(z)\left|\frac{d}{dz}\frac{\psi_R(z)}{\sqrt{\rho_1(z)}}\right|^2,$$

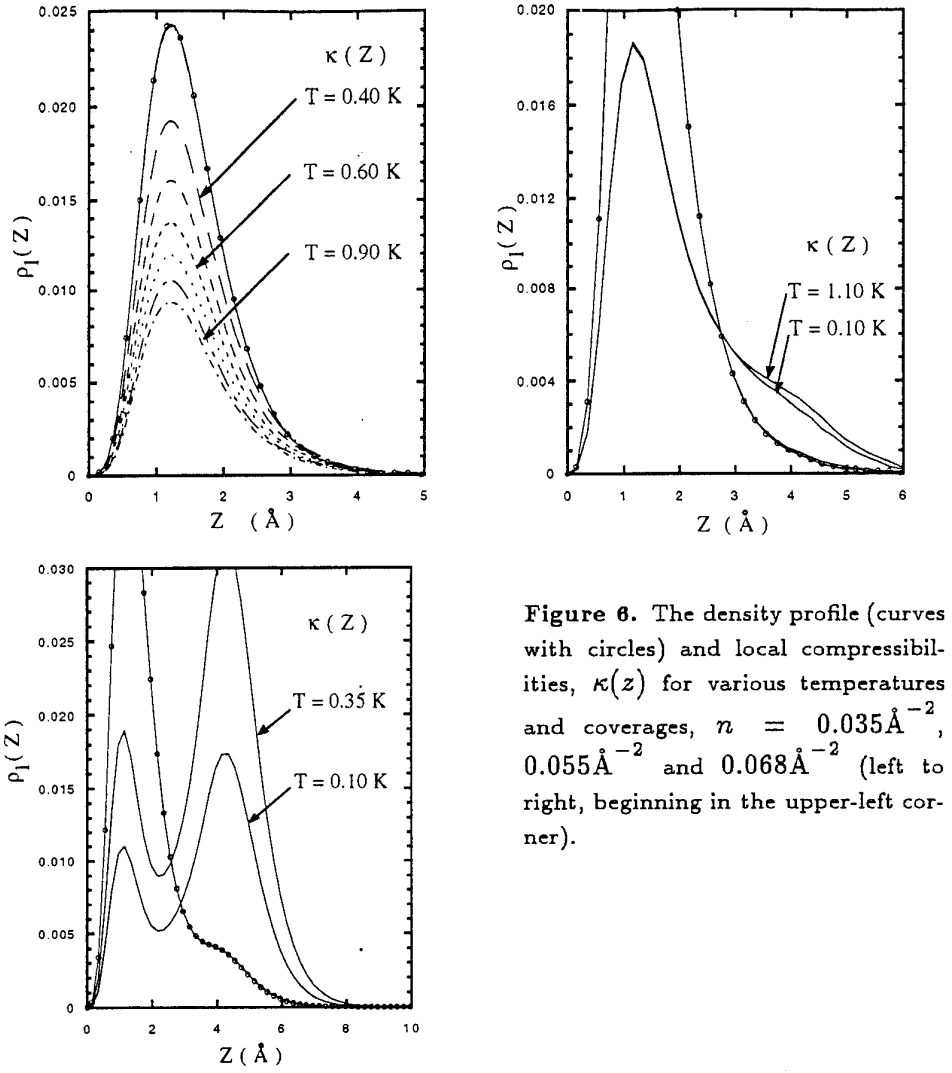

Figure 6. The density profile (curves with circles) and local compressibilities, $\kappa(z)$ for various temperatures and coverages, $n = 0.035\text{Å}^{-2}$, 0.055Å^{-2} and 0.068Å^{-2} (left to right, beginning in the upper-left corner).

and

$$t_q = \frac{\hbar^2 q^2}{2m}.$$

If the excitations of the film are essentially two-dimensional phonons, the excitation function is $\psi_R(r) \sim \sqrt{\rho_1(z)}$ and $E_\perp$ is small. In that case, the thermodynamics of the layered structure will be essentially the same as the one of a two-dimensional system with the same speed of sound. However, when the film develops surface excitations, $E_\perp$ can become quite large, and the dominance of the second term in Eq. (3.17) is further enhanced when the speed of sound becomes small. Consequently, there is a cross-over in the physics which occurs as one term dominates over the other. In Fig. 5, $\delta\mu(T)$ is plotted for three typical coverages. In Fig. 6, the density profile is plotted for the same set of coverages. Also shown are the local compressibilities, $\kappa(z)$ as a function of temperature. The $\kappa(z)$ are scaled to the figure size, *i.e.*, the vertical axis label is for the density profile only. One finds that the physics of the monolayer changes dramatically as a function of the coverage. For $n = 0.035\text{Å}^{-2}$,

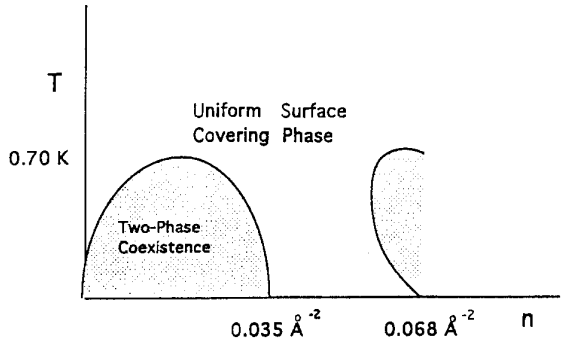

Figure 7. The *speculative* phase diagram for the monolayer. The coexistence regions consist of two-dimensional clusters coexisting with the surrounding vacuum. The boundary of the shaded region is the *spinodal* line.

the local compressibility decreases with the increasing temperature, *i.e.*, the film's rigidity increases. This is the mechanism that allows one cross above the coexistence region if the temperature is above the critical temperature. At $n = 0.055\text{Å}^{-2}$, the film is very stable already at zero temperature. By increasing the temperature the stability changes only slightly. Finally, at $n = 0.068\text{Å}^{-2}$, the local compressibility increases with temperature, *i.e.*, the shoulder in the profile softens even more. Slightly above $T = 0.35K$, the film actually pushes atoms out of the uniform layer, *i.e.*, the film moves into coexistence, already for this coverage. While the profile broadening is always small at these low temperatures, some thermal broadening is observed although it is not readily apparent in the scale in which the figures are plotted.

4. CONCLUSIONS

From a first-principles finite-temperature variational EL theory we have calculated the thermodynamic properties related to the structure of a monolayer of ^{4}He adsorbed on graphite/frozen helium substrate. Properties related to the film's stability are strongly dependent on the coverage of the monolayer. In particular there exists a well-defined two- to three-dimensional crossover coverage (for this substrate, $n_{co} = 0.055\text{Å}^{-2}$). Below n_{co} the temperature dependence of the system is essential one of a 2-dimensional film and above it, the surface excitations are strongly dominate. Although we not yet completed a calculation of the thermodynamic phase diagram, our findings discussed in the previous section indicate that the phase diagram for the monolayer will resemble the one *sketched* in Fig. 7. In particular the the low-coverage coexistence critical temperature will be essentially that of a purely two-dimensional substrate (which is known to have $T_c \approx 0.7K$). The asymmetric coexistence lobe for the second instability occurs because the stability of the film actually decreases with increasing temperature near 0.068Å^{-2}.

ACKNOWLEDGMENTS

This work was supported, in part, by the North Atlantic Treaty Organization under a grant CRG 940127, and the National Science Foundation under grants PHY-9108066 and INT-9014040 (to E. K.) and by the Finnish Academy (to M. S.). We thank P. Crowell, H. Godfrin, H. Lauter, P. Leiderer, P. Nozières, and C. J. Tymczak for many fruitful discussions. B. E. C. thanks the ILL for support. Computational

resources were provided by the Minnesota Supercomputer Institute and the CSC, Helsinki (Finland). Participation in this workshop has been made possible by support from the European and the U. S. Research Office of the U. S. Army.

REFERENCES

[1] P. Leiderer, J. Low Temp. Phys. **87**, 247 (1992).

[2] B. E. Clements, E. Krotscheck, and H. J. Lauter, Phys. Rev. Lett. **70**, 1287 (1993).

[3] Further discussion on the energetics of layer completion can be found in: C. E. Campbell, F. J. Milford, A. D. Novaco, and M. Schick, Phys. Rev. A **1648** (1972).

[4] E. Krotscheck, Q.-X. Qian, and W. Kohn, Phys. Rev. B **31**, 4245 (1985).

[5] B. E. Clements, J. L. Epstein, E. Krotscheck, and M. Saarela, Phys. Rev. B **48**, 7450 (1993).

[6] R. A. Aziz *et al.*, J. Chem. Phys. **70**, 4330 (1979).

[7] E. Krotscheck, Phys. Rev. B **31**, 4258 (1985).

[8] B. E. Clements, E. Krotscheck, H. J. Lauter, and M. Saarela, in *Condensed Matter Theories*, edited by J. W. Clark, A. Sadiq, and K. A. Shoaib (Nova Science Publishers, Commack, NY, 1994), Vol. 9.

[9] E. Krotscheck and C. J. Tymczak, Phys. Rev. B **45**, 217 (1992).

[10] B. E. Clements, H. Forbert, E. Krotscheck, and M. Saarela, J. Low Temp. Phys. **95**, (1994).

[11] P. A. Crowell and J. D. Reppy, Phys. Rev. Lett. **70**, 3291 (1993).

[12] M. Wagner and D. Ceperley, J. Low Temp. Phys. **94**, 185 (1994).

[13] K. A. Gernoth and M. L. Ristig, Phys. Rev. B **45**, 2969 (1991).

[14] C. E. Campbell, K. E. Kürten, M. L. Ristig, and G. Senger, Phys. Rev. B **30**, 3728 (1984).

[15] B. E. Clements, E. Krotscheck, J. A. Smith, and C. E. Campbell, Phys. Rev. B **47**, 5239 (1993).

[16] B. E. Clements *et al.*, Phys. Rev. B (1994), in press.

[17] B. E. Clements, E. Krotscheck, and M. Saarela, Z. Physik B **94**, 115 (1994).

CBF THEORY OF THE SPIN RESPONSES IN NUCLEAR MATTER

A.Fabrocini

Dept.of Physics, University of Pisa
and
INFN, Sezione di Pisa, I-56100 Pisa, Italy;

ABSTRACT. We use Correlated Basis Function theory to compute the longitudinal and transverse dynamical spin responses in nuclear matter, in both the isoscalar and isovector channels. The correlation operator includes spin, isospin and tensor components. Tensor correlations are shown to be responsible for differentiating the longitudinal and transverse responses. Their ratio is compared with the experimental values, as extracted from polarization transfer experiments on medium–heavy nuclei, and found to be in better agreement than previous RPA estimates. Finally, the effect of the one–body spin currents on the transverse electromagnetic response is evaluated. The experimental responses are underestimated by about 30%, in agreement with similar calculations in light nuclei.

1. INTRODUCTION

The description of the response of nuclear systems to external probes has been (and still it is) the goal of large parte of nuclear physics. In this field, Nuclear Matter (NM) plays a particular role because of the advantages coming from being an uniform, infinite system. The unfortunate drawback is that NM does not exist in nature. However, useful information can be gathered by looking at the interior of the nuclei or to the volume term of the mass formulae. Recently, a mass formula has been succesfully used to extract the NM inclusive response to relativistic electrons [1] by inspection of a consistent set of data from several nuclei. These *empirical* NM data may then serve as a test for the predictions of modern, sophisticated many–body theories, as Random Phase Approximation (RPA), Brueckner theory and so on.

Electron scattering has been, by far, one of the most studied phenomena because of the large body of available experiments. However, the nuclear response to exernal spin–isospin fields has actracted the attention of many researchers, after the RPA based prediction of Alberico *et al.* [2] that, at momentum transfer $q \sim 1.75 fm^{-1}$, the response in the isovector spin–longitudinal channel is enhanced and softened, because of the one–pion exchange (OPE) attraction, whereas it is quenched and hardened in the transverse one,

due to short range nucleon–nucleon (NN) correlations.

The ratio of the longitudinal and transverse spin responses has been extracted from measurements of polarization transfer observables for $(\vec{p},\vec{p}')$ and $(\vec{p},\vec{n})$ quasielastic scattering in several nuclei, at $q \sim 1 - 2fm^{-1}$. At these momentum values, both RPA and Distorted Wave Impulse Approximation (DWIA) [3] have predicted an enhancement of the ratio respect to unity. However, no experimental evidence for such an enhancement has been found. A relativistic RPA to the Walecka model [4] in NM, at appropriate density values, does not show appreciable deviations from unity at $\omega \geq 50MeV$, but still overestimates the experimental data at lower energies.

In this contribution, we will discuss how to calculate the dynamical spin responses in NM in the framework of the Correlated Basis Function (CBF) theory. CBF theory has allowed for microscopic and realistic studies of many properties of strongly interacting systems. In particular, in CBF an accurate evaluation of the equation of state [5], based on the realistic hamiltonians, of both nuclear and neutron matter has been obtained. Within the same theory, dynamical NM quantities, as the electromagnetic responses and the one-body Green's functions [6,7] have been evaluated in the past.

In CBF theory, an A–body normalized correlated wave function is given by

$$|n\rangle = \frac{F(1,2,..A)|n\rangle_{FG}}{{}_{FG}\langle n|F^{\dagger}F|n\rangle_{FG}^{1/2}}, \tag{1.1}$$

where $|n\rangle_{FG}$ is a Fermi Gas state and $F(1,2...A)$ is an A-body correlation operator acting on $|n\rangle_{FG}$. A realistic choice of the correlation operator, motivated by the operatorial dependence of the NN interaction, is:

$$F(1,2,..A) = \mathcal{S}[\prod_{i<j} f(i,j)], \tag{1.2}$$

i.e. a symmetrized product of state dependent correlation factors $f(i,j)$, given by

$$f(i,j) = \sum_{n=1,8} f^{(n)}(r_{ij})O^{(n)}(i,j), \tag{1.3}$$

and the operators $O^{(n)}(i,j)$ include central ($n = 1,4$),(1, $\vec{\sigma}_i \cdot \vec{\sigma}_j$, $\vec{\tau}_i \cdot \vec{\tau}_j$, $\vec{\sigma}_i \cdot \vec{\sigma}_j \vec{\tau}_i \cdot \vec{\tau}_j$), isoscalar and isovector tensor ($n = 5,6$) and spin-orbit ($n = 7,8$) components. The usual Jastrow factor is recovered if only the $n = 1$ component is retained. The functions $f^{(n)}(r)$ are variationally determined by minimizing the ground state expectation value of the hamiltonian, $\langle H \rangle$, generally by using the Fermi HyperNetted Chain/Single Operator Chain (FHNC/SOC) cluster summation method [8,9]. In this work, the realistic Urbana v_{14}+TNI model [10] of NN interaction has been used and the spin–orbit ($n = 7,8$) components of the correlation have not been considered.

2. THE RESPONSES

In NM, the isoscalar and isovector dynamical spin responses (ISSR and IVSR, respectively) $S^{\tau=0,1}_{x=L,T}(\mathbf{q},\omega)$, are given by:

$$S^{\tau}_{x}(\mathbf{q},\omega) = \frac{1}{A}\sum_{n} |\langle 0|\rho^{\tau}_{x}(\mathbf{q})|n\rangle|^2 \delta(\omega-\omega_n), \tag{2.1}$$

where the sum goes over the intermediate excited states $|n\rangle$, with excitation energy ω_n. The responses are driven by the fluctuation operators:

$$\rho^{\tau=0}_{L}(\mathbf{q}) = \sum_{i=1,A} (\sigma_i \cdot \hat{\mathbf{q}}) e^{i\mathbf{q}\cdot\mathbf{r}_i}, \tag{2.2}$$

$$\rho^{\tau=0}_{T,\alpha}(\mathbf{q}) = \frac{1}{\sqrt{2}}\sum_{i=1,A} (\sigma_i \times \hat{\mathbf{q}})_\alpha e^{i\mathbf{q}\cdot\mathbf{r}_i}, \tag{2.3}$$

and

$$\rho^{\tau=1}_{L}(\mathbf{q}) = \sum_{i=1,A} (\sigma_i \cdot \hat{\mathbf{q}}) e^{i\mathbf{q}\cdot\mathbf{r}_i} \tau_{z,i}, \tag{2.4}$$

$$\rho^{\tau=1}_{T,\alpha}(\mathbf{q}) = \frac{1}{\sqrt{2}}\sum_{i=1,A} (\sigma_i \times \hat{\mathbf{q}})_\alpha e^{i\mathbf{q}\cdot\mathbf{r}_i} \tau_{z,i}. \tag{2.5}$$

The non energy weighted sums of the responses give the spin static structure functions, $S^{\tau}_{x}(\mathbf{q})$:

$$S^{\tau}_{x}(\mathbf{q}) = \int_0^\infty S^{\tau}_{x}(\mathbf{q},\omega)\, d\omega, \tag{2.6}$$

which can also be computed as expectation values on the ground state:

$$S^{\tau}_{x}(\mathbf{q}) = \frac{1}{A}\frac{\langle 0|\rho^{\dagger\tau}_{x}(\mathbf{q})\rho^{\tau}_{x}(\mathbf{q})|0\rangle}{\langle 0|0\rangle}. \tag{2.7}$$

In CBF theory, the intermediate states appearing in eq.(2.1) belong to the correlated basis constructed with the Correlated States (CS) of eq.(1.1). These CS can be then perturbatively corrected within the same correlated basis. The responses evaluated at the first step of the above procedure will be denoted as *variational*, whereas we will talk of *perturbative corrections to the response* in the second case.

CS are, in general not orthogonal. They have been orthogonalized by following the two–step procedure described in ref.[11]. CS with m hole–n particle $(mh-np)$ excitations are first Schmidt orthogonalized to CS with a lower number of excitations; then they are Lowdin orthogonalized among themselves. These states are called Ortogonal Correlated States (OCS).

The first contribution to the variational responses comes from $(1h1p)$ OCS. These are the only states contributing in the Fermi Gas (FG) model, where the spin responses are given by the usual Lindhard function, showing no difference at all among the channels. The main effect of using $1h1p$ OCS instead of FG states is to quench the peak of the responses

and, if the correlation operator includes tensor components, to separate the longitudinal from the transverse case.

The explicit expression of the $1h1p$ response reads:

$$S^{\tau}_{x,ph}(\mathbf{q},\omega) = \frac{1}{A}\sum_{ph} |\xi^{\tau}_{x}(\mathbf{q},ph)|^2 \delta(\omega - \omega_{ph}), \tag{2.8}$$

with

$$\xi^{\tau}_{x}(\mathbf{q},ph) = \langle 0|\rho^{\tau}_{x}(\mathbf{q})|ph\rangle. \tag{2.9}$$

$2h2p$ and intermediate states with more excitations do not contribute to the FG responses, but they do contribute if a correlated basis is used. Their influence has not been evaluated in this work.

The leading perturbative corrections originate on account of $2h2p$ OCS admixtures in the variational ground and $1h1p$ states. They can be expressed in terms of the correlation and polarization parts of the microscopic self–energy:

$$\Sigma^{CO}(k<k_F, E>e_F) = \frac{1}{2}\sum \frac{\langle 0|H|\mathbf{k}\mathbf{h}_2\mathbf{p}_1\mathbf{p}_2\rangle|^2}{E+e(h_2)-e(p_1)-e(p_2)-\imath\eta}, \tag{2.10}$$

and

$$\Sigma^{PO}(k<k_F, E<e_F) = \frac{1}{2}\sum \frac{\langle \mathbf{k}\mathbf{p}|H|\mathbf{h}_1\mathbf{h}_2\mathbf{p}_1\mathbf{p}\rangle|^2}{E+e(p_1)-e(h_1)-e(h_2)-\imath\eta}. \tag{2.11}$$

k_F is the NM Fermi momentum ($k_F = 1.33 fm^{-1}$ in this paper), $e(x)$ are the single particle energies and e_F is the NM chemical potential. Similar expressions hold for the other momentum and energy regions. The self–energy has been evaluated in CBF, using the same Urbana potential and the effects on the NM longitudinal response and the one–body Green functions have been studied [6,7].

3. THE MATRIX ELEMENTS

This section will be devoted to a brief discussion of the matrix elements $\xi^{\tau}_{x}(\mathbf{q},ph)$ of eq.(2.9).

The correlated matrix element is expanded in Mayer–like cluster diagrams, containing statistical and dynamical correlations. The first ones are associated with exchange Fermi lines, whereas the other ones represent two–body correlations, either of the Jastrow type ($[f^{(1)}]^2 - 1$) or operatorial ($f^{(p>1)}$). The FHNC/SOC method allows for summing the leading, infinite classes of diagrams, when one is dealing with the expectation value of one– and two–body operators on the ground state, as in the case of the evaluation of the energy per particle, the momentum distribution and the static structure functions. The calculation of $\xi^{\tau}_{x}(\mathbf{q},ph)$ cannot be performed at the same level of accuracy. However, again

infinite classes of diagrams can be summed up and the convergence can be studied along the inclusion of higher and higher order terms. An extensive discussion of the calculation of ξ in the case of the charge fluctuaction operator is given in ref.[6]. Here, we will limit ourselves to outline the main features of the matrix elements for the spin responses.

If the correlation is switched off, then the matrix elements are simply given by δ–functions:

$$\xi^0_L(\mathbf{q}, ph) = \delta(\mathbf{q} - \mathbf{p} + \mathbf{h})\delta_{\sigma_z(h)\sigma_z(p)}, \tag{3.1}$$

$$\xi^0_{T,\alpha}(\mathbf{q}, ph) = \frac{1}{\sqrt{2}}\varepsilon_{\alpha\beta z}\delta(\mathbf{q} - \mathbf{p} + \mathbf{h})\delta_{\sigma_\beta(h)\sigma_\beta(p)}, \tag{3.2}$$

and the $\tau = 1$ cases are obtained by multiplying the above expressions by $\delta_{\tau(h)\tau(p)}$. Here we have assumed $\mathbf{q}$ lying along the z–axis.

After the introduction of Jastrow correlations, only exchange diagrams contribute. An infinite set of them can be simply summed by dividing the uncorrelated expressions by $D^{1/2}(h)D^{1/2}(p)$, where

$$D(x) = 1 - \frac{\rho}{4}\int d\mathbf{r}(g_{dd}(r) - 1)L(r)e^{i\mathbf{x}\cdot\mathbf{r}}. \tag{3.3}$$

ρ is the NM density, $g_{dd}(r)$ is the direct–direct radial distribution function and $L(r)$ is a generalized statistical correlation (see ref.[6] for more details).

It is clear from the above equations that the introduction of Jastrow correlations, even if strongly modifies the shape of the free FG responses, does not introduce any distinction between longitudinal and transverse channels. This behavior is still present even if spin and isospin correlations are introduced. It is only the presence of tensor correlations that allows for such a distinction.

This effect is clearly visible if we write down the explicit, not exchanged lowest order contribution, in the operatorial correlation:

$$\xi^0_{L,dir}(\mathbf{q}, ph) = \frac{\delta(\mathbf{q} - \mathbf{p} + \mathbf{h})}{D^{1/2}(h)D^{1/2}(p)}\delta_{\sigma_z(h)\sigma_z(p)}$$
$$\rho\int d\mathbf{r}e^{i\mathbf{q}\cdot\mathbf{r}}2[F^{(1)}(r) + F^{(2)}(r)(3cos^2(\hat{\mathbf{q}}\cdot\hat{\mathbf{r}}) - 1)], \tag{3.4}$$

and

$$\xi^0_{T,\alpha,dir}(\mathbf{q}, ph) = \frac{1}{\sqrt{2}}\varepsilon_{\alpha\beta z}\frac{\delta(\mathbf{q} - \mathbf{p} + \mathbf{h})}{D^{1/2}(h)D^{1/2}(p)}\delta_{\sigma_\beta(h)\sigma_\beta(p)}$$
$$\rho\int d\mathbf{r}e^{i\mathbf{q}\cdot\mathbf{r}}2[F^{(1)}(r) - \frac{1}{2}F^{(2)}(r)(3cos^2(\hat{\mathbf{q}}\cdot\hat{\mathbf{r}}) - 1)], \tag{3.5}$$

where $F^{(1)} = f^{(1)}f^{(2)} + f^{(2)}f^{(2)} - f^{(5)}f^{(5)}$, $F^{(2)} = f^{(1)}f^{(5)} - f^{(2)}f^{(5)} + f^{(5)}f^{(5)}$ and we recall that $f^{(5)}$ is the tensor correlation. In the above expressions, we have not included the isospin components.

It is clear, from eqs.(3.4-5), that if $F^{(2)} = 0$, and so the correlation does not have any tensor part, the L and T responses are identical. When $F^{(2)} \neq 0$, then the responses in the two channels are moved to opposite directions respect to the purely central case.

The ξ matrix elements, with operatorial components, have been computed following the analogous calculation of ref.[6] for the longitudinal electromagnetic response. Besides the two–body, lowest order diagrams, Single Operator Chain (SOC) and separable diagrams (up to linear terms in the vertex corrections) have been included.

4. THE SUM RULES

Let us briefly discuss the results obtained for the sum rules (2.6-7) with only $1h1p$ intermediate OCS. The fluctuaction operators (2.2-5) commute with F when Jastrow correlations are used. In this case, the sum rules are completely exhausted by the $1h1p$ OCS [11], in the sense that the ω–integrals of the $1h1p$ responses coincide with the estimates of $S^{\tau}_{z}(\mathbf{q})$, given by eq.(2.7), if the variational ground state is used. If operatorial correlations, containing spin, isospin and tensor components are introduced, then $[\rho^{\tau}_{z}, F] \neq 0$, and the sum rules are no longer exhausted by $1h1p$ states.

In table I we report the nuclear matter static structure functions for a few q–values, at the empirical saturation density $\rho_{NM} = 0.16\ fm^{-3}$. The isoscalar transverse and the isovector longitudinal sum rules appear to be enhanced by the inclusion of tensor correlations respect to the simple Jastrow estimates , while the isoscalar longitudinal and the isovector transverse ones are depleted. This is in agreement with recent results in light nuclei [12].

In the table, SR1 refers to the results for the static structure functions of eq.(2.6), whereas SR2 shows the g.s. expectaction values of eq.(2.7). The two SR1 lines give the sum rules before and after the Lowdin orthogonalization of the $1h1p$ CS. Finally, the last column gives the sum rules for the Jastrow model.

After orthogonalizing the states, the Jastrow wave function essentially satisfies the sum rule, as expected. This is no longer true for the full operatorial case, because of the mentioned non commutativity of the correlation with the fluctuaction operators. Another source for the differences in the sum rules could be the different cluster expansions employed in the two estimates. However, several checks on their convergence appear to rule out such an explanation.

Particularly badly violated are the sum rules in the isoscalar, $\tau = 0$, channels. This can be understood by explicitely looking into the cluster contributions. In fact, the most important corrections come from the OPEP induced correlations (spin-isospin and tensor–isospin). In the $\tau = 0$ channels, the leading two–body correction is quadratic in $f^{(4)}$ and $f^{(6)}$. It can be seen that the contribution from this term to SR1 is -3 times that to SR2. In the $\tau = 1$ channels, the leading term is linear in the OPEP correlations, and it gives the same contribution to both SR1 and SR2. These differences may point to possible inadequacies of the variational calculation of ground state expectation values for some operators.

	$q(fm^{-1})$	$S_L^{\tau=0}$	$S_T^{\tau=0}$	$S_L^{\tau=1}$	$S_T^{\tau=1}$	S_J
$SR1$	1.0	0.45	0.53	0.64	0.49	0.57
		0.43	0.52	0.60	0.51	0.55
$SR2$		0.59	0.64	0.61	0.53	0.54
$SR1$	1.5	0.65	0.79	1.03	0.67	0.82
		0.62	0.77	0.90	0.71	0.78
$SR2$		0.75	0.84	0.90	0.71	0.78
$SR1$	2.0	0.80	0.99	1.32	0.84	1.01
		0.78	0.97	1.11	0.87	0.95
$SR2$		0.87	0.99	1.09	0.86	0.95
$SR1$	2.5	0.89	1.08	1.38	0.98	1.10
		0.88	1.05	1.18	0.96	1.03
$SR2$		0.95	1.06	1.15	0.96	1.03
$SR1$	3.0	0.93	1.06	1.26	0.98	1.06
		0.91	1.04	1.12	0.96	1.04
$SR2$		0.96	1.04	1.10	0.96	1.04

Table 1. $1h1p$ static structure functions $S_\tau^\tau(\mathbf{q})$ of nuclear matter at saturation density for the Urbana potential.

5. THE RESULTS

This section will be devoted to the results obtained for the spin responses within the CBF theory. The results obtained at the two–body cluster level for the operatorial contributions have already been given in ref.[13]. Here, we will use the full SOC treatment for the matrix elements ξ.

The ISSR and IVSR, with only $1h1p$ intermediate OCS, without self–energy insertions, are shown in fig.(1) at $q = 2.0fm^{-1}$. In the figure, the FG and the Jastrow estimates are also given.

As already stated, tensor correlations have opposite effects in the L and T channels. In the isoscalar channels, the correlations quench the response respect to the FG, pushing strength to higher energies. The effect of the tensor correlations appears sizeable in the longitudinal response, further depleting it. In the isovector case, the situation is reversed: the tensor correlations enhance the longitudinal response and deplete the transverse one. The responses with central correlations, beside the simple Jastrow choice, and no tensor, are very close to the Jastrow ones. These results do not differ appreciably from those of ref.[13], giving confidence in the accuracy of the cluster expansion.

Self energy insertions on top of the hole or particle lines, due to admixtures with $2h1p$ or $2p1h$ CS, have been estimated by means of the optical model of ref.[11], that appears to be quite accurate for the momentum transfers we have considered [6]. The responses, with self energy insertions, are shown in fig.(2). The sum rules remain unchanged, as we

have adopted the optical model. So, the main effect consists in adding a large-ω tail, still preserving the total strengths.

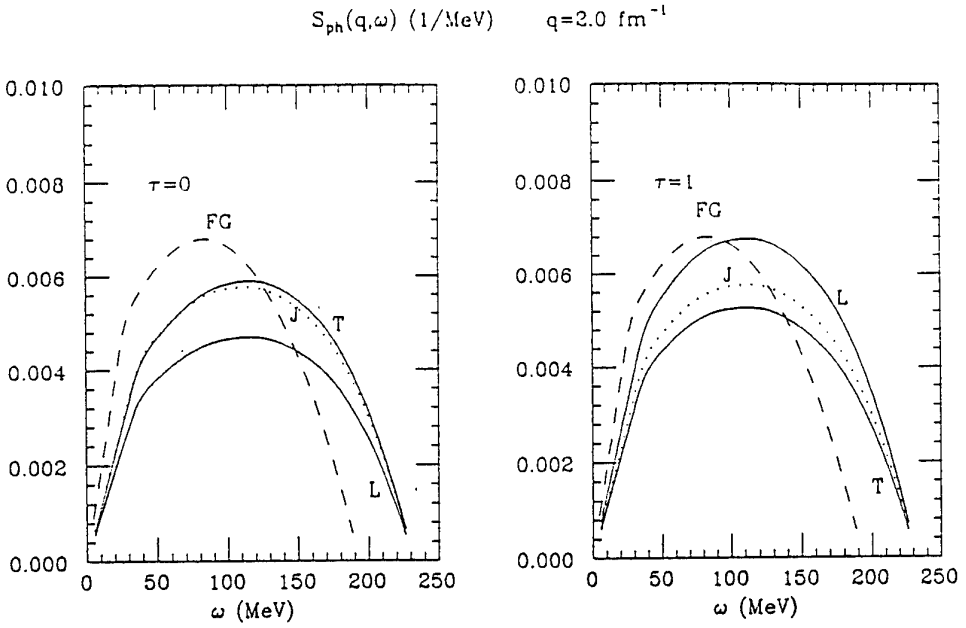

Fig.(1) $1h1p$ spin responses in NM.

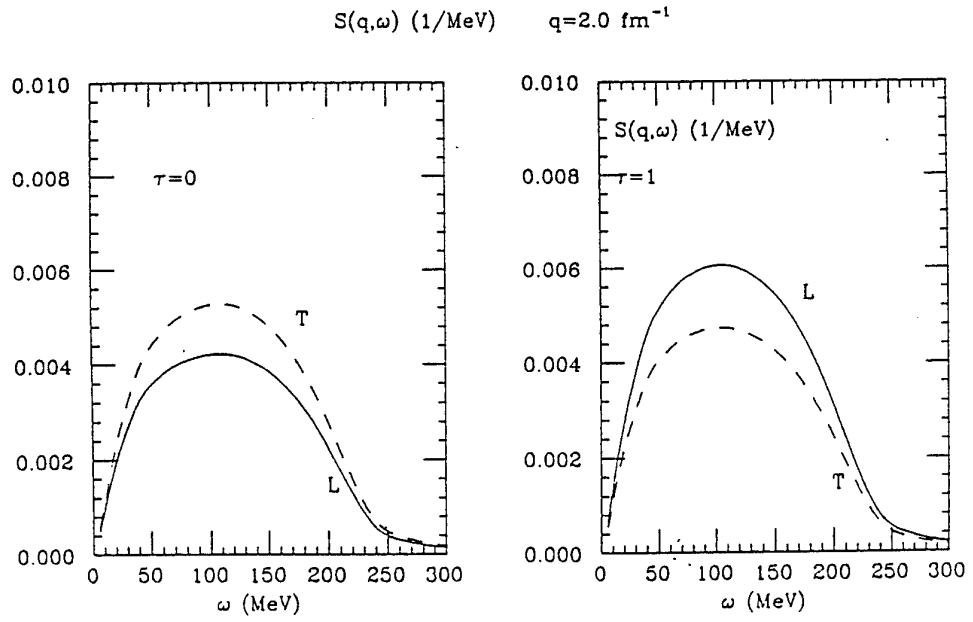

Fig.(2) Spin responses in NM in the optical model.

Finally, fig.(3) compares the CBF spin responses with some of the available experi-

mental data. The plotted quantity is the ratio $R(\mathrm{q},\omega)$, defined as:

$$R(\mathrm{q},\omega) = \frac{2.15}{4.62}\frac{3.62\ S_L^{\tau=1}(\mathrm{q},\omega) + S_L^{\tau=0}(\mathrm{q},\omega)}{1.15\ S_T^{\tau=1}(\mathrm{q},\omega) + S_T^{\tau=0}(\mathrm{q},\omega)}. \tag{5.1}$$

$R(\mathrm{q},\omega)$ has been computed at $q = 1.75\ fm^{-1}$, and it is compared with experimental data for ^{40}Ca from ref.[14], and for ^{208}Pb from refs.[15,16]. The volume RPA estimate of ref.[2] is also given. The CBF ratio appears to be much closer to the experiments than the RPA one. It must ne said that the RPA calculation includes explicit Δ–hole excitations, which increase the RPA value. This effect is absent in the CBF case and it would be really interesting to evaluate it within this approach. The inclusion of surface effects in the RPA ratio lowers it of only ~ 0.2. The CBF results do not show a sensible ω–dependence, in contrast with the relativistic RPA calculation of ref.[4]. $R(\mathrm{q},\omega)$ has been computed also at half of the nuclear matter density, $\rho = \rho_{NM}/2$, as in N–nucleus scattering one is mostly probing the nuclear surface. No meaningful density dependence has been found, and $R(\rho = \rho_{NM}/2)$ differs from $R(\rho_{NM})$ by only a few percent.

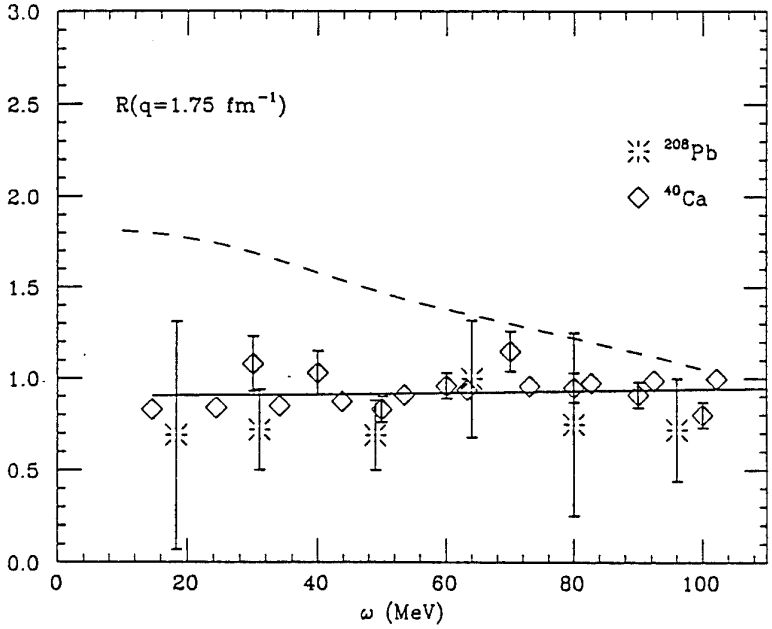

Fig.(3) Ratio of longitudinal and transverse spin responses in NM.

Hadron scattering is strongly distorted. This effect has been evaluated by Ichimura *et al.* [3], and shown to produce a further reduction of the ratio respect to the continuum RPA estimate. Again, a CBF evaluation of distortion would be welcome.

6. THE TRANSVERSE ELECTROMAGNETIC RESPONSE

The double differential cross section for inclusive electron scattering, in the laboratory system, is written as

$$\frac{d^2\sigma}{d\Omega d\epsilon\prime} = \sigma_M\{(\frac{Q^2}{q^2})^2 R_L(\mathbf{q},\omega) + [\frac{1}{2}|\frac{Q^2}{q^2}| + tan^2(\frac{\theta}{2})]R_T(\mathbf{q},\omega)\}, \tag{6.1}$$

where $\epsilon\prime$ and θ are the outgoing electron energy and scattering angle, $Q = (\omega, \mathbf{q})$ is the 4–momentum trasferred to the nucleus, σ_M is the Mott cross section and R_L and R_T are the longitudinal and transverse e.m. responses, respectively.

The longitudinal response, both in NM and finite nuclei, has been object of many investigations. In particular, CBF has shown to be able to reproduce its main feature, *i.e.* a large depletion of the quasielastic peak respect to any mean field prediction, in fairly good agreement with the experimental data in heavy nuclei [6].

The transverse response can be writen in terms of the transverse structure function $S_T(\mathbf{q},\omega)$:

$$R_T(\mathbf{q},\omega) = G^2(\mathbf{q},\omega)S_T(\mathbf{q},\omega), \tag{6.2}$$

$G(\mathbf{q},\omega)$ being the γNN form factor.

$$G(\mathbf{q},\omega) = (1 + \frac{q^2 - \omega^2}{1.81 fm^{-2}})^{-2}. \tag{6.3}$$

$S_T(\mathbf{q},\omega)$ is, in turn, given by:

$$S_T(\mathbf{q},\omega) = \frac{1}{A}\sum_n |\langle n|\hat{J}(\mathbf{q})|0\rangle|^2 \delta(\omega - \omega_n), \tag{6.4}$$

and $\hat{J}(\mathbf{q})$ is the electromagnetic current operator, which is a sum of several terms

$$\hat{J}(\mathbf{q}) = \hat{J}_{conv}(\mathbf{q}) + \hat{J}_{spin}(\mathbf{q}) + \hat{J}_{MEC}(\mathbf{q}). \tag{6.5}$$

The small convection term is usually neglected. Two–body contributions come on account of the Meson Exchange Current (MEC) part of the operator, describing the coupling of the virtual photons directly with the virtual mesons, or with the nucleon via the exchange of a virtual meson. There is a large body of literature about the MEC effects on the transverse response, but we want here to concentrate on the one–body spin term of the current operator, $\hat{J}_{spin}(\mathbf{q})$.

$\hat{J}_{spin}(\mathbf{q})$ is written as

$$\begin{aligned}\hat{J}_{spin}(\mathbf{q}) &= \frac{\imath\mu_0}{e}\sum_{i=1,A} e^{\imath\mathbf{q}\cdot\mathbf{r}_i}[\mu_p\frac{1+\tau_{z,i}}{2} + \mu_n\frac{1-\tau_{z,i}}{2}](\sigma_i \times \hat{\mathbf{q}}) = \\ &= \frac{\imath\mu_0}{e\sqrt{2}}[\mu_+\rho^{\tau=0}_{T,\alpha}(\mathbf{q}) + \mu_-\rho^{\tau=1}_{T,\alpha}(\mathbf{q})],\end{aligned} \tag{6.6}$$

where μ_0 is the Bohr magneton, $\mu_{p(n)}$ is the proton (neutron) magnetic moment (in terms of μ_0) and $\mu_{+(-)} = \mu_p + (-)\mu_n$.

If we use the above expression for the current operator, the transverse e.m. structure function can be expressed in terms of the transverse spin responses:

$$S_T(\mathbf{q},\omega) \simeq S_{T,spin}(\mathbf{q},\omega) = (\frac{\mu_0 q}{e\sqrt{2}})^2[\mu_+^2 S_T^{\tau=0}(\mathbf{q},\omega) + \mu_-^2 S_T^{\tau=1}(\mathbf{q},\omega)]. \qquad (6.6)$$

In fig.(4), the one–body spin NM e.m. transverse response is compared with data from ^{40}Ca, at $q = 330 MeV/c$ [17].

The NM response underestimates the full response by $\sim 30\%$, in agreement with other non relativistic many–body approaches. This result is confirmed also at other q–values in ^{40}Ca, and by a recent analysis of the world data in inclusive e–scattering from ^{56}Fe [18]. MEC are generally thought to be responsible for the missing contribution.

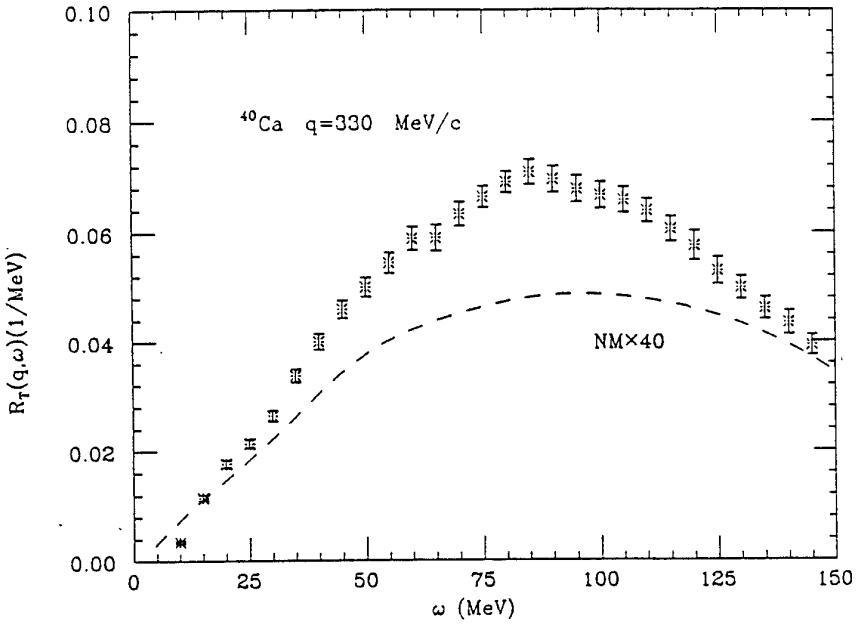

Fig.(4) NM e.m. spin transverse response and experimental data from ^{40}Ca.

7. THE CONCLUSIONS

CBF theory has been adopted to evaluate the spin responses in nuclear matter. It satisfactory describes the currently available experimental results for the ratio between the longitudinal and transverse responses in heavy nuclei. Experimental data for the separated responses will tell us, in the near future, whether the agreement is fortuitous or due to the ability of CBF to correctly describe the effects of the strong NN correlations in the nuclear systems, as it appears from the results obtained within this approach in other nuclear physics problems.

AKNOWLEDGMENTS

The author wants to thank Stefano Fantoni for many invaluable discussions and the European Research Office of the U.S.Army for the partial financial support.

REFERENCES

[1] D.Day *et al.*., Phys.Rev. **C40**(1989)1011; Phys.Lett. **B274**(1992)16.
[2] W.M.Alberico, M.Ericson and A.Molinari, Nucl.Phys. **A379**(1982)429.
[3] M.Ichimura, K.Kawahigashi, T.S.Jorgensen and C.Gaarde, Phys.Rev. **C39**(1989)1446.
[4] C.J.Horowitz and J.Piekarewicz, Phys.Lett. **B301**(1993)321.
[5] R.B.Wiringa, V.Ficks and A.Fabrocini, Phys.Rev. **C38**(1988)1010.
[6] A.Fabrocini and S.Fantoni, Nucl.Phys. **A503**(1989)375.
[7] O.Benhar, A.Fabrocini and S.Fantoni, Nucl.Phys. **A550**(1992)201.
[8] S.Rosati,*From Nuclei to Particles*, A.Molinari ed., Proceedings of the Int.School of Phys. E.Fermi, Varenna, page 73. North-Holland, New York, 1981.
[9] V.R.Pandharipande and R.B.Wiringa, Rev.Mod.Phys. **51**(1979)821.
[10] I.E.Lagaris and V.R.Pandharipande, Nucl.Phys. **A359**(1981)331; Nucl.Phys. **A359**(1981)349.
[11] S.Fantoni and V.R.Pandharipande, Nucl.Phys. **A427**(1984)473.
[12] J.C.Carlson *et al.*, Illinois preprint 1993.
[13] A.Fabrocini, Phys.Lett. **B322**(1994)171.
[14] J.B.McClelland *et al.*, Phys.Rev.Lett. **69**(1992)582.
[15] T.A.Cary *et al.*, Phys.Rev.Lett. **53**(1984)144.
[16] L.B.Rees *et al.*, Phys.Rev. **C34**(1986)627.
[17] Z.E.Meziani *et al.*, Phys.Rev.Lett. **54**(1985)1233.
[18] J.Jourdan, private communication.

CORRELATED DENSITY MATRIX THEORY OF SPATIALLY INHOMOGENEOUS BOSE FLUIDS

K. A. Gernoth

International Centre for Theoretical Physics
Strada Costiera 11, 34014 Trieste, Italy

J. W. Clark

McDonnell Center for the Space Sciences and Department of Physics
Washington University, St. Louis, MO 63130, U.S.A.

M. L. Ristig

Institut für Theoretische Physik
Universität zu Köln, 50937 Köln, Germany

1. INTRODUCTION

During the last decade the method of correlated basis functions has proven successful in microscopic prediction of the ground-state properties and elementary excitations of spatially inhomogeneous systems of liquid ^{4}He [1,2]. The bulk of the work has been done at the Hartree-Jastrow variational level, at which only one-body and two-body correlations are taken into account. At this level, the optimal correlations are to be determined from Euler-Lagrange equations derived by variation of the corresponding energy expectation value with respect to the one-body and two-body correlation functions. A more recent investigation [3] also includes three-body correlations in the trial ground state. In most of the published work, the elementary excitations have been treated within a Feynman description [4] of the wave functions of excited states. Invoking the generality of correlated basis functions (CBF) theory, systematic improvements on the microscopic treatment of excitations that transcend the Feynman picture have recently become available [5].

Nonuniform systems that have received attention within the variational-CBF scheme include liquid ^{4}He films [2,6-8] with or without an adsorbing substrate, ^{4}He clusters [9], and the surface of liquid ^{4}He in a half-space geometry [1,10-12]. The Euler-Lagrange equations, which must be solved numerically, yield the one-body

density describing the spatial inhomogeneity of the system under consideration, the anisotropic two-body distribution function, and, in the form of an eigenvalue equation, the wave functions and energies of elementary excitations. The solutions of the optimization problem also provide input for microscopic evaluation of macroscopically observable quantities, such as the surface tension or chemical potential. Some analytic results may be obtained for the long-range behavior of the two-body correlations and for the spatial shape and dispersion relation of low-lying excitations through expansions in the regime of small excitation energies [13-15].

In view of these past achievements, as well as ongoing theoretical advances, it is timely to attempt an extension of the correlated basis functions theory to spatially inhomogeneous Bose fluids at *nonzero* temperatures. The necessary framework for realizing this aim is furnished by the correlated density matrix theory that has been developed for and quantitatively applied to spatially uniform Bose fluids in Refs. 16 and 17. Here, we will adapt this approach to spatially inhomogeneous systems. In fact, such an extension of inhomogeneous variational theory has already been put to use in recent extensive studies of the ^{4}He vapor-liquid interface [18-20]. The theory itself is elaborated for the first time in this contribution. Rather than focusing on numerical implementation of the generalized Feynman eigenvalue equation and the physical nature of its solutions, we shall present an explicit derivation of the Euler-Lagrange equations for the one-body density and two-body correlations and report further details of the entire variational approach. Currently, the temperature dependence of a variety of quantities and phenomena, such as surface broadening with temperature in ^{4}He films, is being explored within the theory discussed here [21].

We begin our account with a sketch of the basic concepts of the variational correlated density matrix theory of spatially inhomogeneous Bose fluids.

At a given temperature T, the true canonical density operator ρ_{true} of a system of N bosons characterized by a Hamiltonian H is given by $\rho_{\mathrm{true}} = \exp(\beta H)$. The dimensionless inverse temperature β is defined as $\beta = (k_{\mathrm{B}}T)^{-1}$, where k_{B} is the Boltzmann constant. Correlated density matrix theory rests on the Gibbs-Delbrück-Moliere minimum principle [22], which states that in thermodynamic equilibrium the Helmholtz free energy

$$F = E - \beta^{-1}S \tag{1}$$

assumes its minimum value for the true density matrix ρ_{true}. The first term on the right side of Eq. (1) represents the internal energy, while the second is the entropy contribution to the total free energy. It follows that the free energy corresponding to a density operator ρ that departs from the true one provides a rigorous upper bound on the true Helmholtz free energy. This variational property of the free energy functional $F[\rho]$ may be exploited to find the optimal density matrix within a restricted class of trial density matrices.

The first task is then to pose a suitable trial form for the statistical operator ρ, such that the essential dynamical and thermal physics is incorporated, yet the resulting free energy functional remains tractable. Variation of this functional with respect to the freedom present in the *ansatz* for ρ leads to Euler-Lagrange equations determining the optimal ρ of the chosen class. This optimal ρ may be used to estimate an upper bound for the true free energy and to calculate approximations to other thermodynamic quantities of interest as functions of temperature T, such as the

surface tension of liquid ^{4}He [20].

In constructing a trial form for ρ adapted to spatially inhomogeneous Bose systems we follow the lead of the correlated density matrix treatment of uniform Bose systems [16,17]. Accordingly, we employ a trial density operator that contains one-body factors describing the spatial inhomogeneity of the system and two-body factors describing the strong interparticle correlations. The chosen trial operator takes into account the presence of thermal excitations in Feynman approximation. The resulting Euler-Lagrange equations may be cast in the form of a Feynman eigenvalue equation for the spatial shape and energy of the thermal excitations [18-20], a Hartree equation for the square root of the one-body density, and a Schrödinger-like equation for the square root of the two-body distribution function. Self-consistently determined effective one-body and two-body potentials appear as essential ingredients in the coupled set of Euler-Lagrange equations. These optimization equations systematically generalize the corresponding $T = 0$ theory [1,2] of nonuniform Bose liquids to finite temperatures.

In Sec. 2 we introduce the trial form for the statistical operator and calculate the Helmholtz free energy associated with this *ansatz*. The optimization equations for the elementary excitations, for the one-body density, and for the two-body correlations are presented in Sec. 3. Our findings are summarized in Sec. 4, where we also consider avenues for future research in the field of nonuniform Bose fluids at finite temperatures.

2. DENSITY MATRIX AND FREE ENERGY

The program sketched in the preceding section is most conveniently carried through by adopting a coordinate space representation for all operators involved. As argued in Ref. 16, the coordinate space matrix elements $\rho(\mathbf{R}', \mathbf{R}) = \langle \mathbf{R}'|\rho|\mathbf{R}\rangle$ of a density operator ρ takes the general form

$$\rho(\mathbf{R}', \mathbf{R}) = \Psi(\mathbf{R}')\, Q(\mathbf{R}', \mathbf{R})\, \Psi(\mathbf{R})\,. \tag{2}$$

Here, the notation $\mathbf{R} = (\mathbf{r}_1, \mathbf{r}_2, \cdots, \mathbf{r}_N)$ is used to denote the $3N$ spatial coordinates of the system of N bosons. Likewise, we have $\mathbf{R}' = (\mathbf{r}'_1, \mathbf{r}'_2, \cdots, \mathbf{r}'_N)$. For the form (2) to represent a statistical operator of a Bose system, the function Ψ and the incoherence factor Q have to be positive definite. The latter quantity does not contain any factors that depend on only primed or unprimed coordinates alone. At vanishing temperature, the incoherence factor Q becomes unity and the matrix elements $\rho(\mathbf{R}', \mathbf{R}) = \Psi(\mathbf{R}')\Psi(\mathbf{R})$ describe the density operator associated with the state Ψ, which at $T = 0$ is the ground-state wave function. In general, the factors Ψ and Q in Eq. (2) depend on temperature. To simplify the notation, the argument T will be suppressed in writing these and any other quantities that do not carry an explicit dependence on temperature.

Without loss of generality, the function Ψ in Eq. (2) may be expressed as a product of one-body, two-body, ..., N-body factors, i.e., it has the form of a Feenberg wave function [23]. Truncating the general form at the two-body level, we arrive at

the Hartree-Jastrow *ansatz*

$$\Psi(\mathbf{R}) = \frac{1}{Z} \exp\left(\tfrac{1}{2} \sum_{i=1}^{N} t(\mathbf{r}_i) + \tfrac{1}{2} \sum_{i<j=1}^{N} u(\mathbf{r}_i, \mathbf{r}_j) \right). \tag{3}$$

The normalization integral

$$Z = \int \Psi^2(\mathbf{R})\, Q(\mathbf{R}, \mathbf{R})\, d\mathbf{R} = \int \Psi^2(\mathbf{R})\, d\mathbf{R} \tag{4}$$

ensures the unit-norm condition $\mathrm{Tr}(\rho) = 1$. For the reasons given below, we may assume the diagonal matrix elements $Q(\mathbf{R}, \mathbf{R})$ of the incoherence factor Q to be unity, justifying the simplification made in Eq. (4). The convention $Q(\mathbf{R}, \mathbf{R}) = 1$ will facilitate the succeeding calculations significantly.

Adopting the two-body level also for the incoherence factor, we may assume the trial form

$$Q(\mathbf{R}', \mathbf{R}) = \exp\left(\sum_{i,j=1}^{N} \omega(\mathbf{r}_i', \mathbf{r}_j) - \tfrac{1}{2} \sum_{i,j=1}^{N} \left[\omega(\mathbf{r}_i, \mathbf{r}_j) + \omega(\mathbf{r}_i', \mathbf{r}_j') \right] \right). \tag{5}$$

This expression follows from first making an *ansatz* for $Q(\mathbf{R}', \mathbf{R})$ of the form (5), but without the second sum in the exponent. In a subsequent step, this term is subtracted in the exponent of the original *ansatz* for $Q(\mathbf{R}', \mathbf{R})$, yielding the form (5). As a consequence of this operation, the sums $\sum_{i=1}^{N} \omega(\mathbf{r}_i, \mathbf{r}_i)/2 + \sum_{i<j=1}^{N} \omega(\mathbf{r}_i, \mathbf{r}_j)$ and $\sum_{i=1}^{N} \omega(\mathbf{r}_i', \mathbf{r}_i')/2 + \sum_{i<j=1}^{N} \omega(\mathbf{r}_i', \mathbf{r}_j')$ must be added to the exponents in the Hartree-Jastrow expressions for $\Psi(\mathbf{R})$ and $\Psi(\mathbf{R}')$, respectively. As can be easily seen, the latter operation is tantamount to replacing the quantities t and u in Eq. (3) by the functions $t+\omega$ and $u+2\omega$. The form (3) for $\Psi(\mathbf{R})$ is then retrieved by a simple change of notation, namely the redefinition of the quantities $t+\omega$ and $u+2\omega$ as the one-body and two-body functions t and u entering Eq. (3). Both the Jastrow function u and the incoherence function ω heal to zero for large distances and are symmetric under interchange of coordinates. The latter property ensures that the matrix elements $\rho(\mathbf{R}', \mathbf{R})$ are symmetric under particle interchange, a property required for the trial form ρ to describe a system of identical bosons. At zero temperature, the incoherence function ω vanishes and the operator (2) reduces to the statistical operator of the ground-state wave function.

In order to calculate the internal energy $E = \mathrm{Tr}(\rho H)$ corresponding to the trial density operator ρ introduced above, we need to express the Hamiltonian $H = -(\hbar^2/2m) \sum_{i=1}^{N} \nabla_i^2 + \sum_{i<j=1}^{N} v(\mathbf{r}_i, \mathbf{r}_j)$ in terms of its matrix elements $H(\mathbf{R}, \mathbf{R}') = \langle \mathbf{R} | H | \mathbf{R}' \rangle$ in coordinate space. The result reads [16,17]

$$H(\mathbf{R}, \mathbf{R}') = \left(\frac{\hbar^2}{4m} \sum_{i=1}^{N} (\nabla_i \nabla_i' - \nabla_i^2) + \sum_{i<j=1}^{N} v(\mathbf{r}_i, \mathbf{r}_j) \right) \delta(\mathbf{R} - \mathbf{R}'). \tag{6}$$

The first sum in Eq. (6) represents the operator of the non-relativistic kinetic energy of a system of N bosons of mass m, while the second represents the operator of the

total potential energy, made up of bare two-body interactions given by the potential v. The identity (6) together with equations (3)–(5) enable us to form the trace of the operator ρH in coordinate space. The resulting internal energy E may be split into two contributions, yielding

$$E = \mathrm{Tr}(\rho H) = \int \rho(\mathbf{R}', \mathbf{R}) H(\mathbf{R}, \mathbf{R}')\, d\mathbf{R}\, d\mathbf{R}' = E_\Psi + E_\omega\,. \tag{7}$$

The contribution E_Ψ has the form of an expectation value of the Hamiltonian H with respect to a normalized Hartree-Jastrow state Ψ and therefore may be evaluated using the same techniques as in the $T = 0$ case [1,2,7], where Ψ assumes the role of the ground-state wave function. We thus obtain

$$E_\Psi = \langle \Psi | H | \Psi \rangle = \frac{\hbar^2}{2m} \int \left[\nabla \sqrt{\varrho(\mathbf{r})} \right]^2 d\mathbf{r} + \frac{1}{2} \int \varrho(\mathbf{r}_1) \varrho(\mathbf{r}_2) g(\mathbf{r}_1, \mathbf{r}_2) v^*(\mathbf{r}_1, \mathbf{r}_2)\, d\mathbf{r}_1\, d\mathbf{r}_2\,. \tag{8}$$

The first term on the right side of Eq. (8) arises from the spatial inhomogeneity of the one-body density

$$\varrho(\mathbf{r}_1) = \frac{1}{N} \int \Psi^2(\mathbf{R})\, d\mathbf{r}_2 \cdots d\mathbf{r}_N\,. \tag{9}$$

It vanishes in case of a uniform system, characterized by $\varrho(\mathbf{r}) = \text{const}$. Like the one-body density (9), the two-body spatial distribution function g, appearing in the correlation energy term of Eq. (8), may also be written solely in terms of Ψ, leading to

$$\varrho(\mathbf{r}_1) \varrho(\mathbf{r}_2) g(\mathbf{r}_1, \mathbf{r}_2) = \frac{1}{N(N-1)} \int \Psi^2(\mathbf{R})\, d\mathbf{r}_3 \cdots d\mathbf{r}_N\,. \tag{10}$$

The effective potential v^* is given by

$$v^*(\mathbf{r}_1, \mathbf{r}_2) = v(\mathbf{r}_1, \mathbf{r}_2) + \tfrac{1}{4} \big[D(1) + D(2) \big] u(\mathbf{r}_1, \mathbf{r}_2)\,, \tag{11}$$

the operators $D(1)$ and $D(2)$ being defined by

$$D(i) = -\frac{\hbar^2}{2m} \varrho^{-1}(\mathbf{r}_i) \nabla_i \varrho(\mathbf{r}_i) \nabla_i \tag{12}$$

with $i = 1, 2$.

Further exploiting the $T = 0$ theory of spatially inhomogeneous Bose fluids, the bare two-body correlation function u may be eliminated from the energy functional (8) by making use of the hypernetted chain (HNC) equations [24]. In the set of HNC equations, the two-body spatial distribution function g is related to the Jastrow correlation function u via the hypernet equation

$$g(\mathbf{r}_1, \mathbf{r}_2) = 1 + X(\mathbf{r}_1, \mathbf{r}_2) + N(\mathbf{r}_1, \mathbf{r}_2) = \exp\big[u(\mathbf{r}_1, \mathbf{r}_2) + N(\mathbf{r}_1, \mathbf{r}_2) + E(\mathbf{r}_1, \mathbf{r}_2) \big]\,, \tag{13}$$

where functions N, X, and E represent the sum of nodal, non-nodal, and elementary or bridge diagrams, respectively. The relationship between the nodal function N

and the direct correlation function X is established by the Ornstein-Zernike or chain relation

$$N(\mathbf{r}_1,\mathbf{r}_2) = \int \varrho(\mathbf{r}_3)\big[X(\mathbf{r}_1,\mathbf{r}_3) + N(\mathbf{r}_1,\mathbf{r}_3)\big]X(\mathbf{r}_3,\mathbf{r}_2)\,d\mathbf{r}_3\,, \tag{14}$$

completing the set of HNC equations. Formally regarding the quantities $\tilde{N}(\mathbf{r}_1,\mathbf{r}_2) = \sqrt{\varrho(\mathbf{r}_1)\varrho(\mathbf{r}_2)}\,N(\mathbf{r}_1,\mathbf{r}_2)$ and $\tilde{X}(\mathbf{r}_1,\mathbf{r}_2) = \sqrt{\varrho(\mathbf{r}_1)\varrho(\mathbf{r}_2)}\,X(\mathbf{r}_1,\mathbf{r}_2)$ as entries of matrices characterized by continuous indices $\mathbf{r}_1$ and $\mathbf{r}_2$, the chain equation (14) may be cast in the convenient form of the matrix equation $\tilde{N} = (\tilde{X} + \tilde{N})\tilde{X}$.

Supplemented with a prescription for determining the sum of elementary diagrams, $E(\mathbf{r}_1,\mathbf{r}_2)$, the HNC equations (13) and (14) form a closed set of equations for a given one-body density $\varrho(\mathbf{r})$. To be specific, we will resort to the widely used HNC/0 approximation, which has been applied in the majority of works on spatially inhomogeneous Bose fluids carried out within the general scheme described here (see, for example, Refs. 1,2, and 7). In this approximation, the elementary diagrams are neglected, i.e., $E(\mathbf{r}_1,\mathbf{r}_2) \equiv 0$. Exploiting the hypernet equation (13) in HNC/0 approximation, the energy functional E_Ψ may be expressed solely in terms of "dressed" spatial distribution functions, to arrive at the result [1,7]

$$\begin{aligned} E_\Psi = {} & \frac{\hbar^2}{2m}\int\Big[\nabla\sqrt{\varrho(\mathbf{r})}\Big]^2 d\mathbf{r} + \frac{1}{2}\int \varrho(\mathbf{r}_1)\varrho(\mathbf{r}_2)g(\mathbf{r}_1,\mathbf{r}_2)v(\mathbf{r}_1,\mathbf{r}_2)\,d\mathbf{r}_1\,d\mathbf{r}_2 \\ & + \frac{\hbar^2}{4m}\int \varrho(\mathbf{r}_1)\varrho(\mathbf{r}_2)\Big\{\Big[\nabla_1\sqrt{g(\mathbf{r}_1,\mathbf{r}_2)}\Big]^2 + \Big[\nabla_2\sqrt{g(\mathbf{r}_1,\mathbf{r}_2)}\Big]^2\Big\}\,d\mathbf{r}_1\,d\mathbf{r}_2 \\ & - \frac{\hbar^2}{16m}\int \varrho(\mathbf{r}_1)\varrho(\mathbf{r}_2)\Big\{\Big[\nabla_1 g(\mathbf{r}_1,\mathbf{r}_2)\Big]\cdot\Big[\nabla_1 N(\mathbf{r}_1,\mathbf{r}_2)\Big] \\ & \qquad + \Big[\nabla_2 g(\mathbf{r}_1,\mathbf{r}_2)\Big]\cdot\Big[\nabla_2 N(\mathbf{r}_1,\mathbf{r}_2)\Big]\Big\}\,d\mathbf{r}_1\,d\mathbf{r}_2\,, \end{aligned} \tag{15}$$

which form will expedite the variational procedure to be outlined in the next section. The energy E_Ψ has the same functional form as the Hartree-Jastrow ground-state energy at the HNC/0 level. However, the distribution functions ϱ, g, and N must now be taken at temperature T.

In coordinate space, the second energy term in Eq. (7), denoted E_ω, may be written as

$$E_\omega = \frac{\hbar^2}{4m}\int \varrho(\mathbf{r}_1)\left[\nabla_1^2\omega(\mathbf{r}_1,\mathbf{r}_1) - 2\int \delta(\mathbf{r}_1-\mathbf{r}_2)\nabla_1^2\omega(\mathbf{r}_1,\mathbf{r}_2)\,d\mathbf{r}_2\right]d\mathbf{r}_1\,. \tag{16}$$

The energy functional (16) may be further simplified by expanding the function $\Omega(\mathbf{r}_1,\mathbf{r}_2) = \sqrt{\varrho(\mathbf{r}_1)\varrho(\mathbf{r}_2)}\,\omega(\mathbf{r}_1,\mathbf{r}_2)$ as a series in the biorthogonal system of (real) eigenfunctions ψ_ℓ of the eigenvalue equation

$$\int \Omega(\mathbf{r}_1,\mathbf{r}_2)H_0(2)\psi_\ell(\mathbf{r}_2)\,d\mathbf{r}_2 = \Lambda_\ell\,\psi_\ell(\mathbf{r}_1)\,. \tag{17}$$

The operator

$$H_0 = -\frac{\hbar^2}{2m}\frac{1}{\sqrt{\varrho(\mathbf{r})}}\nabla\sqrt{\varrho(\mathbf{r})}\,\nabla\frac{1}{\sqrt{\varrho(\mathbf{r})}} \tag{18}$$

is the operator of the kinetic energy of a single particle of mass m moving in the inhomogeneous background formed by the density profile $\varrho(\mathbf{r})$. The symbol ℓ denotes a complete set of quantum numbers characterizing an eigenstate ψ_ℓ and the associated eigenvalue Λ_ℓ. As we shall see later, an eigenfunction ψ_ℓ describes the spatial shape of an elementary excitation of the Bose system corresponding to quantum number ℓ. It is easily shown that the eigenvalues Λ_ℓ are real and that the orthogonality relations

$$\langle \kappa | H_0 | \ell \rangle = 0 \qquad \text{for} \qquad \kappa \neq \ell \tag{19}$$

hold. Not only the operator H_0, but also the function Ω possesses a diagonal representation in the system of eigenfunctions of the eigenvalue equation (17). Specifically, we have

$$\Omega(\mathbf{r}_1, \mathbf{r}_2) = \sum_\ell \frac{\Lambda_\ell}{\langle \ell | H_0 | \ell \rangle} \psi_\ell(\mathbf{r}_1) \psi_\ell(\mathbf{r}_2) \,, \tag{20}$$

which, inserted in Eq. (16), leads to the simple expression

$$E_\omega = \sum_\ell \Lambda_\ell \,. \tag{21}$$

If we wished only to cast the energy component E_ω as a series of purely diagonal terms, it would have been sufficient merely to assume that Ω has a diagonal representation of the form $\Omega(\mathbf{r}_1, \mathbf{r}_2) = \sum_\ell \Omega_\ell \, \psi_\ell(\mathbf{r}_1) \psi_\ell(\mathbf{r}_2)$, without appealing to the particular eigenvalue equation (17). However, as we shall see in the next section, variation of the free energy with respect to the normal modes ψ_ℓ yields an eigenvalue equation for these states, from which the orthogonality relations (19) immediately follow. For this reason, we have chosen already at this point to introduce, through Eq. (17), a system of normal modes in which the operator H_0 and the function Ω are simultaneously diagonal. The primary purpose of establishing a spectral decomposition of Ω of the type (20) is that it will be needed to calculate the entropy. We stress that the conditions (19) need not be imposed as constraints when varying the free energy with respect to the eigenfunctions ψ_ℓ. They follow automatically from the resulting eigenvalue equation.

In comparison with the internal energy E, finding a useful expression for the entropy S is a task of a somewhat more demanding nature. Here, we will sketch only the merest of essentials. Employing the replica technique we first obtain

$$S = -k_B \mathrm{Tr}(\rho \ln \rho) = -k_B \frac{\partial}{\partial \xi} \ln \Big[\mathrm{Tr}\big(\rho^\xi\big) \Big] \Big|_{\xi=1} \,. \tag{22}$$

For integral values of the parameter ξ, the trace in the logarithm in the right side of Eq. (22) may be written as

$$\begin{aligned} \mathrm{Tr}(\rho^\xi) &= \int \prod_{\gamma=1}^{\xi} \big[\langle \mathbf{R}_\gamma | \rho | \mathbf{R}_{\gamma+1} \rangle \, d\mathbf{R}_\gamma \big] = \int \prod_{\gamma=1}^{\xi} \big[\Psi^2(\mathbf{R}_\gamma) Q(\mathbf{R}_\gamma, \mathbf{R}_{\gamma+1}) \, d\mathbf{R}_\gamma \big] \\ &= \int \prod_{\gamma=1}^{\xi} \big[\Psi^2(\mathbf{R}_\gamma) \, d\mathbf{R}_\gamma \big] \prod_\ell \exp\Big\{ -\frac{\Lambda_\ell}{2} \sum_{a,b=1}^{\xi} \rho_\ell(\mathbf{R}_a) M_{ab} \rho_\ell(\mathbf{R}_b) \Big\} \,, \end{aligned} \tag{23}$$

where we have made use of

$$Q(\mathbf{R}', \mathbf{R}) = \exp\Big\{-\tfrac{1}{2}\sum_{\ell} \Lambda_\ell \big[\rho_\ell(\mathbf{R}') - \rho_\ell(\mathbf{R})\big]^2\Big\}, \tag{24}$$

the density fluctuation operators ρ_ℓ being defined as

$$\rho_\ell(\mathbf{R}) = \sum_{i=1}^{N} \frac{1}{\sqrt{\langle \ell | H_0 | \ell \rangle}} \frac{\psi_\ell(\mathbf{r}_i)}{\sqrt{\varrho(\mathbf{r}_i)}}. \tag{25}$$

The entries M_{ab} of the $\xi \times \xi$ matrix M in the exponent in expression (23) are given by

$$M_{ab} = 2\delta_{ab} - \delta_{a+1,b} - \delta_{a,b+1} \tag{26}$$

with $a, b = 1, \cdots, \xi$. When it occurs, an index $\xi + 1$ is to be replaced by unity. To proceed, in Eq. (23) we replace the expectation value of the product $\prod_\ell \cdots$ with respect to the state $\prod_{\gamma=1}^{\xi} \cdots$ by the product of the expectation values with respect to this state. This approximation is known as the separability assumption [16,23,25]. Physically, interactions between excitations are neglected. Each expectation value in the latter product has the form of a normalization integral of a generalized wave function describing a mixture of bosons of ξ different sorts, and may be evaluated with the help of techniques similar to those applied in the case of spatially uniform Bose mixtures [26]. The final result reads

$$\begin{aligned} \mathrm{Tr}(\rho^\xi) &\approx \prod_\ell \int \prod_{\gamma=1}^{\xi} \big[\Psi^2(\mathbf{R}_\gamma)\, d\mathbf{R}_\gamma\big] \exp\Big\{-\frac{\Lambda_\ell}{2} \sum_{a,b=1}^{\xi} \rho_\ell(\mathbf{R}_a) M_{ab} \rho_\ell(\mathbf{R}_b)\Big\} \\ &= \prod_\ell \det\left[1 + \Lambda_\ell \frac{D(\ell)}{\langle \ell | H_0 | \ell \rangle} M\right]^{-\frac{1}{2}}, \end{aligned} \tag{27}$$

where

$$D(\ell) = \langle \ell |\, 1 + G \,| \ell \rangle. \tag{28}$$

In coordinate space, the kernel of the integral operator G in Eq. (28) is given by

$$G(\mathbf{r}_1, \mathbf{r}_2) = \sqrt{\varrho(\mathbf{r}_1)\varrho(\mathbf{r}_2)}\, \big[g(\mathbf{r}_1, \mathbf{r}_2) - 1\big]. \tag{29}$$

Assuming the eigenfunctions ψ_ℓ to be unit-normalized, the quantity $D(\ell)$ is the generalization of the static liquid structure factor to spatially inhomogeneous systems. The determinants under the product in the right side of Eq. (27) may now be expressed as polynomials in [17]

$$n_\ell = \sqrt{\frac{1}{4} + \Lambda_\ell \frac{D(\ell)}{\langle \ell | H_0 | \ell \rangle}} - \frac{1}{2}, \tag{30}$$

leading to

$$\mathrm{Tr}(\rho^\xi) = \prod_\ell \Big\{\big[1 + n_\ell\big]^\xi - \big[n_\ell\big]^\xi\Big\}^{-1}. \tag{31}$$

Next, the expression (31) is analytically continued to non-integral values of ξ. Inserting the result (31) into Eq. (22) and taking the derivative with respect to ξ yields the formula

$$S = k_B \sum_\ell \Big\{ [1+n_\ell] \, \ln[1+n_\ell] - n_\ell \, \ln[n_\ell] \Big\} \tag{32}$$

for the entropy. We thus arrive at an entropy functional that is formally equivalent to the entropy of a non-interacting gas of excitations obeying Bose statistics. This finding is in concert with the separability approximation, in which it is assumed that excitations do not interact with each other. The result (32) suggests that we interpret the quantities n_ℓ defined in Eq. (30) as the occupation numbers of thermal excitations characterized by quantum numbers ℓ, and introduce the associated excitation energies ϵ_ℓ via the usual formula

$$n_\ell = \frac{1}{\exp(\beta\epsilon_\ell) - 1} \tag{33}$$

for the occupation numbers of a free gas of Bose excitations.

3. EULER–LAGRANGE EQUATIONS

In this section we derive the optimization equations for the density profile $\varrho(\mathbf{r})$ of Eq. (9), for the two-body spatial distribution function $g(\mathbf{r}_1, \mathbf{r}_2)$ of Eq. (10), and for the set of eigenfunctions $\psi_\ell(\mathbf{r})$ of Eq. (17) and the associated excitation energies ϵ_ℓ. The optimization equations follow by varying the free energy functional F, as given by Eq. (1) together with Eqs. (7), (15), (21), and (32), with respect to ϱ, g (or optionally w.r.t $\sqrt{\varrho}$ and $\sqrt{g}$), ψ_ℓ, and Λ_ℓ respectively, while keeping the respective other quantities fixed. In conjunction with the HNC equations (13) and (14) in HNC/0 approximation, the Euler-Lagrange equations constitute a closed set of equations, determining the basic microscopic ingredients in our theory. The results for ϱ, g, and the set of eigenfunctions and excitation energies furnish the raw material for calculating, numerically or analytically, macroscopic thermodynamic quantities as functions of temperature.

We start by varying the Helmholtz free energy with respect to an eigenfunction ψ_ℓ, while keeping all other eigenfunctions, *all* eigenvalues Λ_ℓ, ϱ, g, and thus also the nodal function N fixed. The functional derivative of the occupation probability n_ℓ with respect ψ_ℓ may be obtained using Eqs. (28) and (30). In terms of the notation introduced in the context of the chain relation (14), the resulting Euler-Lagrange equation is equivalent to the eigenvalue equation [18-20]

$$(1 - \check{X}) H_0 |\ell\rangle = E_\ell |\ell\rangle \,, \tag{34}$$

where the one-body kinetic energy operator H_0 is given by Eq. (18). The eigenvalue E_ℓ satisfies

$$E_\ell = \frac{\langle \ell | H_0 | \ell \rangle}{D(\ell)} = \epsilon_\ell \tanh\Big(\frac{\beta\epsilon_\ell}{2}\Big) = \frac{\epsilon_\ell}{1+2n_\ell} \,. \tag{35}$$

The equality of the second and third members of relation (35) is already the Euler-Lagrange equation that follows from variation of the free energy with respect to Λ_ℓ,

while keeping all other eigenvalues, *all* eigenfunctions ψ_ℓ, ϱ, g, and N fixed. The third equality in (35) is a trivial consequence of the identification made in (33). The orthogonality relations (19) are easily deduced from Eq. (34) – for this reason we did not need to impose them as constraints in the variation. Equation (34) may be viewed as a nonlocal Schrödinger equation for collective excitations characterized by quantum numbers ℓ. It generalizes the Feynman eigenvalue equation to finite temperatures and therefore stands as a key result of our formal development. The nonlocal integro-differential operator $\tilde{X}H_0$ incorporates the effects of the strong interparticle correlations, endowing the excited states with their collective nature. At vanishing temperature, the eigenvalue E_ℓ becomes the excitation energy ϵ_ℓ itself and the well-established $T = 0$ Feynman eigenvalue equation [4] is then retrieved from Eq. (34).

Exploiting the generalized Feynman eigenvalue equation (34), we readily obtain the series expansion

$$\tilde{X} = 1 - \sum_\ell \frac{E_\ell}{\epsilon_0(\ell)} |\ell\rangle\langle\ell| \,, \tag{36}$$

for the operator $\tilde{X}$ corresponding to the matrix of elements $\tilde{X}(\mathbf{r}_1, \mathbf{r}_2)$, where we have introduced the notation

$$\epsilon_0(\ell) = \langle\ell|H_0|\ell\rangle \,. \tag{37}$$

For a spatially inhomogeneous system, the energy $\epsilon_0(\ell)$ represents the analog of the kinetic energy $\hbar^2|\mathbf{k}|^2/2m$ of a free particle moving with momentum $\hbar\mathbf{k}$ in a spatially uniform background. In coordinate space representation, the unit operator in the expansion (36) becomes a $\delta-$function. Employing the identity $1 + G = (1 - \tilde{X})^{-1}$, which holds by virtue of the Ornstein-Zernike relation (14), we may form the resolution

$$G = \sum_\ell \frac{H_0|\ell\rangle\langle\ell|H_0}{E_\ell\, \epsilon_0(\ell)} - 1 \tag{38}$$

of the operator G defined, in coordinate space, by Eq. (29).

The optimization equation for the two-body spatial distribution function g is found by varying the Helmholtz free energy with respect to $\sqrt{g(\mathbf{r}_1, \mathbf{r}_2)}$, while keeping the quantities ψ_ℓ, Λ_ℓ, and ϱ fixed. The functional derivative of the nodal function N with respect to g, needed in this procedure, is obtained by exploiting Eqs. (13) and (14) [1]. The Euler-Lagrange equation for $\sqrt{g}$ may be written as

$$\left[D(1) + D(2)\right] \sqrt{g(\mathbf{r}_1, \mathbf{r}_2)} + \left[v(\mathbf{r}_1, \mathbf{r}_2) + w(\mathbf{r}_1, \mathbf{r}_2) + \phi(\mathbf{r}_1, \mathbf{r}_2)\right] \sqrt{g(\mathbf{r}_1, \mathbf{r}_2)} = 0 \,, \tag{39}$$

where the potential v represents the bare two-body interaction and the operators $D(1)$ and $D(2)$ are given by Eq. (12). Let us adopt the notation $\Phi(\mathbf{r}_1, \mathbf{r}_2) = \sqrt{\varrho(\mathbf{r}_1)\varrho(\mathbf{r}_2)}\, \phi(\mathbf{r}_1, \mathbf{r}_2)$. The potential Φ is then defined by the series

$$\Phi = -2 \sum_\ell \frac{E_\ell^2}{\epsilon_0(\ell)} n_\ell[1 + n_\ell] \, |\ell\rangle\langle\ell| \,. \tag{40}$$

In the now-familiar matrix/operator notation, the quantity $W(\mathbf{r}_1, \mathbf{r}_2) = \sqrt{\varrho(\mathbf{r}_1)\varrho(\mathbf{r}_2)}$ $\times w(\mathbf{r}_1, \mathbf{r}_2)$ becomes

$$W = -\frac{1}{2}(H_0\tilde{N} + \tilde{N}H_0) - \frac{1}{2}\tilde{X}H_0\tilde{X} \,. \tag{41}$$

Among the terms contributing to the total effective pair potential $v + w + \phi$ in the Schrödinger-like equation (39), only the potential ϕ carries an explicit temperature dependence. While vanishing at $T = 0$, for finite T it provides for the coupling of the thermal excitations to the two-body distribution function g, and thereby to all other pair functions. With some algebra, the optimization equation (39) may be stated in the equivalent form

$$-H_0\tilde{X} - \tilde{X}H_0 + \tilde{X}H_0\tilde{X} = 2(V_{\rm ph} + \Phi)\,, \tag{42}$$

where $V_{\rm ph}(\mathbf{r}_1, \mathbf{r}_2) = \sqrt{\varrho(\mathbf{r}_1)\varrho(\mathbf{r}_2)}\, v_{\rm ph}(\mathbf{r}_1, \mathbf{r}_2)$, the particle-hole interaction $v_{\rm ph}$ being given by

$$\begin{aligned} v_{\rm ph}(\mathbf{r}_1, \mathbf{r}_2) =& \big[g(\mathbf{r}_1, \mathbf{r}_2) - 1\big]\,\big[w(\mathbf{r}_1, \mathbf{r}_2) + \phi(\mathbf{r}_1, \mathbf{r}_2)\big] + g(\mathbf{r}_1, \mathbf{r}_2) v(\mathbf{r}_1, \mathbf{r}_2) \\ &+ \frac{\hbar^2}{2m}\left\{ \Big[\nabla_1 \sqrt{g(\mathbf{r}_1, \mathbf{r}_2)}\Big]^2 + \Big[\nabla_2 \sqrt{g(\mathbf{r}_1, \mathbf{r}_2)}\Big]^2 \right\}. \end{aligned} \tag{43}$$

Variation of the free energy with respect to $\sqrt{\varrho(\mathbf{r})}$, while keeping all the ψ_ℓ, all the Λ_ℓ, and g fixed, yields a Hartree-like equation for $\sqrt{\varrho(\mathbf{r})}$. Again equations (13) and (14) are employed to determine the functional derivative of the nodal function N with respect to ϱ [1]. The constraint to be imposed in the variation of F with respect to $\sqrt{\varrho}$ is particle number conservation, $\int \varrho(\mathbf{r})\, d\mathbf{r} = \text{const.}$, which brings the chemical potential μ into the optimization equation for $\sqrt{\varrho(\mathbf{r})}$ as a Lagrange multiplier. The final result reads

$$\left(-\frac{\hbar^2}{2m}\nabla^2 + w_{\rm H}(\mathbf{r}) + \phi_{\rm H}(\mathbf{r}) \right) \sqrt{\varrho(\mathbf{r})} = \mu \sqrt{\varrho(\mathbf{r})}\,, \tag{44}$$

where

$$w_{\rm H}(\mathbf{r}_1) = \int \varrho(\mathbf{r}_2) F(\mathbf{r}_1, \mathbf{r}_2)\, d\mathbf{r}_2 - \frac{1}{4}\int \varrho(\mathbf{r}_2) N(\mathbf{r}_1, \mathbf{r}_2) D(2) X(\mathbf{r}_1, \mathbf{r}_2)\, d\mathbf{r}_2 \tag{45}$$

with

$$\begin{aligned} F(\mathbf{r}_1, \mathbf{r}_2) =& g(\mathbf{r}_1, \mathbf{r}_2) v(\mathbf{r}_1, \mathbf{r}_2) + \frac{\hbar^2}{2m}\left\{ \Big[\nabla_1 \sqrt{g(\mathbf{r}_1, \mathbf{r}_2)}\Big]^2 + \Big[\nabla_2 \sqrt{g(\mathbf{r}_1, \mathbf{r}_2)}\Big]^2 \right\} \\ &- \frac{\hbar^2}{8m}\Big\{ \big[\nabla_1 g(\mathbf{r}_1, \mathbf{r}_2)\big] \cdot \big[\nabla_1 N(\mathbf{r}_1, \mathbf{r}_2)\big] \\ &\qquad + \big[\nabla_2 g(\mathbf{r}_1, \mathbf{r}_2)\big] \cdot \big[\nabla_2 N(\mathbf{r}_1, \mathbf{r}_2)\big] \Big\}. \end{aligned} \tag{46}$$

In the full self-consistent Hartree potential $w_{\rm H} + \phi_{\rm H}$ appearing in the optimization equation (44), only the term

$$\phi_{\rm H}(\mathbf{r}) = \sum_\ell \frac{n_\ell[1 + n_\ell]}{\epsilon_0(\ell)}\, E_\ell \left\{ E_\ell\, \varphi_\ell^2(\mathbf{r}) - 2\varphi_\ell(\mathbf{r}) D\, \varphi_\ell(\mathbf{r}) + \frac{\hbar^2}{2m}\big[\nabla\varphi_\ell(\mathbf{r})\big]^2 \right\} \tag{47}$$

depends explicitly on temperature. The one-body functions φ_ℓ are defined as $\varphi_\ell(\mathbf{r}) = \psi_\ell(\mathbf{r})/\sqrt{\varrho(\mathbf{r})}$. The potential (47) describes the effects of the gas of thermal excitations on the density profile ϱ and accordingly vanishes at $T = 0$. The operator D in the second term of Eq. (47) is given by Eq. (12) with $\mathbf{r}_i$ and ∇_i replaced by $\mathbf{r}$ and ∇. In deriving equation (47), we have made use of the generalized Feynman eigenvalue equation (34).

Finally, inserting the series (36) and (40) into the optimization equation (42), we arrive at the series expansion

$$V_{\mathrm{ph}} = \tfrac{1}{2} \sum_{\ell} \frac{\epsilon_\ell^2}{\epsilon_0(\ell)} |\ell\rangle\langle\ell| - \tfrac{1}{2} H_0 \tag{48}$$

for the particle-hole potential V_{ph}, wherefrom the Bogoliubov-like eigenvalue equation

$$(H_0 + 2V_{\mathrm{ph}}) H_0 |\ell\rangle = \epsilon_\ell^2 |\ell\rangle \tag{49}$$

readily follows.

As has already been indicated, the Euler-Lagrange equations (34), (39), and (44) reduce to the corresponding $T = 0$ formulas, derived in Refs. 1 and 2, in the limit of vanishing temperature. Similarly, the optimization equations for spatially uniform Bose systems at finite temperatures, reported in Refs. 16 and 17, are retrieved from Eqs. (34), (39), and (44) by setting $\varrho(\mathbf{r}) = \text{const}$.

4. SUMMARY

In this paper, we have extended the variational Hartree-Jastrow theory of the ground state of spatially inhomogeneous Bose systems to finite temperatures. The theory presented here is a generalization also in the sense that it extends the correlated density matrix approach, formulated previously for uniform Bose fluids, to systems with nonuniform density profiles. The method provides a framework in which the effects of thermal excitations on the spatial structure of a Bose fluid, as represented by the density profile and the two-body distribution function, may be discussed on the basis of an *ab initio* microscopic description of the system. Thermal excitations make their appearance through self-consistently determined one-body and two-body potentials which enter the nonlinear, coupled Euler-Lagrange equations for the one-body density and for the pair distribution function. Since we neglect backflow correlations, the excitations are described by a Feynman eigenvalue equation, suitably generalized to nonzero temperatures. The only external quantities entering the correlated density matrix theory elaborated here are the bare two-body interaction potential and, in actual applications, the boundary conditions to be imposed on the one-body density.

The natural next step within a correlated density matrix approach to spatially inhomogeneous Bose fluids is the incorporation of backflow effects and three-body correlations. This step will be guided by recent progress in the inclusion of such effects in the homogeneous case [27]. More ambitiously, one might envision, as in Ref. 20, the development of a theory that allows phase transitions to take place in regions of inhomogeneous density. Of particular interest is a ^{4}He liquid-vapor

system in which a relatively dense homogeneous phase consisting of superfluid ^{4}He is separated from a relatively dilute homogeneous phase consisting of normal-fluid ^{4}He vapor by an interface regime with planar geometry. The chosen density operator must have the flexibility to provide for the occurrence of a transition in this spatially inhomogeneous interface. Again, valuable guidance is expected from studies of the homogeneous case, for which a theory of the normal-superfluid phase transition is currently under intense development [28-30].

ACKNOWLEDGMENTS

This work was supported in part by the U.S. National Science Foundation under Grant No. PHY-9307484 and the Deutsche Forschungsgemeinschaft under Grant No. Ri 267/23-1. The three of us gratefully acknowledge travel support from the U. S. Army for participation in the 18th International Workshop on Condensed Matter Theories in Valencia, Spain. More specifically, KAG and MLR received support from the European Research Office and JWC from the Army Research Office, Durham. We would like to thank the organizers of the workshop for local support and the Universidad Internacional Menéndez y Pelayo at Valencia for its kind hospitality.

REFERENCES

[1] M. Saarela, P. Pietiläinen, and A. Kallio, Phys. Rev. B **27**, 231 (1983).
[2] E. Krotscheck, G.-X. Qian, and W. Kohn, Phys. Rev. B **31**, 4245 (1985).
[3] B. E. Clements, J. L. Epstein, E. Krotscheck, and M. Saarela, Phys. Rev. B **48**, 7450 (1993).
[4] C. C. Chang and M. Cohen, Phys. Rev. B **11**, 1059 (1975).
[5] B. E. Clements, J. L. Epstein, E. Krotscheck, M. Saarela, and C. J. Tymczak, J. Low Temp. Phys. **89**, 585 (1992).
[6] E. Krotscheck and C. J. Tymczak, Phys. Rev. B **45**, 217 (1992).
[7] L. Szybisz and M. L. Ristig, Phys. Rev. B **40**, 4391 (1989).
[8] L. Szybisz, Phys. Rev. B **41**, 11282 (1990).
[9] S. A. Chin and E. Krotscheck, Phys. Rev. B **45**, 852 (1992).
[10] K. A. Gernoth, J. W. Clark, G. Senger, and M. L. Ristig, in *Condensed Matter Theories*, Vol. 8, edited by L. Blum and F. B. Malik (Plenum Press, New York, 1993).
[11] K. A. Gernoth, J. W. Clark, G. Senger, and M. L. Ristig, Phys. Rev. B, in press.
[12] E. Krotscheck, S. Stringari, and J. Treiner, Phys. Rev. B **35**, 4754 (1987).
[13] B. E. Clements, E. Krotscheck, and M. Saarela, Z. Phys. B **94**, 115 (1994).
[14] L. Szybisz, Z. Phys. B **90**, 341 (1992).
[15] L. Szybisz, Z. Phys. B, in press.
[16] C. E. Campbell, K. E. Kürten, M. L. Ristig, and G. Senger, Phys. Rev. B **30**, 3728 (1984).
[17] G. Senger, M. L. Ristig, K. E. Kürten, and C. E. Campbell, Phys. Rev. B **33**, 7562 (1986).
[18] K. A. Gernoth and M. L. Ristig, Phys. Rev. B **45**, 2969 (1992).

[19] K. A. Gernoth and J. W. Clark, in *Condensed Matter Theories*, Vol. 9, edited by J. W. Clark, A. Sadiq, and K. A. Shoaib (Nova Science Publishers, Commack, New York, 1994).
[20] K. A. Gernoth and J. W. Clark, J. Low Temp. Phys., in press.
[21] E. Krotscheck, private communication.
[22] A. Huber, in *Methods and Problems of Theoretical Physics*, Vol. 37, edited by J. E. Bowcock (North-Holland, Amsterdam, 1970).
[23] E. Feenberg, *Theory of Quantum Fluids* (Academic Press, New York, 1969).
[24] T. Morita and K. Hiroike, Progr. Theor. Phys. **25**, 537 (1961).
[25] C. E. Campbell and E. Feenberg, Phys. Rev. **188**, 396 (1969).
[26] C. E. Campbell, Ann. Phys. (N. Y.) **74**, 43 (1972).
[27] B. E. Clements, E. Krotscheck, J. A. Smith, C. E. Campbell, Phys. Rev. B **47**, 5239 (1993).
[28] G. Senger, M. L. Ristig, C. E. Campbell, and J. W. Clark, Ann. Phys. (N. Y.) **218**, 160 (1992).
[29] M. L. Ristig, G. Senger, M. Serhan, and J. W. Clark, to be published.
[30] R. Pantförder and M. L. Ristig, to be published.

MAGNETICALLY INDUCED WIGNER ELECTRON SOLID AND THE ANYON MODEL

N.H. March

Theoretical Chemistry Department
University of Oxford
5 South Parks Road
Oxford, OX1 3UB
England

1. INTRODUCTION

The purpose of this paper is to summarize our present knowledge of the many–body physics of electron crystallization in zero magnetic field following Wigner([1], [2]) and then to treat the influence of strong magnetic fields on electron crystallization (Durkan, Elliott and March [3]).

The outline of the paper is as follows. In section 2, the basic physical ideas underlying the prediction of Wigner of the transition in the ground state from an electron liquid at high density in the jellium model to an electron crystal at low density will be summarized. What was not known reliably until 1980 was the density at which such a metal–insulator transition would occur. This matter was dealt with in the quantum Monte Carlo computer study of Ceperley and Alder [4] and their work will be briefly discussed also in section 2. Then in section 3 the melting curve of the Wigner electron crystal will be considered.

Section 4 is concerned with the main topic of the paper : namely the study of magnetically induced Wigner solids (MIWS). Starting with the proposals of Durkan, Elliott and March [3], which were motivated by the Hall measurements of Putley [5] on n–type InSb in a magnetic field (see also Somerford [6]; Care and March [7], [8], and later theoretical studies), a key experiment was performed by Andrei et al [9] in which a GaAs/AlGaAs heterojunction was studied in a strong magnetic field applied perpendicular to the plane of the two–dimensional electron assembly. Evidence was presented for the formation of a MIWS at a critical magnetic field, based on the idea that an electron solid can support low–frequency shear while an electron liquid cannot. Strong support for the conclusions of Andrei et al [9] came from the later luminescence experiments of Buhmann et al [10], and from a theoretical study of the melting curves of a three–dimensional Wigner crystal by Lea and March [11], using the earlier work of Kleppmann and Elliott [12]. Then in section 4.1, the proposed melting curve of the MIWS by Buhmann et al [10] is subjected to analysis based largely on thermodynamics (Lea, March and Sung [13]). This exposes remarkable changes in magnetic behaviour taking place as one crosses the melting curve of the MIWS. In section 5, a preliminary interpretation of this behaviour is given using the anyon model to describe the electron liquid in equilibrium with the electron solid (MIWS). Section 5.1 is concerned with progress on the statistical and momentum distribution function of the anyon model. In section 6, the possible relation between this model and the composite Fermion model of Jain [14] is briefly summarized. Section 7 constitutes a summary, together with some suggestions for future study.

2. WIGNER ELECTRON CRYSTALLIZATION IN ZERO MAGNETIC FIELD

Wigner [1, 2] was interested in the correlation energy of electrons in metals. As the simplest model of a metal, he considered jellium, in which electrons interacting via the Coulomb repulsion energy e^2/r_{ij} between electrons i and j separated by a distance r_{ij} move in a non–responsive uniform background of neutralizing positive charge. The ground–state energy per electron, E/N, of this model, in the high density limit $n \to \infty$, where

$$n = 3/4\pi r_s^3, \tag{2.1}$$

with r_s the mean interelectronic spacing, is given by the Hartree–Fock energy

$$\frac{E}{N} = \frac{2.21}{r_s^2} - \frac{0.916}{r_s}. \tag{2.2}$$

Eqn (2.2) corresponds to the energy obtained from a total wave function which is a single Slater determinant of plane waves exp (i **k**.**r**), where $|\mathbf{k}| < k_F$, the magnitude of the wave vector **k** at the Fermi surface. In eqn (2.2), E/N is in Rydbergs if r_s is inserted in units of the Bohr radius $a_0 = \hbar^2/me^2$.

What is apparent from eqn. (2.2) is that, as r_s increases from the high density limit ($r_s \to 0$) the potential (exchange) energy term in eqn (2.2) becomes eventually important compared with the kinetic energy term ($\alpha\ r_s^{-2}$) and then one must refine the single Slater determinantal wave function set out above. This motivated Wigner [1,2] to examine the extreme low density limit $r_s \to \infty$. He stressed that, in this limit (compare eqn (2.2)) the potential energy will eventually dominate the kinetic energy. He clearly recognized that, in the jellium model, the potential energy would be minimized by electrons avoiding each other maximally and that this would be achieved by localization on the sites of a lattice. One must then minimize the Madelung energy and this turns out to lead to the body–centred–cubic lattice as the low density ground state – the so–called quantal Wigner electron crystal. It is this quantal crystal that is our dominant concern in the present work, though it will be helpful in the ensuing discussion to also invoke known results from the classical limit of the jellium model, the so–called one–component plasma (OCP : see for example the book by March and Tosi [15]). Returning to the Madelung energy, one can write instead of eqn (2.2), which is valid as $r_s \to 0$, the low density ground–state energy as $r_s \to \infty$:

$$\frac{E}{N} \to -\frac{1.8}{r_s}, \tag{2.3}$$

which is twice as low as eqn (2.2) would yield. In conventional terms, comparison of eqns (2.2) and (2.3) shows that the exchange energy $-0.9/r_s$ is approximately equal to the correlation energy as $r_s \to \infty$.

2.1 Value to critical density for transition to Wigner electron crystal ground–state

When electron crystallization was reviewed by Care and March [8], there was still a very wide spread of values of the critical value r_s, say r_c, at which the electron liquid would give way to the Wigner electron crystal as the density is lowered. This difficulty was resolved by Ceperley and Alder [4] who reported quantum Monte Carlo calculations for paramagnetic and ferromagnetic liquid phases as a function of r_s, to compare with the Wigner electron crystal phase. Their important conclusion (see Figure 1) was that the critical interelectronic separation r_c at which the ground–state

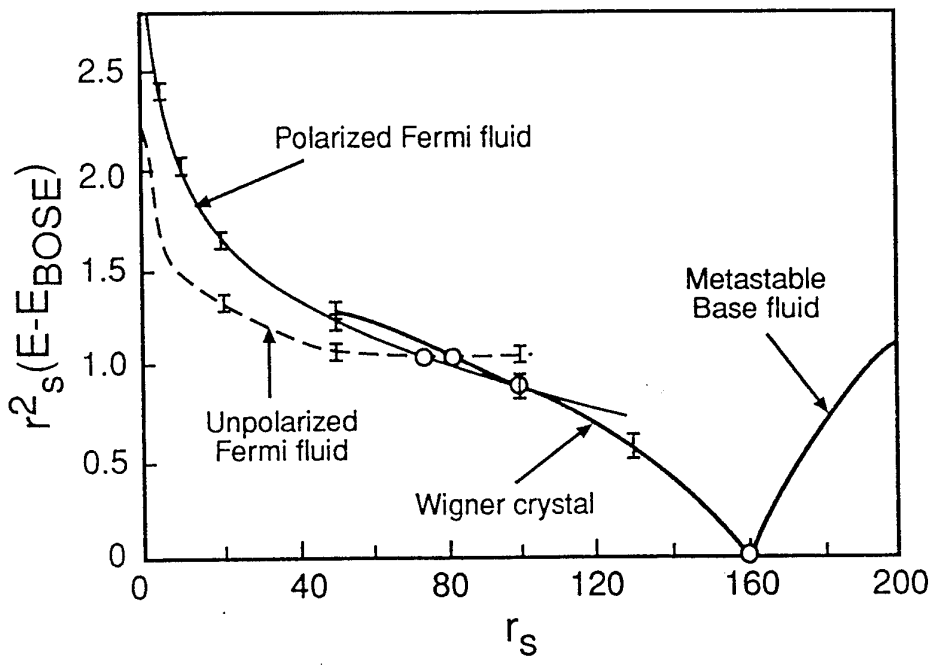

Figure 1 Shows energies of different phases of jellium as a function of mean interelectronic distance r_s defined in eqn (2.1), as calculated by quantal computer simulation. Paramagnetic and ferromagnetic electron liquid phases are compared with the Wigner electron crystal. (Redrawn from Ceperley and Alder [4]).

changed from electron liquid to an electron crystal phase was given by

$$r_c = (100 \pm 20)\, a_0. \tag{2.4}$$

In the body–centred cubic phase, for $r_s > r_c$ in eqn (2.4), the picture of two interpenetrating simple cubic lattices, with electron spins pointing upwards on one lattice and downwards on the other (i.e. a Néel antiferromagnetic electron crystal) is believed to represent correctly the magnetic configuration, but the ferromagnetic state is very close in energy. However, the work of Herman and March [16] strongly suggests that the ferromagnetic state is never stabilized in jellium. These workers also pointed out that the low density energy calculations of Ceperley and Alder [4] are well represented by the results which generalize eqn (2.3) away from the extreme low density limit $r_s \to \infty$, namely

$$\frac{E}{N} = -\frac{1.8}{r_s} + \frac{2.66}{r_s^{3/2}} + \ldots \tag{2.5}$$

The term in eqn (2.5) proportional to $r_s^{-3/2}$ is to be thought of as representing electrons performing harmonic oscillations about the body–centred cubic lattice sites. The coefficient 2.66 then arises from a 'phonon' treatment. Wigner initially used an independent harmonic oscillator (Einstein) model, with wave function

$$\psi = \exp(-\alpha r^2): \tag{2.6}$$

where the exponent α is proportional to $r_s^{-3/2}$. Eqn (2.6) would lead to a coefficient of 3 in the $r_s^{-3/2}$ term in eqn (2.5), instead of the refined value 2.66 given there. However, one merit of the approximate form (2.6) is the immediate recognition that in the insulating Wigner crystal phase for $r_s > r_c$ the momentum distribution n(p) is Gaussian. Plainly therefore, the discontinuity in n(p) at the Fermi momentum $p_F = \hbar k_F$ in the electron liquid phase for $r_s < r_c$ has completely disappeared in the insulting Wigner phase. However, it is relevant to note here that in the one–dimensional Wigner electron crystal, the work of Holas and March [17] has shown that while there is no discontinuity in n(p), some remnants of the Fermi surface persist in the insulating phase through non–analytic character of n(p) at $p = p_F$. This point, as well as the magnetism, remains in need of further study in the quantal Wigner electron crystal.

However, from the point of view of observing this quantal electron crystal in laboratory experiments, it is essential to have knowledge of the melting curve. This is the problem therefore to which we turn next in section 3 immediately below.

3. MELTING CURVE OF QUANTAL WIGNER ELECTRON CRYSTAL IN ZERO MAGNETIC FIELD

Parrinello and March [18] set out the thermodynamics of Wigner electron crystallization in zero magnetic field. One of their most important conclusions can best be made clear by reference to Figure 2 There the melting temperature T_m is

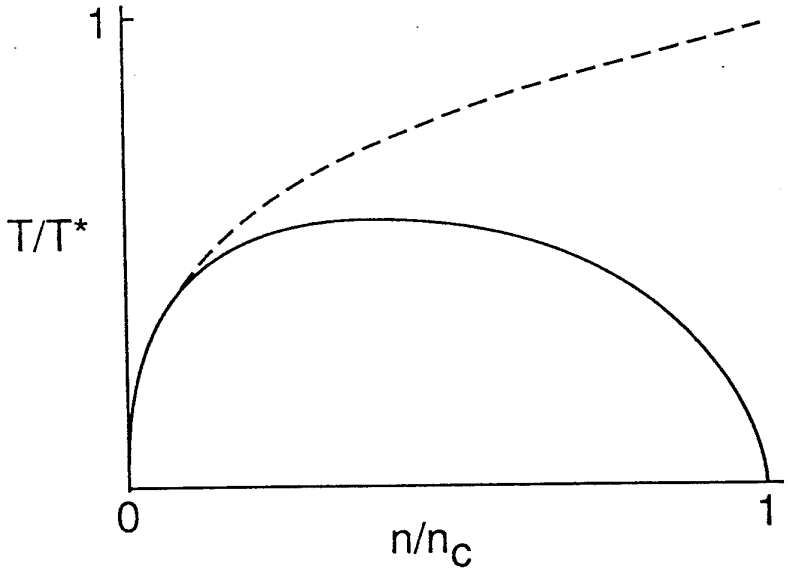

Figure 2 Schematic form of melting curve of Wigner electron crystal in zero magnetic field as a function of reduced density n/n_c, where n_c is the critical density for the liquid–crystal transition in the ground state (T=0). Redrawn from Ferraz et al [20,21].

plotted versus the density n, the critical density $n_c = 3/4\pi r_c^3$ being marked on the (schematic) Fig.2. The low–density limit $n \to 0$ is characterized by the absence of quantum–mechanical tunnelling. Hence in this limit one can use the known result for the classical OCP referred to above. This OCP model exhibits freezing when the customary dimensionless coupling strength Γ, now involving in this classical regime the ratio of Coulombic potential energy to thermal energy, namely

$$\Gamma = (e^2/r_s)/k_B T, \tag{3.1}$$

reaches a critical value $\Gamma_c \sim 170$. Such a transition was known to Brush, Sahlin and Teller [19] in their early computer simulation study and this was subsequently refined by Hansen and coworkers (see, for example, the book by March and Tosi [15]). Eqn (3.1) then translates into a low density asymptote of the melting curve

$$T_m = \text{const } n^{1/3} \tag{3.2}$$

and the constant is determined by $\Gamma_c \sim 170$. This result (3.2) is sketched in Fig.2.

Ferraz, March and Suzuki [20,21] (see also [22]) next interpolated between the asymptote (3.2) and the zero temperature critical density n_c as determined by Ceperley and Alder [4]. They did so by approximate integration of the Clausius–Clapeyron equation for the (assumed) first–order liquid–crystal phase transition. Their main conclusion was that He temperatures would be needed to detect the quantal Wigner electron crystal in laboratory experiments.

4. MAGNETICALLY INDUCED ELECTRON SOLID

The localization of electrons in impure semiconductors was discussed by Durkan et al [3] in relation to measured transport properties (Putley [5]) of highly compensated n–type InSb in an applied magnetic field. In this work, the proposal was made that Wigner electron crystallization could be aided by localization due to strong applied magnetic fields, the magnetic (cyclotron) radius $l_c = (\hbar c/eH)^{\frac{1}{2}}$ providing an important new localization scale. This phenomenon of a magnetically induced Wigner solid (MIWS) has subsequently been observed by Andrei et al [9] in a GaAs/AlGaAs heterojunction. Their findings have been confirmed and extended by the luminescence study of Buhmann et al [10].

Motivated by these experiments, and in particular with the aim of understanding the melting curve of the magnetically induced Wigner solid (MIWS), Lea et al [13] have given the thermodynamics of such melting in a magnetic field. Their results will be utilized immediately below to treat the equilibrium between the electron liquid (compare Laughlin [23]) and the Wigner solid. Remarkable magnetic properties of the electron liquid can then be deduced, following Lea et al [13], by combining the thermodynamic treatment with the 'experimental' phase diagram of Buhmann et al [10].

4.1 Thermodynamics of first–order transition between electron solid and electron liquid

The analogue of the Clausius–Clapeyron equation for melting in a magnetic field was given by Lea et al [13] as

$$(\partial T_m/\partial \nu) = (H/\nu)\Delta M/\Delta S \qquad (4.1)$$

where T_m is the melting temperature. It is to be noted that in the magnetic field H, in the geometry here of an electron assembly in the plane of a heterojunction and in a perpendicular magnetic field, each single–particle state is already confined by the Lorentz force to an area $2\pi\ell_H^2$ and has the discrete energies $(n+\frac{1}{2})\hbar\omega_c$ where $\hbar\omega_c = \hbar^2/m\ell_H^2 = \hbar eH/mc$ is the cyclotron energy. Each of $\nu = 2(\ell_H/r_s)^2$ electrons where r_s is now defined in terms of the areal density n by $\pi r_s^2 = 1/n$. Increasing the field decreases this Landau filling factor ν:

$$\nu = nhc/eH. \qquad (4.2)$$

Finally in eqn(4.1) $\Delta M = M_L - M_S$ is the change of magnetization on melting while $\Delta S = S_L - S_S$ is the corresponding entropy change.

From the schematic phase diagram proposed by Buhmann et al [10] and shown in Figure 3, Lea et al [13] used eqn (4.1) to deduce the magnetization change along the melting curve, as shown schematically in Figure 4. These workers noted that this field dependence of ΔM is very reminiscent of the de Haas – van Alphen effect occurring in metals at larger ν values, suggesting that the magnetism of the electron liquid phase is initimately connected with the exotic variation of ΔM shown in Figure 4. The relation of their proposal to the anyon model will now be briefly summarized [24].

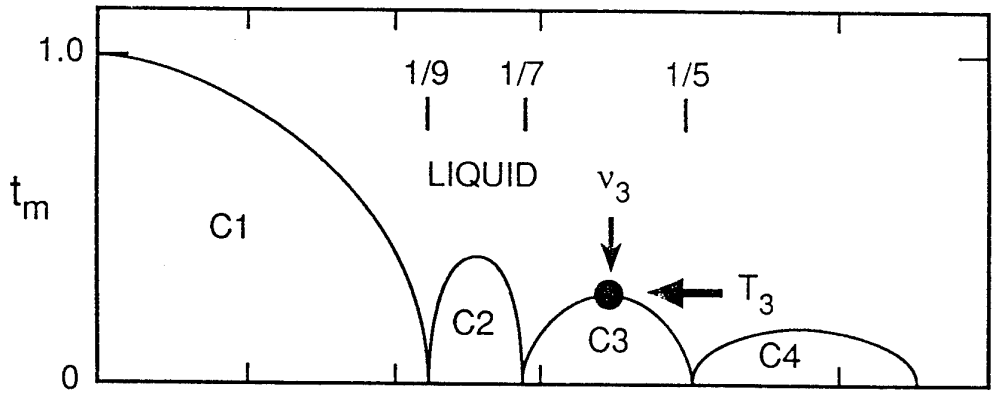

Figure 3 Schematic phase diagram showing magnetically induced Wigner electron solids versus Landau level filling factor ν defined in eqn (4.2). Note the stability of the (Laughlin) electron liquid at $\nu = 1/9$, $1/7$ and $1/5$.

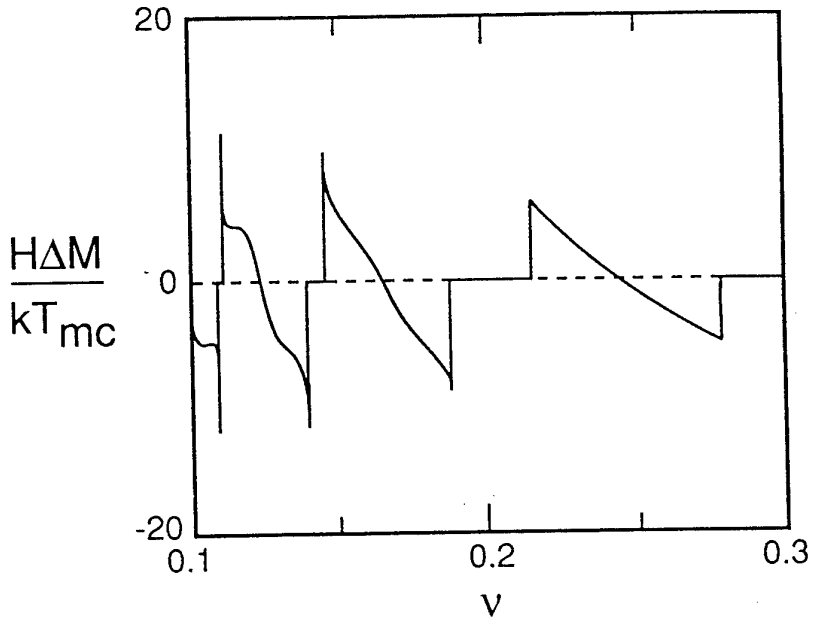

Figure 4 Schematic form of the magnetization of the electron liquid, as a function of Landau level filling factor ν, along the melting curve (after Lea et al [13]).

5. ANYON MAGNETISM AND MELTING CURVE OF FIGURE 3

We use the anyon model only in the classical limit below. We shall see that it can give further insight into the microscopic origin (Lea et al [24]) of the phase diagram of Figure 3. In the anyon model, one has fractional statistics (Wilczek [25]), characterized by a parameter γ, which has the value zero for Fermions and is $\pm$ 1/2 for Bosons.

Using the second virial coefficient of non–interacting two–dimensional anyons (mass m) in a magnetic field (Johnson and Canright [26]; Dowker and Chang [27]), the magnetism ΔM of an anyon gas versus fractional statistics parameter γ is shown in Figure 5. To relate this Figure to a field–dependent magnetization, it is necessary to connect the statistics parameter γ to the Landau filling factor γ. Lea et al [24] give arguments for the approximate relation

$$\gamma = 1/2\nu - \mathrm{j} \qquad (5.1)$$

where the integer j is chosen in such a way that γ varies in the range from $-\frac{1}{2}$ to $+\frac{1}{2}$ as ν decreases. The magnetization of this non–interacting ayon gas has many of the features required to explain qualitatively the phase diagram of the two–dimensional electron solid sketched in Figure 3.

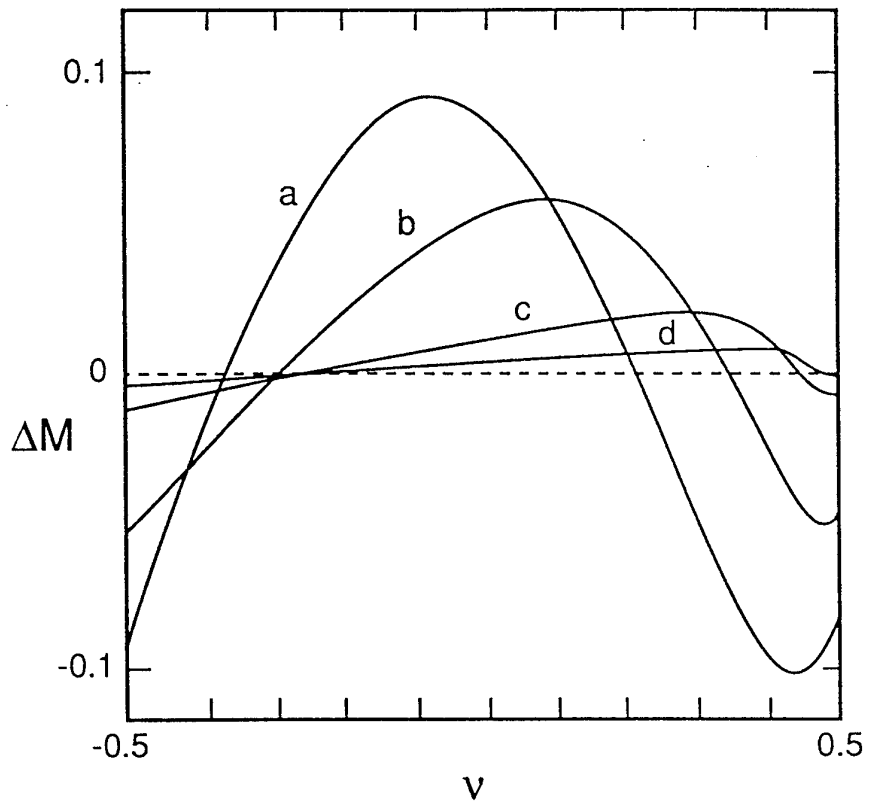

Figure 5 Depicts magnetization ΔM of an anyon gas versus fractional statistics parameter. Different curves (a–d) correspond to different parameters in anyon model. (After Lea et al [24]).

5.1 Statistical and momentum distribution function for anyons

March et al [28]; see also March [29] have treated the statistical distribution function $f(\epsilon)$ for anyons and the closely related momentum distribution function n(k). They start from the treatment of collisions in a gas of Fermions following, for example, Ma [30]. Ma then obtains

$$f(\epsilon)/1\text{–}f(\epsilon) = \exp(-\alpha - \beta\epsilon). \tag{5.2}$$

and for Bosons the factor $1\text{–}f(\epsilon)$ becomes $1+f(\epsilon)$. For anyons, March et al [28] show that

$$f(\epsilon)/1\text{–}a(\gamma)f(\epsilon) = \exp(-\alpha - \beta\epsilon). \tag{5.3}$$

Approximate treatments of $a(\gamma)$ as a function of the fractional statistics parameter γ now exist (March et al, [28]; March [29]) which, at least, correctly interpolate between the Fermion and Boson limits. The relation to the momentum distribution n(k) is also set out in the above references and further details will therefore be omitted here.

6. POSSIBLE RELATION BETWEEN ANYON MODEL AND COMPOSITE FERMION MODEL OF JAIN

6.1 Composite Fermions

The above treatment (Lea et al, [24]) has utilized as an important ingredient the idea of a new kind of Fermionic particle, the composite Fermion (CF). This was proposed by Jain [14,31] to explain the fractional quantum Hall effect (FQHE). Jain argued that in the system treated above, namely a two–dimensional electron system subjected to an intense magnetic field normal to the plane of the electrons, these particles would condense into composite Fermions. Such a composite is an electron carrying an even integer number (2p say) of the vortices of the many–particle wave function, and often can be thought of as an electron binding 2p magnetic flux quanta Φ_0 (= h/e). These composite particles are formed as a result of the Coulomb interaction between the (2d) electrons, and the liquid of strongly interacting electrons is equivalent to a gas of weak interacting composite Fermions. Since these CF's do not experience the flux bound to them, they see an effective magnetic field (Goldman et al [32])

$$B^{*} = B = 2pn\,\Phi_0 \tag{6.1}$$

where n is the electron (and CF) density. In the above equation, the – (+) sign corresponds to the flux binding in the same (opposite) direction as the external field B. The effective Landau level filling factor of composite Fermions, $\nu^{*} = n\Phi_0/B^{*}$ is then related to the electron filling factor $\nu = n\Phi_0/B$ by

$$\nu = \nu^{*}/(2p\nu^{*} \pm 1). \tag{6.2}$$

One of the merits of the CF idea is the straightforward explanation of FQHE of electrons as the integer QHE for composite Fermions. An integer number of filled Landau levels of CF's (ν^{*} =i) corresponds to the electron filling factor $\nu = i/(2pi\pm1)$, which are precisely the sequences of fractions exposed by experiment (Jain [31]; Jain and Goldman, [33]). Transitions from one FQHE state to the next within the sequence are expected to occur when $\nu^{*} = i + \frac{1}{2}$, according to the 'law of corresponding states' (Jain et al [34]) : this is likewise in agreement with experiment (Goldman et al [35]).

Subsequently, Goldman et al [32] have reported transverse magnetic focusing experiments in the vicinity of the Landau level filling factor $\nu = 1/2$. They observe quasiperiodic magnetic focusing peaks for $\nu < 1/2$ and no periodic structure for $\nu > 1/2$ in several double–constriction GaAs heterojunction samples. The quasiperiod and the direction of focusing in all of their samples were found to be in quantitative agreement with that expected from semiclassical transport by composite Fermions of charge $-|e|$.

Wu and Jain [36] have investigated the spectrum of interacting electrons at arbitrary filling actors in the limit of vanishing Zeeman splitting. These workers argue that the CF treatment can explain the low–energy spectrum, provided a hard core condition is imposed on the composite Fermions.

7. SUMMARY PLUS SOME SUGGESTIONS FOR FUTURE STUDY

Electron crystallization, proposed some sixty years ago by Wigner [1], has proved difficult to observe in the laboratory. However, Wigner's original ideas for the jellium model have been amply confirmed by quantal computer simulation [4] as discussed in section 2.1.

For magnetically induced electron solids, proposed by Durkan et al [3] to explain data of Putley [5] on highly compensated n–type InSb, the recent experiments of Andrei et al [9] and Buhmann et al [10] on GaAs/AℓGaAs heterojunctions observe the electron solid and allow the salient features of its melting curve to be sketched. Lea et al [13,24] expose remarkable magnetization of the electron liquid in equilibrium with the MIWS, which can be interpreted, at least qualitatively, using the anyon model.

7.1 Anyon model with two–body interactions

The anyon model was employed above in the interpretation of the exotic magnetic behaviour of the Laughlin electron liquid. While the relation with the composite Fermion picture discussed above remains still to be fully clarified, it is of some interest to note that Gidopoulus and Theophilou [37] have recently included two–body interactions in the anyon model. They have demonstrated, in particular, that the non–analytic behaviour of the second virial coefficient, found by Arovas et al [38], is still retained in the presence of such interactions and independent of the particular form of the interaction. Furthermore, they calculate the second virial coefficient explicitly in the case of a short–range interaction.

We conclude by mentioning a further relevant area in which future work should be fruitful.

7.2 Quantum dots in strong magnetic fields

Advances in nanofabrication technology have allowed the manufacture of 'quantum dots' in which electrons are confined to a small area within a two–dimensional electron assembly (see, eg Kastner [39]). Yang et al [40] have very recently considered the magnetic field dependence of the chemical potential for parabolically confined quantum dots in a strong magnetic field. They demonstrate that approximate expressions, based on the idea that the size of a dot is determined by a competition between confinement and interaction energies, are consistent with exact diagonalization studies for small quantum dots. These workers show that fine structure is present in the magnetic field dependence which requires for its explanation a full many–body treatment and is associated with ground–state level crossings as a function of confinement strength or Zeeman interaction strength. Some of this fine structure is associated by Yang et al [40] with precursors of the bulk incompressible states responsible for the FQHE.

REFERENCES

[1] E.P. Wigner, *Phys.Rev.* **47**, 1002 (1934).

[2] E.P. Wigner, *Trans.Faraday Soc.* **34**, 678 (1938).

[3] J. Durkan, R.J. Elliott and N.H. March, *Rev.Mod.Phys.* **40**, 812 (1968).

[4] D.M. Ceperley and B.J. Alder, *Phys.Rev.Lett.* **45**, 566 (1980).

[5] E.H. Putley, *Proc.Phys.Soc.(London)* **76**, 802 (1960).

[6] D.J. Somerford, *J.Phys.* **C4**, 1570 (1971).

[7] C.M. Care and N.H. March, *J.Phys.* **C4**, L372 (1971).

[8] C.M. Care and N.H. March, *Advances in Physics*, **24**, 101 (1975).

[9] E.Y. Andrei, G. Deville, D.C. Glattli, F.I.B. Williams, E. Paris and B. Etienne, *Phys.Rev.Lett.* 60, 2765 (1988).

[10] H. Buhmann, W. Joss, K. von Klitzing, I.V. Kuhuskim, A.S. Plant, G. Martinez, K. Ploog and V.B. Timofeev, *Phys.Rev.Lett.* **6**, 926 (1991).

[11] M.J. Lea and N.H. March, in "*Disorder in Condensed Matter Physics*", Eds. J.A. Blackman and J. Taguena (Clarendon Press: Oxford,1991) p.431.

[12] W.G. Kleppmann and R.J. Elliott, *J.Phys.* **C8**, 2729 (1975); see also R.J. Elliott and W.A. Kleppman, *J.Phys.* **C8**, 2737 (1975).

[13] M.J. Lea, N.H. March and W. Sung, *J.Phys.Cond. Matter*, **3**, L430 (1991).

[14] J.K. Jain, *Phys.Rev.Lett.* **63**, 199 (1989).

[15] N.H. March and M.P. Tosi, *Coulomb Liquids* (Academic: New York, 1985).

[16] F. Herman and N.H. March, *Solid State Commun.* **50**, 725 (1984).

[17] A. Holas and N.H. March, *Phys.Lett.* **A157**, 160 (1991).

[18] M. Parrinello and N.H. March, *J.Phys.* **C9**, L146 (1976).

[19] S.G. Brush, H.L. Sahlin and E. Teller, *J.Chem.Phys.* **45**, 2102 (1966).

[20] A. Ferraz, N.H. March and M. Suzuki, *Phys.Chem.Liquids*, **8**, 153 (1978).

[21] A. Ferraz, N.H. March and M. Suzuki, *Phys.Chem.Liquids*, **9**, 59 (1979).

[22] H. Nagara, N. Nagata and T. Nakamura, *Phys.Rev.* **A36**, 1859 (1987); N.H. March, *Phys.Rev.* **A37**, 4526 (1988).

[23] R.B. Laughlin, *Phys.Rev.Lett.* **60**, 2577 (1988).

[24] M.J. Lea, N.H. March and W. Sung, *J.Phys.Cond.Matter*, **4**, 5263 (1992).

[25] F. Wilczek, *Fractional Statistics and Anyons* (World Scientific: Singapore, 1990).

[26] M.D. Johnson and G.S. Canright, *Phys.Rev.* **B41**, 6870 (1990).

[27] J.S. Dowker and M. Chang, *ICTP Trieste Report* (1990).

[28] N.H. March, N.I. Gidopoulos, A.K. Theophilou, M.J. Lea, and W. Sung, *Phys.Chem.Liquids*, **26**, 135 (1993).

[29] N.H. March, *J.Phys.Condensed Matter*, **5**, B149 (1993).

[30] S.K. Ma, *Statistical Mechanics* (World Scientific: Singapore, 1985).

[31] J.K. Jain, *Phys.Rev.* **B41**, 7653 (1990); *Adv.Phys.* **41**, 105 (1992); *Comments Condens.Matter Phys.* **16**, 307 (1993).

[32] V.J. Goldman, B. Su and J.K. Jain, *Phys.Rev.Lett.* **72**, 2065 (1994).

[33] J.K. Jain and V.J. Goldman, *Phys.Rev.* **B45**, 1255 (1992).

[34] J.K. Jain, S.A. Kivelson and N. Trivedi, *Phys.Rev.Lett.* **64**, 1297 (1990).

[35] V.J. Goldman, J.K. Jain and M. Shayegan.*Phys.Rev.Lett.* **65**, 907 (1990); see also *Mod.Phys.Lett.* **5**, 479 (1991).

[36] X.G. Wu and J.K. Jain, *Phys.Rev.* **B49**, 7515, (1994).

[37] N.I. Gidopoulos and A.K. Theophilou, *Phys.Rev.* **B49**, 6808 (1994).

[38] D.P. Arovas, J.R. Schrieffer, F. Wilczek and A. Zee, *Nucl.Phys.* **B251**, 117 (1985).

[39] M.A. Kastner, *Mod.Phys.* **641**, 849 (1992).

[40] S.–R.E. Yang, A.H. MacDonald and M.D. Johnson, *Phys.Rev.Lett.* 71, 3194 (1993).

CORRELATIONS AND RELATIVISTIC EFFECTS IN THE MANY-BODY THEORY OF NUCLEAR SYSTEMS

H. Müther

Institute of Theoretical Physics
University of Tübingen
Auf der Morgenstelle 14, D-72076 Tübingen, Germany

1. INTRODUCTION

It is one of the basic aims of theoretical nuclear physics to develop an approximation scheme for the solution of the nuclear many-body problem, which determines the basic properties of directly from a realistic nucleon-nucleon (NN) interaction. Here we use the description realistic NN interaction for models like the One-Boson-Exchange (OBE) model [1], in which the parameters have been adjusted to obtain a detailed fit of the two-nucleon data, i.e. the NN scattering phase shifts and the properties of the deuteron.

These attempts are confronted with two major obstacles. The first one is the necessity to consider the effects of NN correlations which are due to the strong short-range and tensor components in a realistic NN interaction. The importance of the NN correlations is made obvious by the fact that no binding energy of nuclear systems is obtained if these correlations are ignored: A Hartree-Fock (HF) calculation employing e.g. a realistic OBE potential [1] would predict unbound nuclei. Various methods have been developed to include the effects of two-nucleon correlations. One possibility is the so-called Brueckner-Hartree-Fock (BHF) approximation. In this approach one considers a Slater-determinant, which should be an appropriate model wave-function for the nuclear system to be investigated. Solving the Bethe-Goldstone equation yields an effective interaction, the G-matrix, which depends on the bare NN interaction and the model wave-function considered. The self-consistency condition of BHF now requires that the model-wave function, which is needed to set up the Bethe-Goldstone equation, is made identical to the solution of the HF equations using the G-matrix as a kind of effective interaction.

The second obstacle is of a relativistic nature: the strong scalar-meson (σ) exchange part required in realistic meson-exchange potentials [1], gives rise to a significant modification of the Dirac structure of nucleons in the nuclear medium [2].

Therefore relativistic features should be included in the many-body theory of nuclear systems, in order to account for this effect. This modification of the Dirac spinors in the nuclear medium leads to a self-consistency problem beyond the BHF problem outlined above, which includes even the calculation of the matrix elements for the NN interaction, as the evaluation of the matrix elements for an OBE interaction requires the knowledge of the structure of these Dirac spinors. On the other hand the Dirac spinors are determined from the solution of the Dirac equation with a self-energy for the nucleons, which is calculated in terms of the G-matrix evaluated for the OBE interaction.

These self-consistency problems are simplified for nuclear matter since the translational symmetry of this infinite system requires plane waves for the single-particle wave functions to built up the Slater-determinant. Such Dirac BHF (DBHF) calculations have been performed for nuclear matter by, e. g., Shakin and collaborators [3], Brockmann and Machleidt [4], and ter Haar and Malfliet [5]. The basic aspects of this approach have been thoroughly investigated by Horowitz and Serot [6]. Due to the scalar field, the nucleon mass is reduced enhancing the ratio between small and large components of the Dirac spinors. This change in the Dirac spinors yields a reduction of the scalar density, which implies that the attraction due to the exchange of the σ meson in OBE potentials is reduced. At small densities of nuclear matter this loss of attraction is counterbalanced by a reduction of the kinetic energy, which is also caused by the medium dependence of the Dirac spinors. At larger densities the loss of attraction in the NN interaction overwhelms the loss of repulsion in the kinetic energy and for those densities the energy calculated in the DBHF approximation is less attractive than the corresponding energy calculated in the BHF approximation ignoring these relativistic effects.

Consequently the saturation points calculated for nuclear matter in DBHF approximation are shifted to smaller densities as compared to the BHF result. Brockmann and Machleidt succeeded in constructing a realistic OBE potential which fits NN scattering data and also yields DBHF results for nuclear matter in satisfying agreement with the empirical data [4]. The same feature is also observed for the potential "A", defined in table A.2 of ref.[1], which we will consider also in our present investigation.

This success of the DBHF approximation in nuclear matter gives rise to the hope that the same DBHF approximation may also be successful to reproduce the binding energies and radii of finite nuclei. From the discussion above, it is obvious, however, that a complete self-consistent calculation for finite nuclei is rather involved. Therefore we are going to investigate two approximations, in which either the effects of correlations or the relativistic effects are taken from studies of nuclear matter, while the respective other components of the calculation are treated in a self-consistent way directly for the finite nuclei. Some details of these methods and results of such studies [7,8] will be discussed in section 2.

In section 3 we will try to explore other "fingerprints" for the modifications of the Dirac spinors in the nuclear medium as predicted by the DBHF approach. As examples we will consider the relativistic effects on the spin-orbit splitting in the single-particle energies [9] and the energy-dependence of the central part of the optical potential for nucleon nucleus scattering [10].

In order to investigate the discrepancy remaining between the predictions of

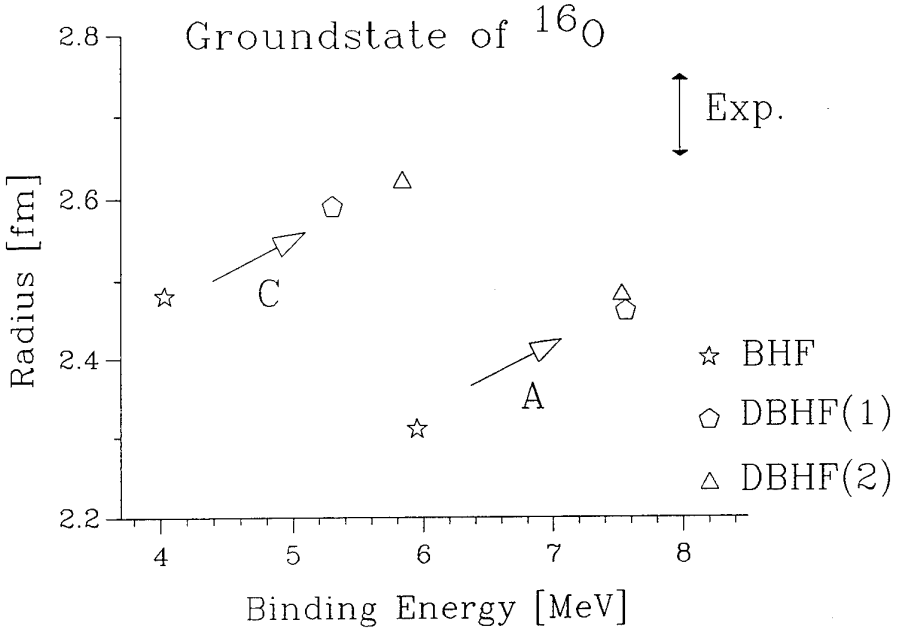

Figure 1. Results on binding energy per nucleon and radius of the charge distribution obtained from various approaches (see text) using OBE potentials A and C.

the DBHF and the experimental data on the groundstate properties of finite nuclei, we consider correlation effects beyond the lowest order Brueckner theory. Within the framework of the self-consistent Green function approach [11] an approximation scheme is presented in section 4, which describes the Green function in terms of a specified number of characteristic poles [12]. A short summary is given in the final section.

2. TWO WAYS TOWARDS DBHF FOR FINITE NUCLEI

For the first of the two approaches we are going to treat the effects of correlations directly for finite nuclei and approximate the Dirac effects from those of nuclear matter in terms of a local density approximation. For that purpose we determine the structure of the Dirac spinors, i.e. the ratio of small to large component in nuclear matter at various densities. Using these Dirac spinors we can evaluate for each density matrix elements of the OBE potential, leading to a density-dependent potential $V(\rho)$. For the various potentials at various densities one can solve the Bethe-Goldstone equation and the BHF problem for finite nuclei using conventional techniques [13,14]. The densities to be used in the calculation of the potential $V(\rho)$ are finally related to

the expectation values for the baryon densities in the different single-particle orbits ρ_i by requesting that for each pair of interacting nucleons, the density ρ is identical to the geometrical average of the densities for the interacting nucleons in orbits i and j.

Results of such DBHF calculations in this approximation "1" (DBHF(1)) on the binding energy and radius of the charge distribution of ^{16}O are displayed in figure 1. These results can be compared with those of a conventional BHF calculation using the same OBE potentials but ignoring the modifications of the Dirac spinors in the medium, i.e. using $V(\rho = 0)$. The BHF results for the 2 potentials A and C are similar to BHF results obtained with other realistic potentials, which means that the results are within the "Coester" band for ^{16}O [15]. Inclusion of the Dirac effects in DBHF(1) results in an increase of the calculated radius and a larger binding energy. This means that the results are significantly closer to the empirical data point. The original discrepancy between BHF and experiment is reduced by approximately a factor of 1/2.

In a second approximation to a self-consistent DBHF calculation for finite nuclei (DBHF(2)), we treat the relativistic effects directly for the finite system and account for correlation effects in a kind of local density approximation. For that purpose we define an effective meson exchange model for nuclear matter. The coupling constants for the effective σ and ω meson exchange are assumed to be density dependent and adjusted in such a way, that at each density the microscopic DBHF results for the binding energy and the self-energy in nuclear matter are reproduced in a Dirac-Hartree-Fock calculation of nuclear matter using this effective meson-exchange model. The density-dependence of the effective meson-coupling constants reflects the density-dependence of the correlation effects in the Brueckner G-matrix. For this effective meson-exchange model we then solve the Dirac-Hartree-Fock equation directly for the finite nucleus. The density parameter in the coupling constants is again related to the local densities determined from the final wave-functions.

Results for this DBHF(2) approximation are also included in figure 1. One finds that the results of DBHF(2) are very close to the corresponding results for the DBHF(1) approximation. As we have used two very different approximation schemes, we can argue that both approximations seem to be very reliable and should yield results very close to a complete DBHF calculation. These DBHF results form a new "Coester" band, which is much closer to the experimental point. Our result that Dirac effects reduce the discrepancy to the experimental point by roughly a factor 1/2, is supported by recent studies of Boersma and Malfliet [16], which are similar to our DBHF(2) calculations.

3. FINGERPRINTS OF RELATVISTIC EFFECTS

The discussion in the previous section demonstrated that the inclusion of relativistic effects in the sense, that Dirac spinors in the nuclear medium might be modified, tends to improve the results on binding energies and radii of nuclei. The next question is: Are there other indications in nuclear structure physics at low energies, which give further evidence to the importance of these relativistic effects. In order to discuss such features we assume that the relativistic self-energy for the nucleon can

be written as a sum of a scalar component and a timelike vector component

$$\hat{\Sigma}(\vec{r}) = \Sigma^s(\vec{r}) + \gamma^0\Sigma^0(\vec{r}) \tag{1}$$

In order to simplify the discussion we ignore the component, which transforms like a spacelike component of a vector, and assume that the components are local. The individual terms are large and of the order of a few hundred MeV, the scalar component Σ^s is attractive while the vector component Σ^0 is repulsive, leading to a cancellation in the sense that the combined effect for solutions of the Dirac equation of positive energy is slightly attractive, in agreement with the weak single-particle potential of nucleon in nuclei. Using an ansatz for the Dirac spinors in finite nuclei of the form [8]

$$\Psi_\alpha(\vec{r}) = \begin{pmatrix} G_a(r) \\ -iF_a(r)\,\vec{\sigma}\cdot\hat{r} \end{pmatrix} \mathcal{Y}_{\kappa_a,m_a}(\Omega) = \begin{pmatrix} g_\alpha(\vec{r}) \\ f_\alpha(\vec{r}) \end{pmatrix} , \tag{2}$$

the Dirac equation for a nucleon accounting for the self-energy of eq.(1) can be written in terms of two coupled first order differential equation for the large (g_α) and small component (f_α)

$$\begin{aligned} \left[m + \Sigma^s(\vec{r}) + \Sigma^0(\vec{r})\right] g_\alpha(\vec{r}) + \vec{\sigma}\frac{\hbar}{i}\vec{\nabla} f_\alpha(\vec{r}) &= E_\alpha g_\alpha(\vec{r}) \\ \vec{\sigma}\frac{\hbar}{i}\vec{\nabla} g_\alpha(\vec{r}) + \left[-m - \Sigma^s(\vec{r}) + \Sigma^0(\vec{r})\right] f_\alpha(\vec{r}) &= E_\alpha f_\alpha(\vec{r}) \end{aligned} \tag{3}$$

By eliminating the small component f_α these two coupled equations can be rewritten in a differential equation of second order for the large component [17], which has the form of a Schroedinger equation

$$\left[-\frac{\hbar^2}{2m}\Delta + U_c(\vec{r}) + \vec{l}\cdot\vec{\sigma}U_{ls}\right] g_\alpha(\vec{r}) = (E_\alpha - m) g_\alpha(\vec{r}) \, . \tag{4}$$

This Schroedinger equation, equivalent to the Dirac equation (3) exhibits two important features:

— It contains a spin orbit term U_{ls}. An inspection of this spin orbit term yields

$$U_{ls} \sim \frac{1}{m(m + \Sigma^s)} \tag{5}$$

— The potential in eq.(4) also contains a central component, which depends on the relativistic energy E of the nucleon to be considered, and can be written

$$U_c(r) = \Sigma^s(r) + \frac{\tilde{E}}{m}\Sigma^0(r) + \frac{\left(\Sigma^s(r)\right)^2 - \left(\Sigma^0(r)\right)^2 + U_{\text{Darwin}}(r)}{2m} \tag{6}$$

with

$$\begin{aligned} U_{\text{Darwin}}(r) =& \frac{3}{4}\left[\frac{1}{D(r)}\frac{dD(r)}{dr}\right]^2 - \frac{1}{rD(r)}\frac{dD(r)}{dr} - \frac{1}{2D(r)}\frac{d^2D(r)}{dr^2} \, , \\ D(r) =& m + E + \Sigma^s(r) - \Sigma^0(r) \, . \end{aligned} \tag{7}$$

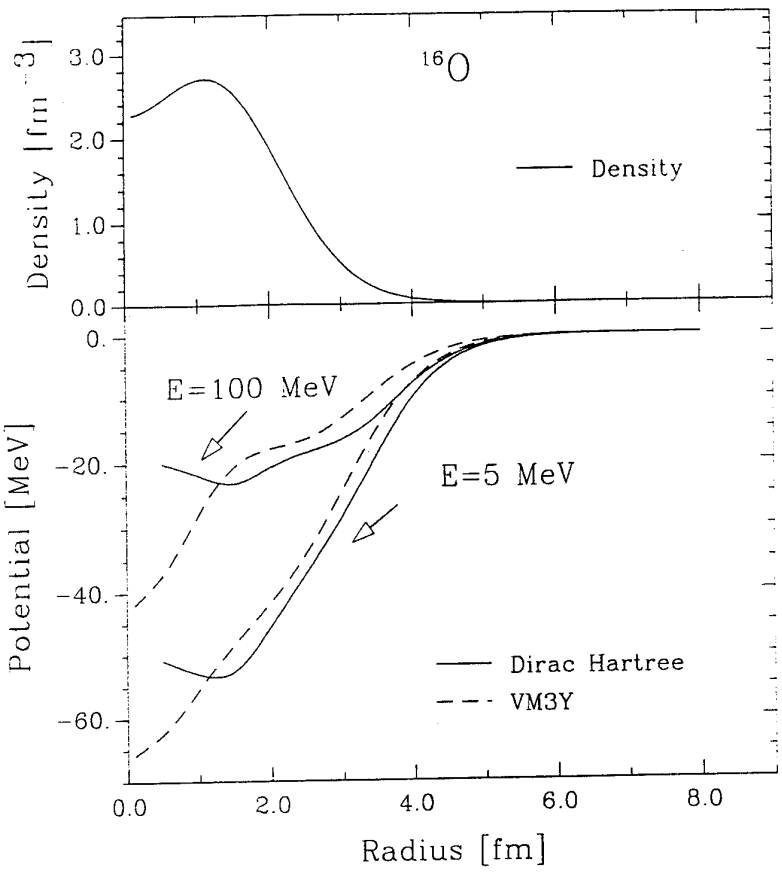

Figure 2. Density distribution and optical potential for ^{16}O. The density distribution displayed in the upper part of the figure has been obtained from the Dirac Hartree calculation of Ref.[8]. For this distribution the local equivalent optical potential of nucleon scattering have been calculated for energies of 5 MeV and 100 MeV, using the Dirac Hartree (solid line) and the non-relativistic folding potential calculated for the M3Y potential (dashed curve)

We will first discuss some features of the spin-orbit term for the example of the spin-orbit splitting of the $p_{3/2}$ and $p_{1/2}$ hole states in ^{16}O and compare it to the splitting of the $d_{5/2}$ and $d_{3/2}$ particle states. Inspecting the experimental data, it is remarkable that the splitting of the d-states is smaller (5.09 MeV) than the splitting of the p orbits (6.18 MeV). Simple spin-orbit terms tend to yield larger values proportional to the orbital angular momentum, i.e. larger splittings for $l = 2$ than for $l = 1$. Also BHF calculations and non-relativistic calculations with inclusion of correction terms in the single-particle potentials predict a larger spin-orbit splitting for the d-shell than for the p-shell [9]. The experimental result can be reproduced only after inclusion of the relativistic effects. The result can be easily understood in terms of the analysis made above. From eq.(5) one can see that the spin orbit term

is large if the effective mass ($m^* = m + \Sigma^s$) is small. This is the case inside the nucleus, where Σ^s is very attractive and reflected in a large spin-orbit splitting for the p-orbits. On the other hand, the local density for the d-orbits is smaller, which leads to a weaker Σ^s and to a weaker spin-orbit term.

It is worth noting that the relativistic effects not only yield a correct description of the spin orbit splitting for the d-shell as compared to the p-shell. If correlation effects are taken into account (2particle-1hole and 3particle-2hole contributions to the self-energy) one obtains also a quantitative description of the spin-orbit term. Also within a non-relativistic many-body calculation one can reproduce the spin-orbit splitting of the p-shell, if the effects of a 3-body force are taken into account [18]. It is not clear, however, whether this 3-body force will also lead to a proper result for the splitting in the d-shell.

In figure 2 we display the baryon density resulting from a Dirac-Hartree calculation for ^{16}O. The coupling constants for the mesons have been determined as described above for DBHF(2), however, restricting the analysis in nuclear matter and also the calculation in finite nuclei to the Dirac-Hartree approximation. The lower part of figure 2 exhibits the local equivalent potential $U_c(r)$ of eq.(7)) for the scattering of nucleons with incident energies of 5 and 100 MeV. According to eq.(5) the contribution of the repulsive vector component Σ^0 is enhanced at the higher energy as compared to the lower energy, leading to a less attractive U_c at 100 MeV. This energy dependence of the real part in the optical potential is needed to reproduce the empirical data of elastic nucleon-nucleus scattering data. This can be seen from the upper part of figure 3, which compares the scattering phase shifts for $l = 0$ nucleons derived from the Dirac equation or the corresponding Schroedinger equivalent potential with empirical phase shifts [19]. To visualize the importance of the energy-dependence we also show results, which are obtained using the Schroedinger equivalent potential for nucleons at 5 MeV for all energies.

Also for the case of nucleon-nucleus scattering one can find mechanisms within a non-relativistic description of nuclear systems, which yield a local potential for nucleon-nucleus scattering, which exhibits the energy-dependence required from experiment. As an example we mention the non-relativistic parameterization of the G-matrix provided by the M3Y approach [20]. It should be mentioned, however, that other non-relativistic parameterizations [21] show similar features. As we want to explore the differences between a relativistic and non-relativistic evaluation of the mean-field contribution to the optical potential, independent on the underlying baryon density, we use the same density distribution as in the Dirac-Hartree approach. For these densities we determine the scattering potential, including the exchange term in a local form with the Slater approximation for the mixed density $\rho(r, r')$ [10].

The resulting local potentials are also displayed in figure 2 (dashed curves) again for nucleons with energies of 5 and 100 MeV. The shapes of the M3Y potentials deviate from those obtained in the Dirac-Hartree approach in a distinct manner. The M3Y potentials tend to be less attractive at the surface and more attractive close to the center. The energy dependence of these local potentials, however, seems to be quite similar to the one obtained in the Dirac-Hartree approach. This can also be seen from the lower half of figure 3, where the phase shifts evaluated with the M3Y folding potential are compared again with empirical data. Fixing the energy-dependence of

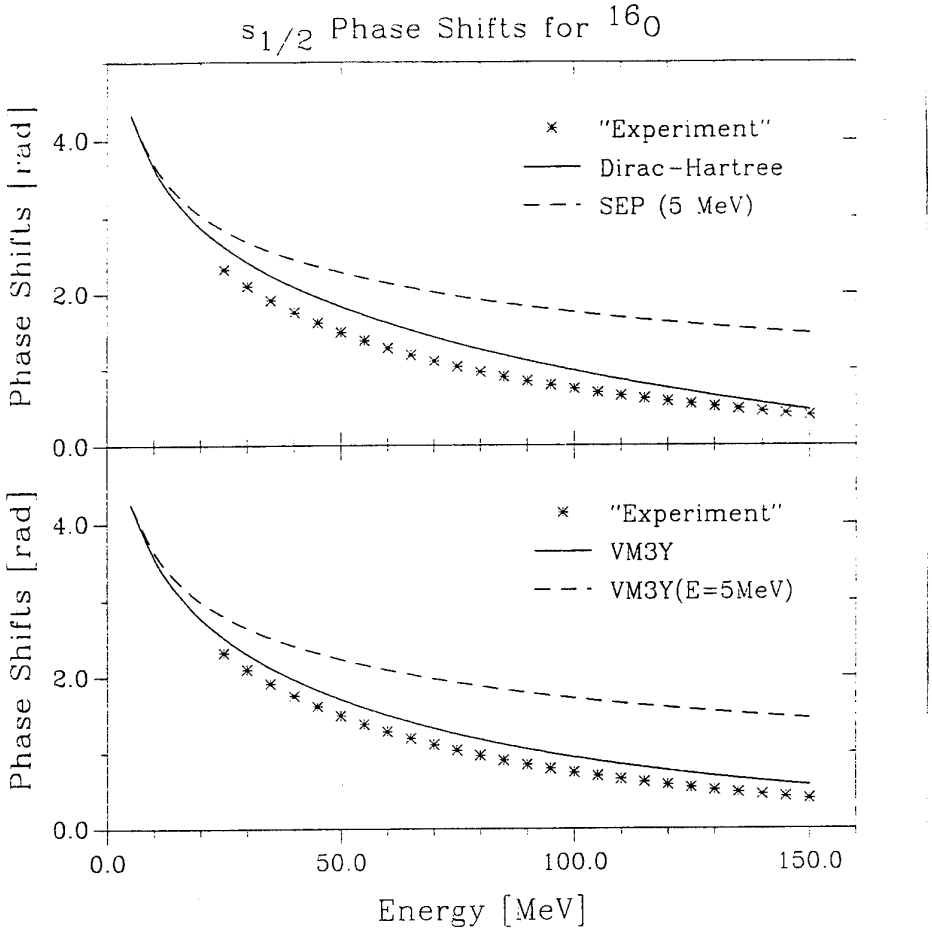

Figure 3. Phase shifts for $l = 0$ scattering on ^{16}O at various energies of the scattered nucleon. Results of the Dirac Hartree calculation are displayed in the upper part while those obtained from the non-relativistic M3Y potential are given in the lower part of the figure. Beside the results of the consistent calculations (solid lines) also phase-shifts obtained for the equivalent local potential at a fixed energy of 5 MeV (dashed line) are presented. For comparison also the phase-shifts obtained from the empirical fit of Ref.[19] are displayed as "experimental" data.

the local potential equivalent to the Fock exchange term again to the one of nucleons at 5 MeV, the dashed curve is obtained.

Within the non-relativistic description, the energy or momentum dependence is due to the strong Fock exchange term in the M3Y parameterization. If one calculates the binding of nuclear matter with this effective interaction, one finds that the dominating contribution to the potential energy arises from the Fock exchange terms. One finds that the Hartree term only yields about 25 percent of the total attraction.

4. BAGEL APPROXIMATION FOR THE GREEN FUNCTION

In the discussion so far we have restricted the discussion of correlation effects to the short-range correlations as they are taken into account in the BHF approximation. In this section we would like to discuss a technique, which allows a systematic extension of this BHF treatment in terms a self-consistent Green function approach. For a first application of this method we consider correlations within a model space, taking into account configurations in an oscillator basis up to and including the 0h1f2p shell. Short-range correlations outside the model space are taken into account by performing all calculations in terms of an appropriate model-space hamiltonian, which is derived from the G-matrix assuming an appropriate Pauli operator for that model space [22]. The contributions to the irreducible self-energy, which are of second order in this residual model space interaction can be written into the form

$$\Sigma^{(2)}_{\alpha\beta}(\omega) = \frac{1}{2}\sum_{p_1,p_2,h} \frac{< \alpha h|G|p_1p_2 >< p_1p_2|G|\beta h >}{\omega - e(p_1,p_2,h) + i\eta} + \frac{1}{2}\sum_{h_1,h_2,p} \frac{< \alpha p|G|h_1h_2 >< h_1h_2|G|\beta p >}{\omega - e(h_1,h_2,p) - i\eta} \tag{8}$$

where we have introduced the abbreviation $e(\alpha,\beta,\gamma) = \epsilon^{HF}_\alpha + \epsilon^{HF}_\beta - \epsilon^{HF}_\gamma$, and the ϵ^{HF}_α are the HF single-particle energies. In eq. (8)) the summations on particle labels like p_1, p_2 and p are restricted to those single-particle states within the model space, which are above the Fermi level, whereas the labels h_1, h_2 and h refer to hole states. It is evident that the first term on the right hand side of eq. (8) refers to the 2 particle - 1 hole contribution to the self-energy, which is already accounted for in the BHF approach, while the second term defines 2 hole - 1 particle contribution. This self-energy can now be inserted into a Dyson equation for the Green function $\mathcal{G}_{\alpha\beta}(\omega)$ taking into account the correlation effects contained in $\Sigma^{(2)}$

$$\mathcal{G}_{\alpha\beta}(\omega) = \delta_{\alpha\beta}g_\alpha(\omega) + \sum_\gamma g_\alpha(\omega)\Sigma_{\alpha\gamma}(\omega)\mathcal{G}_{\gamma\beta}(\omega) \tag{9}$$

$$= \sum_n \frac{< \Psi^A_0|a_\alpha|\Psi^{A+1}_n >< \Psi^{A+1}_n|a^\dagger_\beta|\Psi_0 >}{\omega - \omega^+_n + i\eta} + \sum_m \frac{< \Psi^A_0|a^\dagger_\beta|\Psi^{A-1}_m >< \Psi^{A-1}_m|a_\alpha|\Psi_0 >}{\omega - \omega^-_m - i\eta}\,. \tag{10}$$

The second line (eq.(10)) exhibits the Lehmann representation of the single-particle Green function in terms of the spectroscopic amplitudes $< \Psi^A_0|a_\alpha|\Psi^{A+1}_n >$ and $< \Psi^{A+1}_n|a^\dagger_\alpha|\Psi_0 >$, where a_α ($a^\dagger_\beta$) stands for the single-particle annihilation (creation) operator in the HF basis. The state Ψ^A_0 refers to the ground-state of the A-particle system, while Ψ^{A+1}_n (Ψ^{A-1}_m) stands for the states of the A+1-particle (A-1) system as obtained in the present approach. Also the energy variables $\omega^+_n = E^{A+1}_n - E^A_0$ and $\omega^-_m = E^A_0 - E^{A-1}_m$ are defined in terms of energies obtained for the states of the nuclei with A, $A+1$ and $A-1$ nucleons. The substantial ingredients of the Lehmann

representation of eq. (10) can be obtained from a solution of an eigenvalue problem [23]

$$\begin{pmatrix} \epsilon_\alpha^{HF} & 0 & a_1 & \dots & a_K & A_1 & \dots & A_L \\ 0 & \epsilon_\beta^{HF} & b_1 & \dots & b_K & B_1 & \dots & B_L \\ a_1 & b_1 & e_1 & & & 0 & & \\ \vdots & \vdots & & \ddots & & & & \\ a_K & b_K & 0 & & e_K & & & 0 \\ A_1 & B_1 & & & & E_1 & & \\ \vdots & \vdots & & & & & \ddots & \\ A_L & B_L & 0 & \dots & 0 & & \dots & E_L \end{pmatrix} \begin{pmatrix} X^n_{0,\alpha} \\ X^n_{0,\beta} \\ X^N_1 \\ \vdots \\ X^n_K \\ Y^n_1 \\ \vdots \\ Y^n_L \end{pmatrix} = \omega_n \begin{pmatrix} X^n_{0,\alpha} \\ X^n_{0,\beta} \\ X^n_1 \\ \vdots \\ X^n_K \\ Y^n_1 \\ \vdots \\ Y^n_L \end{pmatrix} . \qquad (11)$$

In writing this equation, we assume that for a given set of conserved quantum numbers (parity, isospin, angular momentum) we have in our model space two HF single-particle states (α, β) and K 2p1h configurations with energies e_i and connecting matrix elements $a_i =< \alpha h|G|p_1p_2 >$. Corresponding for the 2h1p energies E_j and matrix elements b_j. The central point of the BAGEL approximation is to determine the energy and the spectroscopic amplitude of a few "characteristic" states of the $A \pm 1$ system. For that purpose we start from the single-particle states and generate a few more basic 2p1h and 2h1p configurations by applying the corresponding part of the matrix in (11) to the single-particle state. In this way we generate a basis of 2p1h and 2h1p configurations like in the Lanczos scheme for matrix diagonalization (BAGEL = BAsis GEnerated by Lanczos method). It turns out that it is sufficient for many purposes to consider a BAGEL basis with a few basis states only (lets say M 2p1h states and N 2h1p states). The eigenvalues and spectroscopic amplitudes determined from such a BAGEL(M,N) approximation define a single-particle Green function according to eq. (10), which is a very accurate approximation in many investigations.

This approximate Green function contains only a few pole terms. Therefore it may be used to replace the HF approximation of the single-particle Green function in calculating the self-energy (eq.8). This allows a self-consistent treatment of the self-energy and the solution of the Dyson equation [12], which is required to obtain a number conserving approximation for the Green function [11]. Rather stable results (stable with respect to an increase of the BAGEL parameters M and N) are also obtain for the spectral function [23]. A "smoothed" spectral function may be defined by

$$S_\alpha(\omega) = \frac{1}{\sqrt{\pi}\Gamma}\Big[\sum_n \exp -\frac{(\omega-\omega_n^+)^2}{\Gamma^2}| < \Psi_n^{A+1}|a_\alpha^\dagger|\Psi_0 > |^2 + \sum_m \exp -\frac{(\omega-\omega_m^-)^2}{\Gamma^2}| < \Psi_m^{A-1}|a_\alpha|\Psi_0 > |^2\Big] . \qquad (12)$$

In this equation the summation over n is restricted to the poles ω_n^+ above the Fermi energy E_F and the summation over m to those below the Fermi energy. Results for the spectral function at energies below the Fermi energy for ^{40}Ca are displayed in figure 4 and compared to experimental data derived from $(e,e')p$ experiments [24].

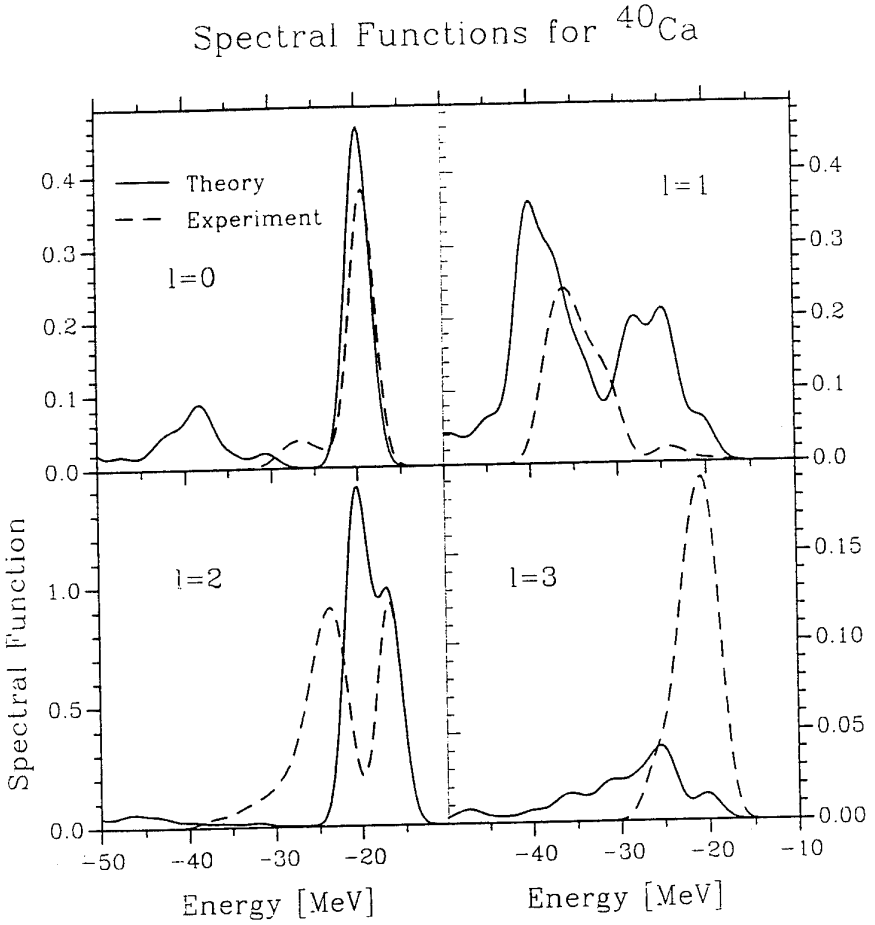

Figure 4. Spectral functions obtained for the nucleus ^{40}Ca for the various orbital angular momenta l in an energy interval [-50 MeV, -10 MeV]. The experimental data are from ref. [24]. Note the different scales for the spectral function in the various parts of the figure

The BAGEL approximation to the single-particle Green function can also be used to evaluate occupation probabilities and expectation values for the radius and the binding energy. Within the model space considered, the inclusion of hole-hole terms yields an extra binding energy (beyond BHF) of around 0.5 MeV per nucleon and an increase of the radius of 0.1 fm for nuclei like 16O and ^{40}Ca [22]. The effect of the hole-hole terms is not very large, it could be sufficient, however, to explain the discrepancy remaining between DBHF and the experimental data.

5. CONCLUSIONS

From the results of our calculations we conclude that the relativistic effects contained in the DBHF approach are very useful to improve our understanding of nuclear structure at low energies. The Dirac effects improve the microscopic description of ground-state properties of finite nuclei considerably. It is quite possible that an extension of the DBHF approach, which accounts also for hole-hole scattering terms [5,22,25] will yield results, which are in good agreement with the experimental data. The Dirac effects provide a very simple explanation for the features of the spin-orbit terms and the energy-dependence of the optical potential. These phenomena may also be described within a non-relativistic approach employing 3-body forces and strong Fock-exchange contributions to the mean field. Therefore it remains a challenge to look for further fingerprints of relativistic effects in nuclear structure physics at low energy. Finally we consider a very powerful approximation scheme for the self-consistent Green function method. This scheme could be used in non-relativistic as well as in relativistic studies of many-body systems.

The work I have been presenting has been done mainly in collaboration with R. Fritz and M. Kleinmann, PhD students of the "Graduiertenkolleg Struktur und Wechselwirkung von Hadronen und Kernen" in Tübingen, and L.D. Skouras from N.R.C.P.S. Demokritos (Greece). I would like to acknowledge the collaboration and the financial support by the DFG (Mu 705/3) and the BMFT.

REFERENCES

[1] R. Machleidt, Adv. in Nucl. Phys. **19**, 189 (1989).
[2] B.D. Serot and J.D. Walecka, Adv. in Nucl. Phys. **16**, 1 (1986).
[3] M.R. Anastasio, L.S. Celenza, W.S. Pong, and C.M. Shakin, Phys. Rep. **100**, 327 (1978).
[4] R. Brockmann and R. Machleidt, Phys. Lett. **149B** 283, (1984).
[5] B. ter Haar and R. Malfliet, Phys. Rep. **149** 207, (1987).
[6] C. J. Horowitz and B. D. Serot, Nucl. Phys. **A464**, 613 (1987).
[7] R, Fritz, H. Müther, and R. Machleidt, Phys. Rev. Lett. **71**, 46 (1993).
[8] R. Fritz and H. Müther, Phys. Rev. **C49**, 633 (1994).
[9] L. Zamick, D.C. Zheng and H. Müther, Phys. Rev. **C45**, 2763 (1992).
[10] M. Kleinmann, R. Fritz, H. Müther, and A. Ramos, Nucl. Phys., in print
[11] W.H. Dickhoff and H. Müther, Reports on Progress in Physics **11**, 1947 (1992).
[12] H. Müther and L.D. Skouras, Phys. Lett. **B 306**, 201 (1993).
[13] H. Müther and P.U. Sauer, *Computational Nuclear Physics 2*, edited by K. Langanke et.al. (Springer, New York 1993) page 30.
[14] H. Müther, R. Machleidt, and R. Brockmann, Phys. Lett. **B 202**, 483 (1988); Phys. Rev. **C 42**, 1981 (1990).
[15] K.W. Schmid, H. Müther, and R. Machleidt, Nucl. Phys. **A530**, 14 (1991).
[16] H.F. Boersma and R. Malfliet, Phys. Rev. **C49**, 233 (1994).
[17] M. Jaminon and C. Mahaux, Phys. Rev. **C40**, 354 (1989).
[18] S.C. Pieper and V.R. Pandharipande, Phys. Rev. Lett. **70**, 2541 (1993).
[19] S. Hama, B.C. Clark, E.D. Cooper, H.S. Sherif, and R.L. Mercer, Phys. Rev. **C41**, 2737 (1990).

[20] G. Bertsch, J. Borysowicz, H. McManus, and W.G. Love, Nucl. Phys. **A 284**, 399 (1977).
[21] P. Czerski, H. Müther, and W.H. Dickhoff, J. Phys. **G 20**, 425 (1994).
[22] H. Müther and L. Skouras, to be published
[23] H. Müther and L. Skouras, Nucl. Phys. **A555**, 541 (1993).
[24] G. Kramer, thesis (University of Amsterdam, 1990)
[25] M.F. Jiang, T.T.S. Kuo, and H. Müther, Phys. Rev. **C40**, 1836 (1989).

CORRELATED DENSITY MATRIX THEORY OF HOMOGENEOUS BOSE SYSTEMS

M. L. Ristig, R. Pantförder, M. Serhan, and G. Senger

Institut für Theoretische Physik,
Universität zu Köln,
D–50937 Köln, Germany.

1. INTRODUCTION

An advanced many-body theory such as the correlated basis functions (CBF) approach [1–3] may provide a unified and adequate formal basis for analyzing and calculating the fundamental structures and properties of quantum fluids, Coulomb liquids, lattice gauge models, spin-systems and other correlated systems with many degrees of freedom, at zero temperature [4–9].

CBF theory may be suitably generalized to the regime of nonzero temperatures $T = (k_B\beta)^{-1}$ (correlated density matrix theory [10]) thus permitting a qualitative structural description of the equilibrium properties of correlated many-body systems and their inherent phase transitions. Steps in this direction have been taken in Refs. [11–14] and Ref. [15], respectively, on the Bose-condensed and the normal phase of liquid ^{4}He or other boson fluids. In the present contribution we outline a unified formalism for dealing with both phases on an equal level that, for example, allows – in a future analysis – a microscopic numerical study of the Bose–Einstein transition.

In CBF theory one seeks an understanding of certain N-body states (ground states and elementary excited states) generated by a Hamiltonian

$$\mathcal{H} = \mathcal{T} + \mathcal{V} = -\sum_{j}^{N} \frac{\hbar^2}{2m} \Delta_j + \sum_{i<j}^{N} v(r_{ij}), \tag{1}$$

for N particles confined to a box of volume Ω in terms of an appropriate set of optimized trial wave functions. The optimization procedure is based on the minimum principle for the ground state energy and the excitation energies, evaluated in the thermodynamic limit ($N/\Omega = \rho =$ constant; $N, \Omega \to \infty$) [2]. At $T > 0$, instead of

working with correlated wave functions, one works with trial N-body density matrices which include the most important correlation effects.

The correlated density matrix approach rests on the Gibbs–Delbrück–Molière minimum principle [10] for the Helmholtz free energy, $F_0 \leq F[\mathcal{W}]$, with a trial N-body density matrix $\mathcal{W}$. For utilizing this theorem we need an explicit construction of the internal energy functional $E[\mathcal{W}] = \mathrm{Tr}\{\mathcal{W}\mathcal{H}\}$ in coordinate space representation,

$$E = \int d\mathbf{R} \int d\mathbf{R}' \delta(\mathbf{R} - \mathbf{R}') \Big\{ \sum_j^N \frac{\hbar^2}{2m} (\nabla_j' \cdot \nabla_j - \Delta_j) + \sum_{i<j}^N v(r_{ij}) \Big\} W(\mathbf{R}, \mathbf{R}') \quad (2)$$

and of the entropy of the system. The configuration of particles $i = 1, 2, ..., N$ is specified by the vector $\mathbf{R} = (\mathbf{r}_1, \mathbf{r}_2, ..., \mathbf{r}_N)$ and $W(\mathbf{R}, \mathbf{R}')$ is a matrix element of $\mathcal{W}$ in coordinate space.

A structural analysis of the multidimensional integral (2) on which we will concentrate in the present study (leaving a study of the entropy to the future) necessitates an explicit evaluation of the radial distribution function,

$$\rho^2 g(|\mathbf{r}_1 - \mathbf{r}_2|) = N(N-1) \int d\mathbf{R}^{(1,2)} W(\mathbf{R}, \mathbf{R}) \quad (3)$$

and its differing components (Section 3). The expression (2) further involves a certain functional derivative $G_{cc}(r)$, i.e., the cyclic distribution function [15].

In addition to the diagonal matrix elements (3) of the reduced two-body density matrix we are also interested in the matrix elements of the reduced one-body density matrix,

$$\rho \rho_1(|\mathbf{r}_1 - \mathbf{r}_1'|) = N \int d\mathbf{R}^{(1)} W(\mathbf{r}_1, \mathbf{R}^{(1)}; \mathbf{r}_1', \mathbf{R}^{(1)}). \quad (4)$$

The integrations in Eqs. (3) and (4) extend over the coordinates $\mathbf{R}^{(1,2)} = (\mathbf{r}_3, ..., \mathbf{r}_N)$ and $\mathbf{R}^{(1)} = (\mathbf{r}_2, ..., \mathbf{r}_N)$, respectively.

If matrix (4) is known we may calculate the momentum distribution of the thermodynamic state by taking the Fourier transform [16],

$$n(k) = n_0 N \delta_{\mathbf{k}0} + \rho \int d\mathbf{r} [\rho_1(r) - \rho_1(\infty)] e^{i\mathbf{k}\cdot\mathbf{r}}. \quad (5)$$

In the Bose-condensed phase the function $\rho_1(r)$ possesses long-range order, $\rho_1(\infty) > 0$, that gives rise to a nonzero value $n_0 > 0$ for the condensate fraction.

In Sections 2 to 4 we develop a microscopic analysis of the reduced matrix elements (3), (4), and present an explicit expression for the internal energy functional (2) that is susceptible for quantitative enumerations. Section 5 summarizes the major results. References [17–19] give a more elaborate report on the present status and future prospects of correlated density matrix theory.

2. REDUCED DENSITY MATRICES

The analysis of the reduced density matrices (3), (4), and related quantities such as the internal energy (2) of interest here may be based on the factor decomposition of the N-body density matrix $\mathcal{W}$ in coordinate space representation [10],

$$W(\mathbf{R},\mathbf{R}') = \mathcal{I}^{-1}\Phi(\mathbf{R})Q(\mathbf{R},\mathbf{R}')\Phi(\mathbf{R}'), \tag{6}$$

where $\mathcal{W}$ is unit-normalized, $\int d\mathbf{R}W(\mathbf{R},\mathbf{R}) = 1$.

For an adequate description of the correlations induced by the two-body potential $v(r)$ at a given temperature we propose that the wave function $\Phi(\mathbf{R})$ is of Jastrow type [10, 15],

$$\Phi(\mathbf{R}) = \exp\frac{1}{2}\sum_{i<j}^{N} u(r_{ij}) \tag{7}$$

or, more accurately, is a Feenberg wave function [20]. For the incoherence factor Q we adopt – in an initial step – the projected ansatz [17]

$$Q(\mathbf{R},\mathbf{R}') = \frac{1}{2\pi i}\oint\frac{dz}{z}e^{1/z}\underset{ij}{\mathrm{Perm}}\{\Gamma(|\mathbf{r}_i - \mathbf{r}'_j|) + Bz\}. \tag{8}$$

The integration in Eq. (8) is to be performed in a mathematically positive direction along a closed path around the origin in the complex z-plane. The function $\Gamma(r)$ is of short range. Nonzero values of the parameter B ($0 \leq B \leq 1$) permit the appearance of off-diagonal long-range order in the density matrix $\rho_1(r)$. This phenomenon is a distinctive signature of a Bose-condensed phase. The normal phase is characterized by $B \equiv 0$. To include effects of phonon excitations one may enlarge the class of functions $Q(\mathbf{R},\mathbf{R}')$ by a factor [21, 10, 15]

$$Q_{ph}(\mathbf{R},\mathbf{R}') = \exp\sum_{i<j}^{N}\gamma(|\mathbf{r}_i - \mathbf{r}'_j|) \tag{9}$$

containing a function $\gamma(r)$ that vanishes asymptotically.

Here we ignore the factor (9) and focus our attention on ansatz (8) in conjunction with Eq. (7). We note that this prescription reduces correctly to the exact density matrix describing the ideal Bose gas [22] by setting $u(r) \equiv 0$ and $\Gamma(r) = \exp[-\pi(r/\lambda)^2]$ where $\lambda = (2\pi\beta\hbar^2/m)^{\frac{1}{2}}$ is the thermal wave length.

For an explicit construction of the internal energy functional and the distribution functions involved we begin our study with the normalization integral

$$\mathcal{I}[u,\Gamma,B] = \int d\mathbf{R}\Phi^2(\mathbf{R})Q(\mathbf{R},\mathbf{R}) \tag{10}$$

and its functional derivatives [15]

$$g(r) = \frac{2}{N}\frac{\delta\ln\mathcal{I}}{\delta u(r)}, \tag{11}$$

$$G_{cc}^{(B)}(r) = \frac{1}{N}\frac{\delta \ln \mathcal{I}}{\delta \Gamma(r)}. \tag{12}$$

In terms of the radial distribution function (11) and the cyclic distribution function (12) the energy (2) reads

$$\frac{E}{N} = \frac{1}{2}\rho \int d\mathbf{r} v^*(r) g(r) + \rho \frac{\hbar^2}{4m} \int d\mathbf{r} \{-\Delta\Gamma(r) + [\nabla_1 \Gamma(r)] \cdot \nabla_1^{(\Gamma)}\} G_{cc}^{(B)}(r), \tag{13}$$

with the Jackson–Feenberg effective potential [2] $v^*(r) = v(r) - (\hbar^2/4m)\Delta u(r)$ and the operator $\nabla_1^{(\Gamma)}$ acting as specified in Ref. [15]. When operating on a term consisting of a Dirac delta function with a constant strength factor, $\nabla_1^{(\Gamma)}$ acts as an ordinary gradient with respect to the coordinate $\mathbf{r}_1$. On the other hand, when operating on a continuous function of $\mathbf{r}_{12}$, it replaces the statistical bond Γ involving coordinate $\mathbf{r}_1$ by its derivative, if such a bond is present in the function, and otherwise yields zero. These are the only possibilities that arise.

To evaluate the reduced one-body density matrix (4) we introduce the generalized normalization integral [18, 19]

$$\mathcal{I}_{2,N-1}[u_{ab}, \Gamma_{ab}, B_a] = \int d\mathbf{r}_1' \int d\mathbf{R} \Phi^2(\mathbf{r}_1', \mathbf{R}) Q(\mathbf{r}_1', \mathbf{R}; \mathbf{r}_1', \mathbf{R}) \tag{14}$$

with $a = 1$ or 2 and $(ab) = (11)$, (12), (21), or (22). The expression (14) is the standard normalization integral for a two-component mixture of $N_1 = 2$ bosons of type 1 with coordinates $\mathbf{r}_1$ and $\mathbf{r}_1'$ and $N_2 = N - 1$ bosons of type 2 with coordinates $\mathbf{R}^{(1)} = (\mathbf{r}_2, ..., \mathbf{r}_N)$. The dynamical and statistical functions corresponding to the two types of bosons in this fictitious mixture are of the special forms $u_{11}(r) = 0, u_{12}(r) = u_{21}(r) = \frac{1}{2}u(r), u_{22}(r) = u(r)$ and $\Gamma_{12}(r) = \Gamma_{21}(r) = \Gamma_{22}(r) = \Gamma(r)$, respectively. Finally, the parameter B_2 takes the value B. The one-body density matrix (4) is then constructed [18, 19] from the integrals (10) and (14),

$$\rho_1(r) = \frac{1}{2}\rho \frac{\mathcal{I}_{2,N-1}}{\mathcal{I}} \frac{\delta \ln \mathcal{I}_{2,N-1}}{\delta \Gamma_{11}(r)}\Big|_{B_1 = B, \Gamma_{11} = \Gamma}. \tag{15}$$

The explicit calculation of the logarithms of the quantities (10) and (14) can be performed by employing standard cluster developments [3, 15, 23] in terms of generalized Ursell–Mayer diagrams [24].

3. SPATIAL DISTRIBUTION FUNCTIONS

The spatial distribution functions (11) and (12) may be evaluated in the thermodynamic limit by constructing an associated generating functional Λ defined in terms of the normalization integral (10) through the relation $\mathcal{I}[u, \Gamma, B] = \Omega^N \exp N\Lambda[u, \Gamma, B]$ where $N \to \infty$. This generator Λ may be systematically evaluated and analysed in terms of standard cluster expansion procedures [2, 3, 15, 17]. Given an expression

for this functional we may thereupon evaluate the functions (11) and (12) in the thermodynamic limit by taking the variational derivatives

$$g(r) = 2\frac{\delta\Lambda[u,\Gamma,B]}{\delta u(r)}\,, \tag{16}$$

$$G_{cc}^{(B)}(r) = \frac{\delta\Lambda[u,\Gamma,B]}{\delta\Gamma(r)}\,. \tag{17}$$

Inspecting the results of this cluster development [15, 17] we may decompose the generator into reducible (factorizable) and irreducible components,

$$\Lambda[u,\Gamma,B] = \Lambda_{\rm irr}[u,\Gamma,B] + \Lambda_{\rm red}[u,\Gamma,B]\,. \tag{18}$$

This result enables us to perform massive resummations of the original expansions yielding compact expressions in terms of irreducible cluster contributions for functions (16) and (17),

$$g(r) = 2\frac{\delta\Lambda_{\rm irr}[u,\Gamma_{cc},B_{cc}]}{\delta u(r)}\,, \tag{19}$$

$$\Gamma(r)G_{cc}^{(B)}(r) = \Gamma_{cc}(r)\Big\{\rho^{-1}\delta(\mathbf{r}) + \frac{\delta\Lambda_{\rm irr}[u,\Gamma_{cc},B_{cc}]}{\delta\Gamma_{cc}(r)}\Big\}\,. \tag{20}$$

In Eqs. (19) and (20) the bare statistical function $\Gamma(r)$ and parameter B appearing in the irreducible generator $\Lambda_{\rm irr}$ are replaced by properly dressed quantities $\Gamma_{cc}(r) = c\Gamma(r)$ and $B_{cc} = b^2cB$. Explicit expressions for the positive renormalization constants c and b are constructed in Ref. [17].

Defining the function $G_{cc}(r) = \delta\Lambda_{\rm irr}[u,\Gamma_{cc},B_{cc}]/\delta\Gamma_{cc}(r)$ we may employ Eqs. (19), (20) to recast the expression (13) for the internal energy into the compact form

$$\begin{aligned}\frac{E}{N} &= \frac{1}{2}\rho\int d\mathbf{r}v^*(r)g(r) - \int d\mathbf{r}\delta(\mathbf{r})\frac{\hbar^2}{2m}\Delta\Gamma_{cc}(r)\\ &\quad + \rho\frac{\hbar^2}{4m}\int d\mathbf{r}\{-\Delta\Gamma_{cc}(r) + (\nabla_1\Gamma_{cc}(r))\cdot\nabla_1^{(\Gamma)}\}G_{cc}(r)\,.\end{aligned} \tag{21}$$

The irreducible forms (19) and (20) are now susceptible to a standard hypernetted-chain (HNC) analysis [3, 15, 17]. In a crucial first step one decomposes functions $g(r)$ and $G_{cc}(r)$ into differing components according to the topology of the statistical bonds $\Gamma_{cc}(r)$ in the diagrammatic representations of these distribution functions. A thorough classification of the set of graphic contributions leads to the decomposition

$$\begin{aligned}g(r) &= 1 + G_{dd}(r) + 2G_{de}(r) + G_{ee}(r)\\ &\quad + 2B_{cc}\big\{2G_{dc}(r) + 2G_{ec}(r) + G_{cc}^{(0)}(r) + 2B_{cc}G_{cc}^{(1)}(r)\big\}\end{aligned} \tag{22}$$

for the radial distribution function (19). The partial distribution functions $G_{dd}(r)$, $G_{de}(r)$, and $G_{ee}(r)$ completely characterize the spatial correlations in the normal phase [15]. The partial distribution functions $G_{dc}(r)$, $G_{ec}(r)$, $G_{cc}^{(0)}(r)$ and $G_{cc}^{(1)}(r)$ only contribute if the system is condensed ($B_{cc} > 0$) [17]. Note that $G_{de} = G_{ed}$, $G_{dc} = G_{cd}$, and $G_{ec} = G_{ce}$.

The analogous decomposition of the cyclic distribution function $G_{cc}(r)$ reads

$$G_{cc}(r) = G_{cc}^{(0)}(r) + B_{cc}\{1 + G_{dd}(r) + 2G_{dc}(r) + G_{cc}^{(1)}(r)\}\,. \tag{23}$$

We may separate the various (G) components of functions (22) and (23) into nodal (N) and nonnodal (X) contributions ($G = X + N$) except the circular component that contains also the statistical function $\Gamma_{cc}(r)$, $G_{cc}^{(0)}(r) = \Gamma_{cc}(r) + X_{cc}^{(0)}(r) + N_{cc}^{(0)}(r)$. The differing N and X portions are related by a set of HNC equations [17]. Seven hypernet equations provide algebraic expressions for the X components in terms of nodal and elementary (E) functions,

$$\begin{aligned}
X_{dd}(r) &= \mathrm{e}^{u+N_{dd}+E_{dd}} - 1 - N_{dd}\,,\\
X_{de}(r) &= [1 + G_{dd}][N_{de} + E_{de} + B_{cc}(N_{dc} + E_{dc})^2] - N_{de}\,,\\
X_{ee}(r) &= [1 + G_{dd}][N_{ee} + E_{ee} + \tfrac{1}{2}(\Gamma_{cc} + N_{cc}^{(0)} + E_{cc}^{(0)})^2\\
&\qquad + \tfrac{1}{2}(\Gamma_{cc} + N_{cc}^{(2)} + E_{cc}^{(2)})^2\\
&\qquad + (N_{de} + E_{de} + B_{cc}(N_{dc} + E_{dc})^2)^2\\
&\qquad + 4B_{cc}(N_{dc} + E_{dc})(N_{ec} + E_{ec})\\
&\qquad + 2B_{cc}(\Gamma_{cc} + N_{cc}^{(2)} + E_{cc}^{(2)})(N_{dc} + E_{dc})^2] - N_{ee}\,,\\
X_{cc}^{(0)}(r) &= [1 + G_{dd}][N_{cc}^{(0)} + E_{cc}^{(0)} + \Gamma_{cc}] - N_{cc}^{(0)} - \Gamma_{cc}\,,
\end{aligned} \tag{24}$$

and

$$\begin{aligned}
X_{dc}(r) &= [1 + G_{dd}][N_{dc} + E_{dc}] - N_{dc}\,,\\
X_{ec}(r) &= [1 + G_{dd}][N_{ec} + E_{ec} + (N_{de} + E_{de})(N_{dc} + E_{dc})\\
&\qquad + (\Gamma_{cc} + N_{cc}^{(2)} + E_{cc}^{(2)})(N_{dc} + E_{dc}) + B_{cc}(N_{dc} + E_{dc})^3]\\
&\qquad - N_{ec}\,,\\
X_{cc}^{(1)}(r) &= [1 + G_{dd}][N_{cc}^{(1)} + E_{cc}^{(1)} + (N_{dc} + E_{dc})^2] - N_{cc}^{(1)}\,,
\end{aligned} \tag{25}$$

where $G_{cc}^{(2)}(r)$ is defined by the (redundant) superposition $G_{cc}^{(2)}(r) = G_{cc}^{(0)}(r) + 2B_{cc}G_{cc}^{(1)}(r)$. For $B_{cc} \equiv 0$ the Eqs. (25) do not enter and Eqs. (24) reduce correctly to the set of hypernet equations that characterizes the normal phase [15]. The associated set of chain equations is conveniently written in momentum space employing the Fourier transforms $S(k), X(k)$ and $N(k)$ of the G, X, and N components, respectively. Forming 3×3 matrices $\hat{\mathrm{S}}(k)$, $\hat{\mathrm{X}}(k)$, and $\hat{\mathrm{N}}(k)$ from these elements,

$$\hat{\mathrm{S}}(k) = \begin{pmatrix} S_{dd} & S_{de} & 2B_{cc}S_{dc} \\ S_{ed} & S_{ee} & 2B_{cc}S_{ec} \\ 2B_{cc}S_{cd} & 2B_{cc}S_{ce} & 2B_{cc}S_{cc}^{(2)} \end{pmatrix} \tag{26}$$

and analogous expressions for $\hat{\mathrm{X}}(k)$ and $\hat{\mathrm{N}}(k)$ we may cast the set of chain equations into the form [15, 19]

$$\hat{\mathrm{N}}(k) = \hat{\mathrm{S}}(k)\hat{\mathrm{M}}_c\hat{\mathrm{X}}(k)\,, \tag{27}$$
$$N_{cc}^{(0)}(k) = S_{cc}^{(0)}(k)\big[\Gamma_{cc}(k) + X_{cc}^{(0)}(k)\big]\,,$$

with the constant matrix

$$\hat{\mathrm{M}}_c = \begin{pmatrix} 1 & 1 & 1 \\ 1 & 0 & 0 \\ 1 & 0 & (2B_{cc})^{-1} \end{pmatrix}. \tag{28}$$

Ignoring the elementary (E) contributions in Eqs. (24) and (25) the HNC equations form a closed set of relations that may be used for computation of the G, X, N components which determine the spatial distribution functions (22) and (23).

4. ONE-BODY DENSITY MATRIX

The structural analysis of the reduced one-body density matrix (4) may be performed in close analogy to the procedure outlined in Section 3 for the radial distribution function.

In the thermodynamic limit we may replace the relation (15) by

$$\rho_1(r) = \frac{1}{2}\exp\{\Lambda^{(2)}[u, \Gamma, B_1, B]\}\frac{\delta\Lambda^{(1)}[u, \Gamma_{11}, \Gamma, B_1, B]}{\delta\Gamma_{11}(r)}\bigg|_{B_1=B.\Gamma_{11}=\Gamma}\,, \tag{29}$$

where the generators $\Lambda^{(1)}$ and $\Lambda^{(2)}$ may be systematically evaluated employing standard cluster expansion techniques. The results in terms of diagrams are given in Refs. [18, 19]. The functionals $\Lambda^{(i)}$, $i = 1, 2$, may be separated into reducible and irreducible portions,

$$\Lambda^{(i)} = \Lambda_{\mathrm{irr}}{}^{(i)} + \Lambda_{\mathrm{red}}{}^{(i)} \tag{30}$$

thus giving way for a compact reformulation of expression (29) in terms of irreducible functions. Earlier CBF results on the one-body density matrix associated with the ground state [23, 25] suggest the resulting irreducible representation

$$\rho_1(r) = n_c N_0(r)\exp\{-Q(r)\} \tag{31}$$

with the strength factor $n_c = \exp Q(r = 0)$. Indeed, a detailed inspection of the explicit results on $\Lambda^{(2)}$ and the variational derivative of generator $\Lambda^{(1)}$ with respect to function $\Gamma_{11}(r)$ in terms of the renormalized (dressed) function $\Gamma_{cc}(r) = c\Gamma(r)$, and dressed parameters $B_{cc} = b^2cB$, $\tilde{B}_{cc} = a^2b^2cB_1$, confirms the structural result (31) in terms of irreducible functions $N_0(r)$ and $Q(r)$. They are composed of nodal (N) portions and elementary (E) pieces, explicitly,

$$\begin{aligned} N_0(r) = {} & \Gamma_{cc}(r) + N_{QQcc}^{(3)}(r) + E_{QQcc}^{(3)}(r) \\ & + B_{cc}[a + N_{QQdc}(r) + E_{QQdc}(r)]^2\,, \end{aligned} \tag{32}$$

$$-Q(r) = N_{QQdd}(r) + E_{QQdd}(r)\,. \tag{33}$$

Results (32) and (33) reduce correctly to the familiar expressions for the dressed statistical factor $N_0(r)$ and the correlation function $Q(r)$ at zero temperature with $B_{cc} = a = 1$, reported in Refs. [23, 25].

The nodal quantities appearing in Eqs. (32), (33) may be constructed from certain spatial distribution functions $G_{Q\alpha\beta}(r)$, $\alpha\beta = (dd), (de), (dc), (cd), (ce)$, from cyclic distribution functions $G^{(i)}_{Qcc}(r)$, $i = 0, 1, 2$, and their nodal and nonnodal components. These functions are related by a corresponding set of HNC_Q equations in analogy to the functions $G_{\alpha\beta}(r)$ and $G^{(i)}_{cc}(r)$ that are the building blocks for the radial distribution function (22) and (23). The explicit form of the HNC_Q equations for the Q-quantities reads [18, 19]

$$\begin{aligned}
G_{Qdd}(r) &= \exp[\tfrac{1}{2}u(r) + N_{Qdd}(r) + E_{Qdd}(r)] - 1\,,\\
G_{Qde}(r) &= [1 + G_{Qdd}][N_{Qde} + E_{Qde} + B_{cc}(N_{Qdc} + E_{Qdc})^2]\,,\\
G_{Qdc}(r) &= [1 + G_{Qdd}][N_{Qdc} + E_{Qdc}]\,,\\
G_{Qcd}(r) &= [1 + G_{Qdd}][N_{Qcd} + E_{Qcd}]\,,\\
G^{(0)}_{Qcc}(r) &= [1 + G_{Qdd}][\Gamma_{cc} + N^{(0)}_{Qcc} + E^{(0)}_{Qcc}]\,,\\
G^{(2)}_{Qcc}(r) &= [1 + G_{Qdd}][\Gamma_{cc} + N^{(2)}_{Qcc} + E^{(2)}_{Qcc} + 2B_{cc}(N_{Qdc} + E_{Qdc})(N_{Qcd} + E_{Qcd})]\,,\\
G_{Qce}(r) &= [1 + G_{Qdd}][N_{Qce} + E_{Qce} + (\Gamma_{cc} + N^{(2)}_{Qcc} + E^{(2)}_{Qcc})(N_{Qdc} + E_{Qdc})\\
&\qquad + (N_{Qcd} + E_{Qcd})(N_{Qde} + E_{Qde})\\
&\qquad + B_{cc}(N_{Qdc} + E_{Qdc})^2(N_{Qcd} + E_{Qcd})]\,,
\end{aligned} \tag{34}$$

The chain equations are analogues of Eqs. (27),

$$\begin{aligned}
\hat{\mathrm{N}}_Q(k) &= \hat{\mathrm{S}}_Q(k)\hat{\mathrm{M}}_c(k)\hat{\mathrm{X}}(k)\,,\\
N^{(0)}_{Qcc}(k) &= S^{(0)}_{Qcc}(k)[\Gamma_{cc}(k) + X^{(0)}_{cc}(k)]\,.
\end{aligned} \tag{35}$$

Neglecting the elementary ingredients we may solve this set of HNC_Q equations for $G_{Q\alpha\beta}(r)$ and $G^{(i)}_{Qcc}(r)$ and their nonnodal and nodal components (HNC/0 approximation).

The resulting solutions may be employed to compute the nodal functions that enter the expressions (32) and (33) for functions $N_0(r)$ and $Q(r)$. In **k**-space we obtain for the Fourier transforms the relations

$$\begin{aligned}
N_{QQdd}(k) &= S_{Qdd}(X_{Qdd} + X_{Qde} + 2B_{cc}X_{Qdc}) + S_{Qde}X_{Qdd}\\
&\quad + 2B_{cc}S_{Qdc}(X_{Qdd} + X_{Qdc})\,,
\end{aligned} \tag{36}$$

$$\begin{aligned}
N_{QQdc}(k) &= S_{Qdd}(X_{Qcd} + X_{Qce} + \Gamma_{cc} + X^{(2)}_{Qcc}) + S_{Qde}X_{Qcd}\\
&\quad + S_{Qdc}(2B_{cc}X_{Qcd} + \Gamma_{cc} + X^{(2)}_{Qcc})\,,
\end{aligned} \tag{37}$$

$$N^{(3)}_{QQcc}(k) = B_{cc}S_{Qcd}(X_{Qcd} + X_{Qce} + \Gamma_{cc} + X^{(2)}_{Qcc}) + B_{cc}S_{Qce}X_{Qcd}$$
$$+ \frac{1}{2}S^{(0)}_{Qcc}(\Gamma_{cc} + X^{(0)}_{Qcc}) + \frac{1}{2}S^{(2)}_{Qcc}(2B_{cc}X_{Qcd} + \Gamma_{cc} + X^{(2)}_{Qcc})\,. \qquad (38)$$

We complete the structural analysis of the irreducible functions (32) and (33) by an explicit evaluation of the renormalization constant a. A cluster development of this quantity through four-body cluster order and selected higher-order contributions [19] reveals that the expansion can be written in the closed form,

$$a = 1 + \rho\int d\mathbf{r}\Gamma_{cc}(r)\{G_{Qdd}(r) + G_{Qdc}(r) - G_{dd}(r) - G_{dc}(r)\}\,. \qquad (39)$$

Since the functions $\Gamma(r)$ and $u(r)$ and therewith the nodal and elementary components of expressions (32) and (33) vanish as $r \to \infty$ the one-body density matrix (31) has the asymptotic property $\rho_1(\infty) = n_c B_{cc} a^2$. At $T = 0$ where $B_{cc} = a = 1$ the condensate fraction n_0 is correctly described by the familiar result [23] $n_0 = \rho_1(\infty) = n_c$. Close to the Bose–Einstein transition, $T \simeq T_\lambda$, this fraction depends linearly on the parameter B_{cc}, $n_0 = \alpha B_{cc}$, with $\alpha = n_c a^2|_{T=T_\lambda}$. The relation provides a microscopic realization of Landau's phenomenological description of continuous phase transitions.

Let us finally address an important consequence of the analysis presented. Equations (31) and (32) specialize at $r = 0$ to

$$\rho_1(0) = N_0(0) = \Gamma_{cc}(0) + N^{(3)}_{QQcc}(0) + E^{(3)}_{QQcc}(0) + B_{cc}\,. \qquad (40)$$

Since $\rho_1(0)$ is unity by construction (4), Eq. (40) implies

$$\Gamma_{cc}(0) + N^{(3)}_{QQcc}(0) + E^{(3)}_{QQcc}(0) + B_{cc} = 1\,. \qquad (41)$$

In Fourier space this condition takes the form of a particle sum rule,

$$\frac{1}{N}\sum_{\mathbf{k}}\{\Gamma_{cc}(k) + N^{(3)}_{QQcc}(k) + E^{(3)}_{QQcc}(k)\} + B_{cc} = \frac{1}{N}\sum_{\mathbf{k}} n(k) = 1\,, \qquad (42)$$

wherein $n(k)$ is the momentum distribution (5). References [17–19] show that Eq. (42) is equivalent to the condition

$$\rho\int d\mathbf{r}\Gamma_{cc}(r)\{\rho^{-1}\delta(\mathbf{r}) + G^{(0)}_{cc}(r)\}$$
$$+ B_{cc}\{1 + \rho\int d\mathbf{r}\Gamma_{cc}(r)[G_{dc}(r) + G^{(1)}_{cc}(r)]\} = 1\,. \qquad (43)$$

For $B_{cc} \equiv 0$ Eq. (43) reduces to the established rule enforcing the conservation of the total number N of bosons in the normal phase [15]. Result (43) may be also interpreted as a condition that determines the renormalization constant c [17].

5. SUMMARY

We have developed some major elements of a correlated density matrix theory for an ab-initio semi-analytic description of strongly correlated boson fluids at finite temperatures in the normal and the Bose-condensed phase. The method suitably generalizes the CBF theory of the ground and excited states of quantum many-body systems. The set of trial density matrices employed here takes account of the correlations in a reasonable first approximation. This ansatz may be systematically improved at later stages of the development or may be adapted to a treatment of inhomogeneous Bose systems [14] or other bosonic phases [8]. We may incorporate backflow or current effects by employing triplet functions $u(\mathbf{r}_1, \mathbf{r}_2, \mathbf{r}_3)$ in addition to the pair pseudopotentials $u(\mathbf{r}_1, \mathbf{r}_2)$ or by working with shadow wave functions, etc. [15].

However, the central problem in the further development is the construction of an explicit expression for the entropy of the Bose system in order to apply the minimum principle for the Helmholtz free energy.

ACKNOWLEDGMENTS

This work was supported in part by the Deutsche Forschungsgemeinschaft under Grant No 267/24 - 1. M. L. R. and M. S. gratefully acknowledge travel support from the European Research Office of the U. S. Army for participation in the 18th International Workshop on Condensed Matter Theories, Valencia, Spain. We thank the organizers of the workshop for local support and the Universidad Internacional Menéndez y Pelayo for its hospitality.

REFERENCES

1. J. W. Clark and E. Feenberg, Phys. Rev. **113**, 388 (1959).
2. E. Feenberg, *Theory of Quantum Fluids*, (Academic Press, New York, 1969).
3. J. W. Clark, in *Progress in Particle and Nuclear Physics*, Vol. 2, edited by D. H. Wilkinson (Pergamon, Oxford, 1979).
4. S. Rosati, in *From Nuclei to Particles*, edited by A. Molinari, Proceedings of the International School of Physics "Enrico Fermi," Course LVII, Varenna, 1981 (North-Holland, Amsterdam, 1982).
5. E. Krotscheck, S. Stringari, and J. Treiner, Phys. Rev. B **35**, 4754 (1987).
6. M. L. Ristig and P. M. Lam, Nucl. Phys. A **328**, 267 (1979).
7. M. L. Ristig, Z. Phys. B **79**, 351 (1990).
8. A. Dabringhaus, M. L. Ristig, and J. W. Clark, Phys. Rev. D **43**, 1978 (1991).
9. K. A. Gernoth, J. W. Clark, G. Senger, and M. L. Ristig, Phys. Rev. B **49**, 15836 (1994).
10. C. E. Campbell, K. E. Kürten, M. L. Ristig, and G. Senger, Phys. Rev. B **30**, 3728 (1984).
11. G. Senger, M. L. Ristig, K. E. Kürten, and C. E. Campbell, Phys. Rev. B **33**, 7562 (1986).

12. B. E. Clements, E. Krotscheck, J. A. Smith, and C. E. Campbell, Phys. Rev. B **47**, 5239 (1993).
13. B. E. Clements and C. E. Campbell, Phys. Rev. B **46**, 10957 (1992).
14. K. A. Gernoth, J. W. Clark, and M. L. Ristig, this volume.
15. G. Senger, M. L. Ristig, C. E. Campbell and J. W. Clark, Ann. Phys. (N.Y.) **218** , 160 (1992).
16. J. W. Clark and M. L. Ristig, in *Momentum Distributions*, edited by R. N. Silver and P. E. Sokol (Plenum, New York, 1989).
17. M. L. Ristig, G. Senger, M. Serhan, and J. W. Clark, to be published.
18. R. Pantförder and M. L. Ristig, to be published.
19. R. Pantförder, Diploma thesis, Universität zu Köln, 1993 (unpublished).
20. J. W. Clark, Nucl. Phys. A **328**, 587 (1979).
21. L. Reatto and G. V. Chester, Phys. Rev. **155**, 88 (1967).
22. R. M. Ziff, G. E. Uhlenbeck, and M. Kac, Phys. Reports **32**, 169 (1977).
23. M. L. Ristig, in *From Nuclei to Particles* edited by A. Molinari, Proceedings of the International School of Physics "Enrico Fermi," Course LVII, Varenna, 1981 (North-Holland, Amsterdam, 1982).
24. J. E. Mayer and M. G. Mayer, *Statistical Mechanics* (Wiley, New York, 1940).
25. M. L. Ristig and J. W. Clark, Phys. Rev. B **14** , 2875 (1976).

CORRELATED EXPANSION BASES FOR STRONGLY INTERACTING SYSTEMS

S. ROSATI[1,2], A. KIEVSKY[2] and M. VIVIANI[2]

[1] *Dipartimento di Fisica, Universita' di Pisa, Piazza Torricelli 2, 56100 Pisa, Italy*

[2] *Istituto Nazionale di Fisica Nucleare, Sezione di Pisa, 56010 S.Piero a Grado, Pisa, Italy*

ABSTRACT.

The problem of the bound and scattering states of three and four nucleons has been investigated using a variational procedure based on the expansion of the wave function of the system in terms of correlated Hyperspherical Harmonic bases. The accuracy of the results so obtained is very satisfactory even in the case of realistic NN interactions. As a consequence, the proposed method can be an alternative to the Faddeev techniques which have been largely investigated in the recent years. An important advantage of the method is that the presence of the coulomb repulsion does not cause any additional difficulty.

1. INTRODUCTION.

The problem of calculating accurate wave functions for systems of strongly interacting particles presents severe difficulties. One way to face the problem is the use of appropriate variational wave functions. In systems such as quantum fluids or nuclei, the strong repulsion at small interparticle distances requires a careful determination of the structure of the system in correspondence to these configurations. To this aim, the use of correlation factors has revealed itself to be a powerfull tool. The variational method based on correlated functions containing a number of trial parameters, has been successfull both for quantum fluids [1], as well as for nuclear matter [2,3] and nuclei [4]. One possibility to further improve the variational approach is to expand the w.f. over a complete set of correlated functions. A straightforward way to determine a basis of this type is to multiply the elements of a standard complete basis by conveniently chosen correlation factors. The correlated Harmonic Oscillator [5] and

correlated Hyperspherical Harmonic bases [6] have been investigated by the authors for the study of nuclear systems. The conclusion is that the latter appears to be more apt to rapidly set up all the important details of the structure. Therefore, through this paper, correlated Hyperspherical Harmonic bases will be considered.

In order to calculate the bound state w.f. of a system the Ritz variational principle will be used. A variational approach can be also applied to the study of scattering states and in this paper the Kohn variational principle will be chosen. The Hyperspherical Harmonic (HH) coordinates are introduced in section 2, where the construction of the bound state w.f. is also discussed. The calculation of the bound states of $A = 3, 4$ systems, in the case of realistic potentials, is the subject of section 3. Scattering states of three and four nucleons are considered in section 4. The merits of the method and its possible extensions to investigate the break–up reaction or larger systems are discussed in the final section.

2. EXPANSION OF THE W.F. IN THE HARMONIC HYPERSPHERICAL BASIS

Let us firstly introduce the following set of $N = A - 1$ Jacobi coordinates $(\mathbf{x}_1, \ldots, \mathbf{x}_N)$ defined as

$$\begin{aligned} \mathbf{x}_N &= \mathbf{r}_2 - \mathbf{r}_1 \ , \\ \mathbf{x}_{N-i+1} &= \sqrt{\frac{2i}{i-1}}(\mathbf{r}_{i+1} - \mathbf{R}_i) \ , \quad (i = 1, \ldots, N) \ , \end{aligned} \tag{2.1}$$

where $\mathbf{r}_i$ is the position of the i-th particle and

$$\mathbf{R}_i = \frac{1}{i}\sum_{j=1}^{i} \mathbf{r}_i \ , \tag{2.2}$$

is the relative center of mass coordinate. The first two particles defining the vector $\mathbf{x}_N$ will be called as the reference particles.

In the second step, the $3N$ HH coordinates are introduced.

$$\rho = \left(\sum_{i=1}^{N} x_i^2\right)^{1/2} \ , \tag{2.3}$$

is the hyperradius and the $N-1$ hyperangles $(\phi_2, \ldots, \phi_N)$ are given by the relations $(\phi_1 = 0)$

$$\begin{aligned} x_N &= \rho \cos\phi_N \\ x_k &= \rho \sin\phi_N \cdots \sin\phi_{k+1} \cos\phi_k \qquad (k = 1, \ldots, N-1) \ . \end{aligned} \tag{2.4}$$

The remaining coordinates are the angular coordinates $\hat{\omega}_i$ of the i–th Jacobi vectors $\mathbf{x}_i$, $i = 1, \ldots, N$. The set of all the angular and hyperangular coordinates determines the hyperangle Ω.

When expressed in terms of the hyperangular coordinates, the Laplace operator has the form

$$\nabla^2 = \sum_{i=1}^{N} \nabla_i^2 = \frac{d^2}{d\rho^2} + \frac{3N-1}{\rho}\frac{d}{d\rho} + \frac{L^2(\Omega)}{\rho^2} \ . \tag{2.5}$$

The HH functions $Y_{[L]}(\Omega)$ are eigenfunctions of the grand angular operator $L^2(\Omega)$ and their explicit expression is reported in ref.[6]. $[L]$ denotes all the quantum numbers necessary to specify a given HH function.

The w.f. of a state with angular momentum J, J_z and total isospin T, T_z can be written as a sum of amplitudes

$$\Psi = \sum_{p} \psi(\mathbf{x}_{1p}, \ldots, \mathbf{x}_{Np}) \ , \tag{2.6}$$

where $\mathbf{x}_{1p} \ldots, \mathbf{x}_{Np}$ are the Jacobi coordinates corresponding to the particles ordered according to the permutation p of the set $1, 2, \ldots, N$. In eq.(2.6) the sum runs over the even permutations p since $\psi(\mathbf{x}_{1p}, \ldots, \mathbf{x}_{Np})$ is taken to be antisymmetric under a permutation of the particles $(1p, 2p)$. Each amplitude has the correct values of the total angular momentum and isospin and it can be expanded in channels. In the LS coupling, a generic channel α is specified by the values $\ell_{1\alpha}, \ell_{2\alpha}, \ldots$ of the angular momenta associated to the Jacobi coordinates, and the couplings of the angular momenta and particle spins and isospins to produce J, J_z and T, T_z. One important parameter is the number N_c of channels necessary for an accurate description of the state of the system. Due to the centrifugal barrier, as the values $\ell_{1\alpha}, \ell_{2\alpha}, \ldots$ increase, the importance of the corresponding channel is reduced. As a consequence, the convergence properties of the expansion can be studied by starting with the lowest allowed angular momenta values and subsequently adding higher order channels. In conclusion, the amplitude ψ in eq.(2.6) is written as

$$\psi(\mathbf{x}_{1p}, \ldots, \mathbf{x}_{Np}) = \sum_{\alpha=1}^{N_c} F_{\alpha p} \Phi_{\alpha p}(x_{1p}, \ldots, x_{Np}) \mathcal{Y}_{\alpha p}(L, S, J, T) \ , \tag{2.7}$$

where $\mathcal{Y}_{\alpha p}$ is the angular–spin–isospin function of the channel, $\Phi_{\alpha p}$ depends on the moduli of the Jacobi coordinates and $F_{\alpha p}$ is a correlation factor. It is worthwhile noticing that in an explicit calculation the expansion basis must be truncated; for this reason it might be convenient to use correlated functions constructed with different sets of Jacobi coordinate. More explicitely, certain system configurations can be more efficiently described in one coordinate set than in another one; as an example, it can be mentioned the d–d cluster configuration in the α–particle. More details can be found in ref.[7]. The radial function $\Phi_{\alpha p}(x_{1p}, \ldots, x_{Np})$ can be expanded in terms of the HH functions in the following way:

$$\Phi_{\alpha p}(x_{1p}, \ldots, x_{Np}) = \sum_{[K]} x_{1p}^{\ell_{1\alpha}} x_{2p}^{\ell_{2\alpha}} \cdots Y_{[K]}(\Omega_p) u_{[K]}^{\alpha}(\rho) \ . \tag{2.8}$$

The functions $u_{[K]}^{\alpha}(\rho)$ are the quantities to be determined by means of a variational procedure.

As regards the correlation factor $F_{\alpha p}$ the following two possible choices are interesting:

a) Pair Correlated HH functions (PHH approach). The correlation factor is taken to depend only on the reference particle coordinates, namely

$$F_{\alpha p} = f_\alpha(|\mathbf{r}_{1p} - \mathbf{r}_{2p}|) \ . \tag{2.9}$$

The function $f_\alpha(r_{ij})$ should describe the relative motion of the pair i,j in the angular–spin–isospin state α and it is chosen as the solution of a Schroedinger–type equation of the form

$$\sum_{\alpha'} \left\{ -\frac{\hbar^2}{m}[\frac{d^2}{dr^2} + \frac{2}{r}\frac{d}{dr} - \frac{\ell_\alpha(\ell_\alpha+1)}{r^2}]\delta_{\alpha\alpha'} + V_{\alpha\alpha'}(r) + \lambda_{\alpha\alpha'}(r) \right\} f_{\alpha'}(r) = 0 \ , \tag{2.10}$$

where $V_{\alpha\alpha'}(r) =< \alpha'|V(i,j)|\alpha >$ ($V(i,j)$ is the interparticle potential). The two–particle state α can be a single state or it can be coupled to other ones. The additional term $\lambda_{\alpha\alpha'}(r)$ in eq.(2.10) is such that $|\lambda_{\alpha\alpha'}(r)| << |V_{\alpha\alpha'}(r)|$ for small r values; its role is to make it possible to satisfy the healing condition $f_\alpha(r) = 1$ for large r values. To this end, a satisfactory choice is $\lambda_{\alpha\alpha'}(r) = \Lambda_\alpha \exp(-\gamma r)$, with Λ_α chosen so as to satisfy the healing condition. The precise value of γ is unimportant and it can be taken $1/\gamma = 2.0$ fm.

With the PHH choice, the dependence of the w.f. on the reference particles is largely given by the correlation function whilst the one on the remaining particles is obtained through the HH expansion and the sum over all the permutations (see eq.(2.6)).

b) Product (Jastrow) Correlated HH functions (CHH approach). The correlation is taken as a product of correlation functions depending only on the interparticle distances. In principle, these functions could be calculated variationally; more easily, they can be chosen as the solution of equations similar to the (2.10). It must be noticed that in a given channel the angle–spin–isospin state of the reference particles is determined, so that the potential to be used in eq. (2.10) is known. For the remaining pair of particles, the situation is in general different and the potential is chosen as an average value of the pair potential on the state of the particles. As an example, in the case of a three–particle system, the correlation factor has the form

$$F_{\alpha p} = f_\alpha(r_{ij}) g_\alpha(r_{ik}) g_\alpha(r_{jk}) \ , \tag{2.11}$$

and the function $g_\alpha(r)$ can be taken [6] as the solution of eq.(2.10) with $V(i,j) = [V_s(i,j) + V_t(i,j)]/2$, where V_s and V_t are the central potentials in the singet and triplet spin states, respectively. More details on the choice of the correlation functions can be found in ref.[6,7].

3. CALCULATION OF THE BOUND STATES OF $A = 3,4$ NUCLEI

A significative example of the merits of the CHH method is given by the calculation of the triton bound state in the case of the Hamada–Johnston (HJ) potential. This potential is a realistic one, and it contains a hard–core repulsion with radius

Method	B(MeV)	T(MeV)	$P_{S'}$(%)	P_D(%)	P_P(%)
CHH	7.06	72.95	1.46	10.18	0.09
Euler[5]	6.87	72.19	1.50	9.95	0.07
ref.[9]	6.5±0.2			9.0	
ATMS[10]	6.00	65.9		8.6	

Table 1. Triton binding energy B, average kinetic energy T and S'-, D- and P-wave percentages for the Hamada–Johnston potential with $N_c = 10$.

$r_c = 0.845$ fm. The results obtained for the triton ground state are presented in table 1 and correspond to a number of channels $N_c = 10$. The improvement of the CHH method with respect to the preceeding variational approaches is sizeable.

It has to be noticed that the presence of a hard–core repulsion requires the w.f. to be zero when any interparticle distance is smaller than r_c. Such a condition can be easily satisfied when using a Jastrow correlation factor. On the contrary, in this case the PHH method is unuseful; similarly, a straightforward generalization of the uncorrelated HH expansion can produce wrong results. Such a situation is verified in the paper of ref.[8] where the w.f. used is different from zero when $r_{ij} = r_c$. As a consequence, the binding energy for the considered problem is misleading: the value $B_3 = 4.30 \pm 0.03$ MeV given in ref.[8] must be compared with our CHH estimate $B_3 =$ 2.112 MeV.

The other NN potential considered here is the AV14 model interaction [11]. The expansion basis is the PHH and the results of the various quantities of interest for the triton and ^{3}He ground states are presented in table 2. For the sake of comparison, also the corresponding estimates from ref.[12] are included. The experimental binding energy of 8.48 MeV (7.72 MeV) for the triton (^{3}He) is not reproduced by using the AV14 potential nor by using any local NN potential. Therefore, we must include Three Nucleon Interaction (TNI) terms in the Hamiltonian. The convergence properties of the PHH expansion is not modified by the presence of TNI terms and the experimental binding can be reproduced when the proper intensity of the TNI is fixed. Among the various TNI existing in the literature, we have studied the Melbourne (MB) [13], Brazil (BR) [14] and Urbana (UR) [15] potentials [16].

An accurate calculation of the four–nucleon bound state is a difficult task due to the large number of channels which must be included. One reason is that for the system there are three Jacobi coordinates and a given value of the total angular momentum can be in general obtained in many different ways; moreover, the radial dependence of each channel involves the hyperradius and two hyperangles. Another motivation is that both the p+^{3}H (n+^{3}He) and the d–d cluster configurations are important to produce the structure of the system. In ref.[7] the alpha particle ground state has been studied by using the AV14 potential with or without the inclusion of TNI terms, by taking into account up to 22 channels. The obtained results, together with the extrapolated value of the binding energy, are reported in table 3 and com-

	^{3}H				
N_c	B(MeV)	T(MeV)	$P_{S'}$(%)	P_D(%)	P_P(%)
8	7.660	45.551	1.128	8.926	0.066
12	7.678	45.645	1.127	8.962	0.076
18	7.683	45.671	1.126	8.967	0.076
ref.[12]	7.684	45.677	1.126	8.968	0.076
	^{3}He				
N_c	B(MeV)	T(MeV)	$P_{S'}$(%)	P_D(%)	P_P(%)
8	7.010	44.687	1.318	8.890	0.065
12	7.027	44.780	1.315	8.926	0.075
18	7.032	44.797	1.314	8.931	0.075
ref.[12]	7.033	44.812	1.314	8.932	0.075

Table 2. Binding energy (B), kinetic energy mean value (T) and S'–, P and D–wave percentages for ^{3}H and ^{3}He in terms of the number of channels N_c. The 26–channels results of ref.[12] are reported in the last row for each case.

pared with the corresponding ones from other methods. It can be noticed that there is an overall agreement between the results from different techniques; however rather small differences do still exist which require more exhaustive calculations.

4. ELASTIC SCATTERING PROCESSES

The method presented in sections 2 and 3 for the study of the bound states of nuclei with $A = 3, 4$ can be extended in a rather straigthforward way to calculate also scattering processes. The w.f. for these states can be written in the form

$$\Psi = \Psi_C + \Psi_A \ . \tag{4.1}$$

The term Ψ_C goes to zero for large interparticle distances; its role is to describe the "core" structure, namely those configurations where all the particles are close to each other. As a consequence, Ψ_C is written as a sum of Faddeev amplitudes, each one being expanded in the correlated HH basis, as in the case of the bound state calculation discussed in the preceeding sections. The second term Ψ_A in eq.(4.1) must reproduce the asymptotic configurations of the system, corresponding to large separations among the two clusters. Ψ_A can also be written as a sum of Faddeev amplitudes. Each amplitude is taken as a product of the two cluster wave functions times a function of their relative distance. This function is chosen equal to the regular or irregular solution of the two–cluster Schroedinger equation without nuclear interaction. Moreover, the angular–spin and isospin momenta are coupled to produce the considered total quantum numbers. The superposition of the two Ψ_A correponding to the regular and

	AV14				
method	B(MeV)	T(MeV)	$P_{S'}$(%)	P_D(%)	P_P(%)
CHH	23.93	94.75	0.35	14.20	0.35
extr.	24.02				
FY[17]	23.87				
GFMC[18]	24.2(2)				
	AV14 + UR				
method	B(MeV)	T(MeV)	$P_{S'}$(%)	P_D(%)	P_P(%)
CHH	27.48	107.20	0.24	16.24	0.64
extr.	27.85				
VMC[15]	27.2(2)	106.6(8)		15.5(1)	
GFMC[18]	28.3(2)	113.3(20)		16.6(2)	

Table 3. Binding energy (B), kinetic energy mean value (T) and S'–, P and D–wave percentages for the alpha–particle ground state, calculated with the AV14 and AV14+UR potential models. In the second row for each potential, extr. means our extrapolated estimate. The Faddeev Yakubovsky (FY), Green–Function Monte Carlo (GFMC) and Variational Monte Carlo (VMC) results are given for the sake of comparison.

irregular solution, together with the cluster term Ψ_C is then determined by means of the Kohn principle [16,19]. Here we limit ourselves to report a few of the results obtained for the p–d and p–^{3}He elastic scattering. In table 4 the phase shifts and mixing parameters for the p–d scattering, as calculated for the lowest channels and using the AV14+BR potential are reported for the incident proton energy Ep= 1.0, 2.0 and 3.0 MeV. The corresponding values shown in the table have been calculated by using a more extended Hilbert space than in reference [16]. The agreement between theory and experiment is reasonable; the minor existing differences are an interesting task for further investigations since they should be related to the quantitative role of TNI terms.

5. CONCLUSIONS

The method discussed in this paper allows for an accurate study of few nucleon systems. Detailed calculations have been performed for $A = 3, 4$. In the first case, the results obtained for the bound state and the N–d elastic scattering below the deuteron threshold are very satisfactory. As an example, the calculated elastic scattering parameters for the n–d process are in a very nice agreement with those obtained by means of the Faddeev approach [20]. The study of the N–d reaction over the breakup threshold is in progress. As regards the bound state of the alpha particle with realistic interactions, the accuracy of the results is appreciable, but not at the same level as

E_p(MeV)	1.0	2.0	3.0
$^2S_{1/2}$	-9.54	-19.8	-27.2
$^4D_{1/2}$	-0.78	-2.28	-3.61
$\eta_{1/2}$	1.85	1.73	1.67
$^4S_{3/2}$	-37.4	-53.5	-63.7
$^2D_{3/2}$	0.45	1.36	2.20
$^4D_{3/2}$	-0.84	-2.46	-3.91
$\varepsilon_{3/2}$	0.83	0.79	0.84
$\zeta_{3/2}$	0.53	0.98	1.39
$\eta_{3/2}$	-0.09	-0.20	-0.32
$^2P_{1/2}$	-3.61	-6.83	-8.85
$^4P_{1/2}$	9.30	17.5	22.0
$\varepsilon_{1/2}$	2.51	3.48	4.46
$^2P_{3/2}$	-3.58	-6.76	-8.72
$^4P_{3/2}$	10.9	20.0	24.5
$\varepsilon_{3/2}$	-0.86	-1.25	-1.67

Table 4. Phase shifts and mixing parameters in degrees, for elastic p–d scattering. Three energy values of the incident proton are considered. The results reported correspond to the AV14 + BR potential.

for the three–nucleon system. We expect that the use of the PHH expansion for the alpha particle will allow for an improvement of the accuracy. Four–nucleon scatterig states have been studied at energies under the breakup of the involved clusters; up to now, only semirealistic central NN interactions have been considered but more extended anlyses of such processes are in progress. Finally, the next step we intend to make is the application of the method to the p–shell nuclei; for the moment only very preliminary results are available. By inspection of the various results so far obtained it can be concluded that the use of a variational approach with suitably correlated wave functions is a powerful tool for the investigation of the few–nucleon systems structure. For systems with A= 3 or 4 the obtained accuracy compares well with the one from the Faddeev and GFMC techniques. As a particular remark, we stress once again that the presence of the Coulomb repulsion does not cause any trouble also in the study of scattering states.

ACKNOWLEDGEMENT.

One of the authors (S.R.) wishes to acknowledge the European Research Office of the U.S. Army for partial travel support.

REFERENCES.

1. Q.N.Usmani, S.Fantoni and V.R.Pandharipande, Phys.Rev. **B26** (1982) 6123; M.Viviani, E.Buendia, S.Fantoni and S.Rosati, Phys.Rev **B38** (1988) 4523
2. V.R.Pandharipande and R.B.Wiringa, Rev.Mod.Phys. **51** (1979) 821; S.Rosati, in *From Nuclei to Particles*, Proc.Int.School E.Fermi, course LXXIX, ed. A. Molinari (North Holland, Amsterdam 1982)
3. R.B.Wiringa, V.Ficks and A.Fabrocini, Phys.Rev. **C43** (1991) 2605; O.Benhar, A.Fabrocini and S.Fantoni , in *Modern Topics in Electron–Scattering*, ed. B.Frois and I.Sick (World Scientific, Singapore 1991)
4. R.Guardiola and M.C.Boscá, Nucl.Phys. **A489** (1988) 45; A.Fabrocini, in *Condensed Matter Theories* Vol.8, ed. L.Blum and F.B.Malik, (Plenum Press, New York 1993), pag.257; J.Carlson, V.R.Pandharipande and R.Schiavilla, in *Modern Topics in Electron–Scattering*, ed. B.Frois and I.Sick (World Scientific, Singapore 1991)
5. A.Kievsky, S.Rosati and M.Viviani, Nucl.Phys. **A501** (1989) 503; A. Kievsky, M. Viviani and S. Rosati, Few–Body Syst. **11** (1991) 111
6. S.Rosati, M.Viviani and A.Kievsky, Few–Body Syst. **9** (1990) 1; M. Viviani, A.Kievsky and S.Rosati, Nuovo Cim. **A105** (1992) 1473; A. Kievsky, M. Viviani and S. Rosati, Nucl.Phys. **A551** (1993) 241;
7. M.Viviani, A.Kievsky and S.Rosati, to be published
8. T.K.Das, H.T.Coelho and J.R.A.Torreão, Phys.Rev **C45** (1992) 2640
9. L.M.Delves and M.A.Hennell, Nucl.Phys. **A168** (1971) 347
10. Y.Akaishi and S.Nagata, Prog.Theor.Phys. **48** (1972) 133
11. R.B.Wiringa, R.A.Smith and T.A.Ainsworth, Phys.Rev. **C29** (1984) 1207
12. H,Kameyana, M.Kamimura and Y.Fukushima, Phys.Rev. **C40** (1989) 974
13. S.A. Coon, M.D. Scadron, P.C. McNamee, B.R. Barrett, D.W.E. Blatt and B.H.J. McKellar, Nucl.Phys. **A317** (1979) 242
14. H.T.Coelho, T.K.Das and M.R.Robilotta, Phys.Rev. **C28** (1983) 1812
15. R.B.Wiringa, Phys.Rev. **C41** (1991) 1585
16. A.Kievsky, M.Viviani and S.Rosati, Nucl.Phys. **A**, in press
17. W.Glöckle and H.Kamada, Nucl.Phys. **A560** (1993) 541; H. Kamada and W. Glöckle, Few–Body Syst.Suppl. **7** (1994) 217
18. J.Carlson, Phys.Rev. **C36** (1987) 2026; **C38** (1988) 1879
19. L.M.Delves, in *Advances in Nuclear Physics* Vol.5, ed. M.Baranger and E.Vogt (New York–London: Plenum Press 1972), p.126
20. D.Hüber, W.Glöckle, J.Golak, H. Witala, H.Kamada, A.Kievsky, S.Rosati and M.Viviani, to be published

Elementary excitations and phase transitions in two-dimensional ^{4}He and thin ^{4}He films

M. Saarela[(1)], B.E. Clements[(2)]
E. Krotscheck[(3)] and F.V. Kusmartsev[(4)]

Report 114/94

[(1)] Department of Theoretical Physics,
University of Oulu,
Linnanmaa, SF-90570 Oulu, Finland

[(2)] Institute Laue Langevin,
38042 Grenoble Cedex, France

[(3)] Department of Physics,
Texas A&M University
College Station, TX 77843, USA

[(4)] Institut for Solid State Physics,
University of Tokyo,
7-22-1, Roppongi, Minato-ku, Tokyo 106, Japan

Oulu August 16, 1994

ISBN 951-42-3954-7
ISSN 0356-1119

ELEMENTARY EXCITATIONS AND PHASE TRANSITIONS IN TWO-DIMENSIONAL ^{4}HE AND THIN ^{4}HE FILMS

M. Saarela[(1)], B. E. Clements[(2)], E. Krotscheck[(3)] and F.V. Kusmartsev[(4)]

[(1)] Department of Theoretical Physics, University of Oulu, SF-90570 Oulu, Finland

[(2)] Institute Laue Langevin, 38042 Grenoble Cedex, France

[(3)] Department of Physics, Texas A&M University, College Station, TX 77843, USA

[(4)] Institut for Solid State Physics, University of Tokyo,
7-22-1, Roppongi, Minato-ku, Tokyo 106, Japan

1. INTRODUCTION

The layered structure of superfluid ^{4}He films [1-4] has inspired increasing interest in two-dimensional ^{4}He superfluid [5-7]. ^{4}He films can be adsorbed on various smooth substrates like graphite, solid hydrogen and alkali metals to mention only a few interesting ones. The number of ^{4}He atoms in such films can be controlled quite accurately which makes it possible to map the growth of atomic monolayers. Knowing the properties of the two-dimensional superfluid ^{4}He is important for understanding this growth process. On the other hand thin films offer an excellent opportunity to study the almost ideal, two-dimensional ^{4}He at varying density. Of course, the major requirement is that the substrate surface is smooth. We have examined these aspects theoretically by carrying out careful many-body calculations of the superfluid in two, three and 1+2 dimensions [8-12].

Several phase transitions can occur in the growth of two-dimensional superfluid ^{4}He films: The superfluidity of films is destroyed at the critical temperature by the Berezinskiĭ-Kosterlitz-Thouless phase transition [13,14] at which macroscopic amounts of unpaired vortices are created. The mechanism responsible for that transition is that the logarithmic holding potential keeping the vortex-antivortex pair bound in a two-dimensional fluid is screened by other pairs which are created with increasing temperature until vortices become free and destroy the superfluid order. Two other phase transitions are encountered by varying the superfluid density at zero temperature. At small densities the fluid becomes unstable against density fluctuations, called the spinodal instability, and at high densities it solidifies. Quite recently a new kind of phase transition has been suggested [5,6]. At low densities it becomes

energetically favorable to create spontaneously vortex-antivortex pairs which possibly arrange themselves into a crystal order. Experimental evidence of that transition is found in third sound measurements by Chen, Roesler and Mochel [15].

In this paper, we use the variational many-body theory to provide an accurate description of the ground state of two-dimensional superfluid ^{4}He and of ^{4}He films. We study "how two-dimensional" the layers in the film are. We then give a microscopic description of vortex-antivortex pair excitations, calculate their dispersion relation at different densities and compare with the two- and three-dimensional phonon-roton spectra. These excitations could be seen in very accurate neutron scattering experiments by Lauter *et al.* [16,12]. At the two-dimensional superfluid densities lower than 0.045 Å^{-2} the vortex-antivortex pair excitation is below the roton minimum and thus reduces the critical superfluid velocity. The spontaneous creation of vortex-antivortex pairs becomes possible at densities below 0.037 Å^{-2}.

The theory for the homogeneous superfluid starts with the variational Jastrow-Feenberg *ansatz* for the ground-state wave function of the form,

$$\Psi_B(\mathbf{r}_1,\ldots,\mathbf{r}_N) = \exp\frac{1}{2}\left[\sum_{i<j} u^{BB}(\mathbf{r}_i,\mathbf{r}_j) + \sum_{i<j<k} u^{BBB}(\mathbf{r}_i,\mathbf{r}_j,\mathbf{r}_k)\right], \qquad (1)$$

and the hypernetted chain (HNC) hierarchy of approximations [17]. Pair and triplet correlations are sufficient for a very accurate description of ^{4}He in two- and three-dimensions as well as for ^{3}He-^{4}He mixtures [8]. The input to the theory is the microscopic Hamiltonian,

$$H_B = -\frac{\hbar^2}{2m_B}\sum_i \nabla_i^2 + \sum_{i<j} V(|\mathbf{r}_i - \mathbf{r}_j|), \qquad (2)$$

where m_B is the ^{4}He mass and $V(|\mathbf{r}_i - \mathbf{r}_j|)$ is the ^{4}He-^{4}He interaction which we take to be the Aziz potential [18]. An important part of the variational approach is the optimization of the many-body correlations by solving the coupled Euler equations

$$\frac{\delta E_B}{\delta u^{BB}(\mathbf{r}_1,\mathbf{r}_2)} = \frac{\delta E_B}{\delta u^{BBB}(\mathbf{r}_1,\mathbf{r}_2,\mathbf{r}_3)} = 0 \qquad (3)$$

where E_B is the energy expectation value of the Hamiltonian (2) with respect to the wave function (1). A property of immediate relevance for the problem of phase transitions is that the Euler equations (3) have *no solution if the assumed geometry is unstable against infinitesimal density fluctuations.* Specifically, the Euler equations (3) have *no liquid solution* when the speed of sound becomes zero (the spinodal instability) or when the oscillations of the pair distribution function extend over the whole fluid (the solidification instability).

The external substrate potential breaks the symmetry of the homogeneous fluid. Thus the wave function of the film also contains a one-particle correlation function,

$$\Psi_S(\mathbf{r}_1,\ldots,\mathbf{r}_N) = \exp\frac{1}{2}\left[\sum_i u^B(\mathbf{r}_i) + \sum_{i<j} u^{BB}(\mathbf{r}_i,\mathbf{r}_j) + \sum_{i<j<k} u^{BBB}(\mathbf{r}_i,\mathbf{r}_j,\mathbf{r}_k)\right]. \qquad (4)$$

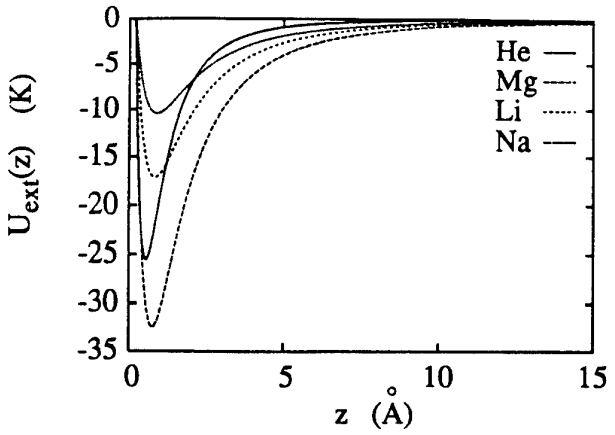

Figure 1. A comparison of the substrate potentials defining the graphite/solid helium model (solid line), and the Mg (long-dashed line), Li (short-dashed line) and Na (dotted line) substrates. The parametrization of the alkali metal potentials is taken from Ref. [19].

The optimization of the energy expectation value leads to three coupled Euler equations for single, pair and triplet correlations. The external potential by itself is not sufficient to cause a strongly layered structure of the film. An important additional ingredient is the behavior of the two-dimensional fluid. It is a liquid bound by roughly 1 K. Its saturation density is 0.043 Å^{-2} and it solidifies at about 0.068 Å^{-2} [20]. This is a fairly low density when compared with the three-dimensional superfluid. The same distance between particles as at the saturation density of the three-dimensional ^{4}He liquid would give a density of 0.078 Å^{-2} for the two-dimensional fluid. We will also show results from the non-local density functional theory (NLDFT) of Ref. [21] which gives a quite incorrect two-dimensional equation of state.

A single vortex in our many-body approach is a topological, singular excitation which can be described by inserting a quantized phase to the wave function,

$$\Psi_v(\mathbf{r}_v, \mathbf{r}_1, ..., \mathbf{r}_N) = e^{\sum_{j=1}^{N} i\phi(\mathbf{r}_v, \mathbf{r}_j)} \psi_v(\mathbf{r}_v, \mathbf{r}_1, ..., \mathbf{r}_N). \tag{5}$$

The coordinate $\mathbf{r}_v$ refers to the position of the vortex and ψ_v contains the response of the superfluid medium. We assume that the vortex is not localized [22], but more like a mobile *quasiparticle* carrying *mass* [23-25,7]. The mass is set equal to the mass of the helium fluid expelled from the vortex core [23]. Its value depends on the vorticity, superfluid density and correlations between the superfluid particles. We determine this vortex mass by a self-consistent many-body calculation.

The creation of a single vortex requires angular momentum and, furthermore, its energy diverges logarithmically with the radius of the sample. In the homogeneous, non-rotating superfluid it is therefore energetically favorable to create pairs of vortices with opposite circulation. The many-body wave function describing these vortex-antivortex pairs contains a phase factor with two centers of circulation of opposite sign. Starting from that phase factor we derive the pairing interaction which diverges logarithmically at large separation. At small distances the coupling to excitations of the superfluid medium causes an important additional attraction. This attraction can drive a phase transition into a new state where macroscopic numbers of vortex-antivortex pairs are spontaneously created. In the long wavelength limit this interaction reproduces the phonon induced attraction by Bardeen, Baym and Pines [26].

The motion of the bound vortex-antivortex pair is best described by letting the center of mass move with a given momentum. We find that the separation between

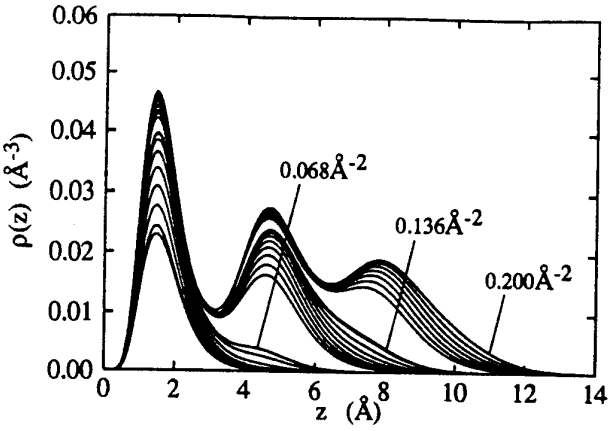

Figure 2. The surface profiles of ^{4}He films adsorbed on graphite/solid helium substrate [10] for different values of coverages are plotted. The profiles correspond to stable surface coverages of 0.033, 0.035, 0.040, ..., 0.065 and 0.068 Å^{-2} for the monolayer, 0.10, 0.105, ..., 0.135, 0.136 Å^{-2} for the double layer, and 0.165, 0.170, ..., 0.200 Å^{-2} for the triple layer.

vortices, as well as the probability of the alignment of vortices perpendicular to the direction of motion, increases with increasing momentum. These results are in qualitative agreement with the behavior of classical vortices [27]. The calculated excitation spectrum shows a quadratic dispersion which is weak at low densities and becomes more pronounced at higher densities. We also calculate the dispersion of the higher lying excited states of the pair.

The remainder of the paper is organized as follows: In the next chapter we present results for thin ^{4}He films and discuss their layered structure. In chapter 3 we briefly describe a single vortex and show the key results. The chapter 4 is devoted to the vortex-antivortex pair and its motion. The last chapter summarizes our work.

2. LAYERED STRUCTURE OF THIN ^{4}HE FILMS

We have studied extensively layered liquid helium in external potentials [10,11]. We assume translational invariance in the $x-y$-plane, *i. e.* the substrate potential is a function of the z-coordinate only. The potentials shown in Fig. 1 provide models for graphite covered with two inert solid layers of helium, and Mg, Li and Na substrates. These potentials cover a representative sample of strengths and ranges; the basic distinction being that Mg, Li and Na potentials are longer range than the graphite/solid helium potential, with Mg being the strongest, and Na the weakest [19]. Our studies provided criteria for when it is allowed to approximate layers in thin ^{4}He films by a rigorously two-dimensional superfluid.

A typical family of density profiles on the graphite substrate is shown in Fig. 2. One of the most striking features of the calculation is that stable, translationally invariant films are *not found for all coverages.* During the growth of a liquid film layers are rigid enough to support two-dimensional "clusters" before ^{4}He "wets" completely the surface. That cluster geometry is not allowed by our wave function and that is why no solution is found at those densities.

The non-uniform growth of these films is the basis of our model for the non-linear increase of the superfluid density seen in the torsional oscillator measurements by Crowell and Reppy [2]. In the transition regions between two uniform configurations, the two-dimensional clusters on top of the "highest" uniform layer are disconnected from the superfluid and can couple, for example through hydrodynamic backflow,

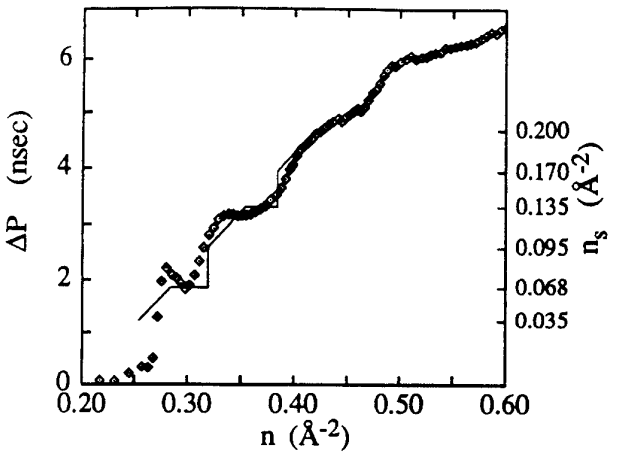

Figure 3. The torsional oscillator periodicity ΔP, taken from Fig. 4 of Ref. [2] (diamonds and left scale) and the connected superfluid surface density from our theory (solid line and right scale) as a function of the total surface density, including the two solid ^{4}He layers.

to the substrate. These clusters behave very similar to single impurity atoms like ^{3}He, whose effective mass can also be determined by torsional oscillator experiments [28]. The numbers obtained above for the range of the uniform phase(s) determine our theoretical estimate of the connected superfluid density as a function of the total surface coverage. It is apparent from Fig. 3 that there is reasonable quantitative agreement between our results and those of Crowell and Reppy. It is known that there is a small surface density dependence in the relation between ΔP and the superfluid density. We believe that this accounts for the slight bending downwards of the experimental curve.

The question to what extent an adsorbed film can be considered as being two-dimensional can be answered by studying the *energetics* of the film. For that purpose, it is convenient to write the ground-state energy/particle of the film in the form

$$E_S = \frac{\hbar^2}{2m_B}\int d^3r \left|\nabla\sqrt{\rho^B(\mathbf{r})}\right|^2 + \int d^3r U_{\rm ext}(\mathbf{r})\rho^B(\mathbf{r}) + E_c \qquad (6)$$

where $\rho^B(\mathbf{r})$ is the density profile, $U_{\rm ext}(\mathbf{r})$ the external potential and E_c the *correlation energy*. In the limit of vanishingly small particle number, the first two terms are equal to the binding energy of a single atom in the substrate potential; the correlation energy is equal to the ground-state energy of the *two-dimensional* system when the film thickness becomes infinitesimal. A similar argument can be made for the chemical potential: *If* the two-dimensional model is a reasonable approximation, then the chemical potential should, as a function of coverage, roughly behave as

$$\mu(n) = \epsilon_0 + \mu_{2D}(n) \qquad (7)$$

where ϵ_0 is the binding energy of a single atom to the substrate, and $\mu_{2D}(n)$ is the chemical potential of a homogeneous, two-dimensional fluid. The estimates of the film energy and chemical potential are exact in the two-dimensional limit, but *how close* an atomic monolayer comes to this depends on the details of the interaction and the substrate potential.

The energetics of the two-dimensional fluid is also relevant for the "wetting" behavior of the liquid. A rough condition for wetting or non-wetting is that one

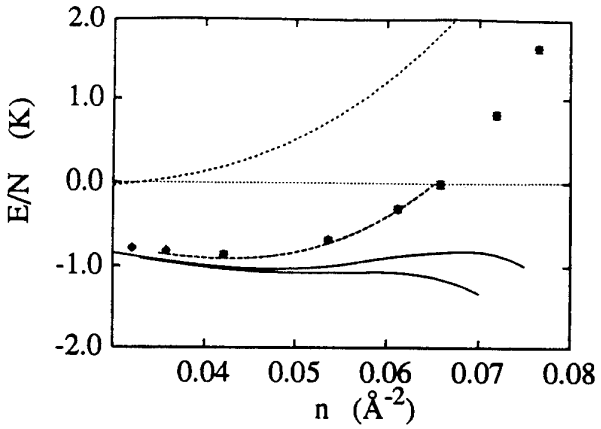

Figure 4. The energy/particle of the two-dimensional ^{4}He as a function of density. The long dashed line is the result of this work. The diamonds with error bars are the Monte Carlo results [20] and the dotted line is the result of the NLDFT. For comparison we show the monolayer correlation energies for the solid H_2 substrate (upper solid curve) and the graphite/solid helium potential (lower solid curve).

should expect a quantum liquid to wet at zero temperature when the binding energy of a single atom added to the energy/particle of the two-dimensional fluid of about 1 K is larger than the chemical potential of an atom in the bulk liquid. The alkali metal, Na, K, Rb and Cs, substrates with single ^{4}He atom binding energies of 4.8, 2.4, 1.8, and 1.5 K, respectively, are examples for substrates where one atomic monolayer will not wet the surface. In the case of sodium we find that a film with two atomic layers can be formed. That is three layers less than predicted in Ref. [19]. We trace the difference back to the different two-dimensional equations of state.

The results for the energy/particle of the two-dimensional ^{4}He are show in Fig. 4. Our results are in excellent agreement with the Monte Carlo data [20] for the whole range of liquid densities. The correlation energies from Eq. (6) of a monolayer on graphite/solid helium and solid hydrogen substrates are also plotted in the same figure. They lie slightly lower than the purely two-dimensional energies and differ increasingly with coverage. This gives one measure of the freedom particles have in z-direction. For comparison we show the two-dimensional energy/particle using the NLDFT of Ref. [21]. That gives the binding energy of -0.06 K at the saturation density of 0.02 Å^{-2}.

Figure 5 shows the coverage dependence of the chemical potential in the film obtained from both our approach and the NLDFT. Again for the monolayer, the chemical potential follows quite closely the estimate of Eq. (7). The comparison with the NLDFT shows basically the same picture. The behavior of the film, however, deviates much earlier from the two-dimensional behavior, which is also plausible since in NLDFT that geometry appears to be energetically unfavorable to the particles. The results for the sound velocities as a function of coverage are also shown in Fig. 5. The increase of the sound velocity with increasing coverage is consistent with the two-dimensional equation of state, but its drop is related to a "ripplon" excitation. That is a surface wave which becomes soft at the density when atoms are pushed from one layer to the next one at the layer completion [12]. In the NLDFT, two-dimensional structures are energetically less favorable. Particles are pushed out of the layers at a lower coverage, and the coverage dependence of the sound velocity becomes smoother [11]. The magnitude of the sound velocity is a very sensitive function of the strength of the substrate potential [10]. A change of the attractive portion by 10 percent can change the sound velocity by almost a factor of two. We can not claim that the accuracy of the substrate potential models is that high.

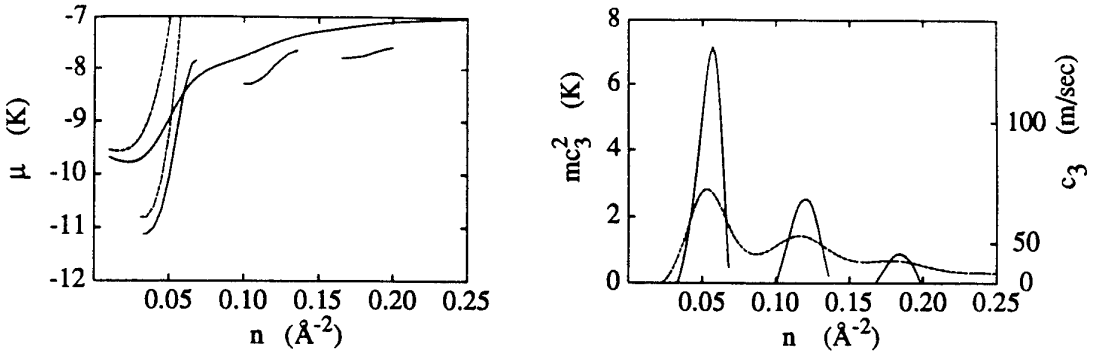

Figure 5. The left figure shows the chemical potential μ of ^{4}He adsorbed to the graphite/solid helium substrate as a function of coverage as obtained in the present work (lower fragmented solid lines) and in NLDFT (upper solid line). Also shown are the estimates of Eq. (7) from the present work (lower dashed line) and NLDFT (upper dashed line) for the monolayer. The right figure shows the incompressibility, mc_3^2 (left scale) and the speed of sound c_3 (right scale) as a function of coverage from the present work (solid line) and NLDFT (dashed line) for the same substrate.

3. QUANTUM VORTEX IN TWO-DIMENSIONAL SUPERFLUID ^{4}HE

A quantum vortex is described by a quantized phase in the many-body wave function of Eq. (5). The gradient of the phase which we will call the *vector potential* is proportional to the superfluid velocity field,

$$\mathbf{A}(\mathbf{r}_v, \mathbf{r}_j) \equiv \nabla_j[\phi(\mathbf{r}_v, \mathbf{r}_j)] = \frac{m_B}{\hbar}\mathbf{v_s}(\mathbf{r}_v, \mathbf{r}_j). \tag{8}$$

The wave function is required to be single valued which gives the familiar quantization condition of the phase $\oint \mathbf{A}(\mathbf{r}_v, \mathbf{r}) \cdot d\mathbf{r} = 2\pi q$. The integer q is the vorticity quantum number of the circulation. The phase transforms into an interaction term in the Hamiltonian. By assuming that the vortex has a finite mass and thus can have kinetic energy we derive the effective Hamiltonian of the *mobile vortex quasiparticle*,

$$H_v = H_B - \frac{\hbar^2}{2m_v}\nabla_v^2 + \sum_{j=1}^{N}\frac{\hbar^2}{2m_B}|\mathbf{A}(\mathbf{r}_v, \mathbf{r}_j)|^2. \tag{9}$$

The value of the vortex mass m_v is a parameter in our approach. We set it equal to mass of the expelled material equivalent with the hollow core model [23] and calculate it self-consistently. Recently Niu, Ao and Thouless also came to the conclusion that the vortex mass must be finite [7].

The vortex singularity polarizes the real part of the many-body wave function. In the Jastrow approach the response of the superfluid is expressed in terms of the vortex-background correlation functions,

$$\psi_v(\mathbf{r}_v, \mathbf{r}_1, ..., \mathbf{r}_N) = e^{\frac{1}{2}\left[\sum_j u^{vB}(\mathbf{r}_v, \mathbf{r}_j) + \sum_{j<k} u^{vBB}(\mathbf{r}_v, \mathbf{r}_j, \mathbf{r}_k)\right]}\psi_B(\mathbf{r}_1, ..., \mathbf{r}_N). \tag{10}$$

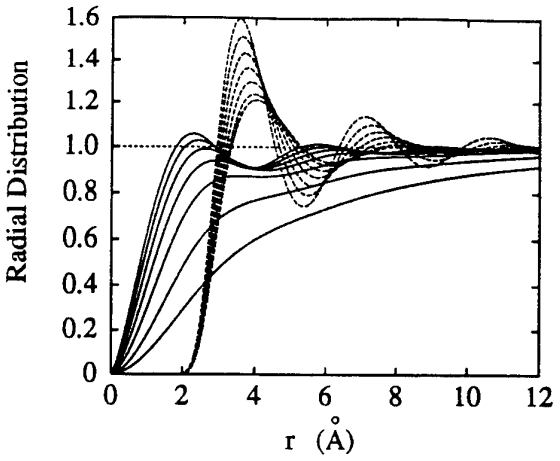

Figure 6. The vortex-^{4}He pair distribution functions, $g^{vB}(r)$, (solid lines) and the ^{4}He - ^{4}He pair distribution functions, $g^{BB}(r)$, (dashed lines) in the two-dimensional liquid ^{4}He are plotted for densities 0.037,..., 0.065 Å^{-2} listed in Table I. The curves with the lowest first peak correspond to the density 0.037 Å^{-2} and those with the highest peak to the density 0.065 Å^{-2}.

These correlation functions are determined by minimizing the energy of the vortex excitation,

$$\mu^v = E_v - E_B = \frac{\langle \psi_v | H_v | \psi_v \rangle}{\langle \psi_v | \psi_v \rangle} - \frac{\langle \Psi_B | H_B | \Psi_B \rangle}{\langle \Psi_B | \Psi_B \rangle}. \tag{11}$$

The first term is the energy of the superfluid with the vortex quasiparticle and the second one is the superfluid in its ground state. The variational ansatz leads to the set of coupled Euler equations,

$$\frac{\delta \mu^v}{\delta u^{vB}(\mathbf{r}_v, \mathbf{r}_1)} = \frac{\delta \mu^v}{\delta u^{vBB}(\mathbf{r}_v, \mathbf{r}_1, \mathbf{r}_2)} = 0, \tag{12}$$

analogous to the problem of a single impurity in the ^{4}He superfluid [29]. The role of the vortex-background interaction is played by the two-dimensional vector potential,

$$|\mathbf{A}(\mathbf{r}_v, \mathbf{r}_j)|^2 = \frac{q^2}{|\mathbf{r}_v - \mathbf{r}_j|^2}. \tag{13}$$

The quantity of main interest which we obtain from the Euler equations is the vortex-background pair distribution function,

$$g^{vB}(\mathbf{r}_v, \mathbf{r}_1) = \frac{\Omega^2}{\mathcal{N}_0} \int d\mathbf{r}_2 ... d\mathbf{r}_N |\Psi(\mathbf{r}_v, ..., \mathbf{r}_N)|^2 \tag{14}$$

with the normalization, $\mathcal{N}_0 = \int d\mathbf{r}_v ... d\mathbf{r}_N |\Psi(\mathbf{r}_v, ..., \mathbf{r}_N)|^2$, and the integration volume Ω. It gives the probability of finding a helium particle at the given distance $|\mathbf{r}_v - \mathbf{r}_1|$ away from the center of the vortex.

The results for the pair distribution functions are shown in Fig. 6 for densities 0.037,..., 0.065 Å^{-2} listed in Table I. The pair distribution function starts from zero quadratically and approaches unity monotonically at the lowest densities. With increasing density, $g^{vB}(r)$ develops a pronounced peak at about 2 Å. This suggests that at high densities only the nearest ^{4}He atoms to the vortex core participate to the circular motion. For comparison we have plotted the pure ^{4}He pair distribution

density	μ^v (K)	μ_c (K)	m_v (amu)
0.037	4.63	1.27	24.3
0.040	5.58	1.32	14.2
0.045	6.90	1.43	8.18
0.050	8.17	1.58	5.61
0.055	9.43	1.77	4.21
0.060	10.7	1.99	3.24
0.065	12.0	2.24	2.73

Table I. The vortex chemical potential, core energy and mass as a function of density.

functions into the same figure. It gives the probability of finding a helium particle when another *helium* is at the origin. The nearest neighbor peak is at 3.8 Å.

Substituting the interaction (13) into the expression for the chemical potential one recovers the familiar logarithmic divergence with the radius, R, of the system. For further discussion we divide the chemical potential into two pieces,

$$\mu^v = \frac{\hbar^2 q^2 \rho^B}{2m_B} \int d^2r |\mathbf{A}(r)|^2 g^{vB}(r) + \mu_c. \tag{15}$$

The first part with the vector potential contains the logarithmic singularity and the second part, μ_c is the non-divergent *core energy*. In Table I we give the full chemical potential, core energy and the vortex mass as a function of density. We have used the radius R=36 Å. Near the saturation density 0.042 Å^{-2} of the two-dimensional ^{4}He the vortex mass is roughly twice the helium mass and becomes "lighter" than helium near the solidification density. In the small density region the vortex mass increases strongly and becomes infinite at the spinodal density 0.032 Å^{-2} where the system becomes unstable against density fluctuation.

4. VORTEX-ANTIVORTEX PAIRS AND PHASE TRANSITIONS

The microscopic model of the vortex-antivortex pair wave function contains two phase factors corresponding to the two centers of circulation,

$$\Psi_{va}(\mathbf{r}_v, \mathbf{r}_a, \ldots, \mathbf{r}_N) = e^{\sum_{j=1}^{N} i[\phi(\mathbf{r}_v,\mathbf{r}_j) - \phi(\mathbf{r}_a,\mathbf{r}_j)]} e^{\frac{1}{2}u^{va}(\mathbf{r}_v,\mathbf{r}_a)} \psi_{va}(\mathbf{r}_v, \mathbf{r}_a, \ldots, \mathbf{r}_N). \tag{16}$$

Vortices are correlated by the factor u^{va}; the real function ψ_{va} depends only on the vortex-helium and helium-helium correlation functions modified by the presence of the other vortex. As in the previous chapter we introduce the vector potential $\mathbf{A}(\mathbf{r}_v, \mathbf{r}_a, \mathbf{r}_j) \equiv \nabla_j [\phi(\mathbf{r}_v, \mathbf{r}_j) - \phi(\mathbf{r}_a, \mathbf{r}_j)]$ and transform it into an interaction in the effective Hamiltonian.

The vortex-antivortex pair is a bound pair. The simplest way to describe its motion is to let the center of mass, $\mathbf{R} = \frac{1}{2}(\mathbf{r}_v + \mathbf{r}_a)$, move by inserting a plane wave

factor into the wave function,

$$\Psi_k(\mathbf{r}_v, \mathbf{r}_a, \mathbf{r}_1, ..., \mathbf{r}_N) = e^{i\mathbf{k}\cdot\mathbf{R}}\tilde{\Psi}_{va}(\mathbf{r}_v, \mathbf{r}_a, \mathbf{r}_1, ..., \mathbf{r}_N; k). \tag{17}$$

All the correlation function in $\tilde{\Psi}_{va}$ become momentum dependent.

The plane wave factor modifies the effective Hamiltonian and brings in two momentum dependent terms,

$$H_{va} = H_B - \frac{\hbar^2}{2m_v}\left[\nabla_v^2 + \nabla_a^2\right] + \frac{\hbar^2}{2m_B}\sum_{j=1}^{N}|\mathbf{A}(\mathbf{r}_v, \mathbf{r}_a, \mathbf{r}_j)|^2|$$
$$+ \frac{\hbar^2}{4m_v}\left[k^2 - 2\sum_{j=1}^{N}\mathbf{k}\cdot\mathbf{A}(\mathbf{r}_v, \mathbf{r}_a, \mathbf{r}_j)\right]. \tag{18}$$

Using this Hamiltonian we calculate the chemical potential of the vortex-antivortex pair at a given momentum k,

$$\mu^{va}(k) = E_{va} - E_B = \frac{\langle\psi_{va}(k)|H_{va}|\psi_{va}(k)\rangle}{\langle\psi_{va}(k)|\psi_{va}(k)\rangle} - \frac{\langle\Psi_B|H_B|\Psi_B\rangle}{\langle\Psi_B|\Psi_B\rangle}. \tag{19}$$

The HNC-equations relate the pair correlation function $u^{va}(\mathbf{r}_v, \mathbf{r}_a)$ to the pair distribution function giving the following expression for $\mu^{va}(k)$,

$$\mu^{va}(k) = \frac{\hbar^2k^2}{4m_v} + 2\mu_c + \int \rho^v\rho^a d^2r_v d^2r_a$$
$$\times\left\{\frac{\hbar^2}{2m_v}\left[(\nabla_v\sqrt{g^{va}(\mathbf{r}_v, \mathbf{r}_a)})^2 + (\nabla_a\sqrt{g^{va}(\mathbf{r}_v, \mathbf{r}_a)})^2\right] + g^{va}(\mathbf{r}_v, \mathbf{r}_a)w_{ind}^{va}(\mathbf{r}_v, \mathbf{r}_a)\right.$$
$$\left.\int \rho^B d^2r_1 g^{vaB}(\mathbf{r}_v, \mathbf{r}_a, \mathbf{r}_1)\left[-\frac{\hbar^2}{2m_v}\mathbf{k}\cdot\mathbf{A}(\mathbf{r}_v, \mathbf{r}_a, \mathbf{r}_1) + \frac{\hbar^2}{2m_B}|\mathbf{A}(\mathbf{r}_v, \mathbf{r}_a, \mathbf{r}_1)|^2\right]\right\}. \tag{20}$$

Here we have ignored the momentum coordinate from the distribution functions.

We divide the square of the vector potential into three parts,

$$|\mathbf{A}(\mathbf{r}_v, \mathbf{r}_a, \mathbf{r}_j)|^2 = |\mathbf{A}(\mathbf{r}_v, \mathbf{r}_j)|^2 - |\mathbf{A}(\mathbf{r}_a, \mathbf{r}_j)|^2 - 2q^2\frac{(\mathbf{r}_a - \mathbf{r}_j)\cdot(\mathbf{r}_v - \mathbf{r}_a)}{|\mathbf{r}_a - \mathbf{r}_j|^2|\mathbf{r}_v - \mathbf{r}_j|^2}, \tag{21}$$

and use the superposition approximation for g^{vaB}. The two first terms then cancel and the last term defines the *direct* part of vortex-antivortex interaction,

$$V_{dir}^{va}(r) = -\frac{q^2\hbar^2\rho^B}{m_B}\int d^2r_1\mathbf{r}\cdot\mathbf{r}_1\frac{g^{vB}(r_1)}{r_1^2}\frac{g^{aB}(|\mathbf{r}_1 - \mathbf{r}|)}{|\mathbf{r}_1 - \mathbf{r}|^2}. \tag{22}$$

This interaction behaves logarithmically at large intervortex distances. The attractive induced potential $w_{\mathrm{ind}}^{va}(\mathbf{r}_v, \mathbf{r}_a)$ is a function of the ^{4}He and ^{4}He-vortex structure functions only, its explicit expression is given in Ref. [30]. The third component of

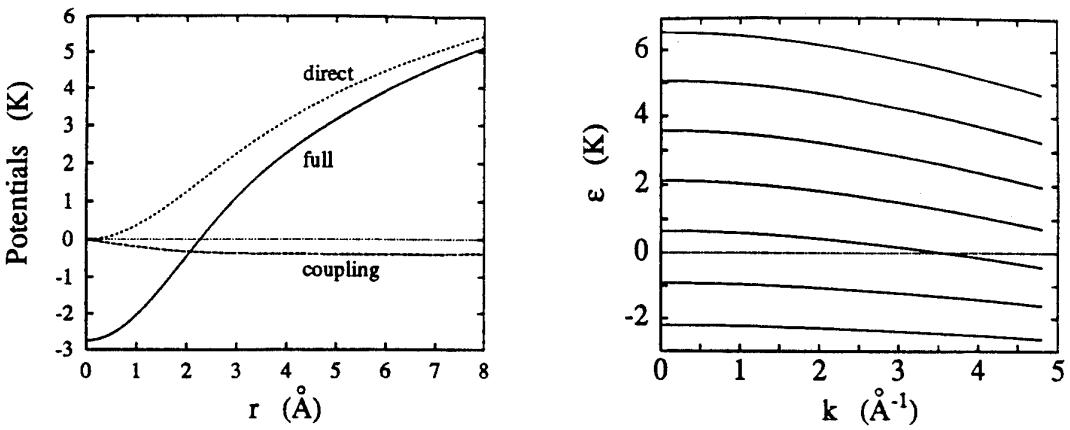

Figure 7. In the left figure three components of the vortex-antivortex interaction are shown at the density 0.045 Å^{-2}. The coupling term is calculated at k=1 Å^{-1}. In the right figure we plot the eigenvalues of the coupled Schrödinger like equations as a function of momentum at densities listed in Table I. The lowest curve is calculated at the density 0.037 Å^{-2} and the highest one at 0.065 Å^{-2}.

the interaction is the $\mathbf{k}\cdot\mathbf{A}$ term. It does not have circular symmetry and gives no contribution if the angle dependence of the $\sqrt{g^{va}(\mathbf{r})}$ is ignored. Therefore we expand $\sqrt{g^{va}(\mathbf{r})}$ in terms of trigonometric functions,

$$\sqrt{g^{va}(\mathbf{r})} = \sum_{even\ m} \xi_m(r)\cos(m\theta) + \sum_{odd\ m} \xi_m(r)\sin(m\theta), \tag{23}$$

where $\mathbf{r} = \mathbf{r}_v - \mathbf{r}_a$, $r = |\mathbf{r}|$, and θ is the angle between $\mathbf{r}$ and $\mathbf{k}$. We use the normalization $\int d^2r\rho^v \sum_m \xi_m^2(r) = 1$. The $\mathbf{k}\cdot\mathbf{A}$ term *couples odd and even m-values*. We have included here only the two first terms in the sum (23). Minimizing $\mu^{va}(k)$ with these approximations with respect to $\xi_m(r)$ results in a set of *coupled Schrödinger-like equations*, with $\xi_m(r)$ playing the role of radial wave functions.

In Fig. 7 we plot the above three components of the interaction. We also show the eigenvalues of the Euler equations as a function of momentum at densities ranging from 0.037 Å^{-2} to 0.065 Å^{-2}. The eigenvalues increase with the density, but decrease with increasing momentum since the attraction of the coupling potential is proportional to the momentum.

Figure 8 shows the chemical potential required to create a vortex-antivortex pair as a function of momentum and density, and the experimental three-dimensional phonon-roton spectrum. Two important features can be seen: At densities below 0.037 Å^{-2}, we find that the chemical potential becomes negative at low momenta. This means that vortex-antivortex pairs can be created spontaneously. The second result is that the dispersion relation near the saturation density of the two-dimensional fluid is quite flat and below the roton minimum. This offers an explanation of the scattering strength seen below the phonon-roton and ripplon bands in the neutron scattering experiments [16]. In the same figure the three lowest excited states are plotted at the density 0.045 Å^{-2}. The states are classified by their radial quantum number. The wave function of the lowest state has no nodes. In the second state the wave function $\xi_{m=0}(r)$ has one node and in the third state $\xi_{m=1}(r)$ has one node.

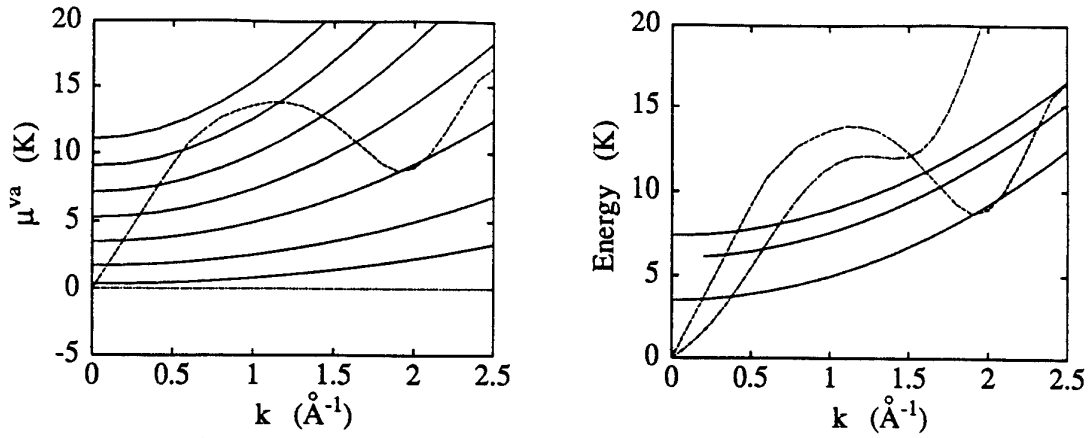

Figure 8. The vortex-antivortex excitation spectrum as a function of momentum at densities listed in Table I (left figure). For comparison we show the experimental phonon-roton spectrum of three-dimensional ^{4}He (dashed line). The right figure shows the three lowest excited states at the density 0.045 Å^{-2} together with the experimental three-dimensional phonon-roton spectrum (dashed line) and the Feynman approximation of the two-dimensional phonon-roton spectrum (dashed-dotted line).

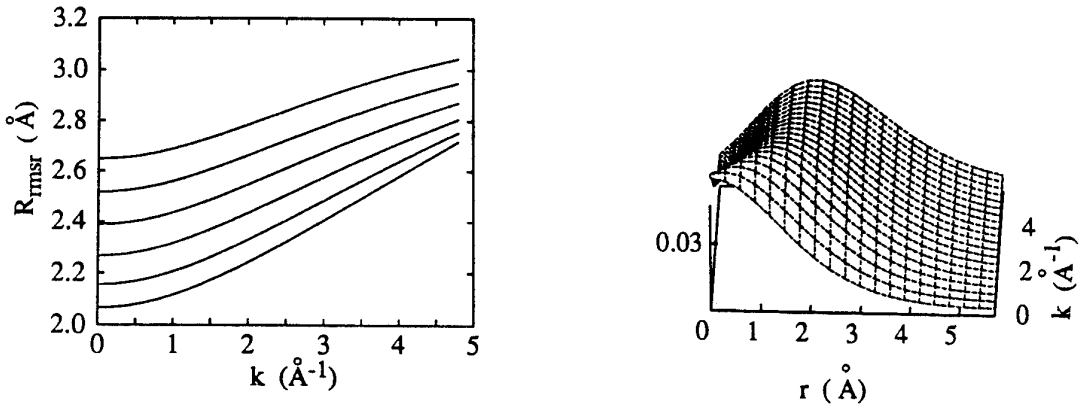

Figure 9. The root mean square radius of the vortex-antivortex separation as a function of momentum at the same densities as in Table I. The radius increases with density (left figure). The right figure shows the distribution function $g_{\perp}^{va}(r)$ in the direction perpendicular to the motion as a function of the separation distance and the momentum. The density is 0.045 Å^{-2}.

The strength of the coupling potential increases with momentum, mixing in more of the m=1 state and thus moving vortices further apart. In Fig. 9 we plot the root mean square radius of the separation which increases both as a function of density and momentum. We also plot $g_{\perp}^{va}(\mathbf{r})$ in the direction perpendicular to the center of mass motion. This gives the probability of finding the pair at the separation distance r. The peak of the probability is moved from the origin at zero momentum to about 2 Å at k=4 Å^{-1}.

Figure 10 shows the two components of the wave function as a function of radius at different momenta. The increasing momentum decreases the $m = 0$ and increases

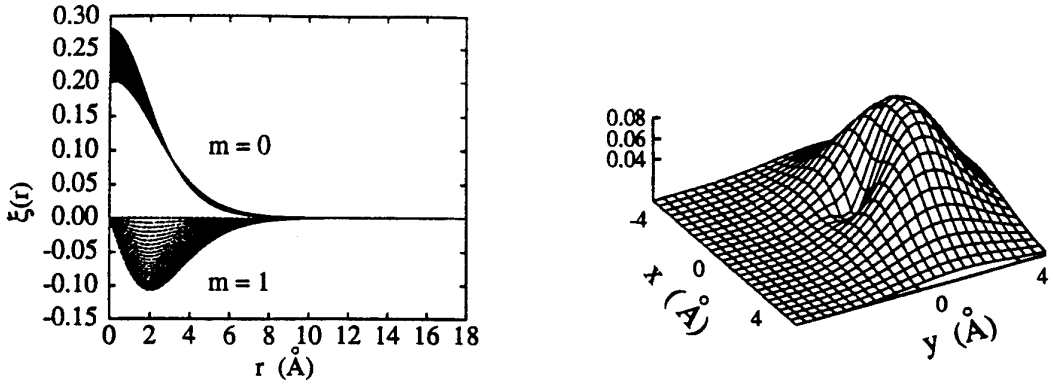

Figure 10. The two components of the vortex-antivortex "wave function" for momenta ranging from 0 $Å^{-1}$ to 5 $Å^{-1}$. The m=0 component decreases and m=1 increases with increasing momentum (left figure). In the right figure we show the $g^{va}(x,y)$ at k=2 $Å^{-1}$.

the $m = 1$ component. We also show $g^{va}(x,y)$ at $|k|$=2 $Å^{-1}$, k pointing to the direction of the negative x-coordinate. One vortex is located at the origin and the surface plot gives the probability of finding the other vortex. The highest probability is clearly in the direction perpendicular to the motion.

5. SUMMARY

We have shown that the properties of the two-dimensional equation of state are important for understanding the growth processes of thin ^{4}He films. This observation makes it highly interesting to study excitation mechanisms in purely two-dimensional superfluid. We have shown that the spinodal and the surface wave instabilities are important in the third sound and torsional oscillator experiments on smooth surfaces.

The vortex-antivortex excitation is a low lying elementary excitation in the two-dimensional quantum fluid. We have derived its dispersion relation and given experimental evidence to support its existence. These are the neutron scattering strength found below the ripplon and roton contributions in Ref. 16 and the second branch in the third sound measurements in Ref. 15. The vortex-antivortex excitation gives a new upper bound for the critical superfluid velocity which we will study in the future.

ACKNOWLEDGMENTS

This work was supported, in part, by the Academy of Finland (to M. S.), by the National Science Foundation under grants PHY-9108066 and INT-9014040 and by the North Atlantic Treaty Organization under grant CRG 940127 (to E. K.). We thank Hans Lauter and Henri Godfrin for interesting discussions in their neutron scattering results. Discussions with Pekka Pietiläinen and Veikko Halonen are also gratefully acknowledged. Participation in this workshop has been made possible by support from the European and the U. S. Research Office of the U. S. Army.

REFERENCES

[1] G. Zimmerli, G. Mistura and M. H. W. Chan, Phys. Rev. Lett. **68** (1992) 60.
[2] P.A. Crowell and J.D. Reppy, Phys. Rev. Lett., **70**, 3291, (1993).
[3] J. M. Mochel and M. T. Chen, Physica B **197** (1994) 278.
[4] M. Wagner and D. Ceperley, J. Low Temp. Phys. **94** (1994) 185.
[5] M. Saarela, B. E. Clements, E. Krotscheck and F. V. Kusmartsev, J. Low Temp. Phys. **93** (1993) 971.
[6] Shou-Cheng Zhang, Phys. Rev. Lett. **71** (1993) 2142.
[7] Q. Niu, P. Ao and D. J. Thouless, Phys. Rev. Lett. **72** (1994) 1706.
[8] E. Krotscheck and M. Saarela, Phys. Rep. **232** (1993) 1.
[9] B. E. Clements, E. Krotscheck and H. J. Lauter, Phys. Rev. Lett. **70** (1993) 1287.
[10] B. E. Clements, J. L. Epstein, E. Krotscheck and M. Saarela, Phys. Rev. B **48** (1993) 7450.
[11] B. E. Clements, H. Forbert, E. Krotscheck and M. Saarela, J. Low Temp. Phys. **95** (1994) 849.
[12] B. E. Clements, H. Forbert, E. Krotscheck, H. J. Lauter, M. Saarela and C. J. Tymczak, Phys. Rev. B **50** (1994) in press.
[13] V.L. Berezinskiĭ, Sov. Phys. JETP **32**, 493 (1971).
[14] J.M. Kosterlitz and D. J. Thouless, J. Phys. **C6**, 1181 (1973), and Prog. Low Temp. Phys. **VIIb**, 373 (1978).
[15] M. T. Chen J. M. Roesler and J. M. Mochel, J. Low Temp. Phys. **89** (1992) 125.
[16] H. J. Lauter, H. Godfrin, V. L. P. Frank and P. Leiderer, Phys. Rev. Lett. **68** (1992) 2484, and private communication.
[17] E. Feenberg, *Theory of Quantum Liquids* (Academic, New York, 1969).
[18] R. A. Aziz, V. P. S. Nain, J. C. Carley, W. J. Taylor and G. T. McConville, J. Chem. Phys. **70** (1979) 4330.
[19] E. Cheng, M. W. Cole, W. F. Saam, and J. Treiner, Phys. Rev. B **46** (1992) 13967.
[20] P. A. Whitlock, G. V. Chester and M. H. Kalos, Phys. Rev. B **38** (1988) 2418.
[21] J. Dupont-Roc, M. Himbert, N. Pavloff, and J. Treiner, J. Low Temp. Phys. **81** (1990) 31.
[22] G.V.Chester, R. Metz, and L. Reatto, Phys. Rev. **175**, 275 (1968).
[23] C.M. Muirhead, W.F. Vinen, and R.J. Donnelly, Phil. Trans. R. Soc. Lond. A **311**, 433 (1984), and Proc. R. Soc. Lond. A **402**, 225 (1985).
[24] J-M Duan and A.J. Leggett, Phys. Rev. Lett. **68**, 1216 (1992).
[25] M. Saarela amd F.V. Kusmartsev, in *Condensed Matter Theories*, ed. by L. Blum and F.B. Malik (Plenum Press, N.Y. 1993) Vol 8, p. 173.
[26] J. Bardeen, G. Baym, and D. Pines, Phys. Rev. **156**, 207 (1967).
[27] R. J. Donnelly, *Quantized Vortices in Helium II* (Cambridge University Press, Cambridge, 1991).
[28] X. Wang and F. M. Gasparini, Phys. Rev. B **38** (1988) 11245.
[29] M. Saarela and E. Krotscheck, J. Low Temp. Phys., **90**, 415 (1993).
[30] J. C. Owen, Phys. Rev. Lett. **47**, 586 (1981).

THEORY OF VALENCE-BOND LATTICE ON SPIN LATTICES

Y. Xian*

Department of Mathematics, UMIST
(University of Manchester Institute of Science and Technology)
P.O. Box 88, Manchester M60 1QD, England

Abstract. Quantum spin-lattice systems in low dimensions exhibit a variety of interesting zero-temperature phases, some of which show non-classical (i.e., non-magnetic) long-range orders, such as dimer or trimer valence-bond order. These symmetry-breaking systems with localized valence bonds are referred to as valence-bond lattices (VBL) in this article. A review of our systematic microscopic formalism based on a proper set of composite operators for the ground and excited states of the VBL systems is given. The one-dimensional (1D) spin-$\frac{1}{2}$ frustrated model is investigated in detail. Several possible VBL systems on the 1D spin-1 chains, the 2D square and *kagomé* lattices are also discussed. That our microscopic theory guarantees the rotational symmetry of the VBL systems is emphasized.

1. INTRODUCTION

Spontaneous symmetry breaking (SSB) (the symmetries of a many-body Hamiltonian not being preserved by its ground state) has always been a fascinating phenomenon in physics. Spin-lattice systems provide ample evidence for such SSB. Perhaps the most well-known example is the ferromagnetic (FM) Heisenberg models which have the classical ground state with all spins pointing in the same direction, say, along the z-axis, thereby breaking the rotational symmetry of its Hamiltonian.

* Email: xian@lanczos.ma.umist.ac.uk

The antiferromagnetic (AFM) counterparts, however, prove much more complicated in quantum mechanics. This is well demonstrated by the fact that even on a bipartite lattice the classical Néel state consisting of two alternating spin-up and spin-down sublattices is no longer the eigenstate of the Hamiltonian. Despite that, a number of AFM systems show a nonzero, albeit reduced, Néel-like order. For example, the 2D spin-$\frac{1}{2}$ AFM Heisenberg model on the square lattice, which has been under intensive study since the discovery of high-temperature superconductors, is now widely believed to possess in its ground state a Néel-like order which is reduced to about two-thirds of the classical value by quantum correlations [1,2].

In addition to the FM phase and Néel-like AFM phase, quantum spin models also exhibit SSB of non-classical (i.e., non-magnetic) types in their ground states, such as the dimerization in a spin chain with two adjacent atoms forming a spin-singlet valence-bond (VB), thereby breaking the chain lattice symmetry. Since the total spin vector of an isotropic spin system is also a good quantum number, those ground states with zero total spin vector certainly have no classical counterparts. Any long-range order in such a many-body ground state must be quantum mechanical in origin and the corresponding broken symmetry is likely to be the lattice symmetry because the rotational symmetry is preserved by such a ground state.

Working in the sector of zero total spin vector has a long history. In fact, the seminal Bethe *ansatz*, which provides exact solutions for the spin-$\frac{1}{2}$ Heisenberg chain, was first proved by Hulthén [3] through finite-size calculations within the framework of resonant valence-bonds (RVB), although the term "RVB" was not used then. Anderson extended this concept of RVB (originally due to Pauline) to frustrated spin-lattice systems [4], and later to the high-temperature superconductor materials [5]. More relevant to the present purposes, Majumdar and Ghosh [6] found that the perfect dimer VB configuration which breaks the lattice translational symmetry is the exact ground state of the important 1D spin-$\frac{1}{2}$ Heisenberg chain at a particular ratio of nearest-neighbour and next-nearest-neighbour coupling constants. In the last six years or so, the VB basis of low-dimensional quantum spin-lattice systems has attracted a lot of theoretical interest [7,8]. In particular, Affleck *et al.* [7] discovered that a homogeneous VB configuration is the exact ground state of a particular spin-1 Heisenberg-biquadratic chain. This finding sheds considerable light on the well-known Haldane conjecture [9] on the nonzero gap in the spin-1 Heisenberg chain. (The term "valence-bond solid" was then used for such a VB state, although it has no conventional symmetry breaking [10].)

An important rigorous result of quantum long-range orders is provided by a series of spin-s $SU(n)$ ($n = 2s + 1$) chains (or the $SU(2)$ spin-s chains with Hamiltonians which project out singlet states). This series of Hamiltonians has been solved by a mapping to the spin-$\frac{1}{2}$ XXZ chain which is integrable by Bethe *ansatz* [11]. By the same mapping, it has been shown that the ground state of the $SU(n)$ model for any $n > 2$ breaks the lattice symmetry with a double degeneracy [12]. The exact values of the corresponding dimerization order parameter have been obtained. In particular, the dimerization order parameters for the $SU(3)$ and $SU(4)$ models are reduced to about 42% and 68% respectively [12].

Although there are no exactly-known examples, it seems possible that spontaneous trimerization, which is characterised by a sequence of spin-singlet states formed from three adjacent spins, may occur for some systems with integer spin quantum

numbers since the trimer state is also a rather stable configuration. Recently this possibility has been discussed for the spin-1 Heisenberg-biquadratic chains over an extended region of the coupling constants [13]. Furthermore, the spontaneous dimerization or trimerization may also occur in higher-order dimensionalities. For example, it has been proposed that the 2D spin-$\frac{1}{2}$ frustrated Heisenberg model on the square lattice may show a column dimer VB order over a small but nonzero region of the coupling constants [14]. A more complicated dimerization picture was suggested for the spin-$\frac{1}{2}$ Heisenberg model on the *kagomé* lattice [15]. The trimerization of spin-1 models on the *kagomé* lattice is also a subject to be discussed in this article.

For convenience, the term "valence-bond lattice" (VBL) is used in this article to represent collectively all those quantum spin-lattice systems in which the simple VB configurations (i.e., dimer or trimer, etc.) are localized with the broken lattice symmetry. One defines a perfect VBL as a regular array of isolated simple VB configurations on a lattice. In general, one expects that the perfect VBL is not the ground state of a given quantum spin-lattice Hamiltonian under consideration. But if the system possesses a VBL long-range order in its ground state, the perfect VBL should be a good starting point. The quantum correlations can then be analysed on the basis of the perfect VBL. This same strategy was employed in 1952 by Anderson [1] in his AFM spin-wave theory, in which the quantum fluctuations from the classical Néel state are described by collective motions of two sets of bosons. The VBL systems are not unlike the quantum Néel-like systems, despite the complication of their ground states being in the sector of zero total spin vector rather than of zero total spin along the z-axis. Similar to the Néel-like systems, where the quantum fluctuations are described by the spin-flip operators (i.e., spin raising and lowering operators) with respect to the Néel model state, I use a proper set of composite operators developed by Parkinson in 1979 [16] to describe the quantum correlations with respect to the perfect VBL model state. A similar spin-wave theory can then be made by a bosonization scheme for those composite operators. But a more systematic approach is provided by a powerful microscopic quantum many-body theory, namely the coupled-cluster method [17], based on those composite operators themselves. The restriction in the sector of zero total spin vector is guaranteed by a very useful and important theorem of the CCM.

Recently, Bishop, Parkinson and Xian [18] have successfully applied the CCM to a number of quantum spin systems, including the spin-$\frac{1}{2}$ AFM Heisenberg model on the square lattice. In their analysis, the Néel state was taken as a model state for the anisotropic-Heisenberg AFM systems. Upon the Néel model state the many-spin correlations are incorporated via a so-called correlation operator consisting of the spin raising and lowering operators with respect to the model state. Within a well-defined systematic approximation scheme amenable to computer-algebraic techniques, they have obtained excellent results for the ground-state energy, excitation spectra, and staggered magnetization as functions of the anisotropy parameter. Their CCM analysis not only produces the numerical results which are among the best estimates available today, but also enables them to study the quantum phase transition of the anisotropic-Heisenberg systems in an extremely systematic fashion [19]. From these experiences, one expects that the CCM analysis should yield similar good quantitative results for the VBL systems.

Because of its simplicity, our microscopic analysis for the spin-$\frac{1}{2}$ frustrated chains is first given. Then the same analysis is extended to other systems, including some spin

models on the 2D square and *kagomé* lattices. The outline of this article is as follows. Sec. 2 considers the few-body systems and introduces the corresponding composite operators and their boson transformations. Sec. 3 is devoted to the study of the 1D spin-$\frac{1}{2}$ frustrated model, firstly by the spin-wave approximation via a bosonization of those composite operators, secondly by the more systematic CCM analysis based on the composite operators themselves. Extension of the same analysis to the other systems, including the spin-1 Heisenberg-biquadratic chains and the some 2D models on the square lattice and the kagomé lattice is discussed in Sec. 4. A general discussion is given in Sec. V. A brief proof of the important symmetry theorem of the CCM is given in the Appendix.

2. FEW-ATOM SYSTEMS AND VALENCE-BONDS

As outlined in Sec. 1, our microscopic theory for a VBL system is based on a set of composite operators which are defined according to the Hilbert space of the corresponding few-atom system. Our discussion here is restricted to the two-atom and three-atom systems. The boson transformation of those composite operators and the spin VB notations are also given.

2.1 Two-Atom Systems

A two-atom system, each with spin $\frac{1}{2}$, has four states, a singlet and triplet states. The singlet state can be written, in the obvious notation, as

$$|0\rangle = \frac{1}{\sqrt{2}}(|\uparrow,\downarrow\rangle - |\downarrow,\uparrow\rangle); \tag{2.1}$$

and the triplet states are, respectively

$$|1\rangle = |\uparrow,\uparrow\rangle, \quad |2\rangle = \frac{1}{\sqrt{2}}(|\uparrow,\downarrow\rangle + |\downarrow,\uparrow\rangle), \quad |3\rangle = |\downarrow,\downarrow\rangle. \tag{2.2}$$

In a matrix representation, one denotes each of these four states by a column matrix with a single nonzero element. Any operator in this Hilbert space can then be written as a 4×4 matrix. Following Parkinson [16], operator A_{mn} is introduced as having only a single non-zero element in a (4×4) matrix, namely $\langle m'|A_{mn}|n'\rangle = \delta_{mm'}\delta_{nn'}$. All single spin operators can now be written in terms of these sixteen, namely

$$s_1^z = \frac{1}{2}(A_{02} + A_{20} + A_{11} - A_{33}), \qquad s_2^z = \frac{1}{2}(-A_{02} - A_{20} + A_{11} - A_{33}), \tag{2.3a}$$

$$s_1^- = \frac{1}{\sqrt{2}}(A_{30} - A_{01} + A_{21} + A_{32}), \quad s_2^- = \frac{1}{\sqrt{2}}(A_{01} - A_{30} + A_{21} + A_{32}), \tag{2.3b}$$

$$s_1^+ = \frac{1}{\sqrt{2}}(A_{03} - A_{10} + A_{12} + A_{23}), \quad s_2^+ = \frac{1}{\sqrt{2}}(A_{10} - A_{03} + A_{12} + A_{23}). \tag{2.3c}$$

The inverse transformations are clearly nonlinear. Therefore A_{mn} has been referred to as a composite operator [13]. In particular, A_{00} corresponds to the spin-singlet projection operator, namely $A_{00} = 1/4 - \mathbf{s}_1 \cdot \mathbf{s}_2$.

We notice that A_{10} (A_{30}) is an operator which increases (decreases) $s^z_{\rm total}$ ($\equiv s^z_1 + s^z_2$) by one unit, while A_{20} leaves $s^z_{\rm total}$ unchanged; their Hermitian conjugates (i.e., transpose matrices) have the opposite effects. Since any of the triplet states can be generated by letting A_{n0} ($n = 1, 2, 3$) operate on the singlet state $|0\rangle$, A_{n0} play the role of creation operators with respect to $|0\rangle$; their transpose matrices correspond to the destruction operators. Using the following algebra

$$A_{mn}A_{kl} = A_{ml}\delta_{nk}, \tag{2.4}$$

which follows by definition, it is easy to see that any A_{mn} can be expressed by a product of A_{m0} and A_{0n}.

For a two-atom system each with spin 1, the dimension of the Hilbert space is nine. The total number of composite operators A_{mn} ($m, n = 0, 1, 2, \ldots, 8$) is eighty-one. Among them are eight pairs of creation and destruction operators with respect to the singlet state. As in the spin-$\frac{1}{2}$ case, if one chooses the the singlet state

$$|0\rangle = \frac{1}{\sqrt{3}}(|1,-1\rangle + |-1,1\rangle - |0,0\rangle), \tag{2.5}$$

the eight pairs of the creation and destruction operators with respect to $|0\rangle$ are then denoted as A_{n0} and A_{0n} ($n = 1, 2, \ldots, 8$) respectively.

2.2 A Three-Atom System

Similar to the two-atom systems discussed above, in order to construct the composite operators of a three-atom system, one should list all of its states. Consider the spin-1 case. There are $3^3 = 27$ states. Ref. [13] lists all of them in detail. Again, the singlet state

$$|0\rangle = \frac{1}{\sqrt{6}}(|0,1,-1\rangle + |1,-1,0\rangle + |-1,0,1\rangle - |0,-1,1\rangle - |-1,1,0\rangle - |1,0,-1\rangle), \tag{2.6}$$

is the first state, and the nine states of $s_{\rm total} = 1$ ($\mathbf{s}_{\rm total} \equiv \mathbf{s}_1 + \mathbf{s}_2 + \mathbf{s}_3$) follow, and so on, until the last state with all three down spins.

As before, A_{00} for the present case is also the spin singlet projection operator by definition, and can be is written as

$$A_{00} = \frac{1}{18}S_{123}(6 + S_{123} - S^2_{123}), \qquad S_{123} \equiv \mathbf{s}_1 \cdot \mathbf{s}_2 + \mathbf{s}_2 \cdot \mathbf{s}_3 + \mathbf{s}_3 \cdot \mathbf{s}_1; \tag{2.7}$$

the creation and destruction operators with respect to the singlet state $|0\rangle$ of Eq. (2.6) are similarly given by A_{n0} and A_{0n} ($n = 1, 2, \ldots, 26$). In Ref. 13, an approximation is made by truncating the Hilbert space from twenty-seven states to the first ten (i.e., restricting to the subspace of $s_{\rm total} = 0$ and 1). In this subspace, there are only nine pairs of creation and destruction operators which can be easily managed.

2.3 Bosonization of Composite Operators

A bosonization scheme for a set of operators usually starts from a reference. The reference of the bosonization scheme (e.g., Holstein-Primakoff transformation) in the

conventional spin-wave theory [1] is either the spin-up state or spin-down state. The reference for our present purpose is clearly the singlet state $|0\rangle$ of the corresponding few-spin system. Therefore, the similarities between operators s^z and A_{00} and between s^+ (s^-) and A_{n0} (A_{0n}) can be clearly seen.

While s^z and $s^\pm$ obey the usual $SU(2)$ angular momentum algebras, from Eq. (2.4), it is easy to see that A_{mn} obey the following pseudo-spin algebra,

$$[A_{mn},\ A_{kl}] = A_{ml}\delta_{nk} - A_{kn}\delta_{lm}. \tag{2.8}$$

Therefore, A_{mn} has also been referred to as a pseudo-spin operator. From Eq. (2.8) one can make the following Dyson-Maléev-like transformation,

$$A_{00} = 1 - \sum_{n=1}^{d-1} a_n^+ a_n;\ \ A_{n0} = a_n^+ A_{00},\ A_{0n} = a_n;\ \ A_{mn} = a_m^+ a_n, \tag{2.9}$$

where $m, n = 1, 2, \ldots, d-1$ with d the Hilbert space dimensionality of the few-atom system, and where a_n, a_n^+ are $(d-1)$ sets of boson operators, obeying the usual boson commutation, $[a_m,\ a_n^+] = \delta_{mn}$.

By definition, the singlet state $|0\rangle$ is the vacuum state of the bosons, namely, $a_n|0\rangle = 0,\ n = 1, 2, \ldots d-1$. The physical states correspond to the vacuum state $|0\rangle$ and the $(d-1)$ states with only one boson excited. Furthermore, as the matrix elements between the physical and unphysical subspaces are equal to zero, the transformation given by Eqs. (2.9) is exact at zero temperature just as in the case of the conventional spin-wave theory [1].

2.4 Valence Bonds

In the above analysis, the singlet state is always taken as the reference with respect to which creation and destruction operators are defined. This is the essence of our microscopic theory for the VBL systems.

As is well known, spin singlet states can be conveniently represented in terms of VB which in turn can be expressed by Schwinger bosons [7,8]. Schwinger boson represention is given by the following transformation,

$$s^+ = a^+ b,\ \ s^- = a b^+,\ \ s^z = \frac{1}{2}(a^+ a - b^+ b), \tag{2.10}$$

where a, a^+ and b, b^+ obey the usual boson commutations. It should be emphasized that Schwinger bosons are used here purely for the notational purpose. They should not be confused with the bosonization scheme of Eq. (2.9). A spin-s state with $s^z = m$ $(-s \le m \le s)$ is written in the Schwinger reprsentation as

$$|s, m\rangle = \frac{(a^+)^{s+m}}{\sqrt{(s+m)!}} \frac{(b^+)^{s-m}}{\sqrt{(s-m)!}} |V\rangle, \tag{2.11}$$

where $|V\rangle$ is the vacuum state of the bosons. A spin VB between atoms i and j is defined by a number of the so-called VB operators [8]

$$C_{ij}^+ = a_i^+ b_j^+ - a_j^+ b_i^+, \tag{2.12}$$

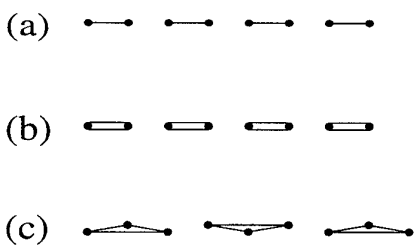

Fig. 1. Three VB configurations: (a) spin-$\frac{1}{2}$ dimer, (b) spin-1 dimer and (c) spin-1 trimer. A single bond is defined by C_{ij}^{+} of Eq. (2.12).

acting on the vacuum state $|V\rangle$. Using Eq. (2.11), it is easy to see that the spin-singlet states of Eqs. (2.1), (2.5) and (2.6) can be conveniently written respectively, apart from the trivial normalization factors, as one-bond $C_{12}^{+}|V\rangle$, two-bond $(C_{12}^{+})^2|V\rangle$, and three-bond $C_{12}^{+}C_{23}^{+}C_{31}^{+}|V\rangle$ configurations.

A general VB configuration can be easily drawn for a spin-s many-spin system. In Fig. 1, two dimer and one trimer configurations are shown. A many-spin ground state with zero total spin vector [$\mathbf{s}_{\text{total}}$ ($\equiv \sum_i \mathbf{s}_i$) $= 0$] is in general given by a linear summation of all independent VB configurations in which each atom is linked by $2s$ VBs [7,8]. In general, different many-spin VB states are not orthogonal to one another. This makes working in the VB basis very difficult. But the ground state of some interesting quantum systems is dominated by a particular VB state consisting of an array of independent simple VBs such as those shown in Fig. 1. These are the VBL systems defined in Sec. 1. In the following sections, a systematic microscopic theory is developed by taking these perfect VBLs as the reference state and by employing the creation and destruction operators A_{n0} and A_{0n} with respect to this reference.

3. THE SPIN-$\frac{1}{2}$ FRUSTRATED CHAINS

3.1 Spin-Wave Theory

The 1D spin-$\frac{1}{2}$ frunstrated model is perhaps the simplest model with spontaneous dimerization. The model consists of N atoms each with spin $\frac{1}{2}$ on a chain with nearest-neighbour and next-nearest-neighbour interactions. The Hamiltonian is simply

$$H = \sum_{i=1}^{N} (\mathbf{s}_i \cdot \mathbf{s}_{i+1} + J\mathbf{s}_i \cdot \mathbf{s}_{i+2}), \tag{3.1}$$

where J is the coupling constant, the usual periodic boundary condition is assumed, and even N and a unit lattice spacing are also chosen for convenience. At $J = 0$, H is the well-known Heisenberg model which was solved exactly by Bethe *ansatz* [3]; its ground state is gapless and has no long-range order. At $J = \frac{1}{2}$, the ground state is given by the dimer VB configuration as shown in Fig. 1 (a) with a double degeneracy

[6],

$$|D\rangle = \prod_{r=1}^{N/2} |0\rangle_{2r-1,2r}, \tag{3.2}$$

where the notation $|0\rangle_{i,j}$ represents the singlet state of the pair given by Eq. (2.1). Let r denote each dimer in Fig. 1 (a), and $\mathrm{s}_1(r)$ and $\mathrm{s}_2(r)$ the two spins of the dimer, Eq. (3.1) becomes

$$H = \sum_{r=1}^{N/2} \big[\mathrm{s}_1(r)\cdot\mathrm{s}_2(r) + \mathrm{s}_2(r)\cdot\mathrm{s}_1(r+1) + J\mathrm{s}_1(r)\cdot\mathrm{s}_1(r+1) + J\mathrm{s}_2(r)\cdot\mathrm{s}_2(r+1)\big]. \tag{3.3}$$

One can then express H in terms of the composite operators A_{mn} by Eqs. (2.3).

As discussed in Sec. 2, since the flutuations with respect to $|D\rangle$ can be described by operators A^r_{n0} and A^r_{0n} $(n = 1, 2, 3)$, one can derive the equations of motion for all of these three sets of pairs. By employing the usual decoupling approximations and taking $A_{00} \approx 1$, it is easy to derive the spin-wave spectra (i.e., eigen modes). Parkinson [16] employed this method to obtain the triplet spectrum of the Heisenberg model $(J = 0)$.

Application of bosonization scheme not only provides a more systematic means to obtain the excitation spectra, but also allows one to study the ground-state properties as well. By Eqs. (2.9), one can further express H in terms of the three sets of bosons (a polynomial up to sixth order). Diagonalization of the quadratic parts of H by the usual Bogoliubov transformations, one can easily obtain the ground-state energy E_0 and excitation spectra ω_q within the spin-wave approximation. They are given by respectively

$$\frac{E_0}{N} = \frac{3}{4}\int_0^\pi \frac{dq}{\pi}\big[\sqrt{1-(1-2J)\cos 2q} - 1\big] - \frac{3}{8}, \tag{3.4}$$

and

$$\omega_q = \sqrt{1-(1-2J)\cos 2q}. \tag{3.5}$$

Eq. (3.5) agrees with that of Parkinson at $J = 0$ [16]. A dicussion of these results is left to the end of this section.

3.2 The Coupled-Cluster Method

The CCM has been successfully applied to a wide range of quantum many-body problems in both physics and quantum chemistry [17]. The interested reader is referred to Ref. [17] for the general formalism of the CCM and to Ref. [18] for its particular application to the spin systems with the Néel-like order. Here its extension to the VBL systems is considered.

(a). The Ground State

The CCM *ansatz* for the ground ket state is $|\Psi_g\rangle = \mathrm{e}^S|\Phi\rangle$, where $|\Phi\rangle$ is the so-called model state which is usually chosen as an uncorrelated many-body wavefunction, and where S is the many-body correlation operator consisting purely of the creation operators with respect to $|\Phi\rangle$. For the VBL problem under consideration,

it is quite natural to choose the perfect VBL state as the model state. The creation operators with respect to this model state are clearly given by any combination of those operators A^r_{n0} with $n = 1, 2, \ldots, d-1$ where d is the dimensionality of the corresponding few-spin system and r denotes its vector position in the VBL. Their Hermitian conjugates A^r_{0n} are the corresponding destruction operators.

The Schrödinger equation of the ground state, after a simple manipulation, can then be written as

$$\mathrm{e}^{-S} H \mathrm{e}^{S} |\Phi\rangle = E_g |\Phi\rangle, \tag{3.6}$$

where E_g is the ground-state energy, and where the similarity-transformed Hamiltonian can be expressed as a series of nested commutators, namely

$$\mathrm{e}^{-S} H \mathrm{e}^{S} = H + [H, S] + \frac{1}{2!}[[H, S], S] + \cdots, \tag{3.7}$$

which usually terminates at the fourth-order for most Hamiltonians with pair-interaction potentials [17,18]. So does the present case if the Hamiltonian contains a finite-order polynomial of the destruction operators.

Now let us focus on the spin-$\frac{1}{2}$ dimerization. The model state $|\Phi\rangle = |D\rangle$. There are three creation operators, namely A_{10}, A_{20} and A_{30}. If one restricts to the sector of zero s^z_{total} ($\equiv \sum_i^N s^z_i$), the correlation operator $S = \sum_{n=1}^{N/2} S_n$, with

$$\begin{aligned} S_1 &\equiv \sum_{r=1}^{N/2} \mathcal{S}_r A^r_{20}, \quad S_2 \equiv \sum_{r,r'}{}' \left[\mathcal{S}^{(1)}_{r,r'} A^r_{10} A^{r'}_{30} - \frac{1}{2!} \mathcal{S}^{(2)}_{r,r'} A^r_{20} A^{r'}_{20} \right], \\ S_3 &\equiv \sum_{r,r',r''}{}' \left[\mathcal{S}^{(1)}_{r,r',r''} A^r_{10} A^{r'}_{30} A^{r''}_{20} - \frac{1}{3!} \mathcal{S}^{(2)}_{r,r',r''} A^r_{20} A^{r'}_{20} A^{r''}_{20} \right], \end{aligned} \tag{3.8}$$

etc. In Eq. (3.8) the primes on the summations imply exclusion of the terms with any pair of indices being equal.

The ground-state energy is obtained by taking the inner product of the Schrödinger equation (3.6) with the model state $|D\rangle$ itself, namely

$$E_g = \langle D | \mathrm{e}^{-S} H \mathrm{e}^{S} | D \rangle; \tag{3.9}$$

and the correlation coefficients $\{\mathcal{S}_{r,r',\ldots}\}$ in Eqs. (3.8) are determined by the coupled set of equations obtained by taking inner products of Eq. (3.6) with states constructed from the corresponding destruction operators, namely

$$\langle D | A^r_{02} \mathrm{e}^{-S} H \mathrm{e}^{S} | D \rangle = 0, \quad \forall r, \tag{3.10}$$

for the one-body equation; and

$$\langle D | A^r_{01} A^{r'}_{03} \mathrm{e}^{-S} H \mathrm{e}^{S} | D \rangle = 0, \quad \langle D | A^r_{02} A^{r'}_{02} \mathrm{e}^{-S} H \mathrm{e}^{S} | D \rangle = 0, \quad \forall r, r' (\neq r) \tag{3.11}$$

for the two-body equations. The three-body equations and higher-order many-body equations are obtained in a similar fashion.

The exact energy equation (3.9) can be straightforwardly derived as

$$\frac{E_g}{N} = \frac{1}{8}[(1-2J)(2b_1^{(1)} + b_1^{(2)} - a) - 3], \tag{3.12}$$

where the lattice symmetry is used to set accordingly $\mathcal{S}_r = a$, $\mathcal{S}^{(l)}_{r_1,r_2} = \mathcal{S}^{(l)}_{r_2,r_1} = b_r^{(l)}$, with $l = 1, 2$ and $r = r_2 - r_1$.

The exact one-body equation (3.10) can also be easily derived. It couples only to the two-body coefficients. Similarly, the two-body equations (3.11) couple only to the one-body and the three-body coefficients, and so on. One clearly needs to employ an approximation scheme for a practical calculation. The most common approximation of the CCM is the SUBn scheme which retains up to n-body correlation operators. Here the SUB2 scheme is considered, namely $S \to S_{\rm SUB2} = S_1 + S_2$ and $S_n = 0$ for $n \geq 3$. The one-body equation (3.10) yields an interesting solution, $a = 0$, implying no one-body correlations for the dimerization problem. Furthermore, the two-body equations (3.11) provide a solution in which the two sets of two-body coefficients are identical, namely

$$b_r^{(1)} = b_r^{(2)} \equiv b_r. \tag{3.13}$$

We notice that the model state $|D\rangle$ is in the sector of $\mathrm{s}_{\rm total} = 0$, and the one-body correlation operator S_1 will take the state out of this sector. We also notice that the two-body correlation operator S_2 commmutes with $\mathrm{s}_{\rm total}$ if and only if Eq. (3.13) is satified. All these imply that the ground state in our SUB2 approximation remains in the sector of $\mathrm{s}_{\rm total} = 0$ despite the fact that we started with operators in the sector of $s^z_{\rm total} = 0$. In fact, this nice property also holds at higher-order approximations in the above CCM analysis. Appendix provides a brief proof for a general theorem which states that the CCM coupled equations [e.g., Eqs. (3.10) and (3.11)] at any level of approximations always provide at least a solution which guarantees the symmetry of the model state if this symmetry is one of those belonging to the model Hamiltonian. This is certainly a big advantage because it is much more difficult to work in the sector of $\mathrm{s}_{\rm total} = 0$ than of $s^z_{\rm total} = 0$.

The energy equation is now reduced to

$$\frac{E_g}{N} = \frac{3}{8}[(1-2J)b_1 - 1], \tag{3.14}$$

and, after simplification, the two equivalent two-body equations are given by

$$\frac{1}{2}\sum_{\rho=\pm 1}(K_3\delta_{r\rho} + K_2 b_r - 2K_1 b_{r+\rho} + K_1 \sum_{r'\neq 0} b_{r'} b_{r+\rho-r'}) = 0, \quad r \neq 0 \tag{3.15}$$

with $K_1 \equiv 1-2J$, $K_2 \equiv 4(1-2K_1 b_1)$, and $K_3 \equiv K_1(1+4b_1^2) - 2(1+2J)b_1$. A simpler approximation can be made from Eq. (3.15), namely the SUB2-2 scheme which retains only the single coefficient, b_1. Eq. (3.15) then reduces to

$$1 - 2J + 2(3-2J)b_1 - 9(1-2J)b_1^2 = 0, \tag{3.16}$$

which is easily solved. The full SUB2 equation (3.15) can also be solved analytically by a Fourier transformation method in a similar fashion as described in Ref. 18. Here only the final result is given by the following self-consistency equation for b_1,

$$b_1 = \frac{1}{3K_1}\left(2 - \frac{K_2}{2}\frac{1}{2\pi}\int_{-\pi}^{\pi} dq\,\sqrt{1 - k_1\cos 2q + k_2\cos^2 2q}\right), \tag{3.17}$$

where the constants k_1 and k_2 are defined by

$$k_1 \equiv \frac{1}{K_2^2}(4K_1K_2 + 8K_1^2 b_1 - 4K_1^2 X), \quad k_2 \equiv \frac{4K_1(K_1 - K_3)}{K_2^2}, \tag{3.18}$$

and where $X \equiv \sum_{r=1}^{N/2} b_r b_{r+1}$, which can be calculated self-consistently as b_1 of Eq. (3.17). After b_1 is determined as a function of J, the ground-state energy is obtained by Eq. (3.14). Again the discussion of these results is left to the end.

(b). The Excited States

The CCM *ansatz* for the excited state is $|\Psi_e\rangle = X|\Psi_g\rangle = X\mathrm{e}^S|\Phi\rangle$, where $|\Psi_g\rangle$ is the ground state as determined above and X is the excitation correlation operator consisting only of the creation operators as S does. Using the Schrödinger equations for the ground and excited states, one obtains

$$\mathrm{e}^{-S}[H, X]\mathrm{e}^S|\Phi\rangle = eX|\Phi\rangle, \quad e \equiv E_e - E_g. \tag{3.19}$$

In the so-called SUB(2,1) scheme, one retains up to two-body correlations in S and one-body correlations in X, namely, $S \to S_{\mathrm{SUB2}} = S_1 + S_2$ and $X \to X_1$. Therefore one writes,$X_1 = \sum_r \mathcal{X}_r A_{10}^r$. The other two one-body excitation operators are given by replacing A_{10} by A_{20} and A_{30} respectively. The coefficient $\mathcal{X}_r$ is determined by the inner product of Eq. (3.19) with state $A_{10}^r|\Phi\rangle$. A Fourier transformation readily yields the following excitation spectrum with a lattice momentum q,

$$e_q = \frac{K_2}{4}\sqrt{1 - k_2\cos 2q + k_2\cos^2 2q}, \tag{3.20}$$

where the constants K_2, k_1 and k_2 are as defined before. The other two excited states with operator A_{20} and A_{30} produce the same spectrum. Therefore e_q is a triplet spectrum as expected.

3.3 Discussion

Fig. 2 shows the results of the ground-state energy per atom as a function of J from the spin-wave approximation, and from the SUB2-2 and full SUB2 schemes of the CCM. The numerical results [20] of Tonegawa and Harada, obtained by extrapolating the finite-size calculations for $J < 1/2$, and the exact results by Parkinson of the $N = 20$ system for $J > 1/2$, are also included for comparison. At $J = 1/2$ (i.e., the Majumdar-Ghosh point) both spin-wave theory and the CCM approximations give the exact result of $-3/8$. This is not surprising because both take the dimer state $|D\rangle$ as their model state. At $J = 0$ (the Heisenberg point), spin-wave theory yields -0.4498, while the SUB2-2 and full SUB2 schemes yield $-0.4268, -0.4298$ respectively. They all agree with the exact result of -0.4432 by the Bethe ansatz [3]. But we notice that at $J = 0$ spin-wave theory produces divergent results for other physical quantities such as the dimerization parameter discussed later. Furthermore, as can be seen from Fig. 2, the energy curve of spin-wave theory is symmetric about $J = 1/2$, while

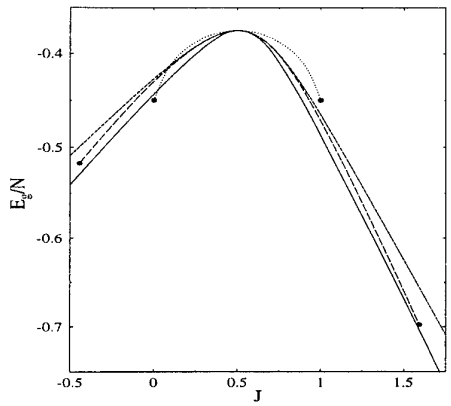

Fig. 2. Ground-state energy per atom as a function of J. Shown are the results from the spin-wave theory (dotted), the SUB2-2 scheme (short-dashed), and the full SUB2 scheme (long-dashed). The terminating points are indicated. The numerical results of Ref. [20] are also included (solid).

the extremely simple SUB2 scheme gives much better results for a wide range of the coupling constant J when compared with the numerical results of Ref. [20].

We notice that both spin-wave theory and the SUB2 scheme have two terminating points $J_c^{(1),(2)}$, beyond which, namely for $J < J_c^{(1)}$ and $J > J_c^{(2)}$, there is not real solution. For spin-wave theory, the two points are given by $J_c^{(1)} = 0$ and $J_c^{(2)} = 1$, while $J_c^{(1)} = -0.4443$ and $J_c^{(2)} = 1.591$ from the SUB2 scheme. The corresponding energy values of the SUB2 scheme are -0.5172 and -0.6977 respectively. In the past we had identified the SUB2 terminating points as the phase transition critical points of the anisotropic-Heisenberg models [18]. This is strongly supported by the calculations of the spin correlation functions and order parameters within the same CCM analysis. The following discussion of the triplet spectra of the spin-wave excitations also supports that the two terminating points $J = J_c^{(1),(2)}$ of the present dimerization case may again correspond to the quantum phase transitions of the frustrated systems.

The triplet spectra of Eq. (3.5) and Eq. (3.20) have the same qualitative behaviour. Fig. 3 shows the schematical plot of the spectrum from the SUB(2,1) scheme of the CCM at several values of J. The spectrum clearly shows a nonzero gap between the two terminating points and the gap collapses at both the terminating points. In particular, the triplet spectrum is flat with a gap value of 1 at $J = 1/2$. This flatness implies no coupling between pairs of spins (dimers) at $J = 1/2$ within the approximations. Since the simple dimer state $|D\rangle$ is the exact ground state at this point, the two-body correlation can be easily included in the excitation operator X and the corresponding two-body coefficients can be determined by a simple variational procedure similar to the well-known Feynman theory for the excitation spectrum of the ^{4}He superfluid [21]. Hence the excitaion operator with a lattice momentum q is

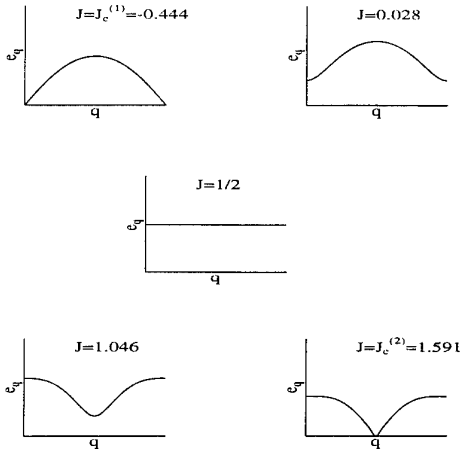

Fig. 3. Schematic plots of the triplet excitaions spectrum in the SUB(2,1) scheme at several values of J.

written as,

$$X_q = \sum_r e^{2iqr} A^r_{10} + \sum_{r,r'} f_q(r,r') A^r_{10} A^{r'}_{20}. \tag{3.21}$$

Taking $f_q(r,r')$ as the variational parameter to optimise the expectation value of the Hamiltonian, it is found that the gap in the spectrum is reduced by half at $q = 0$ and π, but remains at 1 at $q = \pi/2$ [22]. (The preliminary calculations of the similar SUB(2,2) scheme not only yield similar results at $J = 1/2$ but the whole spectrum as a function of J.) These results of the triplet spectrum from such a low-order approximation seem to agree with a more substantial calculation at $J = 1/2$ by Shastry and Sutherland [23]. They obtained the spectrum of a soliton-like excitation with a minimum gap of 0.25 at $q = 0$ and π and a maximum gap of about 1 at $q = \pi/2$. Tonegawa and Harada's numerical calculations [20] confirmed the nonzero gap at $J = 1/2$ and in the nearby region. They predicted that the gap collapses at $J_0 \approx 0.3$, while Haldane [24], who used a fermion representation, predicted this value to be about 1/6. Recently, J_0 has been estimated by the conformal field theory to be about 0.2411 [25]. In any case, this gapless point may correspond to a phase transition from the dimerized phase to a critical phase similar to the Heisenberg model at $J = 0$.

A more intriguing situation occurs for $J > 1/2$, where the triplet spectrum of both spin-wave theory and the SUB(2,1) scheme has a minimum at $q = \pi/2$. This certainly reminds us of the magneto-roton excitations in the fractional quantum Hall effects [26]. As J increases, the minimum (spin-roton gap) decreases and finaly at $J = J_c^{(2)}$, it collapses at $q = \pi/2$. Whether or not this suggests a phase change in the spatial periodicity of the system from double to four-fold, for example, is still unclear. The numerical calculations of the spin-spin correlation function [20] certainly show a more complicated feature for $J > 1/2$. In particular, the short-range four-fold Néel order ($\uparrow\uparrow\downarrow\downarrow\uparrow\uparrow\downarrow\downarrow\cdots$) is observed for $J > 1/2$, contrast to the case of $J < 1/2$ where

the ordinary short-range two-fold Néel order ($\uparrow\downarrow\uparrow\downarrow\cdots$) is observed [27]. As we know, at $J = \infty$, the model Hamiltonian of Eq. (3.1) becomes two uncoupled Heisenberg chain with a double lattice spacing showing a four-fold spatial periodicity. Clearly, higher-order calculations are needed to obtain a clearer picture.

To conclude this section, it should be pointed out that the dimerization order parameter, defined by $D \equiv \langle \mathbf{s}_{i-1} \cdot \mathbf{s}_i \rangle - \langle \mathbf{s}_i \cdot \mathbf{s}_{i+1} \rangle$, can be easily obtained within spin-wave theory and the SUB2 scheme of the CCM. In spin-wave theory, for example, D is found to be nonzero in the region of $0 < J < 1$ and gradually diminish when J moves toward the two terminating points; but at the two terminating points ($J = 0, 1$), D diverges to $-\infty$, implying a breakdown of spin-wave theory. The SUB2 scheme of the CCM, however, yields converging results even at the two terminating points, as it is the case in our previous CCM analysis for the 1D anisotopic-Heisenberg model [18]. Since it also involves the ground bra state which is not manifestly the Hermitian conjugate of the ground ket state in the CCM, our CCM analysis for the dimerization order parameter and correlation functions will appear elsewhere.

4. OTHER SYSTEMS

4.1 The Spin-1 Chains

Recently, the 1D Heisenberg-biquadratic spin-1 chain has attracted much attention because it provides very rich and interesting quantum phases. The model Hamiltonian is given by

$$H = \cos\theta \sum_i \mathbf{s}_i \cdot \mathbf{s}_{i+1} + \sin\theta \sum_i (\mathbf{s}_i \cdot \mathbf{s}_{i+1})^2, \quad s = 1 \tag{4.1}$$

where the coupling between spins is parametrized by θ. The FM phase is restricted to the region of $\pi/2 \leq \theta \leq 5\pi/4$, and the rest is non-FM.

There are a number of exact results available at several values of θ. In particular, at $\theta = -\pi/2$, the system is exactly known to be dimerized with a nonzero gap and the corresponding order parameter is about 42% of the perfect dimer state [11,12]. At $\tan\theta = 1/3$, the ground state is given by a homogeneous VB configuation with a nonzero energy gap but with no lattice symmetry breaking [7]. At $\theta = \pi/4$, the model is again integrable, the ground state clearly shows a triple spatial periodicity and the excitation spectrum becomes gapless at the lattice momentum $q = 0$ and $2\pi/3$ [28]. Based on these exact results, one tends to conclude that the system may show different phases representing by the following three VB states, the dimer state as shown in Fig. 1 (b), the trimer state in Fig. 1 (c) and the homogeneous VB state [7]. The expectation values of the Hamiltonian with respect to these three trial wavefunctions can be straightforwardly obtained as

$$\frac{E_0}{N} = \begin{cases} -\frac{4}{3}\cos\theta + 2\sin\theta, & \text{homogeneous;} \\ -\cos\theta + \frac{8}{3}\sin\theta, & \text{dimer;} \\ -\frac{2}{3}\cos\theta + \frac{10}{9}\sin\theta, & \text{trimer.} \end{cases} \tag{4.2}$$

These values are shown in Fig. 4 as a function of θ, together with the numerical results from finite-size exact calculations [18]. One sees that the dimer state has

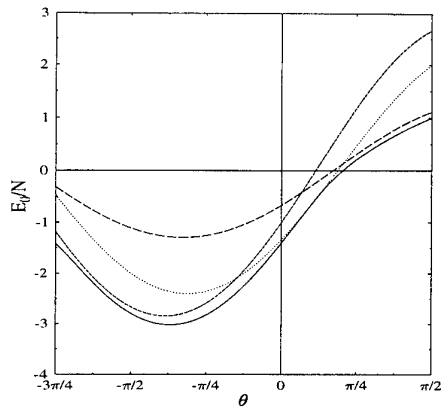

Fig. 4. Expectation values of the 1D spin-1 Hamiltonian as a function of θ with respect to the three simple VB states: homogeneous (dotted), dimer (short dashed), and trimer (long dash). Also shown are the results from finite-size exact calculations (solid).

lower energy than that of the homogeneous VB state for $\theta < \tan^{-1}(-1/2) \approx -26.6°$; for larger θ, however, the homogeneous VB state has lower energy. In particular, the homogeneous VB state is the exact ground state at $\tan\theta = 1/3$ [7]. At even larger θ, it is interesting to see that the trimer state has the lowest energy. This occurs when $\theta > \tan^{-1}(3/4) \approx 36.9°$. The lower envelope of the three curves is in general quite close to the 'exact' results over the entire non-FM region. This crude approximation certainly seems to give a clear picture for the three-phase diagram of the spin-1 system, so far as the ground-state energy is concerned. Of course, the precise locations of the boundaries between these phases given here are not to be trusted because of the gross simplification.

From the above analysis, it is clear that one can extend our previous calculations to the study the dimerization around the region of $\theta = -\pi/2$ and possible trimerization about $\theta \geq \pi/4$. Chubukov [29] applied a dimerized spin-wave theory using the Holstein-Primakoff bosonization to the Hamiltonian of Eq. (4.1) and indeed he found that over an extended region, the dimerized spin-wave excitations are stable. One certainly desires to obtain also other physical quantities, such as the ground-state energy, dimerization order parameter and the corresponding four-spin correlation functions, etc. The CCM analysis described in Sec. 3 for the spin-$\frac{1}{2}$ model can certainly provide a systematic means to obtain these physical quantities.

The possible trimerization of the spin-1 chain was discussed in Ref. [13] where the equations of motion were derived for the creation and destruction operators A^r_{n0} and A^r_{0n} ($n = 1, 2, \ldots, 26$) with r denoting each of the trimers in Fig. 1 (c). After a truncation in the Hilbert space, namely restricting to $n = 1, 2, \ldots, 9$, the trimerized spin-wave spectra were obtained. The lowest mode shows a nonzero gap associated with the trimerization, and this gap collapses at precisely $\theta = \pi/4$ and $\theta = \pi/2$. In particular, at $\theta = \pi/4$, the spectrum becomes gapless at lattice momentum $q = 0$ and $2\pi/3$ with a spin-wave velocity of $3/\sqrt{5} \approx 1.342$. This spectrum compares well with

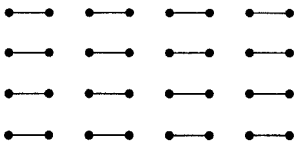

Fig. 5. A column dimer VB state for the 2D frustrated Heisenberg model on the square lattice.

the exact result of Sutherland [28], which has a spin-wave velocity of $\sqrt{2}\pi/3 \approx 1.481$. At $\theta = \pi/2$, where the system is known to become FM, a constant zero spectrum was obtained. Again, the CCM analysis using A^{-}_{n0} and A_{0n} ($n = 1, 2, \ldots, 26$) with the trimer model state should provide more systematic and reliable results.

4.2 The Spin-$\frac{1}{2}$ Frustrated Model on the Square Lattice

The 2D spin-$\frac{1}{2}$ frustrated Heisenberg model on the square lattice is described by the following Hamiltonian

$$H = \frac{1}{2}\sum_{i,\rho} \mathbf{s}_i \cdot \mathbf{s}_{i+\rho} + \frac{1}{2}J\sum_{i,\rho'} \mathbf{s}_i \cdot \mathbf{s}_{i+\rho'}, \tag{4.3}$$

where i runs over all lattice sites, and ρ and ρ' over all nearest-neighbour and next-nearest-neighbour (diagonal) sites respectively. Because its possible relevance to the high-temperature superconductors, a variety of techniques has been applied to this model [14]. One now generally believes that the system shows the classical Néel-like order [ordering wavevector $\mathbf{Q} = (\pi, \pi)$] for small J and the collinear magnetic order [$\mathbf{Q} = (0, \pi)$] for $J \approx 0.65$ or larger. Between these two phases, i.e., $0.35 < J < 0.6$, no Néel-like nor collinear order is observed. Although there is no clear consensus on the zero-temperature structure for this nonmagnetic region, the column dimerized phase shown in Fig. 5 has been proposed [14]. In particular, Chubukov again applied his dimerized spin-wave theory to the Hamiltonian of Eq. (4.3). His results seem to agree with the numerical calculations which suggest that the column dimer VB state may be stable around $J = 1/2$. But it is fair to say that a more systematic approach is needed before one can reach the definite conclusion on the dimerization of the 2D square lattice. It is quite straightforward to extend our CCM analysis for the 1D spin-$\frac{1}{2}$ frustrated chain described in Sec. 3 to the present 2D case. We will report these results soon.

4.3 The Spin-1 Models on the *Kagomé* Lattice

Spin models on the *kagomé* lattice are another group of frustrated systems because the ground state of the classical Ising model on the *kagomé* lattice has infinite degeneracy. In addition to their intrinsic theoretical interest, some spin models on the *kagomé* lattice may have been realized in experiments. For example, in a layered compound Sr-Cr-Ga-O, the $s = 3/2$ Cr^{3+} ions form a stack of dense *kagomé* lattices

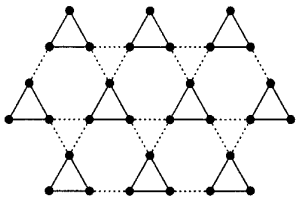

Fig. 6. The spin-1 *kagomé* lattice.

separated by more dilute triangular lattices [30]. And the spin-$\frac{1}{2}$ Heisenberg model on the *kagomé* lattice has been proposed to explain the interesting phenomena observed in the experiments with ^{3}He atoms deposited on the graphite substrate [15].

Here the case of the spin-1 models on the *kagomé* lattice is considered. It is useful to study the following trimerized Hamiltonian,

$$H(J) = \left(\sum_{\langle ij \rangle} + J \sum_{(ij)} \right) \mathbf{s}_i \cdot \mathbf{s}_j, \quad s = 1, \tag{4.4}$$

where, as shown in Fig. 6, $\langle ij \rangle$ denote the solid bonds and (ij) the dashed bond. The symmetric model is given by $J = 1$. At $J = 0$, the perfect trimer VB configuration (i.e., solid bonds in Fig. 6) is the exact ground state. Therefore one expects that the trimerized spin-wave theory discussed in Sec. 4.1 for the spin-1 chain should be a good approximation for at least small J. I have applied the method of equation-of-motion for the operators A^r_{n0} and A^r_{0n} with $n = 1, 2, \ldots, 9$, restricting the Hilbert space of each trimer (denoted by the new lattice vector r) to the first ten states. The trimerized spin-wave spectra have been obtained as functions of J. Unfortunately, the spectra are found to be stable only when $J \leq 1/2$, and the symmetric point $J = 1$ seems to be beyond this simple spin-wave approximation.

However, similar to the 1D spin-1 case discussed earlier, one can in general consider the spin-1 Heisenberg-biquadratic model on the *kagomé* lattice. This model is given by adding a quadratic term to Eq. (4.4),

$$H' = J' \sum_{i,\rho} (\mathbf{s}_i \cdot \mathbf{s}_{i+\rho})^2, \tag{4.5}$$

where, as before, ρ denotes nearest-neighbour sites on the *kagomé* lattice. From the experience of the 1D spin-1 chain, one expects that the quadratic term of of Eq. (4.5) may stabilize the trimer VB state over an extended region of J' and even at the symmetric point of $J = 1$. This work is in progress.

5. CONCLUSION

In this article, I have described our microscopic approach to the quantum spin systems with an anticipated VBL long-range order. The perfect VBL consisting of

independent simple VBs is taken as the model state and the corresponding composite operators first developed by Parkinson are employed. Two approximation schemes are developed, firstly a spin-wave theory via bosonization transformation and secondly the more systematic analysis within the framework of the CCM. The general formalism for the quantum correlations in the ground and excited states of the VBL systems are given. In particular, the simple 1D spin-$\frac{1}{2}$ frustrated model have been investigated in detail as a demonstration. The extensions of our approach to the spin-1 Heisenberg-biquadratic chain and to the 2D frustrated models on the square lattice and *kagomé* lattice are also discussed. The preliminary results presented in this article are quite promising indeed. There is much more work to do. I wish to report our new results in the near future.

ACKNOWLEDGEMENTS

I am grateful to R.F. Bishop for introducing me the powerful CCM and for constant encouragement without which this work would not be possible, and to J.B. Parkinson for providing the numerical results of finite-size calculations prior to publication. I also wish to express my gratitude to R. Guardiola and J. Navarro for the introduction of the computer algebra package (REDUCE) which was used to derive those coupled set of equations in the CCM analysis. The partial travel support from the European Research Office of the United States Army is also acknowledged.

APPENDIX
SYMMETRY THEOREM OF THE COUPLED-CLUSTER METHOD

In Sec. 3.2, the SUB2 scheme of the CCM provides a solution which preserves the rotational symmetry (i.e., $s_{\rm total} = 0$) of the model state $|D\rangle$, although one started with the operators in the sector of $s^z_{\rm total} = 0$. This is true in any general application of the CCM. A brief proof of the following theorem is given in this Appendix: the CCM equations at any level of approximations always provide at least a solution which guarantees the symmetry of the model state if this symmetry is one of those belonging to the Hamiltonian.

Let Λ be a symmetry operator, associated with which the model state $|\Phi\rangle$ has an eigenvalue λ_0, namely $\Lambda|\Phi\rangle = \lambda_0|\Phi\rangle$. Let Hamiltonian H commutes with Λ, $[\Lambda, H] = 0$. Therefore, one has

$$\Lambda H|\Phi\rangle = \lambda_0 H|\Phi\rangle. \qquad (A.1)$$

(I). *Eigen operator representation.* Let C_I^+ and C_J^+ be the multi-configurational creation operators with respect to $|\Phi\rangle$, with the set-indices I and J respectively labeling the general multi-particle cluster configurations. The corresponding destruction operators are denoted as C_I and C_J respectively. Assuming that C_I^+ commutes with Λ,

$$[\Lambda, C_I^+] = 0, \quad \forall I, \qquad (A.2)$$

but C_J^+ does not. Instead, C_J^+ has the following commutations,

$$[\Lambda, C_J^+] = \lambda_1'(J) C_J^+, \quad \lambda_1'(J) \neq 0, \quad \forall J. \qquad (A.3)$$

Therefore one has for any positive integer n

$$\Lambda(C_I^+)^n|\Phi\rangle = \lambda_0(C_I^+)^n|\Phi\rangle, \quad \forall I, \tag{A.4}$$

and

$$\Lambda C_J^+|\Phi\rangle = \lambda_1(J)C_J^+|\Phi\rangle, \quad \lambda_1(J) \equiv \lambda_0 + \lambda_1'(J). \tag{A.5}$$

The CCM correlation operator S is defined as

$$S \equiv \sum_I{}' \mathcal{S}_I C_I^+ + \sum_J \mathcal{S}_J C_J^+, \tag{A.6}$$

where the prime implies that the identity term, $C_0^+ \equiv \mathbf{1}$, is excluded. The correlation coefficients $\{\mathcal{S}_I, \mathcal{S}_J\}$ of Eq. (A.6) are determined by the following sets of the coupled equations,

$$\langle\Phi|C_I e^{-S} H e^S|\Phi\rangle = 0, \quad \forall I\ (\neq 0), \tag{A.7a}$$
$$\langle\Phi|C_J e^{-S} H e^S|\Phi\rangle = 0, \quad \forall J, \tag{A.7b}$$

where the expansion of the similarity-transformed Hamiltonian

$$e^{-S} H e^S = H + [H, S] + \frac{1}{2!}[[H, S], S] + \cdots, \tag{A.8}$$

will terminate at a finite order if H contains a finite number of destruction operators.

We notice that the states $H|\Phi\rangle, [H, C_I^+]|\Phi\rangle, [[H, C_I^+], C_{I'}^+]|\Phi\rangle, \ldots$, all have the eigen value λ_0 for Λ by Eqs. (A.1) and (A.4). However, the state $C_J^+|\Phi\rangle$ has a different eigenvalue, $\lambda_1(J)$ $(\neq \lambda_0)$. Therefore they must be orthogonal to one another, namely

$$\langle\Phi|C_J H|\Phi\rangle = 0, \quad \forall J \tag{A.9a}$$
$$\langle\Phi|C_J[H, C_I^+]|\Phi\rangle = 0, \quad \forall J, I \tag{A.9b}$$
$$\langle\Phi|C_J[[H, C_I^+], C_{I'}^+]|\Phi\rangle = 0, \quad \forall J, I, I' \tag{A.9c}$$

etc. Using Eq. (A.8), one immediately concludes that Eqs. (A.7) have at least a solution given by $\mathcal{S}_J = 0$ for all J. If this solution is taken, the correlation operator S of Eq. (A.6) preserves the symmetry of $|\Phi\rangle$.

(II). *Non-eigen operator representation.* let $C_I^+ \equiv (C_I^+(0), C_I^+(1), ..., C_I^+(n_I - 1))$ be the multi-configurational creation operators with respect to $|\Phi\rangle$, with n_I the dimension of the symmetry Λ within a set I. Assuming $C_I^+(n)$ do not have the commutations as in Eq. (A.2) or Eq. (A.3). Let the corresponding correlation coefficients be $\mathcal{S}_I \equiv (\mathcal{S}_I(0), \mathcal{S}_I(1), ..., \mathcal{S}_I(n_I - 1))$. The CCM correlation operator is then written as

$$S = \sum_I{}' \mathcal{S}_I \cdot C_I^+ \equiv \sum_I{}' [\mathcal{S}_I(0)C_I^+(0) + \mathcal{S}_I(1)C_I^+(1) + \cdots + \mathcal{S}_I(n_I - 1)C_I^+(n_I - 1)], \tag{A.10}$$

where the primes again imply exclusion of the identity term, $I = 0$.

As before, the correlation coefficients $\{\mathcal{S}_I(i), i = 0, 1, ..., n_I - 1\}$ are determined by the following set of the coupled equations

$$\langle\Phi|C_I(i)\mathrm{e}^{-S}H\mathrm{e}^{S}|\Phi\rangle = 0, \quad i = 0, 1, ..., n_I - 1 \text{ and } \forall I \ (\neq 0). \tag{A.11}$$

Let $B_I^+ \ [\equiv (B_I^+(0), B_I^+(1), ..., B_I^+(n_I - 1))] = T_I \cdot C_I^+$, where T_I is a c-number $(n \times n)$ matrix and is chosen such that $B_I^+(0)$ commutes with the symmetry operator Λ, namely

$$[\Lambda, B_I^+(0)] = 0, \quad \forall I, \tag{A.12}$$

but

$$[\Lambda, B_I^+(j)] = \lambda_j'(I)B_I^+(j), \quad \lambda_j'(I) \neq 0, \quad j = 1, ..., n_I - 1 \text{ and } \forall I. \tag{A.13}$$

Multiplying Eq. (A.11) by the corresponding elements of the c-number Hermitian matrix of T_I, and after a simple summation, one derives the following equivalent equations

$$\langle\Phi|B_I(j)\mathrm{e}^{-S}H\mathrm{e}^{S}|\Phi\rangle = 0, \quad j = 0, 1, ..., n_I - 1 \text{ and } \forall I \ (\neq 0), \tag{A.14}$$

where S can be equivalently written as

$$S = \mathcal{S}_I' \cdot B_I^+, \quad \mathcal{S}_I' \equiv \mathcal{S}_I \cdot T_I^{-1}. \tag{A.15}$$

According to (I), there is at least a solution to Eq. (A.14) hence to Eq. (A.11) in which $\mathcal{S}_I'(j) = 0$ for all $j \neq 0$. If this solution is chosen, the symmetry of the model state is preserved. Q.E.D.

REFERENCES

1. P.W. Anderson, Phys. Rev. **86**, 694 (1952); T. Oguchi, *ibid.* **117**, 117 (1960).
2. E. Manousaki, Rev. Mod. Phys. **63**, 1 (1991); T. Barnes, Int. J. Mod. Phys. C **2**, 659 (1991).
3. H.A. Bethe, Z. Phys. **71**, 205 (1931); L. Hulthén, Ark. Mat. Astron. Fys. A **26**, No. 11 (1938).
4. P.W. Anderson, Mater. Res. Bull. **8**, 153 (1973).
5. P.W. Anderson, Science **235**, 1196 (1987).
6. C.K. Majumdar and D.K. Ghosh, J. Phys. C **3**, 91 (1970); J. Math. Phys. **10**, 1388, 1399 (1969).
7. I. Affleck, T. Kennedy, E. Lieb, and H. Tasaki, Phys. Rev. Lett. **59**, 799 (1987).
8. D.P. Arovas, A. Auerbach, and F.D.M. Haldane, Phys. Rev. Lett. **60**, 531 (1988).
9. F.D.M. Haldane, Phys. Lett. **93A**, 464 (1983); Phys. Rev. Lett. **50**, 1153 (1983).
10. There is, however, a hidden symmetry breaking in the valence-bond solid. See K. Rommels and M. den. Nijs, Phys. Rev. Lett. **59**, 2578 (1987).
11. J.B. Parkinson, J. Phys. C **20**, 21 (1988); M.N. Barber and M.T. Batchelor, Phys. Rev. B **40**, 4621 (1989); A. Klümper, Europhys. Lett. **9**, 815 (1989); I. Affleck, J. Phys.: Condens. Matter **2**, 405 (1990).

12. Y. Xian, Phys. Lett. A **183**, 437 (1993).
13. Y. Xian, J. Phys.: Condens. Matter **5**, 7489 (1993).
14. R.R.P. Singh and R. Narayanan, Phys. Rev. Lett. **65**, 1072 (1990); A.V. Chubukov and Th. Jolicoeur, Phys. Rev. B **44**, 12050 (1991); N. Read and S. Sachdev, Phys. Rev. Lett. **66**, 1773 (1991); H.J. Schulz, T.A.L. Ziman, and D. Poilblanc, preprint (1994).
15. V. Elser, Phys. Rev. Lett. **62**, 2405 (1989); J.B. Marston and C. Zeng, J. Appl. Phys. **69**, 5692 (1991).
16. J.B. Parkinson, J. Phys. C **12**, 2873 (1979).
17. R.F. Bishop and H. Kümmel, Phys. Today **40(3)**, 52 (1987); R.F. Bishop, Theo. Chim. Acta **80**, 95 (1991).
18. R.F. Bishop, J.B. Parkinson, and Y. Xian, Phys. Rev. B **43**, 13782 (1991); **44**, 9425 (1991); J. Phys.: Condens. Matter **4**, 5783 (1992); J. Phys.: Condens. Matter **5**, 9169 (1993).
19. R.F. Bishop, R.G. Hale and Y. Xian, UMIST preprint (1994).
20. T. Tonegawa and I. Harada, J. Phys. Soc. Japan **56**, 2153 (1987); and courtesy of J.B. Parkinson.
21. R.P. Feynman and M. Cohen, Phys. Rev. **102**, 1189 (1956); H.W. Jackson and E. Feenberg, Rev. Mod. Phys. **34**, 686 (1962).
22. Y. Xian, unpublished.
23. S.S. Shastry and B. Sutherland, Phys. Rev. Lett. **47**, 964 (1981); W.J. Caspers, K.M. Emmett, and W. Magnus, J. Phys. A **17**, 2697 (1984).
24. F.D.M. Haldane, Phys. Rev. B **25**, 4925 (1982).
25. K. Okamoto and K. Nomura, Phys. Lett. A **169**, 433 (1992).
26. S.M. Girvin, A.H. MacDonald, and P.M. Platzman, Phys. Rev. Lett. **54**, 581 (1985); S.M. Girvin, in *Quantum Hall Effects* (ed. R.E. Prange and S.M. Girvin), Springer-Verlag, New York, 1987, p. 353.
27. I am grateful to C. Zeng for pointing out this to me.
28. B. Sutherland, Phys. Rev. B **12**, 3795 (1975).
29. A.V. Chubukov, Phys. Rev. B **43**, 3337 (1991).
30. A.P. Ramiresz, G.P. Espinosa, and A.S. Cooper, Phys. Rev. B **45**, 2505 (1992), and references there in.

STATISTICAL KERNEL POLYNOMIAL METHOD FOR MEGADIMENSIONAL HAMILTONIANS

H. Röder

Dept. of Physics, University of Bayreuth
W–95440 Bayreuth, Germany

R. N. Silver
MS B262 Theoretical Division
Los Alamos National Laboratory
Los Alamos, NM 87545, USA

1. INTRODUCTION

In many areas of modern numerical studies one is faced with the problem of diagonalising large matrices. Since in typical diagonalization algorithms required storage scales with the dimension N of the matrix as $O(N^2)$ and cpu time as $O(N^3)$, the limiting matrix dimensions is a few times 10^4. In the case where the matrices are very sparse, algorithms that make use of the sparsity of the matrix can be used. These algorithms, like the Lanczos method, the conjugate gradient method and the vector iteration, use only matrix vector multiplications (MVMs) to extract a few, isolated eigenvalues. All programming effort can be concentrated on fast and efficient MVMs. The Lanczos method, especially, has been used succesfully in many studies of ground state properties of strongly interacting fermions and quantum mechanical spin systems. If one is interested in thermodynamic properties, one needs more than just ground state information. To generate a complete set of eigenvalues using Lanczos diagonalization, or related methods, may require a number of MVMs far exceeding N. Invoking such procedures which exactly calculate all individual eigenenergies can be both irrelevant and impractical for statistical mechanics. Precise information on integrated numbers of states can be far more important than good energy resolution. Approximate methods may be adequate to meet the goals of the calculation, and they may be preferred if the computational expense is dramatically reduced.

In this spirit, we propose a new statistical method [1], scaling as $O(N)$ for sparse Hamiltonians, for estimating the density of states (DOS) and thermodynamic functions. The method may also be applicable to many other areas of science and

engineering where statistical estimates of properties of huge matrices may suffice. We presume the matrix is sufficiently large that the only practical operation is repeated MVM. Input to our procedure should be an efficient algorithm to multiply the Hamiltonian matrix onto any initial vector. This is the same as required by the Lanczos method. For a small number of MVMs and when only low energy resolution is required, a variety of methods exist to estimate DOS from a small number of power moments [2]. But when higher energy resolution is needed, determination of DOS from pure power moments has been shown to be ill-conditioned [3].

Our approach begins by putting lower and upper bounds on energies in the DOS. If these are not known in advance, they can be calculated efficiently by Lanczos diagonalization. These bounds define an interval for an orthogonal polynomial (*modified moment*) expansion of the DOS. Such expansions are known to be well-conditioned [3]. A stochastic method to estimate polynomial moments of the DOS uses MVM on Gaussian random vectors and polynomial recurrence relations. The DOS estimate is taken to be a modified kernel polynomial [4] constructed from polynomial moments. The modification is chosen to damp the Gibbs phenomenon which occurs for abrupt truncation of series expansions. We term the output of this procedure a *kernel estimate.*

A kernel estimate is a *controlled* approximation to the DOS and quantities formed from it. It equals the exact DOS 'convolved' with a known kernel (resolution function) plus additive noise with known covariance properties. In this sense, kernel estimates are similar to experimental data taken by a spectrometer, with resolution and statistical accuracy at the discretion of the experimenter. Energy resolution is inversely proportional to the number of MVM's, M. Noise covariance is inversely proportional to the number of random vectors, J, and it is calculable from the DOS. For purposes of discussion, let us assume the Hamiltonian is sparse so each MVM requires an operation count proportional to N. Cpu time to calculate a kernel estimate to a given statistical accuracy and fractional energy resolution scales at least as fast as $O(N \times J \times M)$. Memory scales as $O(3 \times N + M)$. However, for thermodynamic and other integrated properties of DOS, the required number of random vectors can decrease as N increases because of a statistical averaging effect, resulting in sublinear scaling with N. Indeed, for extremely large N we usually find one random vector to be sufficient to determine thermodynamic functions except at the lowest temperatures.

Section 2 develops the kernel polynomial representation of densities of states, thermodynamic functions, and operator expectation values in the canonical ensemble. And it discusses damping of the Gibbs phenomenon. Section 3 presents a stochastic method to calculated polynomial moments of a DOS, and estimate statistical errors on kernel estimates. Section 4 illustrates the method for the DOS and thermodynamic functions of the Heisenberg antiferromagnet. Section 5 concludes.

2. KERNEL POLYNOMIAL ESTIMATES OF DOS

Our goal is to calculate DOS of an $N \times N$ Hamiltonian $\mathbf{H}$, defined as

$$D(\varepsilon) = \frac{1}{N} \sum^{N} \delta(\varepsilon - \varepsilon_n) \quad , \tag{1}$$

where ε_n are eigenenergies. From this, we wish to calculate thermodynamic functions.

The first step is to put lower, ε_l, and upper, ε_u, bounds on energies in DOS. If these are not known a priori, they can be determined by Lanczos diagonalization [5] using the same MVM routine required for calculating kernel estimates. Sufficient accuracy is typically obtained with less than 30 MVM's. A scaled Hamiltonian matrix, $\mathbf{X}$, is defined by $\mathbf{H} = c\mathbf{X} + d$ where $c \equiv (\varepsilon_u - \varepsilon_l)/2$ and $d \equiv (\varepsilon_u + \varepsilon_l)/2$. Eigenvalues of $\mathbf{X}$ satisfy $-1 \leq x_n \leq +1$.

We assume the scaled DOS can be represented by an orthogonal polynomial expansion,

$$D(x) = \frac{1}{N}\sum_{n=1}^{N}\delta(x - x_n) = w(x)\sum_{m=0}^{\infty} a_m T_m(x) \quad . \tag{2}$$

In principle, any orthogonal polynomials defined over this interval could be used. But manipulations of Chebyshev polynomial expansions are particularly simple because they are isomorphic to Fourier series. The $T_m(x)$ are taken to be Chebyshev polynomials of the first kind defined by recurrence relations,

$$T_o(x) = 1 \quad ; \quad T_1(x) = x \quad ; \quad T_{m+1}(x) = 2xT_m(x) - T_{m-1}(x) \quad . \tag{3}$$

Their weight function is $w(x) = 1/\sqrt{1-x^2}$. They are orthogonal satisfying

$$\int_{-1}^{1} w(x)T_m(x)T_n(x)dx = \frac{\pi}{2}\delta_{m,n} \quad \{m,n \geq 1\} \quad ; \quad \pi \quad \{m = n = 0\}. \tag{4}$$

Defining $\theta \equiv \arccos(x)$, T_m may be expressed in terms of trigonometric functions

$$T_m(x) = \cos(m\theta) \quad . \tag{5}$$

Equation (2) is analogous to a Fourier series

$$D(x) = \frac{1}{\sin(\theta)}\sum_{m=0}^{\infty} a_m \cos(m\theta) \quad . \tag{6}$$

A *kernel polynomial of degree M* [4] is defined by

$$\int_{-1}^{1} K_M(x, x_o)D(x_o)dx_o = \sum_{m=0}^{M} a_m T_m(x) \quad . \tag{7}$$

for arbitrary a_m. It generates truncated series expansions of $D(x)$. However, abrupt truncation of a Fourier series will result in lack of uniform convergence ('ringing') at jump discontinuities in a DOS. This is known as the Gibbs phenomenon [6]. We prefer to use *modified kernel polynomials* defined by

$$\int_{-1}^{1} \tilde{K}(x, x_o)D(x_o)dx_o = w(x)\sum^{M} a_m g(m, M)T_m(x) \quad . \tag{8}$$

The $g(m,M)$ are *Gibbs damping factors*, which are positive smoothly decreasing functions satisfying $g(0,M)=1$ and $g(M,M)=0$. They may also implicitly depend on M. Eq. (8) is satisfied by

$$\tilde{K}(x,x_o)=\frac{2w(x)}{\pi}[\frac{1}{2}+\sum_{m=1}^{M}g(m,M)T_m(x)T_m(x_o)] \quad . \tag{9}$$

We consider only $g(z)$ which produce the limit,

$$\lim_{M-\infty}\int_{-1}^{1}\tilde{K}(x,x_o)D(x_o)dx_o=D(x) \quad , \tag{10}$$

corresponding to the completeness property of orthogonal polynomials. At finite M, $\tilde{K}(x,x_o)$ is peaked at $x=x_o$ with a full-width-half-maximum (FWHM) proportional to $1/M$. Normalization is preserved, $\int_{-1}^{1}\tilde{K}(x,x_o)dx=1$.

We now consider approximations to DOS constructed by identifying a_m in Eq. (2) with polynomial moments of the true DOS,

$$a_0=\frac{1}{\pi} \quad ; \quad \{m\geq 1\} \quad a_m=\frac{2}{\pi}g(z)\mu_m \qquad \mu_m\equiv\int_{-1}^{1}T_m(x)D(x)dx \quad . \tag{11}$$

This corresponds to a *kernel estimate* of DOS constructed from M moments,

$$D_K(x)=\int_{-1}^{1}\tilde{K}(x,x_o)D(x_o)dx_o \quad . \tag{12}$$

$\tilde{K}$ is the effective *resolution function* for this kernel polynomial 'spectrometer'. Eq.(12) is a Fredholm integral equation of the 1st kind preserving normalization.

The usefulness of a kernel estimate depends on the height of the peak at $x\approx x_o$ and rapidity of its fall at large $|x-x_o|$. This property is controlled by the choice of Gibbs damping factor, $g(z)$. A variety of Gibbs damping factors have been proposed in the literature, designed to suppress Gibbs phenomena at the expense of the rate of convergence of series. For our problem, this translates to suppressing Gibbs oscillations in $\tilde{K}(x,x_o)$ at large $|x-x_o|$ at the expense of the FWHM of the central peak at $x\approx x_o$. As M becomes large, the central peak in $\tilde{K}(x,x_o)$ narrows, and D_K will uniformly converge to $D(x)$, provided $g(z)$ are appropriately chosen. Fortunately an optimal Gibbs damping functions can be found in the mathematics literature [7]. Optimal means that the half width of the central peak is minimized under the constraint that the DOS remains positive everywhere. This leads to the following form of the Gibbs damping factors:

$$g(m,M)=\sum_{k=0}^{M-m}c_kc_{k+m} \quad , \quad c_m=c_0U_m(\lambda) \quad , \quad \lambda=\cos(\frac{\pi}{M+2}) \quad . \quad \sum_{m=0}^{M}c_m^2=1. \tag{13}$$

where U_m are Chebychew polynomials of the second kind.

Kernel estimates yield simple moment expansions of thermodynamic functions. Using the relation

$$e^{-u\cos(\theta)} = I_o(u) + 2\sum_{n=1}^{\infty}(-1)^n I_n(u)\cos(n\theta) \quad , \tag{14}$$

an exact expansion of the partition function is

$$Z \equiv N\int_{\varepsilon_l}^{\varepsilon_u} e^{-\beta(\varepsilon-\varepsilon_l)}D(\varepsilon)d\varepsilon = Ne^{-\beta c}\left[I_o(\beta c)\mu_o + 2\sum_{m=1}^{\infty}(-1)^m I_m(\beta c)\mu_m\right] \quad . \tag{15}$$

The I_m are modified Bessel functions and $\beta = 1/T$. (Note, the Legendre polynomial variant of kernel estimators yields expansions in half-integer modified Bessel functions.) In practice, this series may be truncated without significant systematic error because the I_m fall off rapidly with increasing m. Machine precision provides a limit on the number of moments possible in practice.

Matrix operators may be defined which are analogous to the functions discussed in this section. For a scaled Hamiltonian matrix $\mathbf{X}$, $T_m(\mathbf{X})$ is the corresponding *polynomial operator*, and $\tilde{K}(x,\mathbf{X})$ is the corresponding *kernel operator*. Thus, polynomial moments are

$$\mu_m = \frac{1}{N}Tr\{T_m(\mathbf{X})\} \quad . \tag{16}$$

The kernel estimate for a DOS may be written

$$D_K(x) = \frac{1}{N}Tr\{\tilde{K}(x,\mathbf{X})\}. \quad . \tag{17}$$

We shall use these definitions in the next section.

Kernel estimates may be extended to operator expectation values. For example, consider a matrix operator $\mathbf{O}$. A kernel estimate for its thermodynamic expectation value,

$$\overline{O} \equiv \frac{Tr\{\mathbf{O}e^{-\beta\mathbf{H}}\}}{Z} \quad , \tag{18}$$

is given by

$$\overline{O}_K = \frac{1}{Z_K}\int_{-1}^{1} e^{-\beta(cx+d)}Tr\{\mathbf{O}\tilde{K}(x,\mathbf{X})\}dx \quad . \tag{19}$$

And, similar to the partition function, expansions can be derived for such operator expectation values in terms of modified Bessel functions and moments of the form $\mu_m(\mathbf{O}) \equiv Tr\{\mathbf{O}T_m(\mathbf{X})\}/N$.

3. STOCHASTIC EVALUATION

Use of Gaussian random vectors for the stochastic calculation of polynomial moments has been discussed previously [8] in the context of maximum entropy methods for estimating DOS. Here, we consider application of Gaussian random vectors to calculate kernel estimates of DOS

We propose a statistical estimator for D_K,

$$\widehat{D}_K(x) = \frac{1}{J}\sum_{j=1}^{J} < G(j)|\tilde{K}(x,\mathbf{X})|G(j) > \quad . \tag{20}$$

The $|G(j)>$ are Gaussian independent random vectors of unit variance, defined by

$$|G(j)> \equiv \frac{1}{\sqrt{N}}\sum_{k=1}^{N} a_k(j)|k> \tag{21}$$

where $|k>$ are convenient basis states for the Hamiltonian. The a_k are components of an N dimensional random vector, $\mathbf{a}$, *i.i.d.* (independently and identically drawn) from a Gaussian distribution of unit variance. Its probability is

$$P[\mathbf{a}] = \frac{1}{(2\pi)^{N/2}} \exp\left(-\frac{\mathbf{a}^\dagger \mathbf{a}}{2}\right) \quad . \tag{22}$$

The *statistical expectation value* for any function $O(\mathbf{a})$ is

$$\mathbf{E}[O] \equiv \int d\mathbf{a} P[\mathbf{a}] O(\mathbf{a}) \quad . \tag{23}$$

For example, $\mathbf{E}[a_k(j)] = 0$, $\mathbf{E}[a_k(j)a_l(j')] = \delta_{k,l}\delta_{j,j'}$, etc. Therefore,

$$\mathbf{E}[\widehat{D}_K(x)] = D_K(x) \quad , \tag{24}$$

so $\widehat{D}_K(x)$ may be termed an *unbiased estimator* for $D_K(x)$.

An efficient procedure to calculate DOS begins with an unbiased estimator for moments,

$$\widehat{\mu}_m = \frac{1}{J}\sum_{j=1}^{J} < G(j)|T_m(\mathbf{X})|G(j) > \quad . \tag{25}$$

The recurrence relation for 1st kind Chebyshev polynomials is applied to each independent Gaussian random vector, $|G(j)>$,

$$T_o(\mathbf{X})|G(j)> = |G(j)> \qquad T_1(\mathbf{X})|G(j)> = \mathbf{X}|G(j)>$$

$$T_{m+1}(\mathbf{X})|G(j)> = 2\mathbf{X}T_m(\mathbf{X})|G(j)> - T_{m-1}(\mathbf{X})|G(j)> \quad . \tag{26}$$

Moments are constructed using

$$T_{2m}(x) = 2T_m(x)T_m(x) - 1 \qquad T_{2m-1}(x) = 2T_m(x)T_{m-1}(x) - x \quad . \tag{27}$$

Thus, unbiased estimators are

$$\widehat{\mu}_{2m} = \frac{1}{J}\sum_{j}^{J} (2 < G(j)|T_m(\mathbf{X})T_m(\mathbf{X})|G(j) > - < G(j)|G(j) >) \quad , \tag{28}$$

and similarly for $\widehat{\mu}_{2m-1}$. First kind Chebyshev polynomials are especially convenient because calculation of M moments requires $M/2$ MVM's per random vector. The memory required for this recurrence procedure is for two vectors, which is $2N$.

The success of this procedure should be judged on how efficiently it achieves the scientific goals of the calculation. Are the systematic and statistical errors acceptable in exchange for the significant reduction in computational effort? Systematic errors are easily evaluated by studying convergence with increasing numbers of moments, as discussed in the previous section. Calculation of statistical errors begins by expanding a random vector $|G(j)>$ in eigenstates $|n>$ of $\mathbf{X}$,

$$|G(j)> = \frac{1}{\sqrt{N}} \sum_{n=1}^{N} b_n(j)|n> \quad . \tag{29}$$

Define a random variable $\delta D_K(x) \equiv \widehat{D}_K(x) - D_K(x)$, such that

$$\delta D_K(x) \equiv \frac{1}{N} \sum_{n=0}^{N} \tilde{K}(x, x_n) \frac{1}{J} \sum_{j=1}^{J} (b_n^2(j) - 1) \quad . \tag{30}$$

The $\mathbf{b}(j)$ are related to $\mathbf{a}(j)$ by the orthonormal transformation which diagonalizes $\mathbf{X}$. Hence, sampling $\mathbf{a}(j)$ from a Gaussian distribution of unit variance is equivalent to sampling $\mathbf{b}(j)$ in the same way. The $\mathbf{b}(j)$ have analogous expectation values to those for $\mathbf{a}(j)$. In particular $\mathbf{E}[b_n^2(j)] = 1$, so $\mathbf{E}[\delta D_K(x)] = \mathbf{0}$. The most important relation for calculating statistical errors is

$$\mathbf{E}[(b_n^2(j) - 1)(b_{n'}^2(j') - 1)] = 2\delta_{n,n'}\delta_{j,j'} \quad . \tag{31}$$

Then,

$$Cov(x, x') = \mathbf{E}[\delta D_K(x) \delta D_K(x')] = \frac{2}{JN^2} \sum_{n=0}^{N} \tilde{K}(x, x_n) \tilde{K}(x', x_n) \quad . \tag{32}$$

This may be approximated by

$$Cov(x, x') \approx \frac{2}{JN} \int_{-1}^{1} \tilde{K}(x, x_o) \tilde{K}(x', x_o) D_K(x_o) dx_o \quad . \tag{33}$$

Most often we are interested in an integrated function of the DOS, say $I \equiv \int_{-1}^{1} I(x) D(x) dx$. This would be approximated by a kernel estimate, i.e. $I \approx I_K \equiv \int_{-1}^{1} I(x) D_K(x) dx$. Statistical errors are given by the square root of the variance,

$$\mathbf{E}[(\delta I_K)^2] = \int I(x) I(x') Cov(x, x') dx dx' \quad . \tag{34}$$

Systematic errors are usually assumed to be independent of statistical errors. If so, then $\tilde{K}(x, x_o)$ may be interchanged legitimately with $\delta(x - x_o)$ as needed in these expressions. The resulting final estimate for the *fractional statistical error* is

$$f_I \equiv \frac{\mathbf{E}[(\delta I)^2]}{I} \approx \frac{2 \int_{-1}^{1} I^2(x) D_K(x) dx}{JN \int_{-1}^{1} I(x) D_K(x) dx} \quad . \tag{35}$$

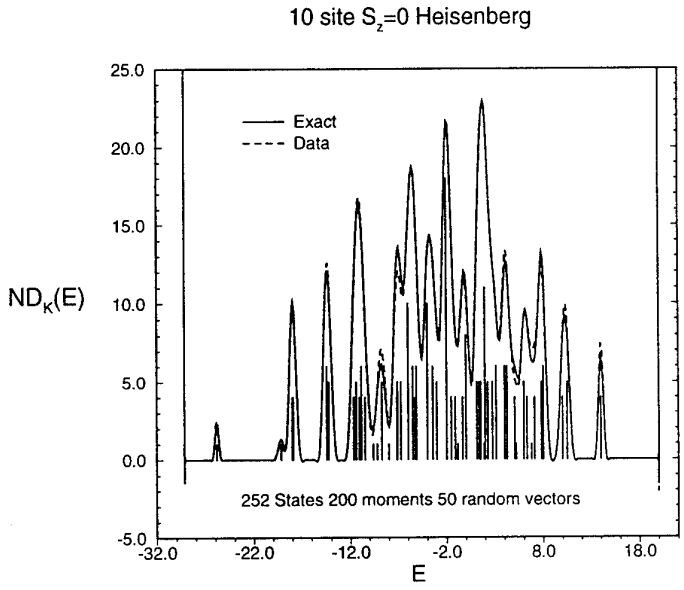

Figure 1. DOS for the $S_z = 0$ sector of the 10 site Heisenberg antiferromagnet. There are 252 states and 54 distinct energies. The vertical lines are at energies of eigenstates and their height equals their degeneracy. 'Exact' corresponds to the predicted kernel estimate in the absence of noise. 'Data' is the kernel estimate obtained using 50 random vectors.

Note, two integrated functions of DOS estimated from the same data would be statistically covariant and not independent.

Equation (35) makes explicit the dependence of statistical errors on the number of random vectors, matrix dimension, and integrated function desired. These parameters control rates of convergence for this method. To improve accuracy in practical calculations at a fixed N, we should compare the relative magnitude of systematic and statistical errors. If systematic errors are larger, the number of moments should be increased. If statistical errors are larger, the number of random vectors should be increased.

Provided $D(x)$ and $I(x)$ do not vary rapidly with N, f_I decreases with both the number of random vectors, J, and the dimension of the Hamiltonian, N. Thus, there can be a statistical averaging effect as N increases requiring fewer random vectors to achieve a desired f_I. In this case, sub-linear scaling of cpu time with N may be obtained for sparse Hamiltonians. Indeed, for thermodynamic functions of extremely large Hamiltonians, we find one random vector to be sufficient except at the lowest temperatures. Also, f_I decreases with the support of $I(x)$. A smaller number of Gaussian random variables, $b_n(j)$, contribute, and so statistical errors are larger. At one extreme, where $I(x) = \delta(x - x_o)$ corresponding to an individual point in the DOS. $D(x_o)$, f_I is infinite. At another extreme, where $I(x) = 1$ corresponding to

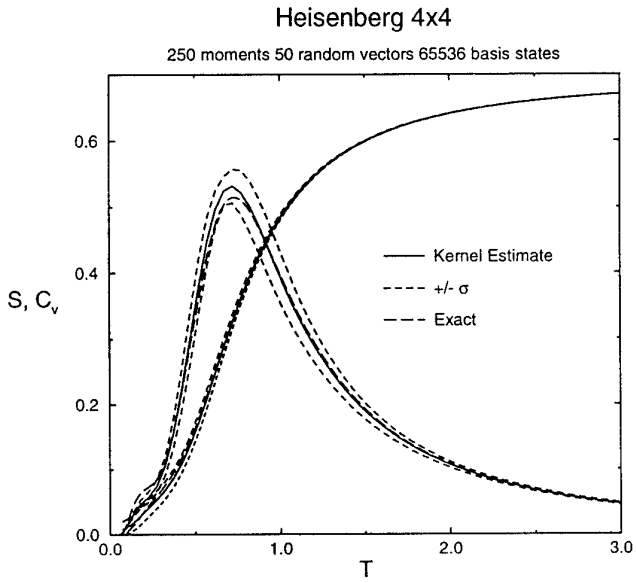

Figure 2. Thermodynamic functions of the 16 site Heisenberg antiferromagnet as obtained by kernel estimates (solid curve) with statistical error bars (short dashed curve) and by exact diagonalization (long dashed curve) [9]. Shown are the entropy, S, and specific heat at constant volume, C_v, per electron plotted against temperature, T

the normalization, $f_I = \sqrt{2/JN}$ and is negligible. For thermodynamic quantities where $I(x) \propto \exp(-\beta cx)$, f_I increases as temperature decreases. The f_I on $D_K(x_o)$, which is an integrated quantity with $I(x) = \tilde{K}(x, x_o)$, increases with the number of moments, M, because the kernel narrows.

4. APPLICATION TO THE HEISENBERG ANTIFERROMAGNET

We illustrate the performance of the kernel method by applying it to DOS and thermodynamic functions of the two-dimensional Heisenberg antiferromagnet on a square lattice. This model consists of a spin one-half electron on each site interacting via a nearest neighbor spin-spin coupling. Periodic boundary conditions are imposed. If the unit cell has N_s sites, the number of states is $N = 2^{N_s}$.

Figure 1 demonstrates the performance of kernel estimates in a simple case involving only a few states. Shown are results for the $S_z = 0$ sector for 10 sites and $N = 252$. This can easily be diagonalized exactly using standard $O(N^3)$ routines. The number of distinct energies is 54. Vertical lines are positioned at the energy of each eigenstate and their height equals the degeneracy. The solid curve shows the kernel estimate predicted using 200 exact polynomial moments and higher order Gibbs damping. This corresponds to a simple convolution of the exact DOS with the known kernel (resolution function). Note the sharp resolution for states at edges of

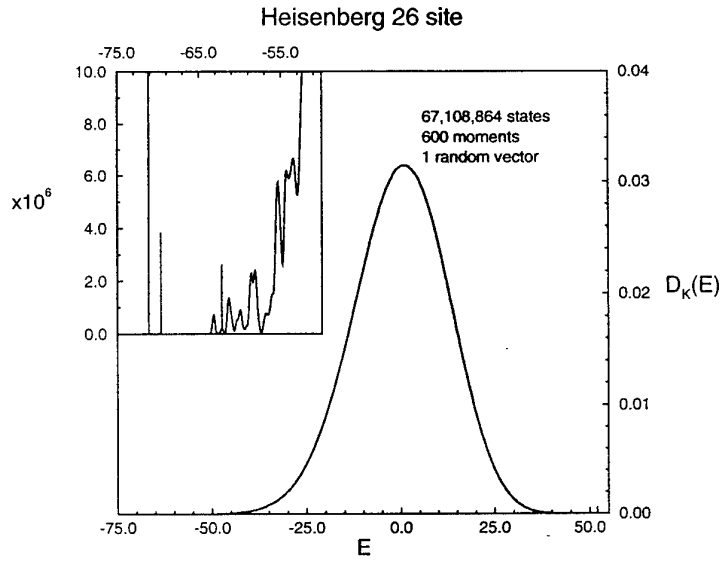

Figure 3. Kernel estimates of the DOS for the 26 site Heisenberg antiferromagnet having 67, 108, 864 states obtained with 600 moments and 1 random vector

the spectrum which were initially determined by Lanczos diagonalization. The dashed curve shows the kernel estimate obtained by stochastic evaluation of moments using 50 random vectors. The small disagreement between the two curves is statistical noise due to use of a stochastic method. In general, statistical errors will affect only the number of states in features of the DOS and not their energies. Thus, if the goals of the calculation are only energies of isolated peaks or features in DOS such as band edges, a single random vector may suffice. Energy resolution may be improved by increasing the number of moments. Statistical noise may be reduced by increasing the number of random vectors.

Exact diagonalization results are available [9] for all of the eigenvalues of the 16 site Heisenberg antiferromagnet which has $N = 65536$. Exact diagonalization proceeds optimally by first reducing the Hamiltonian to block diagonal form as much as possible using symmetries. Cpu time scales as $O(N_b^3)$ for each block, where N_b is the block dimension, and memory scales as $O(N_b^2)$. For example, by invoking spin conservation the largest block of the 16 site Hamiltonian corresponds to $S_z = 0$ having 12870 states. By invoking translational invariance the largest block can be further reduced to approximately $12870/16 \approx 805$ states. Exact diagonalization can readily be performed with such block sizes. But this becomes impractical for larger numbers of sites with larger block sizes. The MVM's used in Lanczos and kernel estimates are also most efficiently performed by invoking symmetries to reduce the Hamiltonian to block diagonal form. But the MVM routine creates the Hamiltonian

for each multiply without storing it, so the maximum memory requirement for kernel estimates is a few times N_b and the cpu time scales as $O(N_b \times J \times M)$ for each block. Detailed comparisons of exact diagonalization and MVM techniques depend on the advantage taken of symmetry properties of the Hamiltonian as well as the goals of the calculation. But, in general, memory requirements and cpu time can be orders of magnitude smaller for kernel estimates compared to exact and Lanczos diagonalization, if the quantity desired involves DOS.

In addition to the partition function, Eq. (14), thermodynamic functions include the entropy

$$S = \log(Z) + \beta\overline{\varepsilon} \quad , \tag{36}$$

and specific heat

$$C_v = \beta^2 \left(\overline{\varepsilon^2} - \overline{\varepsilon}^2\right) \quad . \tag{37}$$

These quantities are related by

$$C_v = T\frac{dS}{dT} \qquad \beta = \frac{1}{T} \quad . \tag{38}$$

Such thermodynamic quantities are estimated using a kernel estimate for each quantity, such as $\overline{\varepsilon^2} \approx \overline{\varepsilon^2}_K$, entering these expressions.

Statistical errors may also be estimated for the entropy

$$\mathbf{E}[(\delta S)^2] \simeq \frac{2N}{JZ_K^2} \int d\varepsilon e^{-2\beta\varepsilon} D_K(\varepsilon) \left[1 - \beta\varepsilon + \beta\overline{\varepsilon}_K\right]^2 \tag{39}$$

and specific heat

$$\mathbf{E}[(\delta C_v)^2] \simeq \frac{2N\beta^2}{JZ_K^2} \int d\varepsilon e^{-2\beta\varepsilon} D_K(\varepsilon) \left[\varepsilon^2 - 2\overline{\varepsilon}_K\varepsilon - \overline{\varepsilon^2}_K + 2\overline{\varepsilon}_K{}^2\right]^2 \quad . \tag{40}$$

The errors again scale approximately as $1/\sqrt{N}$, since $Z_K \propto N$. Statistical errors on these integrated quantities are not independent at different temperatures. Full error properties should be described by a covariance matrix.

Figure 2 compares kernel estimates of thermodynamic functions to exact results. The solid lines are kernel estimates of the the entropy per electron and specific heat per electron for the 16 site model obtained with 250 moments and 50 random vectors. The number of moments is well beyond the point where systematic errors become negligible compared to statistical errors. The plots use the same units as [9]. Short dashed curves indicate one standard deviation statistical errors on the kernel estimates. Long dashed curves are the exact results [9]. Kernel estimates agree with exact results within statistical errors. Fractional statistical error increases as temperature is decreased.

Figure 3 demonstrates that kernel estimates do work for truly mega-dimensional Hamiltonians. A kernel estimate is shown of the DOS for the 26 site Heisenberg antiferromagnet having $N = 67,108,864$. This DOS was obtained using 600 moments and 1 random vector. Note the remarkable smoothness of the DOS. The lack of statistical fluctuations in comparison with the 16 site DOS is due to the three orders of magnitude larger number of states. Fluctuations in coeffecients of individual states

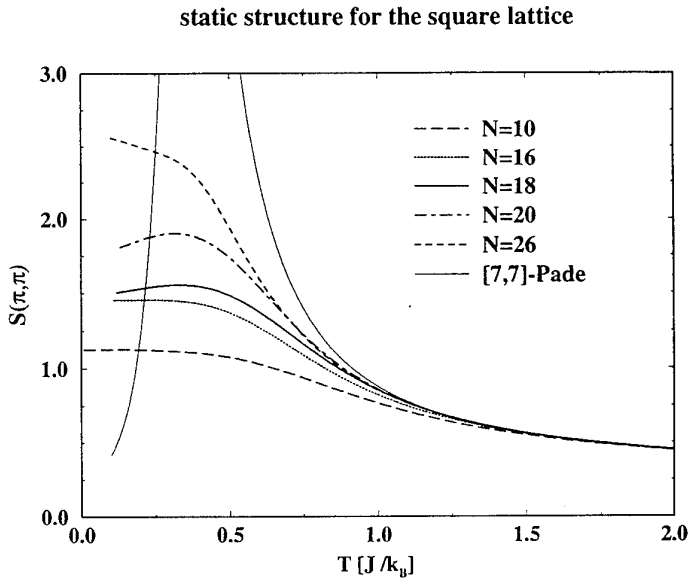

Figure 4. Static structure factor for the spin half Heisenberg model on a square lattice. The data for $N = 10$ have been obtained by exact diagonalization, for $N = 16..26$ we show results from the Kernel Polynomial approximation.

(including the Gaussian distribution of b_n) average out in the DOS estimate. The insert shows the low energy portion of the DOS using a vertical scale magnified by 4×10^3. Structure due to individual states is observable on such a fine vertical scale. The height of peaks for isolated states will have large error bars because only one random vector was used. But large features in DOS where many states contribute will have small statistical errors.

Figure 4 compares the static structure factor for various finite lattices with the result of high temperature series calculation [10]. The static structure factor is defined as:

$$S(\mathbf{q} = (\pi, \pi)) = \frac{1}{N} \sum_{\mathbf{R}_i - \mathbf{R}_j} \exp(-i\mathbf{q}(\mathbf{R}_i - \mathbf{R}_j))\mathbf{S}_i\mathbf{S}_j$$

For high enough temperatures, where the finite size effects are small and the high temperature expansion is valid, we obtain excellent agreement. At smaller temperatures the high temperature expansion deviates due to an unphysical pole, but our results still behave sensibly. Below $T = 0.5$ drastic finite size effects cause the interpretation to be very difficult.

5. CONCLUSION

We have proposed a new *kernel method* to estimate densities of states (DOS)

and statistical mechanical properties of huge Hamiltonian matrices. The method uses only matrix vector multiplications on random vectors, the same algorithm required for Lanczos diagonalization. Therefore, kernel estimates are economical in cpu time and memory, scaling as $O(N)$ for large sparse Hamiltonians. They achieve excellent accuracy and efficiency for integrated functions of DOS such as thermodynamic functions and operator expectation values in the canonical ensemble. This is accomplished by relaxing the energy resolution for individual states. Canonical ensemble expectation values are expressed as an orthogonal polynomial moment expansion using modified Bessel functions. The method also provides estimates of statistical error, and systematic errors may be reduced by increasing the number of moments. Kernel estimates have a linear data-independent relation to the true DOS. They are based on well-developed concepts in analysis and statistics. We believe the comparative simplicity and efficiency of kernel estimates will make them an important addition to the arsenal of methods for attacking huge matrix problems.

ACKNOWLEDGEMENTS

We thank G. Baker for pointing out the relation of our approach to kernel polynomials, R. Singh and N. Elstner for supplying the coefficients of the high temperature series, and E. Rezayi for supplying exact results for the thermodynamics of the 16 site Heisenberg antiferromagnet. This research was supported in part by the U. S. Department of Energy.

REFERENCES

[1] R. N. Silver, H. Roeder, to appear in Int. J. of Mod. Phys. **C**
[2] L. R. Mead, N. Papanicolacu, J. Math. Phys. **25**, 2404 (1984).
[3] J. C. Wheeler, M. G. Prais, C. Blumstein, Phys. Rev. B**10**, 2429 (1974).
[4] G. Szegö, *Orthogonal Polynomials*, American Mathematical Society, Providence, 1939.
[5] J. K. Cullum, R. A. Willoughby, *Lanczos Algorithm for Large Symmetric Eigenvalue Computations*, Birkhäuser, Boston (1985).
[6] See, for example, G. Arfken, *Mathematical Methods for Physicists*, Academic Press, Inc., 1985, Sec. 14.5.
[7] G. Meinardus in *Approximation of Functions: Theory and Numerical Methods*, Springer Tracts in Natural Philosphy, Volume 13, 1967
[8] J. Skilling, in *Maximum Entropy and Bayesian Methods*, ed. J. Skilling, Kluwer, Dordrecht, 455-466 (1988).
[9] H. Shi, E. H. Rezayi, Phys. Rev. B**43**, 13618 (1991).
[10] N. Elstner, private communication

CLUSTER APPROACH TO ATOMIC NUCLEI: ALPHA-CHAIN STATES IN ^{12}C

G.S. Anagnostatos

Institute of Nuclear Physics,
National Center for Scientific Research " Demokritos",
Aghia Paraskevi, Attiki, 15310 Greece

1. INTRODUCTION

Carbon 12 is among the 4N nuclei which are mainly studied by using the Bloch-Brink a-cluster model [1] and its variations. A common characteristic of many of these a-cluster models is that the α-particles involved in a specific nucleus are considered proformed and thus this nucleus appears in the framework of these models as an aggregate of α-particles subunits. Despite the apparent successes of these models, however, the wealth of nuclear reactions does not support this α-particle composition of nuclei even for the 4N nuclei. This serious handicap of these models has been overcome by considering that the alpha-particles involved may dissolve into nucleons since, for cluster separations reaching zero, antisymmetrization forces the cluster wave fuction into some shell model limit. Thus, the geometries in these improved α-cluster models arise through the long-range effects of antisymmetrization and the mean field combined with a preference for simple underlying structures [1-2]. Such structures in the literature range from three-dimensional[3-4] high symmetry shapes to two-dimensional[1] configurations and even to completely linear[1,5-6] arrangements.

In the present study an alternative approach is considered where indeed nucleons and not α-particles compose the nuclei and thus possible α-particles and their spatial distributions in nuclei are derived. Specifically, the semiclassical[7] part of the Isomorphic Shell Model is employed. The semiclassical instead of the quantum mechanical part[8] of the model is utilized since this part is closer to the α-cluster models and thus a comparison between them is easier and more comprehensive. An outline of the model is given in the next

section. Here, only a very brief comparison is attempted for the geometry involved in this model and that in the α-cluster models[1,3].

In the α-cluster models, several geometries are chosen for a particular nucleus based on symmetry arguments for the α particles involved and then the binding energy is used for the final selection of geometry. In the isomorphic shell model,however, a common geometry for all nuclei is derived by packing the nuclear shells[7] (whose average forms result from the independent particle assumption) after taking the nucleon finite size into account. The part of this geometry utilized by the nucleons of a specific nucleus results from the search for the maximum binding energy, which defines the average form and size of the cluster structure representing the specific nucleus.

The well studied α-cluster models[1] of the nucleus and the isomorphic shell model [7,8] appear, at first glance, as two completely independent approaches of studying the atomic nucleus. However, there is a fundamental common feature that brings these two approaches very close to each other. This feature is the very fact that both models are based on the mean positions of their constituent particles (i.e.,of α-particles and of nucleons, respectively.) Thus, in a broader sense the isomorphic shell model may be thought that it provides the required dissolution of the α-particles into their nucleons which is common for all nuclei [7,8] and precisely consistent with the Pauli principle [9-12]. After this important remark the two models may be viewed as two similar approaches converging into one.

Demonstration of the above is successfully obtained here by taking throughout this paper ^{12}C as an example. The good results obtained in the present paper point to many other applications in the future refering to light, medium, and even heavy nuclei.

2. THE ISOMORPHIC SHELL MODEL

The isomorphic shell model is a microscopic nuclear-structure model that incorporates into a hybrid model the prominent features of single-particle and collective approaches in conjunction with the nucleon finite size.[7,8]

The single-particle component of the model is along the lines of the conventional shell model with the **only** difference that in the model the nucleons creating the central potential are the nucleons of each particular nuclear shell alone, instead of all nucleons in the nucleus as assumed in the conventional shell model.[8] That is, our Hamiltonian is analyzed into partial state-dependent Hamiltonians for neutrons (N) and for protons (Z) as follows, where crossing terms between partial Hamiltonians of different shells, have been omitted.

$$\begin{aligned} H &= {}_{N}H + {}_{Z}H \\ &= {}_{N}H_{1s} + {}_{N}H_{1p} + {}_{N}H_{1d2s} + \ldots \end{aligned} \tag{1}$$

$$+ {}_Z H_{1s} + {}_Z H_{1p} + {}_Z H_{1ds} + \ldots$$

While a finite square-well or Woods-Saxon potential would be a more realistic choice of the potential, for reasons of simplicity, we take the harmonic oscillator (HO) potential without spin-orbit coupling, where the expressions of the mean square radius and of the energy eigenvalues, necessary in demonstrating the model, are exceptionally simple and have closed mathematical forms. In addition, the appearance of the finite negative constants $-{}_N V_i$ and $-{}_Z V_i$ in the neutron and the proton harmonic oscillator potentials below, reduces the boggling impression given when an infinite potential is used for determining total-binding energies.

Thus, for each partial neutron or proton Hamiltonian we take

$$ {}_N H_i = {}_N V_i + {}_N T_i = -{}_N \bar{V}_i + \frac{1}{2} m({}_N \omega_i^2) r^2 + {}_N T_i \tag{2}$$

$$ {}_Z H_i = {}_Z V_i + {}_Z T_i = -{}_Z \bar{V}_i + \frac{1}{2} m({}_Z \omega_i^2) r^2 + {}_Z T_i \tag{3}$$

That is, each harmonic oscillator potential has its own state-dependent frequency ω. These ω are **not** taken as adjustable parameters, but all are determined from the harmonic oscillator relation[13]

$$\hbar\omega = \left(\frac{\hbar^2}{m < r^2 >} \right) \left(n + \frac{3}{2} \right), \tag{4}$$

where n is the harmonic oscillator quantum number and $< r_i^2 >^{1/2}$ is the average radius of the relevant high fluximal shell determined by the semiclassical part of the model specified below.

The solution of the Schrodinger equation with Hamiltonian (1), in spherical coordinates, is

$$\Psi_{nlm}(r, \theta, \phi) = R_{nl}(r) Y_l^m(\theta, \phi), \tag{5}$$

where $Y_l^m(\theta, \phi)$ are the familiar spherical harmonics and the expressions for the $R_{nl}(r)$ are given in several books of quantum mechanics and nuclear physics, for example see Table 4–1 of Ref. 13.

The only difference between our wave functions and those in these books is the different ω's as stated in (2) – (3) above. Those of our wave functions, however, which have equal l value, because of the different $\hbar\omega$, are not orthogonal, since in these cases the orthogonality of Legendre polynomials does not suffice. Orthogonality, of course, can be obtained by applying established procedures, e.g., the Gram-Schmidt process.

According to Hamiltonian (1), the binding energy of a nucleus with A nucleons in the case of orthogonal wave functions takes the simple form given by (6)

$$BE = 1/2(\bar{V}.A) - 3/4\left[\sum_{i=l}^{A}\hbar\omega_i(n+3/2)\right], \tag{6}$$

where $\bar{V}$ is the average potential depth[8]. The coefficients $1/2$ and $3/4$ take care of the double counting of nucleon pairs in determining the potential energy.

Applications and details of the quantum mechanical part of the model are given in Ref. 8. Here an application of the semiclassical part (see Refs. 7 and 14-19) in the place of the quantum mechanical part of the model is considered in the spirit of Ehrenfest's theorem,[20] which for the observables of position ($\mathbf{R}$) and momentum ($\mathbf{P}$) takes the form

$$\frac{d}{dt} < \mathbf{R} > = \frac{1}{m} < \mathbf{P} > \quad \text{and} \tag{7}$$

$$\frac{d}{dt} < \mathbf{P} > = - < \nabla V(\mathbf{R}) > \tag{8}$$

The quantity $< \mathbf{R} >$ represents a set of three time-dependent numbers $\{< X >, < Y >, < Z >\}$ and the point $< R > (t)$ is the centre of the wave function at the instant t. The set of those points which correspond to the various values of t constitutes the trajectory followed by the centre of the wave function.

From (7) and (8) we get

$$m\frac{d^2}{dt^2}\mathbf{R} = - < \nabla V(\mathbf{R}) > \tag{9}$$

Furthermore, it is known that, for the **special** case of the harmonic oscillator potential assumed by the isomorphic shell model in (3), the following relationship is valid

$$< \nabla V(\mathbf{R}) > = [\nabla V(\mathbf{r})]_{\mathbf{r}=<\mathbf{R}>}, \quad \text{where} \tag{10}$$

$$[-\nabla V(\mathbf{r})]_{\mathbf{r}=<\mathbf{R}>=\mathbf{F}} \tag{11}$$

That is, for this potential the average of the force over the whole wave function is rigorously equal to the classical force F at the point where the centre of the wave function is situated. Thus, for the special case (harmonic oscillator) considered, the motion of the centre of the wave function precisely obeys the laws of classical mechanics. Any difference between the quantum and the classical description of the nucleon motion exclusively depends on the degree the wave function may be approximated by its centre. Such differences will

contribute to the magnitude of deviations between the experimental data and the predictions of the semiclassical part of the model employed here.

Now, in the semiclassical treatment[7] the nuclear problem is reduced to that of studying the centres of the wave functions presenting the constituent nucleons or, in other words, of studying the average positions of these nucleons[7]. For this study the following two assumptions are employed by the isomorphic shell model[7].

i) The neutrons (protons) of a closed neutron (proton) shell, considered at their **average** positions, are in **dynamic equilibrium** on the sphere presenting the average size of that shell.

ii) The average sizes of the shells are determined by the **close-packing** of the shells themselves, provided that a neutron and a proton are represented by **hard spheres** of definite sizes (i.e., $r_n = 0.974$ fm and $r_p = 0.860$ fm).

It is apparent that assumption (i) is along the lines of the conventional shell model, while assumption (ii) is along the lines of the liquid-drop model.

The model employs a specific equilibrium of nucleons, considered at their average positions on concentric spherical cells, which is valid whatever the law of nuclear force may be[21]: assumption (i). This equilibrium leads uniquely to Leech[21] (equilibrium) polyhedra as average forms of nuclear shells. All such nested polyhedra are closed-packed, thus taking their minimum size: assumption (ii). The cumulative number of vertices of these polyhedra, counted successively from the innermost to the outermost, reproduce the magic numbers each time a polyhedral shell is completed[7] (see the numbers in the brackets in Fig. 1 there and in this paper).

For one to conceptualize the isomorphic shell model, he should first relate this model to the conventional shell model. Specifically, the main assumption of the simple shell model, i.e. that each nucleon in a nucleus moves (in an average potential due to all nucleons) independently of the motion of the other nucleons, may be understood here in terms of a **dynamic equilibrium** in the following sense.[7] Each nucleon in a nucleus is **on average** in a **dynamic equilibrium** with the other nucleons and, as a **consequence**, its motion may be described independently of the motions of the other nucleons.

From this one realizes that dynamic equilibrium and independent particle motion are **consistent** concepts in the framework of the isomorphic shell model.

In other words, the model implies that at some instant in time (reached **periodically**) all nucleons could be thought of as residing at their individual average positions, which coincide with the vertices of an equilibrium polyhedron for each shell. This system of particles evolves in time according to each independent particle motion. This is possible, since axes standing for the angular-momenta quantization of directions are **identically** described by the rotational symmetries of the polyhedra employed.[9–12] For example, see Ref.

11, where one can find a complete interpretation of the independent particle model in relation to the symmetries of these polyhedra. Such vectors are shown in Fig. 1 for the orbital angular-momentum quantization of directions involved in all nuclei up to $N = 20$ and $Z = 20$.

Figure 1. The isomorphic shell model for the nuclei up to $N = 20$ and $Z = 20$. The high-symmetry polyhedra in row 1 (i.e. the zerohedron, the octahedron and the icosahedron) stand for the average forms for neutrons of (a) the $1s$, (c) the $1p$ and (e) the $1d2s$ shells, while the high-symmetry polyhedra in row 2 (i.e. the zerohedron, the hexahedron (cube) and the dodecahedron) stand for the average forms of (b) the $1s$, (d) the $1p$ and (f) the $1s2s$ shells for protons. The vertices of polyhedra stand for the average positions of nucleons in definite quantum states (τ, n, l, m, s). The letters h stand for the empty vertices (holes). The z axis is common for all polyhedra when these are superimposed with a common centre and with relative orientations as shown. At the bottom of each block the radius R of the sphere exscribed to the relevant polyhedron and the radius ρ of the relevant classical orbit, equal to the maximum distance of the vertex-state (τ, n, l, m, s) from the axis ${}_n\theta_l^m$ precisely representing the orbital angular momentum axis with definite n,l and m values, are given. Curved arrows shown help the reader to visualise for each nucleon round what axis is rotated, where close (open) arrows show rotations directed up (down) the plane of the paper. All polyhedra vertices are numbered as shown. The backside (hidden) vertices of the poluhedra and the related numbers are not shown in the figure.

Since the radial and angular parts of the polyhedral shells in Fig. 1 are well defined, the coordinates of the polyhedral vertices (nucleon average positions) can be easily computed. These coordinates up to $N = Z = 20$, needed here for the application of the model on ^{12}C (see next section), are already published in footnote 14 of Ref. 14, and in footnote 15 of Ref. 15. These coordinates correspond to the relevant R values of the exscribed polyhedral spheres given in Fig. 1 (see bottom line at each block).

According to the isomorphic shell model[7], the nucleon average positions of a nucleus are distributed at the vertices of the polyhedral shells as shown, for example, in Fig. 1. The specific vertices occupied, for a given (closed- or open-shell) nucleus at the ground state, form a vertex configuration (corresponding to a state configuration) that possesses a maximum binding energy (BE) in relation to any other possible vertex configuration. This maximum BE vertex configuration defines the average form and structure of the ground state of this nucleus. All bulk (static) ground-state properties of this nucleus (e.g. BE, rms radii, etc.) are derived as properties of this structure, as has been fully explained in Ref. 7 and will become apparent below.

The quantities estimated by the model in the framework of its semiclassical part [7,14,16] (see next section) are potential energy V_{ij}, Coulomb energy $(E_c)_{ij}$; average kinetic energy $< T >_{nlm}$; odd-even energy E_δ; binding energy E_{BE}; collective rotational energy $E_{\rm rot}$; rms charge, mass and effective radii $< r^2 >^{1/2}$; and electric quadrupole moment using (12)–(22).

$$V_{ij} = 1.7(10^{17})\frac{e^{-(31.8538)r_{ij}}}{r_{ij}} - 187\frac{e^{-(1.3538)r_{ij}}}{r_{ij}}, \tag{12}$$

where the internucleon distances r_{ij} are estimated following Fig. 1 or (the same) the corresponding coordinates of polyhedral vertices.[14–15]

$$(E_C)_{ij} = \frac{e^2}{r_{ij}}, \tag{13}$$

where distances r_{ij} are computed as explained above.

$$< T >_{nlm} = \frac{\hbar^2}{2M}\left[\frac{1}{R^2_{\rm max}} + \frac{l(l+1)}{\rho^2_{nlm}}\right], \tag{14}$$

where $R_{\rm max}$ is the outermost polyhedral radius (R) plus the relevant nucleon radius (i.e., $r_n = 0.974$ fm or $r_p = 0.860$ fm), i.e., the radius of the nuclear volume in which the nucleons are confined, M is the nucleon mass, ρ_{nlm} is the distance of the vertex (n, l, m) from the axis ${}_n\theta^m_l$ (see Fig. 1 and Ref. 16).

$$E_{BE} = -\sum_{\substack{\text{all nucleon}\\ \text{pairs}}} V_{ij} - \sum_{\substack{\text{all proton}\\ \text{pairs}}} \frac{e^2}{r_{ij}} - \sum_{\text{all nucleons}} < T >_{nlm} - E_\delta + E_{\rm rot}, \tag{15}$$

where distances r_{ij} are estimated as above and E_δ is a correction "odd-even" term familiar from the liquid drop model. Here E_δ value is equal to zero for even-Z even-N nuclei for which the potential in (12) is exclusively derived[14] and thus no correction is needed, while for odd-A nuclei its value is taken equal[13] to 80/A MeV, i.e.

$$E_\delta = \frac{80}{A} \tag{16}$$

$$E_{\rm rot} = \frac{\hbar^2 I(I+1)}{2J}, \tag{17}$$

where J is the moment of inertia of the rotating part of the nucleus given by (18)

$$J = \sum_i^{N_{\rm rot}} m\rho_i^2 = m\sum_i^{N_{\rm rot}} \rho_i^2 = mN_{\rm rot} < r^2 >_{\rm rot}, \tag{18}$$

where $N_{\rm rot}$ is the number of nucleons participating in the collective rotation and
$< r^2 >_{\rm rot}$ is the rms radius of these nuclei.

The term $E_{\rm rot}$ in (15) is meaningful for the ground state **only** for the cases where the angular speed ω due to independent particle motion is comparable (about equal) to that due to collective motion in such a way that these two motions are coupled even at the ground state, i.e., for these cases the adiabatic approximation is not valid.

$$< r^2 >_m^{1/2} = \left[\frac{\sum_{i=1}^Z R_i^2 + \sum_{i=1}^N R_i^2 + Z(0.8)^2 + N(0.91)^2}{Z+N}\right]^{1/2}, \tag{19}$$

$$< r^2 >_{ch}^{1/2} = \left[\frac{\sum_{i=1}^Z}{Z} R_i^2 + (0.8)^2 - (0.116)\frac{N}{Z}\right]^{1/2}, \tag{20}$$

where the subscripts ch and m refer to charge and mass, R_i is the radius of the ith proton or neutron average position from Fig. 1, Z and N are the proton and the neutron numbers of the nucleus, 0.8 and 0.91 fm are the rms radii of a proton and of a neutron, and -0.116 fm^2 is the ms charge radius of a neutron.[22] The 0.91 fm value for a neutron is taken from the 0.8 fm value for a proton by considering proportionality according to the sizes of their bags 0.974 and 0.860 fm, respectively, i.e. $0.91 = 0.8(0.974/0.860)$.

$$< r^2 >_{\rm eff}^{1/2} = \left[< r^2 >_m + < r^2 >_{\rm rot}\right]^{1/2} \tag{21}$$

$$eQ'_{\rm intr.} = \sum_i eQ'_i = e\sum_{i=1}^Z R_i^2(3\cos^2\theta_i - 1), \tag{22}$$

where Q' stands for the intrinsic quadrupole moment, R_i is the radius of the i^{th} proton average position, and θ_i is the corresponding azimuthal angle with respect to the quantisation axis.

3. CALCULATIONS AND DISCUSSION

In the α-cluster model of the nucleus referring to α-chain states, ^{12}C (N=3) is the key nucleus since an α-chain structure for Be^8 (N=2) is apparent and since the appearance of such structure for heavier nuclei ($N \geq 4$) could be associated to ^{12}C structure particularly if the α-chain states of these heavier nuclei could be thought of as forming molecular structures of the type ^{12}C $+(N-3)\alpha$, either ^{12}C + ^{8}Be or ^{12}C + ^{12}C. Thus in the following we will concentrate on ^{12}C.

The average structure of ^{12}C, in the framework of the isomorphic shell model, comes from Fig.1 by considering the states (1s and $1p_{3/2}$) involved in this nucleus. Specifically, from Fig.1 the average nucleon positions numbered 1–2 (for 1s neutrons), 3–4 (for 1s protons), 5–8 (for $1p_{3/2}$ neutrons), and 11–14 (for $1p_{3/2}$ protons) are depicted as shown in Fig.2(a) by employing the same numbers. Thus, Fig.2(a) contains part of Fig.1 and so, as mentioned, all coordinates of the average nucleon positions involved are known.[14,15] Further, Fig.2(b) is almost identical to Fig.2(a) and only slightly differs with respect to the average positions of the two 1s protons (nos. 3–4). Specifically, due to the absence of $1p_{1/2}$ neutrons in ^{12}C (nos. 9–10) whose average positions together with those of 1p3/2 neutrons (nos.5-8) determine the symmetry of the average positions for the 1s protons, these two latter positions can relax getting closer to the average positions for the $1p_{3/2}$ neutrons (nos. 5–8) in such a way that their corresponding nucleon bags come in contact.This relaxation of the two proton average positions leads to larger binding energy for ^{12}C.

Further in the model, each set of the following four nucleon average positions numbered (1–4), (5, 7, 11, 13) and (6, 8, 12, 14) consists of two protons and two neutrons with the same n and l quantum numbers which are close together for the instant depicted by Fig.2(a) and (b). Thus, in the model each of these three sets can be considered as an α-particle. Considering now the center of gravity for each of these α-particles, Fig.2(c) results, where indeed these three α-like particles are in a row forming a linear chain. For later moments, of course, each of the four nucleons composing any one of the above three α-particle like structures will evolve by following its independent particle motion. That is, each nucleon will rotate in an orbital round its own axis of orbital angular momentum vector as schematically shown by arrows in Fig.1.

In the framework of the isomorphic shell model now the observables of rms charge radius and of binding energy can be estimated. Specifically,

from Eq.(20) since all R_i involved in Fig.2(a) and (b) are known[7] (namely, $R_{1s-protons} = 1.554$ fm, and $R_{1p-protons} = 2.541$ fm; see Figs.1(b) and (d)), the charge rms radius is computed equal to 2.37 fm for each of the Figs.2(a) and (b) ($< r^2 >^{1/2}_{ch,exp} = 2.37$ fm). Also, from Eqs.(12)-(15) since all coordinates of the nucleon average positions[14-15] and the radial distances involved in Figs.2(a) and (b) (namely in fm, $R_{max} = 2.511 + 0.974$, $\rho_{1p-proton} = 2.075$, $\rho_{1p-neutron} = 2.511$, also $E_{rot} = 0$; see Figs.1(c) and (d) are known[14-15], the binding energy for Figs.2(a) and (b) are computed equal to 86.0 MeV and 94.2 MeV, respectively.

Figure 2. Average forms for ^{12}C, according to the isomorphic shell model, composed of the average positions of the constituent nucleons. Part (a) stands for the first 0^+ excited state at 7.65 MeV and part (b) for the ground state. Average nucleon positions are numbered as shown by using for the same position the same number as in Fig.1.Thus, one can observe that for the positions shown in Fig.1(a)-(d) those numbered (9)-(10) for neutrons and (15)-(16) for protons are the only not present in Fig.2. Fig.2(c) comes from either Fig.1(a) or Fig.1(b) when each of the three sets of four close-by nucleons (two neutrons and two protons) of same n and l numbered (1–4), (5, 7, 11, 13) and (6, 8, 12, 14) are assumed forming a sort of an α particle. Axes labelled 1, 2 and 3 stand for $C2$ symmetry axes and those labelled $R_{0_1^+}$ and $R_{0_2^+}$ for rotational axes referring to the first (0_1^+) and to the second (0_2^+) 0^+ levels.

Fig.2(a) and (b) have been found to be the two average-nucleon-position configurations with the largest binding energies with respect to any other possible configuration for ^{12}C involving s and p or even d states and coming from Figs.1(a) - (f). Thus, Fig.2(b) is associated with the ground state and Fig.2(a) with the 7.653 ± 0.3, $J^\pi = 0_2^+$ excited state[23] of ^{12}C possessing 92.2 MeV and 84.55 MeV experimental binding energies,[24] respectively. The inbetween excited state[23] at 4.4392 ± 0.3, $J^\pi = 2_1^+$, will be discussed shortly. Center-of-mass corrections are not included.

Table 1. Theoretical predictions and experimental values for the ground state (0_1^+) and first 0^+ excited state (0_2^+) of ^{12}C.

Approach			Energy (MeV)	rms charge radius (fm)	Intrinsic quadrupole moment $(\text{fm})^2$
	0_1^+		92.2[b]	2.40±0.25[c]	±21[d]
Experiment	0_2^+		7.65		
Isomorphic	0_1^+		94.2	2.37	21
shell model	0_2^+		8.2	2.37	21
α-particle	0_1^+ (triangle)	V1	72.7		
model[a]		V2	64.3		
with forces		B1	62.0	2.62	−43[f]
V1, V2, B1	0_2^+ (chain)	V1		15.0	3.27[e]
		V2		8.7	
		B1		6.1	

[a] See Ref. 3
[b] See Ref. 23
[c] See Ref. 25
[d] See Ref. 27
[e] See Ref. 30
[f] See text (Section 3) for other calculated values (e.g.-21.6 fm^2)

It is satisfying that the present predictions are close to the experimental values for the binding energies but also for the radii[25]. The comparison is even more to our favour if we consider the corresponding α-model predictions[3] given in Table 1. However, a more detailed comparison with α-cluster models is going to be made later.

As seen from Figs.2(a) and (b), the deformation of the average shapes for the ground state and the 0_2^+ excited state of ^{12}C is apparent. In these figures the axes of symmetry and the corresponding axes of rotation are also shown. Specifically, the axis of rotation labelled $R_{0_1^+}$ is perpendicular to both axes of symmetry labelled 2 and 3, while the axis of rotation labelled $R_{0_2^+}$ is defined from the proton average positions nos. 3 and 4 and is perpendicular to the axis of symmetry labelled 1.

Since all coordinates involved in Figs.2(a) and (b) are known[14−15], by applying Eq.(18) the relevant moments of inertia are estimated. Namely,

$$J_a = 42.6 \text{ M.fm}^2 \text{ and}$$
$$J_b = 28.03 \text{ M.fm}^2 \quad ,$$

where M stands for the nucleon mass and the contribution to the moment of inertia coming from the finite nucleon size has been empirically incorporated equal to 0.165 M.fm^2 for each nucleon participating in the collective rotation.

By assuming no variation of the moment of inertia with angular momentum and by applying Eq.(17) the bands corresponding to the rotational axes labelled $R_{0_1^+}$ and $R_{0_2^+}$ are those given in Table 2.

Table 2. Rotational ground state and 0_2^+ excited bands of ^{12}C.

Band	J^π	Experiment[a] J^π	Energy (MeV)	Isomorphic shell model (MeV)	α-particle models[b] (MeV)
	2^+	2^+	4.44	4.28	2.76[c]
0_1^+	4^+	(4^+)	14.08	14.28	
	6^+		28.9	29.98	
	0^+	0^+	7.65	7.65	7.65
0_2^+	2^+	(0^+)	10.3	10.4	8.90
	4^+			16.9	12.1

[a] See Ref. 23
[b] See Ref. 31
[c] See Ref. 30

The second band is what is usually considered by the α-cluster models[3] as corresponding to the linear α-chain states for ^{12}C. Of course, the existence of such a band is not clearly supported by the experimental data.[23] Its existence exclusively depends on whether in the future the J^π for the state 10.3 ± 3 MeV will be found to be 2^+ in place of the present tentative[23] assignment (0^+).

What is really different between the present approach and the α-cluster models is the nature of the first band, i.e. of the ground-state band in Table 2. In these models α-particles are arranged at the corners of an equilateral triangle[3] for the ground state of ^{12}C. Such triangular configuration of α-particles round the nuclear center is based on the assumption that the α-particle is a fundamental constituent of ^{12}C nucleus. In such a case by considering any reasonable $\alpha - \alpha$ interaction, the most compact structure (and thus with maximum binding energy) is that of an equilateral triangle and should be assigned to the ground state of ^{12}C. In the framework of the present

model, however, nucleons and not α-particles are the constituents of any nucleus and it is the Pauli principle together with the maximum binding energy which determine what average nucleon positions are occupied and eventually what is the average shape of a specific nucleus. The good agreements between the experimental data and the predictions of the present model concerning the member states of the ground state band[23] lend support to the present approach,where a linear instead of a triangular average shape for the ground state of ^{12}C is employed.

Finally, an estimation of the electric quadrupole moment of ^{12}C is made which constitutes a very sensitive test of the angular distribution of the average structure for any nucleus. Dealing with average values, the intrinsic quadrupole moment is given[13] by (22) where, for Fig.2(b) representing the ground state of ^{12}C each R_i has been specified[7] above (see R values in Fig.1) and the corresponding θ_i is the azimuthal angle for the proton average position i with respect to the axis 1 (see Fig.2), which is the quantization axis for all vectors presenting quantization of direction[9-12] for orbital angular momenta shown in Fig.1 (namely,[26] $\theta_{3,4} = 90°$ and $\theta_{11-14} = 35°\ 15'52''$). It is satisfying that the resulting value $eQ'_{\rm intr} = 21.0$ fm^2 is identical to the measured[27] absolute value of the intrinsic quadrupole moment. The corresponding value coming from the α-cluster model[3] used for the construction of Table 1 is -43 fm^2, while more recent calculations[28] give -21.6 fm^2 and[41] -21.7fm^2. Hence, the difference between the present model and the Bloch- Brink model concerning the electric quadrupole moment essentially lies in the sign of the Q'_{intr}.

4. CONCLUSIONS

In the present study of ^{12}C the isomorphic shell model[7,8] has been employed as a cluster approach to atomic nuclei, where consideration of the nucleon finite size[7] constitutes one of the main features of the model. This feature allows the packing and clusterization in a nucleus.[7] What are really packed in the model are the shells themselves[7] taken as entities. Thus, only nucleons necessary for the shell packing are in contact. That is, the model does not support general packing of nucleons which should lead to much higher density. It is satisfying that this packing of shells reproduces a magic number[7] each time a saturated shell is added into the packing. The close reproduction of binding energies and sizes in many nuclei by both the quantum[8] and semiclassical[7] parts of the model lends support to the present approach and makes its results reliable.

A prolate average shape with a sizable positive intrinsic quadrupole moment is predicted for ^{12}C which can be considered as a linear chain of three α-particles, when each two close-by pairs of neutrons and protons with the same n and l quantum numbers (sort of α-particle) are presented by their center of gravity. Such a linear α-chain has already been predicted by α-

cluster models.[3] However, here the α-chain stands for **both** the excited 0_2^+ state[23] at 7.65 MeV (as in these models) and the ground state (instead of an equilateral triangle in these models[3]). The good agreements with experimental values for all observables examined, superior to those from α-cluster models, support the credibility of the present approach. Of course, the difference in the sign of the deformation cannot be ignored. However, despite much effort the quantitative experimental evidence is inconclusive[28]. Most of it derives from model-dependent analysis of electron scattering and hadron scattering data. Some of these analyses are inherently insensitive to the sign of the deformation and there are indications that the values obtained are projectile dependent and also that the findings strongly depend on the assumption that the nuclear charge distribution is spheroidal.[28].Besides the sign the most recent estimation[28-29] of $|Q_0|$ range from 21.6 to 24.0 fm^2 which are in good agreement with our prediction of 21.0 fm^2.

The above conclusions are further strengthened by the fact that the isomorphic shell model used here employs no adjustable parameters. It uses, of course, two numerical parameters for the sizes of neutron and proton bags[7,16] and four parameters for the two-body potential[14] employed, but these totally six parameters are universal parameters of the model constant for all properties in all nuclei. In the present approach no ad hoc assumption has been made and all predictions are based on the isomorphic shell model, all of whose numerals necessary for its implementation have been published independently a long time ago.

ACKNOWLEDGMENT

I would like to thank the European Research Office of the U.S. Army for partial financial support.

REFERENCES

1. D.M. Brink,"The alpha-particle model of light nuclei", In *Proc. Int. School of Physics ,"Enrico Fermi", Course XXXVI* (Ed. C. Bloch), New York: Academic Press, 1966, 15pp.
2. W.D.M. Rae, A.C. Merchant, and J. Zhang,"Geometry and collectivity in the Bloch-Brink alpha-cluster model",*Phys. Lett.* B Vol. 321, 1994, pp.1-5
3. D.M. Brink, H. Friedrich,A. Weiguny, and C.W. Wong ,"Investigation of the alpha-particle model for light nuclei",*Phys. Lett.* Vol. 33 B, 1970, pp. 143-146.

4. D. Robson,"Evidence for the tetrahedral nature of ^{16}O". *Phys. Rev. Lett.* Vol. 42, 1979, pp. 876-879.
5. W.D.M. Rae and A.C. Merchant,"Shape eigenstates and other one - and two - dimensional alpha - cluster structures in light nuclei", *Mod. Phys. Lett.* A Vol.8, 1993, pp. 2435-2447; J. Zhang and W.D.M. Rae, "Systematics of 2-dimensional alpha-cluster configurations in 4N nuclei from ^{12}C to ^{44}Ti" ,*Nucl. Phys.* A Vol. 564, 1993, pp. 252-270.
6. A.C. Merchant and W.D.M. Rae,"Systematics of alpha-chain states in 4N-nuclei", *Nucl. Phys.* A Vol. 549, 1992, pp. 431-438.
7. G.S. Anagnostatos,"Isomorphic shell model for closed-shell nuclei", *Int. J. Theor. Phys.*, Vol. 24, 1985, pp. 579-613.
8. G.S. Anagnostatos,"Multiharmonic nuclear Hamiltonian", *Can J. Phys.*, Vol. 70, 1992, pp. 361-364.
9. G.S. Anagnostatos,"Angular structure of unique spherical shells", *Lett. Nuovo Cimento*, Vol. 22, 1978, pp. 507-512.
10. G.S. Anagnostatos, "The geometry of the quantization of angular momenta(**l,s,j**) in field of central symmetry", *Lett. Nuovo Cimento*, Vol. 28, 1980, pp. 573-577.
11. G.S. Anagnostatos,"Symmetry description of the independent particle model", *Lett. Nuovo Cimento*,Vol. 29, 1980, pp. 188-192.
12. G.S. Anagnostatos, J. Yapitzakis, and A. Kyritsis,"Rotational Invariance of orbital-angular-momentum quantization of direction for degenerate states",*Lett. Nuovo Cimento* Vol. 32, 1981, pp. 332-336.
13. W.F. Hornyak, "Single-particle shell model", In:*Nuclear Structure*, New York: Academic Press 1975, pp. 233-282.
14. G.S. Anagnostatos and C.N. Panos,"Effective two-nucleon potential for high-energy heavy-ion collisions",*Phys. Rev.* C Vol. 26, 1982, pp. 260-264.
15. G.S. Anagnostatos and C.N. Panos,"Simple static central potentials as effective nucleon-nucleon interactions",*Lett.Nuovo Cimento* Vol. 41, 1984, pp. 409-416.
16. C.N. Panos and G.S. Anagnostatos,"Comments on A relation between average kinetic energy and mean-square radius in nuclei",*J. Phys.* G Vol. 8, 1982, pp. 1651-1658.
17. G.S. Anagnostatos, "Classical equations- of- motion model for high- energy heavy- ion collisions", *Phys. Rev.* C Vol. 39, 1989, pp. 877-883.
18. G.S. Anagnostatos,"Semiclassical simulation of finite nuclei" *Can J. Phys. Rev.* C Vol. 42, 1990, pp. 961-965.
19. G.S. Anagnostatos, T.S. Kosmas, E.F. Hefter, and C.N. Panos, "Semiclassical approximation for the isotopic shift of charge radii in Ca isotopes",*Can J. Phys.* Vol. 69, 1991, pp. 114-123.

20. E. Merzbacher John Wiley and Sons,"Quantum Mechanics", *Inc.,New York*, 1975.

21. J.Leech,"Equilibrium of sets of particles on a sphere", *Math. Gaz.* Vol. 41, 1957, pp. 81-90.

22. C.W. de Jager, H. de Vries, and C. de Vries, " Nuclear charge and magnet- ization- density- distribution parameters from elastic electron scattering", At. Data *Nucl. Data Tables* Vol. 14, 1974, pp. 479-508.

23. F. Ajzenberg-Selove and T. Lauritsen, "Energy levels of light nuclei A=11-12" , *Nucl. Phys.* A Vol. 433, 1985, pp. 1-158.

24. A.H. Wapstra and N.B. Grove,"The 1971 atomic mass evaluation", *Nucl. Data Tables* Vol. 9, 1971, pp. 267-301.

25. J.H. Fregeau and R. Hofstadter, "High-energy electron scattering and nuclear structure determinations.III. Carbon-12 nucleus",*Phys. Rev.* Vol. 99, 1955, pp. 1503-1509.

26. H.S.M. Coxeter,"Definitions of symbols used in the tables", In: *Regular Polytopes*, New York: Macmillan Company 1963, pp. 290-305.

27. P.H. Stelson and L. Grodzins,"Nuclear transition probability, B(E2), for $0^+_{g.s} - 2^+_{first}$ transitions and deformation parameter,β_2", *Nucl. Data*, Sec. A Vol. 1, 1965, pp. 21-102.

28. M. Kamimura,"Transition densities between the O^+_1, 2^+_1, 4^+_1, O^+_2, 2^+_2, 1^-_1 and 3^-_1 states in ^{12}C derived from the free-alpha resonating-group wavefunctions",*Nucl. Phys.* A Vol. 351, 1981, pp. 456-480.

29. W.J. Vermeer, M.T. Esat, J.A. Kuehner and R.H. Spear, " Electric quadru- pole moment of the first excited state of ^{12}C", *Phys. Lett.* B Vol. 122, 1983, pp. 23-26.

30. N.de Takacsy,"The structure of ^{12}C in a cluster model with varying Hinge angle", *Nucl. Phys.* A Vol. 178, 1972, pp. 469-478.

31. A.C. Merchant,private communication.